

DEPOSITIONAL AND DIAGENETIC ENVIRONMENTS
OF THE GORDON SUBGROUP (ORDOVICIAN),
GUNNS PLAINS, N.W. TASMANIA.

by

AZAM ALI KHWAJA

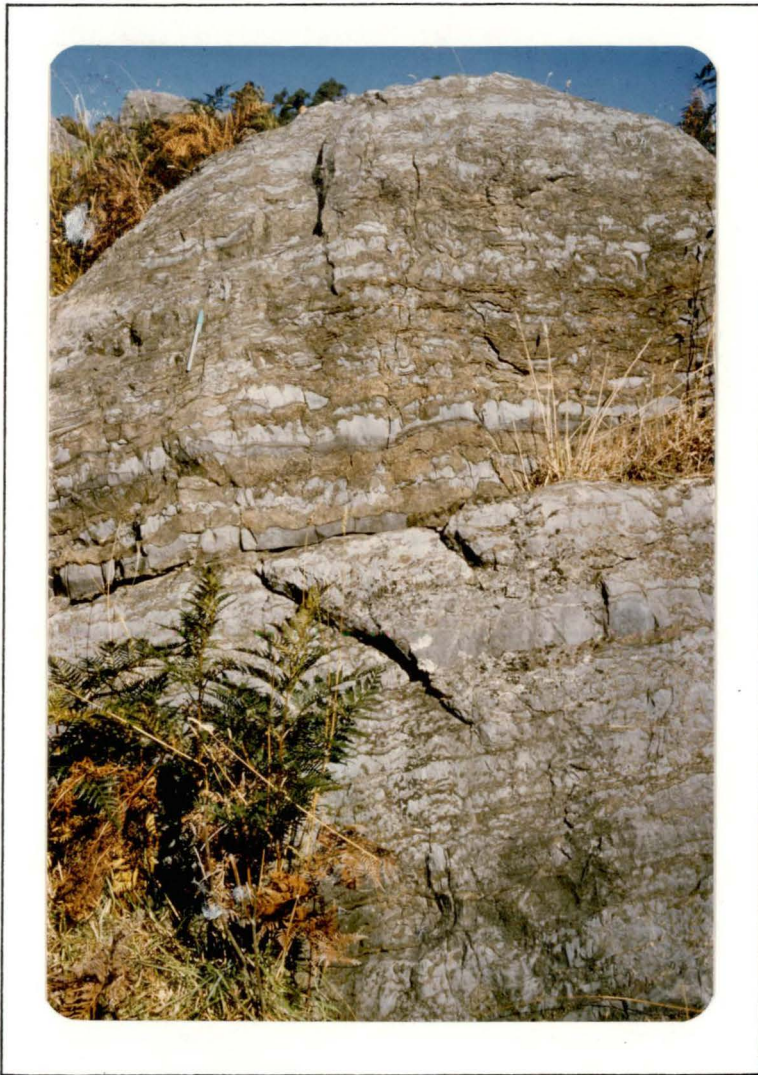
Submitted in partial fulfilment of the requirements
for the degree of Doctor of Philosophy
at the University of Tasmania.

HOBART

July, 1980

This thesis contains no material which has been accepted for the award of any other degree or diploma in any university and, to the best of my knowledge and belief, contains no copy or paraphrase of material previously published or written by another person, except where due reference is made in the text of this thesis.

A. A. Khwaja
July, 1980.



Frontispiece: Alternating limestone and dolomite sequence from section GPW. Note the upward increase in the dolomite content.

ABSTRACT

The Ordovician Gordon Subgroup at Gunns Plains is represented by over 450 m of carbonates. Three major peritidal carbonate environments (subtidal, intertidal and supratidal) are recognized. Microfacies observed are (a) subtidal - sparse and packed biomicrites, biosparites, pelbiomicrites, fossiliferous micrites, and micrites; (b) intertidal - sparse biomicrites, biopelmicrites and pelbiomicrites, pelmicrites and pelsparites, intrapelsparites, intrabiomicrites, intraoncosparites, intramicrites and intrasparites, intraclast-bearing micrites, intraclast-bearing fossiliferous micrites, other minor allochem-bearing micrites and dismicrites; (c) supratidal - dismicrites, fossiliferous micrites, intraclast-bearing fossiliferous micrites, intraclast-bearing micrites and intramicrites. Abundant mudcracks, birdseyes, and vertical and random burrows characterize the supratidal and intertidal facies, while diverse fossil types and random bioturbation features are characteristic of the subtidal facies.

Carbonate sedimentation took place dominantly during regressions as shown by asymmetric cyclicity. These depositional regressions represent progradation of the supratidal sequences. Microfacies variation suggests supratidal conditions in the south and subtidal conditions in the north of the study area. Ca, Mg, Sr, Na, Mn and Fe concentrations reflect depositional and diagenetic environments, in particular dolomitization and dedolomitization.

In most samples studied, an equigranular mosaic of finely crystalline, euhedral to subhedral, ideal to ferroan dolomite commonly ranging in size from 10 to 50 μ occurs in burrows, in and around intraclasts, and along mudcrack margins. Vertical distribution of the dolomite content in the sections indicate different episodes of dolomitization, of varying

intensity, at the end of each regressive cycle. This early diagenetic dolomite is representative of tidal flats undergoing sabkha diagenesis.

Dedolomitization textures are easily recognizable in this limestone. Both petrographic and chemical studies (Ca and Mg scans across dolomite crystals) demonstrate dedolomitization. The degree to which individual dolomite crystals are affected is highly variable ranging from a small clot to a whole dedolomitized rhomb. Observation of these textures suggests that most have formed as a result of the centripetal type of dedolomitization. The complex nature of occurrence of the dedolomite fabrics has been the main obstacle in making a quantitative petrographic estimate of the dedolomite content.

A first attempt has been made to estimate the dedolomite content by combining volumetric estimates of the dolomite content and their Mg/Ca molar ratios. Curves representing different percentages are constructed with the Mg/Ca = 1 curve corresponding to zero percent dedolomitization. As most of the dolomites in the study area are ideal dolomites, dedolomitization is implied for cases in which the dolomite content and the Mg/Ca ratio deviate from the Mg/Ca = 1 curve. The degree of dedolomitization in the studied sections ranges up to 69%.

Vertical variation of the dedolomite content appears to be related to the regressive phases, generally being abundant in the supratidal environment or where supratidal is absent, in the upper intertidal environment of each cycle. Increase of dedolomitization towards the supratidal suggests that dedolomitizing solutions were derived from a landward source. The variable amount of dedolomite in the different depositional cycles indicates that dedolomitization occurred in episodes of various intensity at the end of each cycle.

Trace element relationships inferred for dedolomitization are losses of Sr, Na and Mg, and a gain in Mn. The relationship of iron to dedolomitization remains uncertain. Sr and Mn concentrations obtained for the dedolomitizing solutions are similar to those of aragonite, implying that the transformation of aragonite to calcite had not been completed.

The $\delta^{18}\text{O}$ values of dedolomites (-4.0 to $-5.0\text{‰}_{\text{PDB}}$) are within the limits given by Keith and Weber (1964) for marine carbonates. The samples show a tendency towards a depletion in ^{18}O with increasing dedolomite content. Water to rock ratios (open and closed system) and initial values of the dedolomitizing solutions show that sea-water could not have been responsible for dedolomitization. The $\delta^{18}\text{O}$ values in the dolomites (-2.1 to $-5.6\text{‰}_{\text{PDB}}$) are heavier compared to calcites analyzed from the same sample. It is believed that the initial enrichment prior to dedolomitization in dolomites must have been significantly different. The $\delta^{18}\text{O}$ values in limestones (-5.4 to $-8.6\text{‰}_{\text{PDB}}$) reflect re-equilibration. Comparison with recent rain and cave waters shows that this re-equilibration most probably took place during early diagenesis. The $\delta^{13}\text{C}$ values in dedolomites ($+0.2$ to $-0.6\text{‰}_{\text{PDB}}$), dolomites ($+1.8$ to $-0.7\text{‰}_{\text{PDB}}$) and limestones ($+1.6$ to $-1.5\text{‰}_{\text{PDB}}$) are also believed to have undergone re-equilibration during early diagenesis.

It is proposed that, in cases where the dedolomite fabrics have been recognized, the trace element concentrations for dolomitization may not be valid unless the geochemical changes due to dedolomitization are also taken into account.

CONTENTS

	page
ABSTRACT	i
CONTENTS	iv
LIST OF FIGURES	vi
LIST OF TABLES	x
 Chapter 1 INTRODUCTION	
Statement of Problem	1
Location	1
Physiography	3
Methods	3
Acknowledgements	5
 Chapter 2 GENERAL GEOLOGY AND STRATIGRAPHY	
Previous Work	7
Geological Setting	7
Cambrian Stratigraphy	8
Ordovician Stratigraphy	9
Denison Subgroup	10
Gordon Limestone Subgroup	11
 Chapter 3 PETROGRAPHY	
Mesoscopic	17
Microscopic	18
Allochems	19
Structures	22
Carbonate Rock Types (Microfacies)	28
Micrite	28
Fossiliferous micrite	30
Intraclast-bearing micrite	31
Intraclast-bearing fossiliferous micrite	34
Other allochem-bearing micrites	36
Dismicrite	39
Biomicrite and biosparite	40
Pelmicrite and pelsparite	45
Biopelmicrite and pelbiomicrite	48
Intramicrite and intrasparite	49
Intrabiomicrite and intrabiosparite	52
Intrapelsparite	54
Intraoncomicrite	56
Distribution of Microfacies and Depositional Environment	57
 Chapter 4 DOLOMITIZATION	
Introduction	73
Petrology	74
Vertical Distribution	80
Geochemistry	82
Strontium	89
Sodium	92
Iron and manganese	97
Vertical variation of Mg/Ca, Sr/Ca, Mn/Ca and Fe/Ca molar ratios	97
Origin of dolomites	100

	page
Chapter 5 DEDOLOMITIZATION	
Introduction	104
Petrography	106
Regeneration of Earlier Texture	120
Type of Dedolomitization	121
Type of Dolomite Affected by Dedolomitization	123
Chemical Evidence for Dedolomitization	124
Estimation of the Dedolomite Content	128
Vertical Distribution of Dedolomite Content	135
Relationship of Trace Elements to Dedolomitization	138
Strontium	138
Manganese	143
Iron	148
Sodium	151
Origin of Dedolomites	154
Chapter 6 STABLE-ISOTOPE STUDIES	
Introduction	158
Sample Preparation and Analytical Procedure	158
Dedolomites	162
Dolomites	173
Limestones	175
Chapter 7 SUMMARY AND CONCLUSIONS	178
REFERENCES	184
Appendices	
A Petrographic data recording sheet	197
A.1 Sample locations and descriptions	198
B.1 Dissolution of samples for analyses	208
B.2 Preparation of standard solutions	209
C.1 Atomic absorption spectroscopy	211
C.2 Chemical data - A.A.S.	212
D X-ray fluorescence analysis (XRF)	215
E X-ray diffraction analysis (XRD)	217
F Electron-microprobe analysis (SEM)	219

List of Figures

	page
Figure 1.1 Locality map of the Gunns Plains area	3
1.2 Simplified geological map showing sampled outcrops. The letters shown refer to stratigraphic sections (see also Figs. 2.1 and 2.2).	4
2.1 Simplified cross-section of the Gunns Plains Limestone, also showing the position of the sections	13
2.2 Generalized stratigraphic column (composite section) and the dominant environment of deposition	15
3.1 Micrite with vertical and horizontal burrows. Note the occurrence of dolomite within two burrows.	24
3.2 Mudcracked, algal micrite with abundant vertical burrows	24
3.3 Fossiliferous micrite - wide variation in grain size of fossils	29
3.4 Fossiliferous micrite - moulds of fossils with early and late cements	29
3.5 Intraclast-bearing finely crystalline dolomite. Note wide variation in dolomite crystal size within intraclasts.	32
3.6 Mudcracked, dolomitic, intraclast-bearing fossiliferous micrite	32
3.7 Micrite grading into pellets with fossils, pellets and intraclasts	37
3.8 Dismicrite with abundant bulbous birdseyes	37
3.9 Alternating dismicrite and micrite	38
3.10 Dismicrite overlain by dolomitized algal mat	38
3.11 Gastropod biomicrite. The gastropods are re-crystallized and filled with micrite	41
3.12 Biosparite. The moulds of gastropods are filled with micrite	41
3.13 Biomicrite with abundant pelmatozoan fragments and micrite envelopes	43
3.14 Biosparite with calcareous algae	43
3.15 Pelmicrite, faintly laminated and containing silt size quartz	45
3.16 Dolomitic pelmicrite with abundant quartz	46
3.17 Intrasparite grading upwards into dolomite	50
3.18 Erosional contact between intrasparite and dolomicrite	50
3.19 Oolitic intrabiosparite with some intraclasts containing skeletal material	51
3.20 Intrabiosparite. The intraclasts are composed of micrite, dolomite and scattered quartz grains	51

	page
Figure 3.21 Intrapelsparite. The intraclasts are composed of micrite, few dolomite rhombs and scattered quartz	53
3.22 Intrapelsparite. Note the wide variation in grain size of intraclasts	53
3.23 Intrapelsparite - flat pebble conglomerate. Note upward decrease in grain size and erosional contact	55
3.24 Dolomitic intraoncomicrite. Note skeletal fragment in core and irregular outline of oncolite. The bryozoan fragment partly overlies oncolite	55
3.25 Vertical distribution of the microfacies and depositional environments in section GPR	59
3.26 Vertical distribution of the microfacies and depositional environments in section GPD	60
3.27 Vertical distribution of the microfacies and depositional environments in section GPB	61
3.28 Vertical distribution of the microfacies and depositional environments in section GPW	62
3.29 Vertical distribution of the microfacies and depositional environments in section GPL	63
3.30 Simplified energy and rock response profiles across a stable cratonic shelf. Energy zones X, Y and Z of Irwin (1965) are also shown	68
3.31 A general model depicting the environments of deposition during any period of time within the Gunns Plains Limestone	70
4.1 Equigranular mosaic of fine crystalline euhedral to subhedral dolomite	75
4.2 Rounded intraclast composed of dolomite. The dolomite has also invaded the micrite matrix	75
4.3 Horizontal burrow filled with dolomite of variable size	77
4.4 Broken shell with convex side up. Note the unreplaced micrite beneath the shell suggesting downward seepage of the dolomitizing brines	77
4.5 Vertical variation of the dolomite content in the laterally equivalent sections GPL, GPW and GPB and the interpreted depositional environments	79
4.6 Vertical variation of the dolomite content in sections GPR and GPD	81
4.7 Relationship of Sr/Ca molar ratio to Mg/Ca molar ratio in section GPL	87
4.8 Relationship of Sr/Ca molar ratio to Mg/Ca molar ratio in section GPW	88
4.9 Relationship of Na/Ca molar ratio to Mg/Ca molar ratio in section GPW	90
4.10 Relationship of Na/Ca molar ratio to Mg/Ca molar ratio in section GPL	91

	page
Figure 4.11 Relationship of Mn/Ca molar ratio to Mg/Ca molar ratio in section GPL	93
4.12 Relationship of Mn/Ca molar ratio to Mg/Ca molar ratio in section GPW	94
4.13 Relationship of Fe/Ca molar ratio to Mg/Ca molar ratio in section GPL	95
4.14 Relationship of Fe/Ca molar ratio to Mg/Ca molar ratio in section GPW	96
4.15 Vertical variation of the major and minor elements in section GPW	98
4.16 Vertical variation of the major and minor elements in section GPL	99
4.17 A general model for dolomitization in the Gunns Plains Limestone	101
5.1 Clots of finely crystalline calcite (dedolomite) on dolomite	108
5.2 Clots of finely crystalline calcite on dolomite. Note the gradation of clots into a mosaic of anhedral calcite crystals (composite calcite rhombohedra)	108
5.3 Composite calcite rhombohedra - crossed nicols	110
5.4 Composite calcite rhombohedra and abundant rhombic pores. Note the presence of anhedral calcite crystals within rhombic pores - crossed nicols	110
5.5 Partly to completely dedolomitized rhombs. The black organic laminae are believed to be algal mats	112
5.6 Breached dedolomite zones in a micrite matrix. Crossed nicols	112
5.7 Patches of dedolomite	113
5.8 Enlarged view of one of the patches	113
5.9 Palimpsest texture. Arrows point to boundaries of former dolomite crystals. Iron oxide rims are also visible	114
5.10 Ghosts of earlier dolomite crystals in a micrite matrix. Lacy calcite lenses to the right of centre in the photomicrograph. Crossed nicols	114
5.11 Dedolomitized rhombs with dark boundaries. Some show effects of leaching. Crossed nicols	117
5.12 Dolomite rhombs with calcite cores (dedolomite)	117
5.13 Rhombic pores	118
5.14 Electron microprobe scans of a partly dedolomitized rhomb of dolomite	125
5.15 Electron microprobe scans of a partly dedolomitized rhomb of dolomite	126
5.16 X-ray distribution maps of Mg and Ca in a dolomite crystal with irregular outlines. Petrographic observations showed clots of dedolomite within the crystal	127

	page
Figure 5.17 Plot of Mg/Ca molar ratio against the dolomite percentage. The straight line ($Mg/Ca = 1$) representing the ideal dolomite has been drawn taking $Mg/Ca = 0.5$, $0.3 = 50\%$ and 30% dolomite	129
5.18 Plot of Mg/Ca molar ratios against the dolomite percentage. The area between $Mg/Ca = 1$ and the x-axis has been divided to represent different percentages of dedolomitization	130
5.19 Plot of Mg/Ca molar ratios against the dolomite percentage.	132
5.20 Vertical distribution of the dolomite percentage and dedolomite percentage	136
5.21 Vertical distribution of the dolomite percentage and dedolomite percentage in section GPW	137
5.22 Plot of Sr/Ca molar ratio against the dedolomite percentage in sections GPL and GPW	139
5.23 Plot of Mn/Ca molar ratio against the dedolomite percentage in section GPW	144
5.24 Plot of Mn/Ca molar ratio against the dedolomite percentage in section GPL	146
5.25 Plot of Fe/Ca molar ratio against the dedolomite percentage in sections GPW and GPL	149
5.26 Plot of Na/Ca molar ratio against the dedolomite percentage in sections GPW and GPL	152
5.27 A general model for dedolomitization in the Gunns Plains Limestone	156
6.1 Plot of $\delta^{13}C$ and $\delta^{18}O$ data. Line separating fresh water and sea-water samples after Keith and Weber (1964)	161
6.2 Relationship of Mg/Ca molar ratio with (a) $\delta^{13}C$, (b) $\delta^{18}O$. Relationship of dedolomite with $\delta^{13}C$ and $\delta^{18}O$ shown in (c) and (d) respectively	163
6.3 Relationship between δC_a^O and W/R ratio for closed system	167
6.4 Relationship between δC_a^O and W/R ratio for open system	169
6.5 Permissible values of dedolomitizing solutions and W/R ratio. The field lies away from sea-water of present-day composition, thus ruling it out as the agent of dedolomitization.	171
E.1 X-ray diffractograms of several samples	218

List of Tables

	page
Table 3.1 Important indicators used in delineating depositional environments	27
3.2 Distribution (%) of the microfacies in the studied sections	58
3.3 Summary of observed features in section GPR	65
3.4 Summary of observed features in section GPD	66
3.5 Summary of observed features in the laterally equivalent sections GPB, GPW and GPL	67
4.1 Comparison of the visual and point count estimates of dolomite percentage	78
4.2 Chemical data obtained by X-ray fluorescence	83
4.3 Correlation coefficients for major and minor elements	84
4.4 Atomic absorption analyses from different parts of the same sample	85
4.5 Distribution (mean and standard deviation of molar ratios) related to interpreted environments	102
5.1 Petrographic criteria for recognition of dedolomites	107
5.2 Distribution (mean) of trace elements in sections GPL and GPW	155
6.1 Series 1 isotope analyses	159
6.2 Series 2 isotope analyses	159
6.3 Series 3 isotope analyses	159
D.1 Instrument settings for XRF analysis	216

Chapter 1

INTRODUCTION

STATEMENT OF PROBLEM

The aims of the study are to reconstruct the depositional and diagenetic environments of the Ordovician limestone exposed at Gunns Plains, independently and collectively from petrographic and geo-chemical criteria, and on lateral and vertical successions of facies.

Most studies dealing with ancient carbonate rocks emphasize the physical and biological characteristics of a depositional setting, in addition to the lateral and vertical facies relationships. This study uses the same integrated approach. The investigation of diagenesis differs from other studies in that the process of dedolomitization has also been considered in addition to the commonly discussed dolomitization process. This is the first study to propose a method for estimating the dedolomite content and to indicate its relationship with some trace elements commonly thought to be associated with dolomitization. Knowing the overprints of dedolomitization on the dolomites allows for a clearer understanding of the dolomitization process in terms of trace element geochemistry. Additional evidence is discussed on the basis of Scanning Electron Microscopy (SEM) and on stable isotopic variation in oxygen and carbon.

LOCATION

Gunns Plains, named after the first man to survey the region in 1860, lies between latitudes $41^{\circ}15'$ and $41^{\circ}21'$ south and longitudes 146° and $146^{\circ}04'$ east in the north-west of Tasmania (Fig. 1.1).

Access to Gunns Plains is along a 32 kilometre all-weather metalled road, which joins the Bass Highway at Ulverstone.

PHYSIOGRAPHY

At the southern extremity of the Dial Range, the hill-locked valley of Gunns Plains is 8 kilometres in length from north to south. The River Leven flows along the western side of the valley. The topography is conditioned by the different rock types. The valley floor has been largely carved out of the limestone, while at the northern and southern extremities are narrow gorges cut into hard conglomerates and other older resistant rocks. Underground streams, sink holes and caverns, typical of the limestone terrains influenced by the karst cycle, are well developed.

METHODS

An initial reconnaissance of the area was undertaken in July 1975. Due to the discontinuous nature of the outcrops, a continuous stratigraphic section could not be obtained. Sampling was subsequently limited to five outcrops designated GPR, GPD, GPB, GPW and GPL (Fig. 1.2). Samples were collected at each major lithological change except in sections GPW and GPL where more detailed sampling was carried out. A Jacobs staff and tape were used to measure the stratigraphic thicknesses on traverses at right angles to strike to within the nearest centimetre.

All specimens were cut and polished in the laboratory. Thin sections and acetate peels (both unstained and stained with Alizarin-red and potassium ferricyanide) were prepared from the polished slabs,

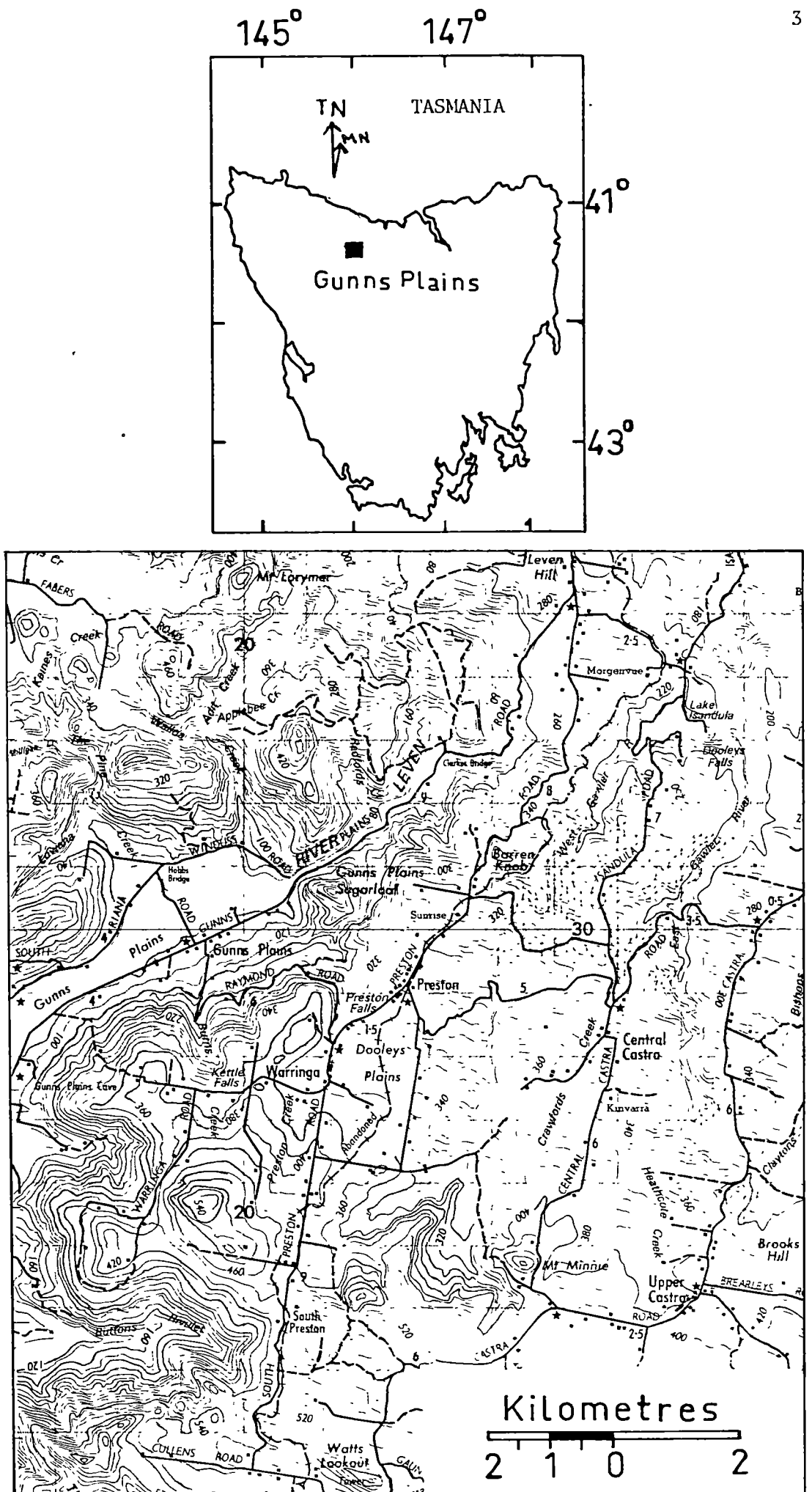


Fig. 1.1 Locality map of Gunns Plains area.

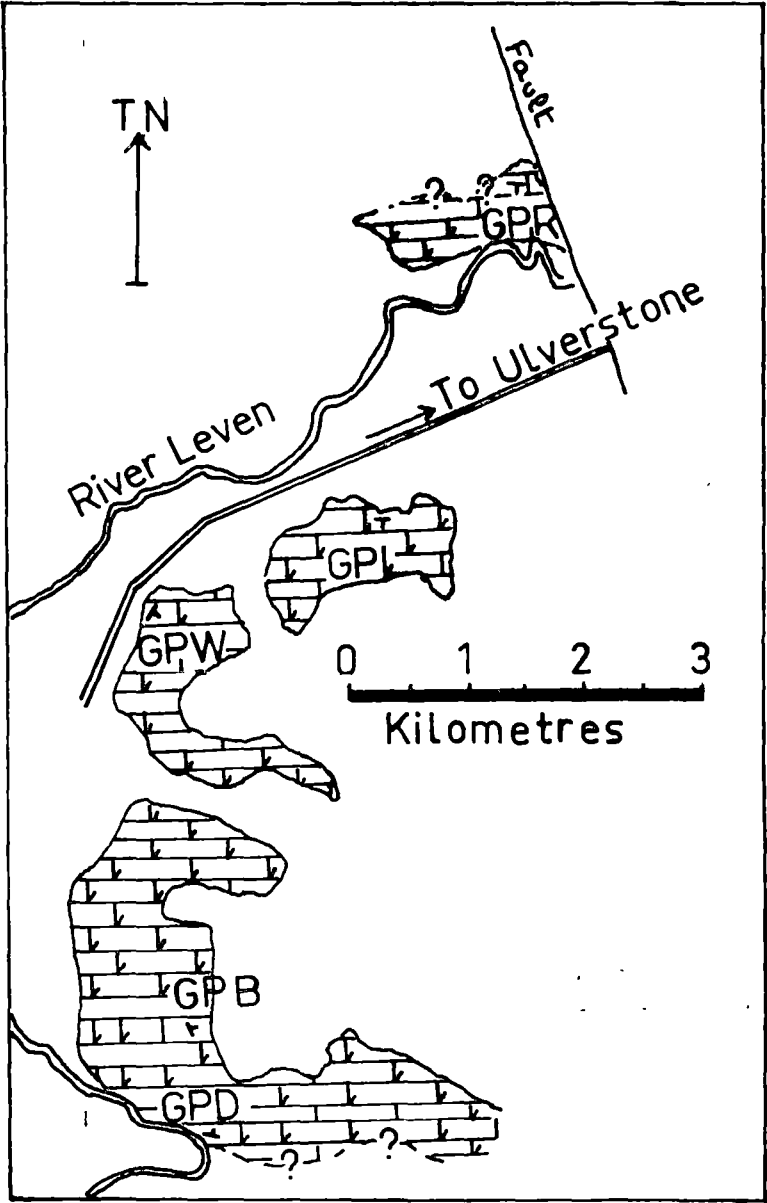


Fig. 1.2 Simplified geological map showing sampled outcrops. The letters shown refer to stratigraphic sections (see also Figs. 2.1 and 2.2).

and studied under the microscope. All the observable petrographic features of each sample were entered on petrographic data recording sheets (Appendix A). For the description of the rocks, the terminology and classification scheme of Folk (1962) is applied with some modifications. Carbonate rock types identified are listed in Appendix A.1.

A fresh slab of each sample from sections GPW and GPL was finely crushed, dissolved in 1N hydrochloric acid (Appendix B.1) and standard solutions prepared (Appendix B.2). The insoluble residue percentages were determined and the soluble carbonate fractions analysed for Ca, Mg, Sr, Mn, Fe and Na using atomic absorption spectroscopy (AAS; Appendix C.1). Chemical data is listed as Appendix C.2. Twenty-one samples from sections GPL and GPW were analysed by X-ray Fluorescence (XRF) for major and minor elements (Appendix D). In addition, twenty samples were analysed by X-ray Diffraction (XRD; Appendix E). Thirty-two limestones, dolomitic limestones and dolostones, and dedolomites were analysed for stable isotope variation in oxygen and carbon. Five samples were selected for electron microprobe analyses (Appendix F).

ACKNOWLEDGEMENTS

Sincere thanks are due to Dr. C.P. Rao for suggesting this project, and for his guidance and supervision throughout the study. I am indebted to the members of the staff at the University of Tasmania, especially Professor D.H. Green, Dr. M.R. Banks and Dr. C.F. Burrett for their advice and comments.

This work has benefitted greatly from discussions with Dr. C. Eastoe, Dr. J.L. Walshe, Dr. M. Ahmad, Dr. D.C. Green and Mr. I.H. Naqvi. Dr. D.C. Green along with Mr. R.N. Woolley of the Mines Department are also thanked for their supervision and assistance during the stable-isotope determinations. The constant help of Mr. P. Robinson during all

stages of analytical work, and of Mr. W. Doran during lapidary work is greatly appreciated. The help of Mr. W. Jablonski of the Central Science Laboratory during electron microprobe work is sincerely acknowledged.

I wish also to acknowledge the helpful discussions and comments of my fellow post-graduate students at the University of Tasmania, especially A. Bush, G. Jenner, K. Kenna, J. Laurie, J. Odell, D. Seymour and B. Stait.

The invaluable assistance of J. Pongratz with the typing is gratefully acknowledged.

The study was partly financed by the Government of Pakistan. Quaid-e-Azam University, Islamabad, granted study leave to the author. Mr. and Mrs. L.R. Lee are thanked for their kind hospitality during my visits to the study area. Finally, for her support and encouragement, I am indebted to Shamsa, my wife.

CHAPTER 2

GENERAL GEOLOGY AND STRATIGRAPHYPREVIOUS WORK

No detailed sedimentological work on the limestone had been carried out prior to the present study, although numerous workers have contributed towards the understanding of the geology of the area with emphasis on palaeontology, stratigraphy, structure and economic aspects.

Twelvetrees (1903, 1909) was the first person to assign the limestone at Gunns Plains to the (Ordovician) Gordon River Limestone, earlier recognized by Gould (1866) as a separate unit of "Early Silurian" age. Hughes (1957) and Banks (1962) have summarized the earlier works in their reviews. A detailed geological map (the Sheffield Quadrangle, 1 inch to 1 mile) was compiled in 1959 by Jennings, Burns, Mayne and Robinson of the Department of Mines. Later, Burns (1963) and Jago *et al.* (1977) made some modifications.

GEOLOGICAL SETTING

The Palaeozoic deposition began in narrow troughs developed between and within Precambrian blocks. These troughs formed part of the Tasman Geosyncline (Schuchert, 1916) which extended along eastern Australia from Queensland to Tasmania. In Tasmania the central Precambrian region (like the others in Tasmania) became a geanticline during the Cambrian and is known as the Tyennan Geanticline. Rocks of the Tyennan Geanticline were metamorphosed during the Precambrian Frenchman Orogeny. (term introduced by Spry, 1962, p.124). Similar rocks constitute the Forth Nucleus (term introduced by Burns, 1963, p.43), northeast of Gunns Plains, on the north coast. The Rocky Cape Geanticline, to the west of the Forth Nucleus and

the Badger Head Geanticline, to the east are the other Precambrian blocks of the region. The Precambrian rocks in the Rocky Cape and Badger Head Geanticlines are comparatively unmetamorphosed (Burns, 1963), but were extensively folded during the Penguin Orogeny (Penguin Movement of Spry, 1962, p.124).

Between the Rocky Cape and Tyennan Geanticlines and the Forth Nucleus, the main area of Cambrian deposition was the Dundas Trough. It formed an arcuate belt around the northern and western margins of the Tyennan Geanticline. Close to the edge of this belt are acid to intermediate volcanic rocks forming what is known as the Mount Read Volcanic Arc. It is intruded by granites (Williams, 1976).

The north trending offshoot of the Dundas Trough between the Forth and Rocky Cape Geanticline is the Dial Range Trough (Burns, 1963, p.43). It broadens at the southern end near Gunns Plains to join the regional Dundas Trough (Burns, 1963, p.75). Gunns Plains is thus situated close to the junction of two major Cambrian troughs.

CAMBRIAN STRATIGRAPHY

The Cambrian rocks occurring in the Dial Range Trough were correlated by Banks (1956) with the Dundas Trough on the West Coast of Tasmania. In the Dial Range, north Gunns Plains area, the Cambrian rocks vary in thickness from about 1790 m to more than 3175 m (Burns, 1963). The oldest rocks are the massive intermediate to acid volcanic rocks more than 300 m thick called the Lobster Creek Volcanics followed unconformably by more than 1120 m of predominantly mudstones belonging to the Cateena Point Subgroup. Unconformably overlying the Cateena Point Subgroup rocks is the Barrington Chert varying in thickness from 75 m to more than 850 m. They grade laterally into the Radfords Creek Subgroup

rocks consisting predominantly of mudstones. No complete succession has yet been established for this Subgroup. In the southern Gunns Plains area, rocks equivalent to those in the northern part are found. These correlates of the Dundas Group are also described as the Gog Range Greywacke (Jennings *et al.*, 1963) of unknown thickness. Burns (1963) identified quartzite conglomerates consisting of rounded pebbles in a matrix of quartz sand in them and correlated these with the Radfords Creek Subgroup.

The Cambrian rocks underwent deformation during and after their deposition. Carey and Banks (1964) named this deformational phase the Tyennan Orogeny, and the unconformity between the Dundas Group (and its equivalents) and the overlying Ordovician Junee Group rocks the Jukesian Movement. According to Burns (1963), Cambrian sedimentation ceased in the Dial Range Trough on the formation of an axial anticlinal structure during the Jukesian Movement.

ORDOVICIAN STRATIGRAPHY

Unconformably overlying the Cambrian rocks of the Radfords Creek Subgroup in the north Gunns Plains area and the Gog Range Greywacke in the south are siliceous clastics which have been correlated with the Ordovician Owen Conglomerate (Bradley, 1954). These terrestrial and shallow marine conglomerate beds and sandstones are conformably overlain by a limestone sequence and together they represent the Ordovician Junee Group at Gunns Plains.

In the type area (the Florentine Valley), the Junee Group rocks cover virtually the whole Ordovician Period. It is divided into a lower, dominantly clastic sequence (Denison Subgroup) and an upper carbonate sequence (Gordon Limestone Subgroup) (Corbett and Banks, 1975).

In much of Tasmania, the basal member of the Junee Group is a conglomerate which passes up into a sandstone termed the Moina Sandstone (Jennings *et al.*, 1959) or the Caroline Creek Sandstone (Banks, 1962). Overlying the sandstone is the Gordon Limestone Subgroup, although in the Florentine Valley (type area), the sandstones are overlain by mudstones of the Florentine Valley Formation.

Denison Subgroup

The sandstone (Moina Sandstone) and conglomerate (Roland Conglomerate) grouped by Johnston (1888) into the Magog Group occur in the southern Gunns Plains area. The Roland Conglomerate unconformably overlies the Cambrian Gog Range Greywacke and the basal beds usually contain fragments of the underlying Cambrian rocks. The typical rock is a dense recrystallized quartz conglomerate composed of subrounded quartz, quartzite and quartz schist fragments. There is a general decrease in grain size and increase in degree of sorting and roundness of the pebbles upwards. The Roland Conglomerate is terrestrial and probably fluvial in origin (Jennings, 1963).

Lying unconformably above the Roland Conglomerate is the Moina Sandstone, in which, besides sandstones and quartzite are conglomerate beds which resemble the underlying Roland Conglomerate. With the onset of Moina Sandstone deposition, the environment changed to shallow marine as indicated by the occurrence of tubicolar casts, a few brachiopods, gastropods and trilobite fragments. South of Buttons Rivulet, no exposure of limestone was seen by the author (this area being covered by Quaternary talus), although limestone is shown on the Sheffield Quadrangle map (Jennings *et al.*, 1959).

At the northern end of Gunns Plains, the clastics underlying the Gordon Limestone are called the Dial Subgroup (Burns, 1963, p.135).

The succession is Gnomon Mudstone conformably or unconformably overlain by the Duncan Conglomerate, which is followed by the Moina Sandstone. The Moina Sandstone, underlying the Gordon Limestone (section GPR), in Kaines Creek and Walloa Creek (see fig. 1.1) is represented by a conglomerate. This conglomerate differs from the Duncan Conglomerate in the type of pebbles, a higher degree of sorting and by the occurrence of well-defined beds of fine to medium sandstone. The conglomerate has a sand-size matrix of rock fragments forming up to 30% of the rocks. Nearly 50% of the pebbles are composed of rounded, subspherical, white quartz with a mean diameter of about 25 mm. Subrounded pebbles of 50 mm mean diameter form about 20% of the rock, while micaceous quartzite pebbles having a mean diameter of about 75 mm total about 30% of the rock. In some of these conglomerates, 60% of the pebbles have a mean diameter of about 17.5 mm and are composed of white quartz.

Unlike material in the Roland Conglomerate (south of Gunns Plains), which has been mainly derived from Cambrian rocks, the pebbles at the base in the conglomerate north of Gunns Plains (below section GPR) are composed of Precambrian rocks. On the basis of this lithological dissimilarity, Burns concluded that the Magog Group and Dial Subgroup rocks were deposited at the same time, but in different basins of sedimentation under different conditions of transport.

Gordon Limestone Subgroup

The only detailed stratigraphic studies of the Gordon Limestone Subgroup have been done in the Florentine Valley (type area) and at Mole Creek. In the type area, the Gordon Limestone Subgroup is represented by a 2000 m sequence, dominantly of limestone, ranging in age from Arenigian (the Karmberg Limestone) to Early Llandoveryian (the Westfield Beds) (Corbett and Banks, 1974).

The succession in the Florentine Valley is as follows (after Corbett and Banks, 1974):

GORDON LIMESTONE SUBGROUP	Westfield Beds	
	Benjamin Limestone	Upper Limestone Member Lords Siltstone Lower Limestone Member
	Cashions Creek Limestone	
	Karmberg Limestone	Wherrets Chert Member

Overlying the Florentine Valley Formation (Denison Subgroup) is the Karmberg Limestone. It consists of calcareous siltstone and impure nodular limestone at the base, followed by a 100 to 180 m thick cherty limestone (Wherrets Chert Member). Above this micritic limestone is a thick bedded oncolitic limestone formation (of Chazy age) called the Cashions Creek Limestone. The Cashions Creek Limestone is followed upwards by the 1200 m thick Benjamin Limestone ranging in age from Chazy to Maysvillian. It is divisible into two limestone members named the Lower and Upper Limestone Members and separated in places by a siltstone member (the Lords Siltstone). Overlying the Benjamin Limestone is a siltstone and sandstone unit called the Westfield Beds.

At Gunns Plains, the carbonate rocks are over 450 m thick. The contact between these carbonate rocks representing the Gordon Limestone Subgroup and the underlying clastics, equivalents of the Denison Subgroup, is not exposed at either end (northern and southern) of the Gunns Plains syncline. The top of the limestone is also commonly covered by Tertiary basalts, although in the centre of the syncline, south of the Gunns Plains Cave there is a small outcrop of quartzite, the lowest unit of the Silurian and Devonian Eldon Group.

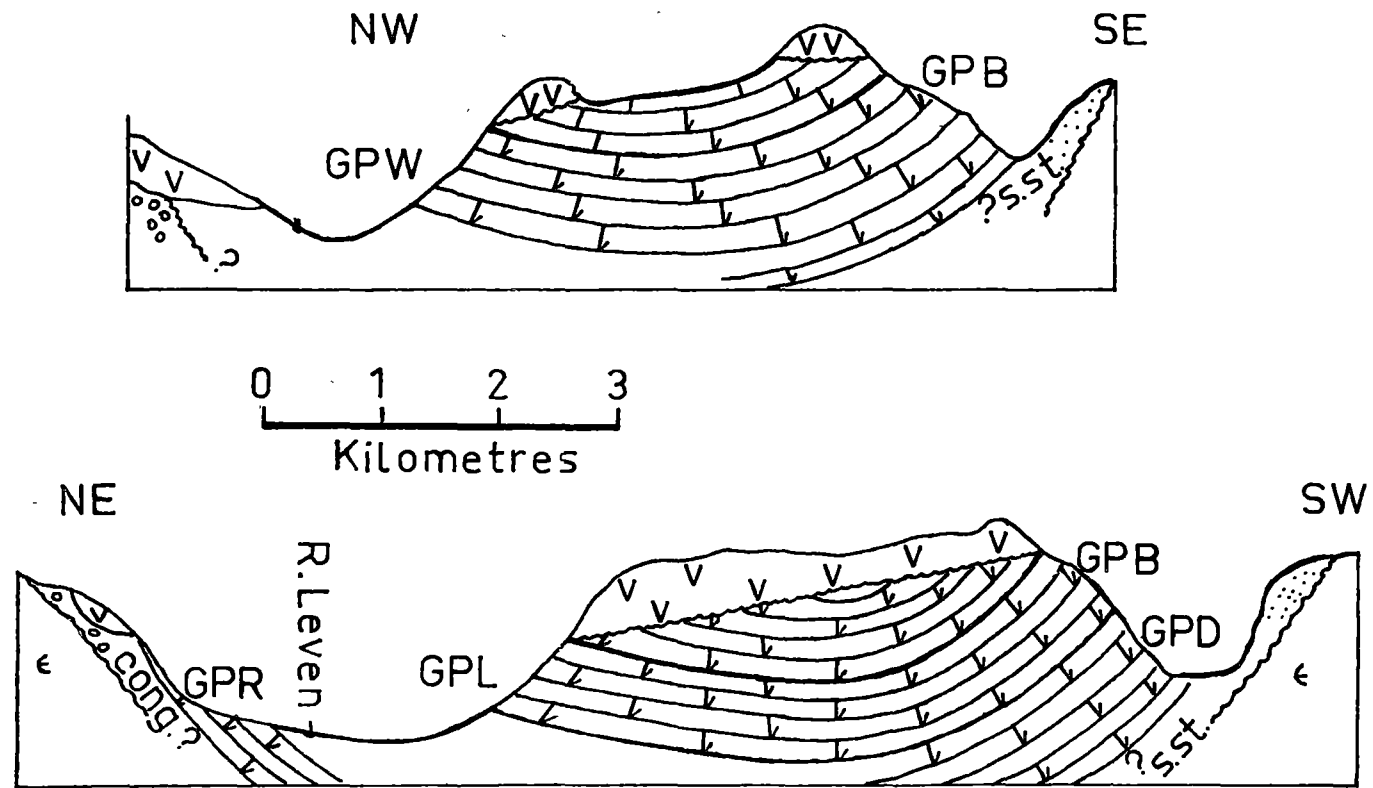
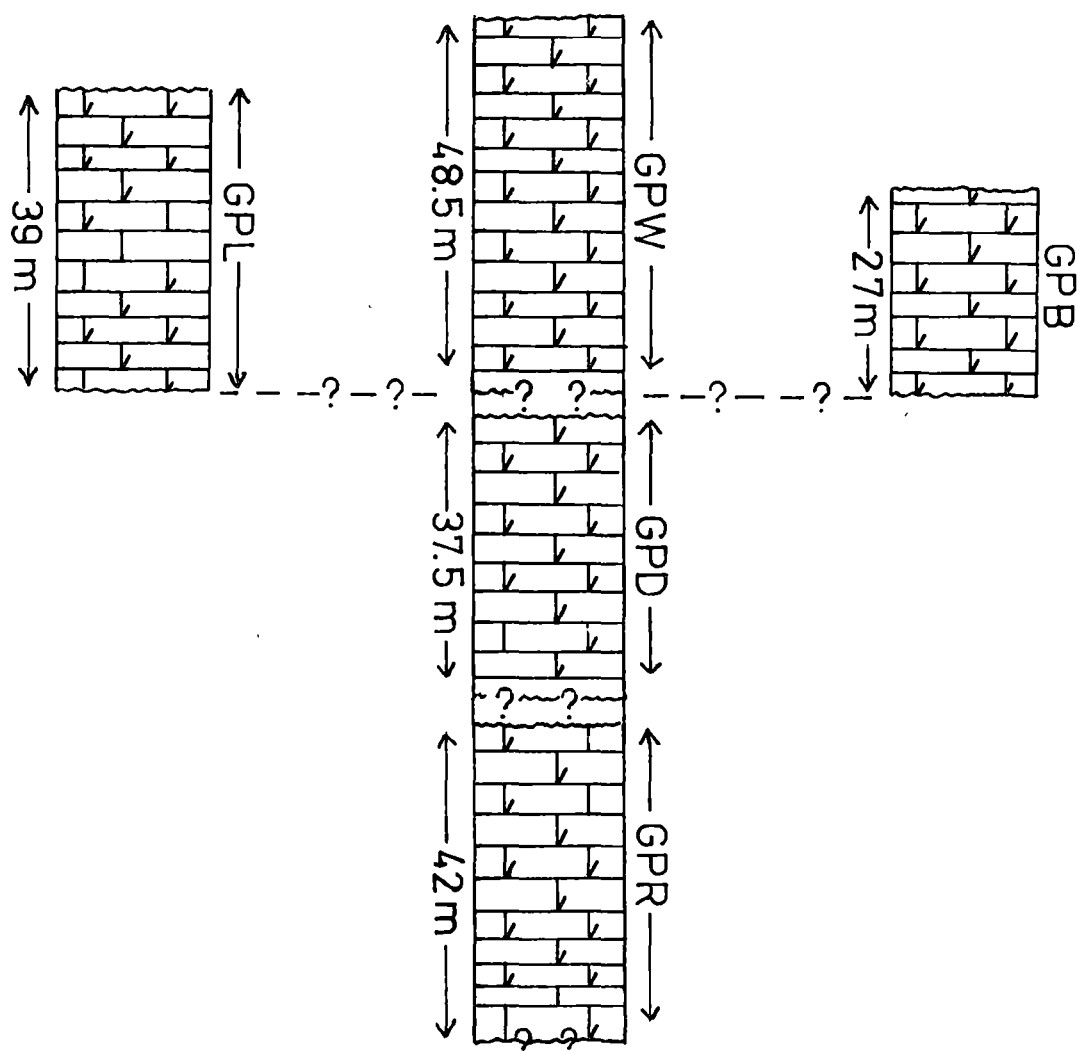


Fig. 2.1 Simplified cross-section of the Gunns Plains Limestone, also showing the position of the sections.

As the limestone occurrence at Gunns Plains is a mappable unit, it can be described as a formation. The name Gunns Plains Limestone is proposed for this mappable unit. A continuous stratigraphic section could not be obtained due to the discontinuous nature of the outcrops. However, a composite section can be made from the sampled outcrops, whose relationship is shown in a cross section (fig.2.1).

Various carbonate rock types in these predominantly well-bedded, micritic, dolomitic limestones have been recognized. Lithologically they are similar to the Benjamin Limestone in the Florentine Valley. The Gunns Plains Limestone represents mostly progradational tidal flat sequences, which in vertical succession show asymmetric cyclicity. Detailed lithological description and a discussion of the depositional environments of the individual sections are discussed in the following chapters. The generalized stratigraphic column (composite section) and the major palaeo-environmental interpretation of the Gunns Plains Limestone is shown in fig. 2.2. Sections GPB, GPW and GPL are lateral equivalents. The upper part of the composite section is from section GPW, as it has the maximum thickness. Although the upper limit of section GPW is covered by Tertiary basalts, its proximity to the top of the measured (composite) section is thought to be within 100 m. The base of the composite section is represented by section GPR, where faults and folds occur. This complicated structure and the thick vegetation cover made the measurement of stratigraphic thickness difficult. Repetition of beds is a possibility and therefore the thickness shown for section GPR may not represent the correct thickness.

The fossil content in the Gunns Plains Limestone is variable ranging from 0% to 56% by volume in the studied samples. The average fossil content in the sections is as follows: GPR - 7%, GDP - 8%, GPW - 7%, GPB - 7% and GPL - 9%. Dominantly broken, diverse fossil types



- GPR: mostly intertidal
- GPD: mostly intertidal and subtidal
- GPW: mostly supratidal and intertidal
- GPB: mostly supratidal and subtidal
- GPL: mostly intertidal and subtidal

Fig. 2.2 Generalized stratigraphic column (composite section) and the dominant environment of deposition. For details of vertical distribution of the microfacies and depositional environments, see Figs. 3.25, 3.26, 3.27, 3.28 and 3.29.

of brachiopods, bryozoans, corals, crinoids, gastropods, pelecypods; or individual fossil types may be present. Banks (1957) recognized corals such as *Propora*, heliolitids, favositids, *Favistella* and colonial stauriaceans; stromatoporoids; the bryozoan *Rhinidictya*; rhynchonnellid brachiopods and trilobites from section GPW. He recognized *Tetradium*, heliolitids, *Favistella*; *Rhinidictya*; rhynchonnellids, and asaphid trilobites from section GPL.

In specimens gathered during this study, orthoconic nautiloids were found to occur in sections GPW and GPL; and filamentous algae in section GPW. Kenna (pers. comm., 1979) identified corals *Tetradium petaliforme* in section GPR; *Propora* cf. *hirsuta*, *Foerstephyllum* of *vacuum* group and a stromatoporoid, ?*Beatricea*, from section GPW. Burrett (1978) identified the conodont fauna *Phragmodus undatus*, *Plectodina* cf. *furcata*, *Drepanoistodus suberectus*, *Belodina compressa*, *Chirognathus monodactylus*, *Plectodina aculeata* and *Panderodus gracilis* from sections GPW and GPL. The conodont fauna indicates a Blackriveran to Kirkfieldian age for sections GPW and GPL.

Chapter 3

PETROGRAPHYMESOSCOPIC

The parameters used for defining lithologies in the field do not correspond accurately with those used for microscopic description. Thus, the differentiation into carbonate rock types in the field was only a rough approximation. Amongst the different carbonate rocks, biomicrites are easily recognizable. They mostly occur in thin bands, except near the top of section GPW where they are more widespread.

The limestone is generally well-bedded, although some units which appear to be single beds are in fact seen to be thinly laminated under the microscope. Wherever parting planes were observed, they seemed to correspond to the original bedding planes. Graded-bedding and cross bedding on a mesoscopic scale were not seen.

V-shaped mudcracks are commonly observable, whereas stylolites, even if present, are not always observed. Among stylolites, the saddle and lobe pattern of variable frequency is most common and is generally parallel to bedding. Cross-cutting stylolites and stylolites cutting across bedding were also observed, but not commonly in section GPR.

The dolomite layers are more coarse-grained than the limestones. They are dominantly yellowish-brown and show positive relief on weathered surfaces. This could be ascribed to differential weathering. Dolomitic burrows are easily recognizable in the bioturbated rock units.

MICROSCOPIC

The features observed during the petrographic examination of peels and thin sections are outlined in the petrographic data recording sheet enclosed as Appendix A. Included are petrographic variables like volumetric percentages of allochems, fossil types, intraclast composition and shape; depositional textures - homogeneity, grain groundmass ratio, textural maturity; structures - birdseyes, bioturbation, mudcracks, sedimentary unit thickness; diagenetic fabrics - spar type, dolomite colour, size, shape and fabric; dedolomites; vanished evaporites. All the petrographic properties were quantified after a scheme developed by Rao and Naqvi (1977).

In order to identify the carbonate rock types, the terminology and classification scheme developed by Folk (1959, 1962) was used with a few modifications. This scheme was preferred primarily for the reason that it provides a framework in which a number of new parameters can be included without affecting the relationship between the allochemical (carbonate grains) and orthochemical (matrices or bonding agents) constituents.

Due to the significance of the allochems in naming carbonate rock types according to Folk's classification, their occurrence and associated sedimentary structures are detailed below and are followed by a description of the major carbonate rock types in the Gunns Plains Limestone. The vertical distribution of the allochems and structures in the measured sections is shown in Figs. 3.25, 3.26, 3.27, 3.28 and 3.29. All percentages mentioned for the allochems are volumetric estimates.

ALLOCHEMS

Fossils

Fossils in the form of skeletal debris are the most common allochemical constituents of the Gunns Plains Limestone. The percentage of samples in the measured sections which contain at least one percent of skeletal debris is as follows: GPB = 63%, GPW = 73%, GPL = 95%, GPD = 83% and GPR = 65%. Most of the fossils have been recrystallized and this, combined with the fact that in peels the fossil debris is seen in two dimensions only has made it difficult to identify most of them below Phylum or Class level. (For species identified by different workers, see Chapter 2, p.16.)

The most abundant fossil remains are those of gastropods and brachiopods occurring independently or in association with other types like calcareous algae, bryozoans, corals, echinoderms, nautiloids, sponge spicules, pelecypods, stromatoporoids and trilobite fragments. In a very few samples, bryozoans, pelecypods or stromatoporoids were found to be the only fossil representatives. The common size of skeletal debris is about 6 mm, but all size ranges from 0.01 mm to >6 cm (a stromatoporoid) occur. Although very fine skeletal grains cannot be recognized as such [as Feray *et al.* (1962) have shown after experimental crushing of shell material], their contribution to the Gunns Plains Limestone is most likely very significant even though the origin remains unknown.

The skeletal grains occur mostly in association with other kinds of allochems. Intraclasts followed by pellets (pelloids) were the most frequently found allochems in association with the skeletal grains. Post-depositional changes, commonly resulting in recrystallization, affect nearly all the samples and may lead to total obliteration of the grains.

Microsparite formed as a result of recrystallization was found to have affected the echinodermal plates less than other skeletal grains. Ferroan calcite spar is not common and only rarely the replacement of shell structure by ferroan dolomite was observed. Wave-action was possibly the main agent responsible for the well-fragmented skeletal grains. Micrite envelopes are common. Geopetal fabrics are not always present, and the same holds true for sparry cement fillings.

Intraclasts

Following Folk (1962), the term intraclasts is here limited to allochems larger than 0.2 mm in diameter. In the measured sections, the percentage of samples which contain at least one percent intraclasts as their allochemical constituent is as follows: GPB = 55%, GPW = 53%, GPL = 47%, GPD = 27% and GPR = 38%. The size range of intraclasts varies from the minimum limit of 0.2 mm to 30 mm, although the common range in the studied samples is between 4 mm and 10 mm. All shapes from angular to rounded were observed but predominantly the intraclasts are subangular to subrounded. Generally the larger intraclasts, except the flat-pebble conglomerates, are angular in shape and commonly show brecciation, while the other smaller intraclasts are mostly the result of erosion and reworking of earlier deposited sediments.

The intraclasts are commonly composed of micrite, but others composed of biomicrite, pelmicrite and dismicrite are also present. Another notable feature of some intraclasts is their dolomitic composition (see Figs. 3.5, 3.18 and 3.20) with no dolomite being present in the surrounding matrix. In a few samples, intraclasts ranging in size from fine sand to conglomerate-size occur (Figs. 3.22 and 3.23). These grains seem to be erosional rather than of faecal origin. In the studied samples, intraclasts may be the only allochems present or they may occur

in association with fossils, pellets, oolites, oncolites and algal mats. Sedimentary structures - birdseyes, mudcracks and bioturbation features may or may not be present in association with the intraclasts.

Pellets

Pellets as defined by Folk (1959) are "structureless", rounded, spherical to elliptical or ovoid micritic grains less than 0.2 mm in diameter. McKee and Gutschick (1969) proposed the name "Peloid" for pebbles of an indeterminate origin, but following Folk, the name pellet has been used in this study although probably all pellets are not of faecal origin. Their abundance in the Gunns Plains Limestone shown as percentages of samples containing at least one percent pellets is as follows: GPB = 13%, GPW = 18%, GPL = 21%, GPD = 21% and GPR = 38%. Pellets are probably more abundant in the measured sections than the visual estimates indicated. This is based on the observation that pellets were often difficult to distinguish from the micrite matrix, and in some cases patchy recrystallization and dolomitization could be seen obliterating the original pellet texture.

In the studied samples, most of the pellets are brown in colour and vary in shape from spherical to ovoid. All sizes between 0.05 mm and 0.2 mm were observed, but commonly the pellets in a single sample are characterized by one size only. The pellets occur in a micrite matrix or surrounded by sparry calcite cement. Usually spar cemented pellets have hazy boundaries, probably indicating incipient recrystallization spreading from the cement into the pellets. In a very few cases, gradations from pellets in a micrite matrix to spar-cemented pellets can be observed in a single sample. The pellets may occur in association with other allochems. Skeletal grains in subordinate or dominant amounts to the pellets are the most frequently found allochems, followed by intraclasts.

Oolites

Oolites as defined by Folk (1959) are particles which must show radial or concentric structure, or both. In the present study the term "oolite" following Rao and Carozzi (1971), is used to designate a grain which consists of a core (nucleus) and an accretionary envelope showing fibro-radiated structures, or both.

No oolites were found to occur in sections GPB, GPD and GPR. Even in sections GPW and GPL they are rare, only 2% of the samples in section GPW and 6% in section GPL contain 1 to 17% oolites. All oolites are less than 0.5 mm in diameter and have been affected by recrystallization to varying degrees. Mostly the original nuclei have acted as centres of recrystallization resulting in a pseudospar fabric containing ghosts of the oolitic nuclei. A few oolites have core linings of fibrous calcite. Sometimes recrystallized, well-rounded grains without any visible internal structure (as in Fig. 3.19) occur associated with the oolites. These have been included with oolites in the present study. Oolites with concentric structure were not observed in the Gunns Plains Limestone. In all cases, the oolites occur associated with other allochems, skeletal fragments being the most frequent in a micritic or sparry matrix.

STRUCTURES

While undergoing deposition and diagenesis the carbonate rocks acquire some characteristic features which affect not only the allochemical constituents but the matrices also. These primary and secondary features (structures) in certain combinations help in deciphering the natural sequence of events in ancient carbonate rocks by analogy with the recent. The sedimentary structures observed in the studied samples are laminations, bioturbations, birdseyes and mudcracks.

Laminations

The Gunns Plains Limestone at mesoscopic scale is a well-bedded sequence. Under microscopic examination some samples in all the sections were observed to be thinly laminated with the individual laminae less than 1 mm in thickness. The laminae within a sample may be parallel to each other, either flat or wavy, or they may be truncated by overlying laminae. They are of micritic or dolomitic composition. In some cases, skeletal fragments and burrows with distinct outlines are present.

The wavy, laminated dolomicrite containing mostly anastomosing, black (organic) laminae and rarely very small unrecognizable skeletal debris are considered to represent algal mats. They correspond to the cryptalgalaminated sediments of Aitken (1969) and are stromatolites by the definition of Logan *et al.* (1964), but they differ from other stromatolites in lacking pronounced doming. The algal mats are common in all the sections.

Current laminations, another distinct type, were also recognized in sections GPB and GPW. They are best represented in section GPW between 27 and 32 m above the base. Broken shells, oriented randomly in some cases or with the convex side up in others, are found in these current laminated rocks. Shells with the convex side up acted as "tent structures" during dolomitization, so that no dolomite occurs immediately underneath them (see Fig. 4.4). Scour-and-fill structure, horizontal lamination, vertical burrows, a few oolites and intraclasts also occur. One sample (49099) shows cross-bedding.



Fig. 3.1. Micrite with vertical and horizontal burrows. Note occurrence of dolomite within two burrows.

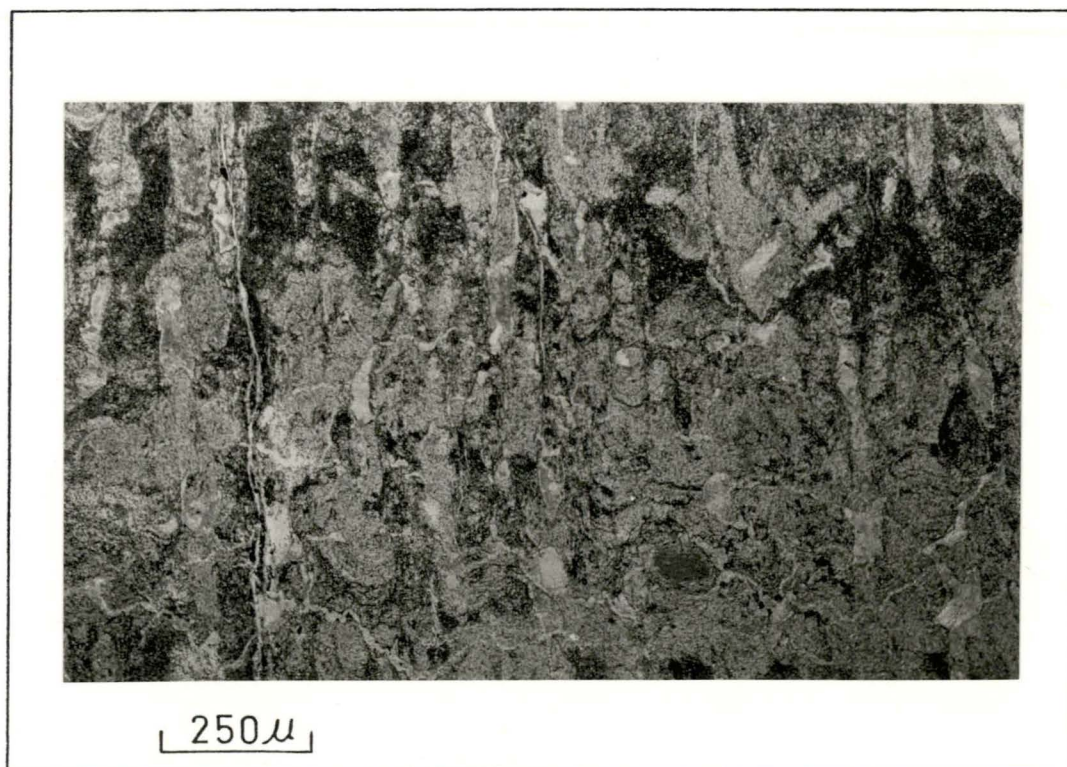


Fig. 3.2. Mudcracked, algal micrite with abundant vertical burrows.

Bioturbation Structures

The bioturbation structures record the activity of organisms after deposition, but before lithification. In this study, the term "bioturbation structure" refers to burrows greater than 1 mm in diameter. Thus, they are differentiated from borings which are usually less than 1 mm in diameter. The bioturbation structures were found to occur in all the measured sections of the Gunns Plains Limestone. Burrowing could not be quantified in the same way as allochem percentages, but for each sample, if present, the type of burrow (vertical, horizontal or random) was recorded. If 0 to 25% of the peel/thin section showed burrows, it was recorded as rare, 25 to 50% as common and above 50% as abundant. The burrows usually stand out as circular to elongate disruptions of the matrix. They are mostly filled with dolomite and in some cases, a slightly different sediment type than the matrix occurs within the burrows which may contain very small skeletal fragments with slightly swirled fabric. When observed, the full length of the burrows is greater than the width. In laminated sediments, especially in section GPB, vertical burrows with distinct outlines commonly disrupt the laminae. These burrows unlike some others of uniform width are wider near their openings. Overall the burrows in the Gunns Plains Limestone constitute what Seilacher (1967) terms the "Skolithos" and "Cruziana" facies.

Birdseye Structures (also referred to as fenestral fabrics by Tebutt *et al.*, 1965)

Following Shinn (1968), the term "birdseye structure" is used to designate tiny blebs of calcite or anhydrite. These structures are common in the Gunns Plains Limestone and like the bioturbation structures, their abundance in each sample was recorded as rare (0 to 25%), common

(25 to 50%) or abundant (over 50%). Shinn (1968) recognized two types of birdseye - planar and bulbous (bubble-like) vugs. In the studied samples, the bulbous type, commonly ranging in size from 1 mm to 4 mm and filled with calcite, is the dominant form. All the measured sections contained samples with birdseyes, occurring with or without allochems, burrows and mudcracks.

Mudcracks (Dessication cracks)

All the measured sections in the Gunns Plains Limestone showed abundant mudcracks. They are mostly intralaminar mudcracks commonly varying from 4 mm to 10 mm in polygon diameter. In plan view, the mudcracks showed curvilinear or nearly rectilinear sides. Dolomitization has resulted in obscuring the boundary between the polygons. The mudcracks were found to occur in samples containing all types of allochems. In a few cases, birdseyes were observed in the mudcracked polygons.

The significance of the above-mentioned variables in deciphering depositional environments is well-documented in the literature. Table 3.1 compiled from many sources lists most of the variables and their depositional environments. In ancient carbonate rocks, the depositional environments are interpreted by analogy with modern areas such as Persian Gulf, Shark Bay, Bahamas and others (see Bathurst, 1976 for summaries of many workers' results), and the petrographic variables listed in Table 3.1 are believed to be the imprints of the physical, biological and chemical conditions that characterized the depositional setting (e.g. Rigby and Hamblin, 1972; Ginsburg, 1975).

Table 3.1

IMPORTANT INDICATORS USED IN DELINEATING DEPOSITIONAL ENVIRONMENTS

(Compiled from many sources.)

Indicator	Supratidal	Intertidal		Subtidal
		Upper	Lower	
Birdseyes			-----	
Mudcracks			-----	
Vertical burrows	-----		-----	
Random burrows			-----	
Algal mat			-----	
Intraclasts	-----			-----
Flat-pebble	-----			
Oncolites				-----
Algae				
Brachiopods			-----	
Cephalopods			-----	
Gastropods	-----			
Pelecypods	-----			
Bryozoans			-----	
Corals			-----	
Ostracods	-----			
Pelmatozoans			-----	
Trilobites			-----	

CARBONATE ROCK TYPES (MICROFACIES)

It has been mentioned previously (p. 18) that for each sample studied a petrographic data recording sheet enclosed as Appendix A was used. Based on this recorded data, the following is a general description of the carbonate rock types and their interpreted depositional environment. These carbonate rock types are considered as microfacies following Gubler *et al.* (1967).

1. Micrite

The most abundant constituent of the carbonate rocks in the study area is micrite, which commonly occurs in association with allochems. Micrite in the absence of allochems (pure micrite) can form a rock in its own right (Folk, 1959, p.68). Only 4% of the samples from section GPR in the Gunns Plains Limestone do not contain any allochems or birdseye structures and thus are "micrite" carbonate rock types.

The notable feature of these samples is that abundant burrows (random) have disturbed the homogeneous character of the rocks as in Fig. 3.1. It can be seen that the micrite in the burrows is slightly lighter in colour than the yellowish-brown micrite of the matrix or the burrows may be partly or completely filled with dolomite (see also Fig. 4. 3).

Studies of recent carbonates show that pure carbonate mud accumulates in a range of environments grading from the backreef lagoons (e.g. British Honduras, Florida Bay) to the tidal flat complex (e.g. Bahama Bank). Micrite is of polygenetic origin (Lobo and Osborne, 1973) and is interpreted to have formed from such lime muds. Presence of random burrows, and absence of birdseyes and mudcracks suggests a probable subtidal environment of deposition for this microfacies in quiet water conditions.

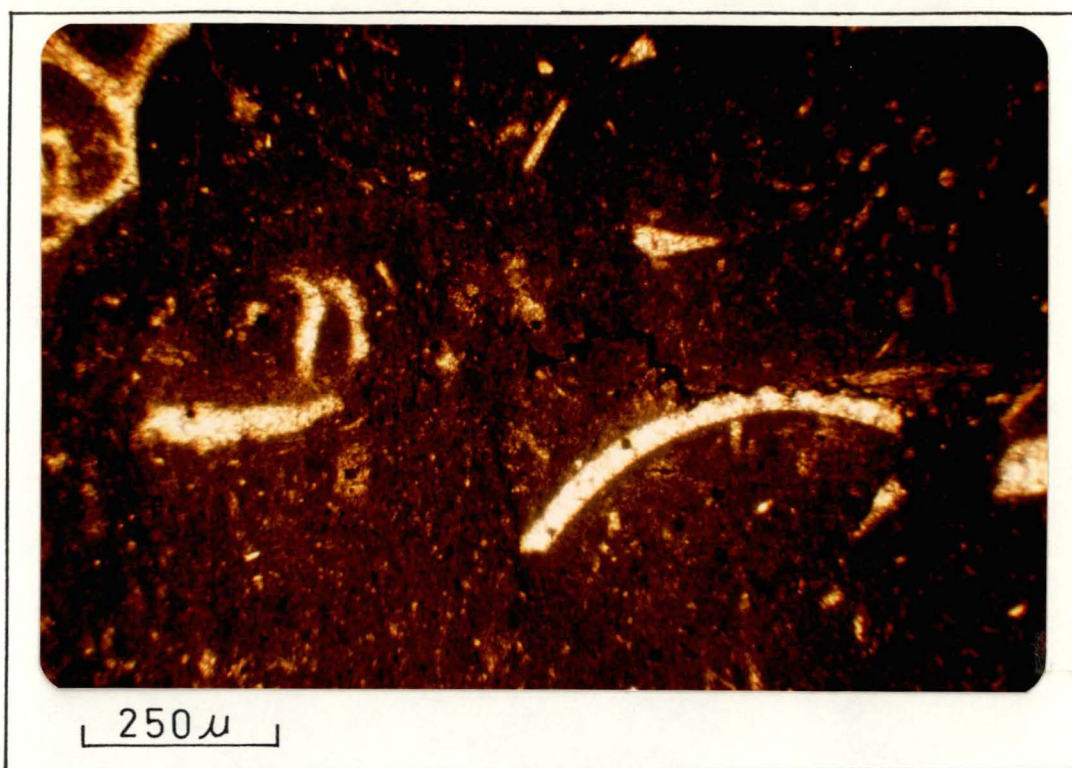


Fig. 3. 3. Fossiliferous Micrite. Note the wide variation in grain size of fossils.

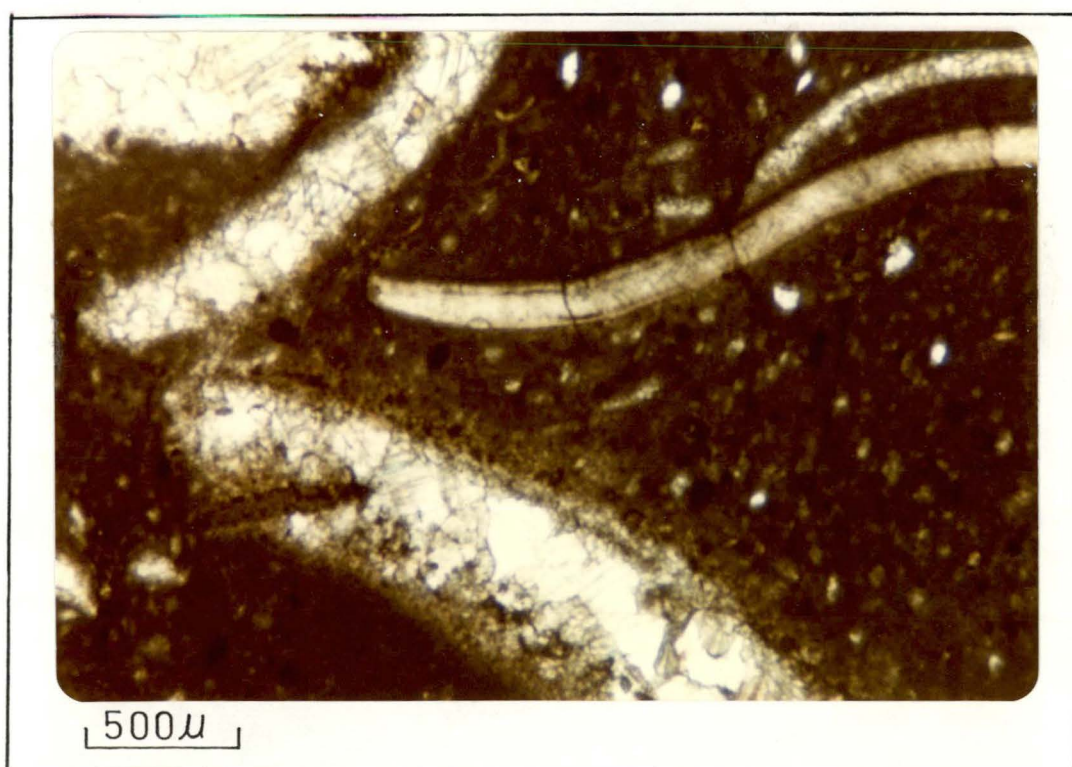


Fig. 3. 4. Fossiliferous Micrite. Note moulds of fossils with early and late diagenetic cements.

2. Fossiliferous Micrites (fossil-bearing micrite)

This is described as micrite having fossils ranging up to 10% as the only allochems. The grain to groundmass ratio in all cases is less than 1:9. The percentages of fossiliferous micrites in the studied sections are GPB = 15%, GPW = 21%, GPL = 31%, GPD = 35% and GPR = 13%.

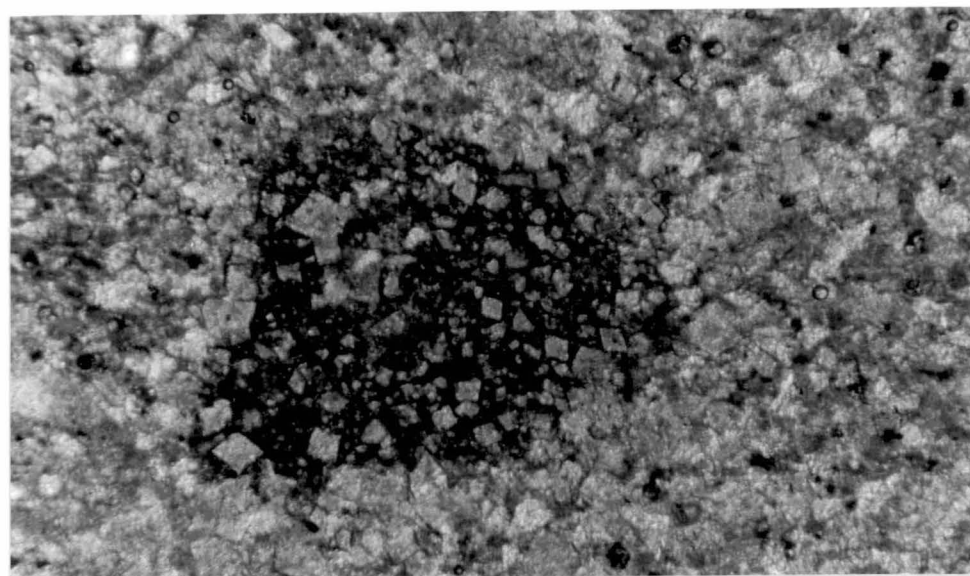
The mean content of fossils in the fossiliferous micrites is 5%. Commonly the fossils like those shown in Fig. 3.3 occur as broken, dis-oriented fragments scattered randomly in a micrite matrix. There is a wide variation in the grain size of skeletal debris and often the type of fossil cannot be determined due to their small size with even some so small as to make it difficult to differentiate from the micrite matrix. In some samples, diverse fossil types like algae, brachiopods, bryozoans, crinoids and trilobite fragments are recognizable or rarely the fossils may occur as moulds filled with early and late cements (Fig. 3.4). Some shells in section GPW are oriented with their convex side up (Fig. 4.4). The micrite is visible only beneath the shell, elsewhere being replaced by dolomite. The distribution of birdseyes, mudcracks and burrows in the studied sections is shown below (see also Figs. 3.25, 3.26, 3.27, 3.28 and 3.29).

	Birdseyes	Mudcracks	Burrows
GPB	in 60% samples rare, common or abundant	in 40% samples	vertical - common random - rare
GPW	in 43% samples common	35%	in 50% samples vertical - rare, common or abundant
GPL	in 43% samples rare to common	27%	mostly vertical - common. In some random - common to abundant
GPD	in 15% samples common	-	vertical - common random - common
GPR	in 50% samples rare	43%	dominantly vertical ranging from common to abundant.

The dominance of unrecognizable broken forms even in samples with no visible bioturbation structures suggests extensive fragmentation and abrasion of skeletal material. On the other hand, absence of spar in the samples suggests lack of winnowing and indicates that overall quiet water conditions prevailed in the environment. Most of the samples contain birdseyes and/or mudcracks, which are significant indicators of subaerial exposure. Also, vertical burrows (for environmental range see Table 3.1) are more common than the random burrows. The fossiliferous micrites are believed to have formed mostly in the intertidal and supratidal environments, although a few samples containing algae, bryozoans, pelmatozoans and trilobite fragments with no birdseyes and mudcracks are interpreted to have formed in the subtidal environment. Samples from section GPW with convex side up oriented shells are believed (Reineck and Singh, 1975, p.176) to have formed in channels.

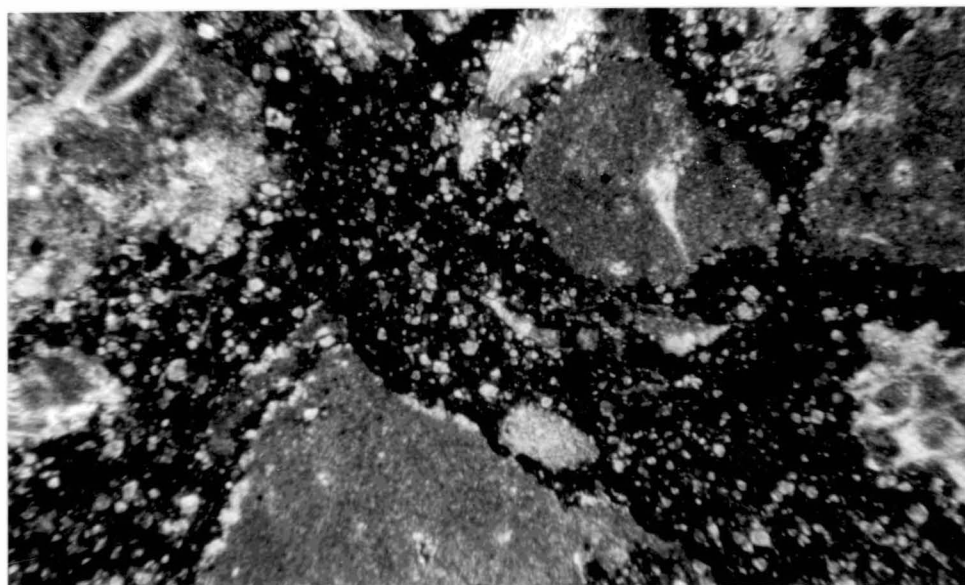
3. Intraclast-bearing Micrite

Intraclast-bearing micrite is defined as micrite having intraclasts as the only major allochems. Skeletal debris, if present, constitutes



250 μ

Fig. 3.5. Intraclast bearing finely crystalline equigranular dolomite. Note dolomitization of intraclast and wide variation in dolomite crystal size within intraclast.



1 mm

Fig. 3.6. Mudcracked, dolomitic, intraclast bearing fossiliferous micrite.

less than 1% of the total allochemical content. The intraclasts in these micrites do not exceed 20%, thereby limiting the grain to ground-mass ratio to being less than 2:8. The percentages of intraclast-bearing micrites in the sections are GPB = 8%, GPW = 13%, GPL = 2% and GPR = 4%. No sample from section GPD belongs to this microfacies.

Some of the observed features are summarized below:

	Intraclast range	Shape	Composition	Birdseyes	Burrows
GPB	up to 14%	angular to subangular	micrite	rare to common	if present, random-common
GPW	14%	subangular to rounded	micrite, dolomite	if present are rare to common	vertical-rare random-rare
GPL	11%	subangular	micrite	rare to abundant	random-common
GPR	3%	subrounded to rounded	micrite	rare	random-abundant

As mentioned above, the intraclasts are mainly composed of micrite. Except for the upper intraclast range of 14% and occurrence in a micrite matrix, they are quite similar to those occurring in the intrasparites (Figs. 3.17 and 3.18). The intraclasts composed of dolomite in section GPW may differ in that the dolomite is of variable size. Fig. 3.5 is a photomicrograph from section GPW showing an intraclast being replaced by dolomite of variable crystal size. Common to rare mudcracks are present in most of the samples.

According to Folk (1962), intraclasts are commonly formed by erosion of a widespread layer of semi-consolidated carbonate sediment. This erosion may be submarine or due to wave attack on exposed mud-cracked carbonate flats. Abrasion of these eroded fragments (intraclasts) results in their becoming rounded and indicates high-energy conditions. Mostly the intraclasts are subangular in shape, except the 3% of samples from section GPR and some from section GPR, which contain

subrounded to rounded intraclasts. This suggests that overall quiet water conditions prevailed at the time of deposition of this microfacies. Presence of mudcracks in most of the samples indicates subaerial exposure of the samples after deposition, which may or may not have been periodic. Additional evidence for subaerial exposure is provided by the occurrence of birdseyes in the mudcracked samples. An intertidal to supratidal environment of deposition is envisaged for this microfacies.

4. Intraclast-bearing Fossiliferous Micrite

Intraclast-bearing fossiliferous micrite is defined as micrite containing less than 20% intraclasts and up to 10% fossils. Other allochems, if present, constitute less than 1% of the total allochemical content. The grain to groundmass ratio is less than 3:7. The percentages of intraclast-bearing fossiliferous micrite samples in the studied sections are: GPB = 8%, GPW = 21%, GPL = 25%, GPD = 14% and GPR = 11%.

Some of the observed features are detailed below:

Intraclast mean		Shape	Fossil mean
GPB	4%	angular to sub-angular	5%
GPW	4%	angular to rounded, but mostly subangular	4%
GPL	3%	subrounded to rounded - common angular to sub-rounded - rare	5%
GPD	2%	subangular to rounded	5%
GPR	6%	angular to sub-rounded	3%

The intraclasts are dominantly composed of micrite, except some samples from section GPW, where the intraclasts like in the intraclast-bearing micrites of this section show variable composition with both micrite and dolomite occurring in them. The fossils occur as broken pieces scattered randomly in the micrite matrix. They show a wide, variety, from very small unidentifiable fragments to recognizable forms, predominantly of brachiopods and gastropods. Rarely bryozoans (Fig. 3.6), pelmatozoans and trilobite fragments were observed.

~~commonly~~ ~~rather~~ ~~but~~ Samples containing only one type (mostly gastropods or brachiopods) are also present. Fig. 3.6 is a photomicrograph of a dolomitic intraclast-bearing fossiliferous micrite showing intraclasts, bryozoan and some other unidentifiable fossil fragments. No birdseyes were observed in section GPD. In other sections, when present, birdseyes are rare to common. About half the samples have mudcracks. Nearly all the samples contain vertical or random burrows ranging from rare to abundant.

The occurrence of broken fragments in mostly burrowed rocks suggests that biological activity may have been responsible for this fragmentation. On the other hand, differences in roundness of the associated intraclasts, which is believed to reflect their abrasional history indicates wave activity as another possible mechanism. Thus the possibility exists of both biological activity and wave action as the agents responsible for skeletal fragmentation. The likely depositional environment for this microfacies is believed to have been the intertidal zone with only a few samples containing angular intraclasts, common birdseyes, mudcracks with or without vertical burrows being formed in the supratidal environment.

5. Other Allochem-bearing Micrites

In addition to the above three common types of allochem-bearing micrites, other types were also recognized in the Gunns Plains Limestone. Allochems in various combinations occur. If present, the intraclasts, oolites and oncolites are each less than 20%, and the fossils and pellets are each less than 10%. These rare combinations of allochems in a micrite matrix occur in sections GPR, GPL and GPW where they form 1%, 6% and 2% of the samples respectively.

The combination of allochems observed were pellets (range 3 to 6%) and fossils (2 to 8%); pellets (2 to 4%), fossils (6 to 8%) and intraclasts (2 to 7%); fossils (4 to 7%) and oolites (up to 15%); fossils (3 to 7%), intraclasts (up to 3%) and oolites up to 3%); or fossils (3 to 7%), pellets (up to 6%) and oolites (5 to 13%).

Fig. 3.7 is a photomicrograph of one such sample from section GPL showing unidentifiable broken skeletal debris, pellets and angular to subrounded intraclasts. Overall micrite predominates over spar in the sample. In other samples fossils show all gradations from very small unidentifiable fragments to recognizable fragments (mostly brachiopods, gastropods and trilobite fragments). Pellets are sparsely distributed and not concentrated at one place. The intraclasts are composed of micrite and vary in shape from subangular to rounded. Oolites showing radial structure with recrystallized nucleus or ghosts of oolites with no visible structure usually occur surrounded by microsparite, but micrite predominates in the whole sample. Commonly birdseye structures and mudcracks are absent, but bioturbation structures are present. In addition to the above-mentioned combinations of allochems, a single sample each from sections GPR and GPW consists of algal micrite.

Fig. 3.2 is a photomicrograph of such a sample. The mudcracked algal mat layers have been disturbed by abundant vertical burrows of variable

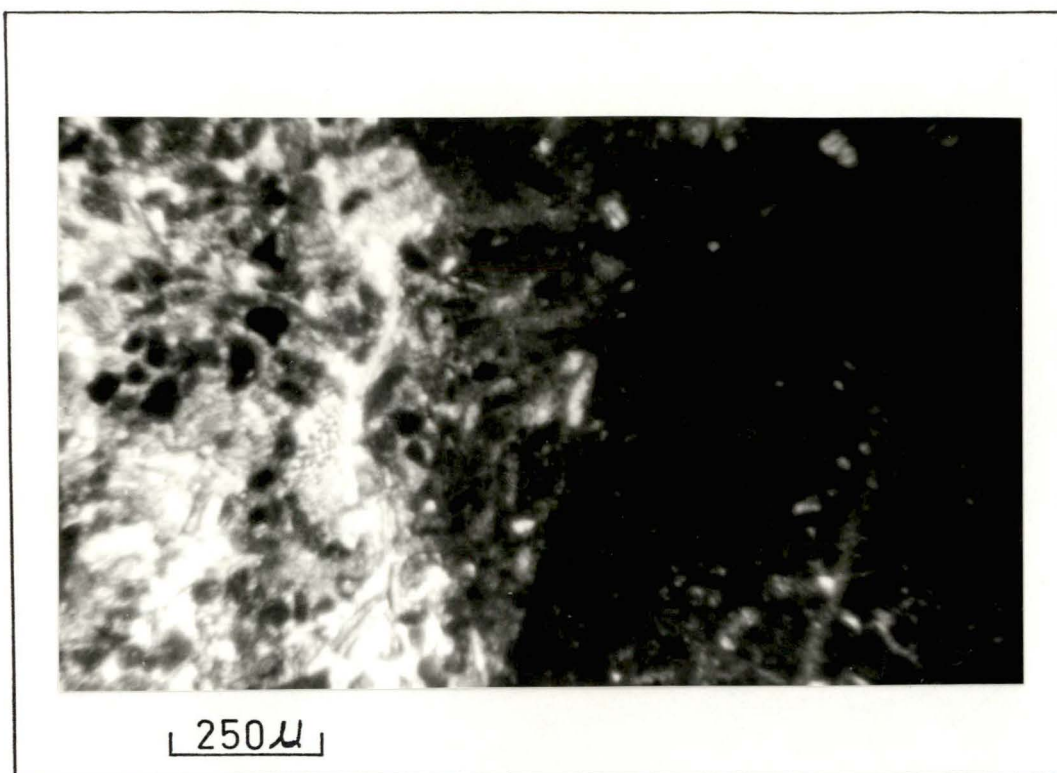


Fig. 3. 7. Micrite grading into sparite with fossils, pellets and intraclasts.

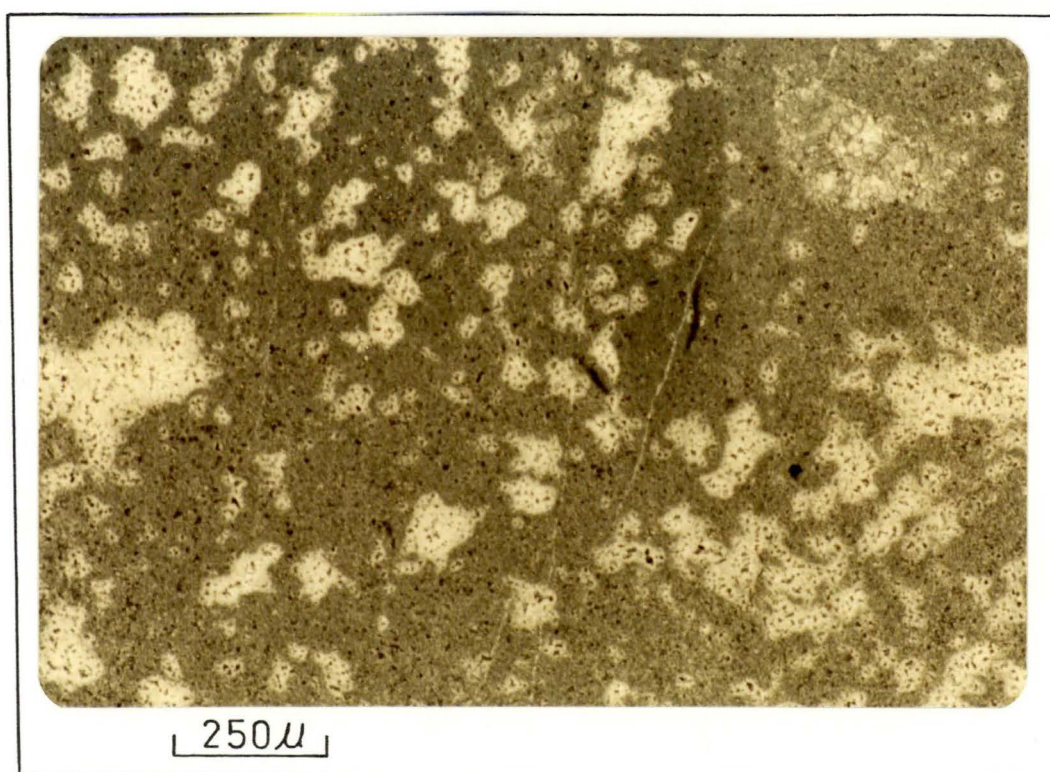


Fig. 3. 8. Dismicrite with abundant bulbous birdseyes.

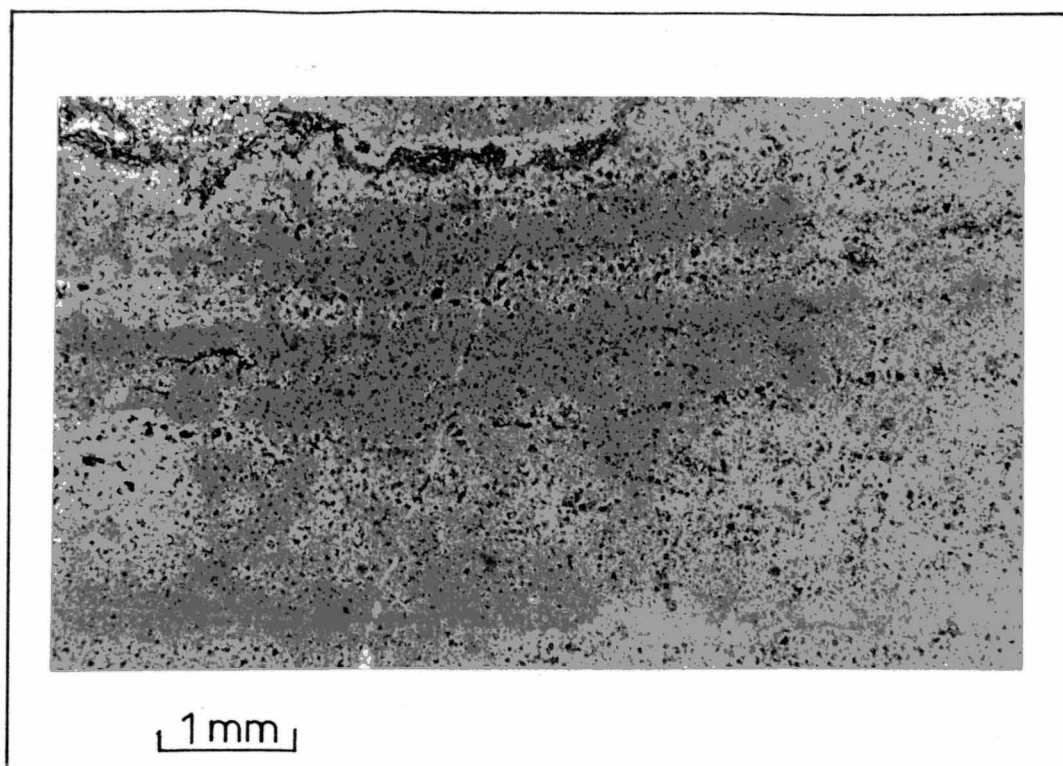


Fig. 3.9. Alternating dismicrite and micrite. At top is a stylolite.

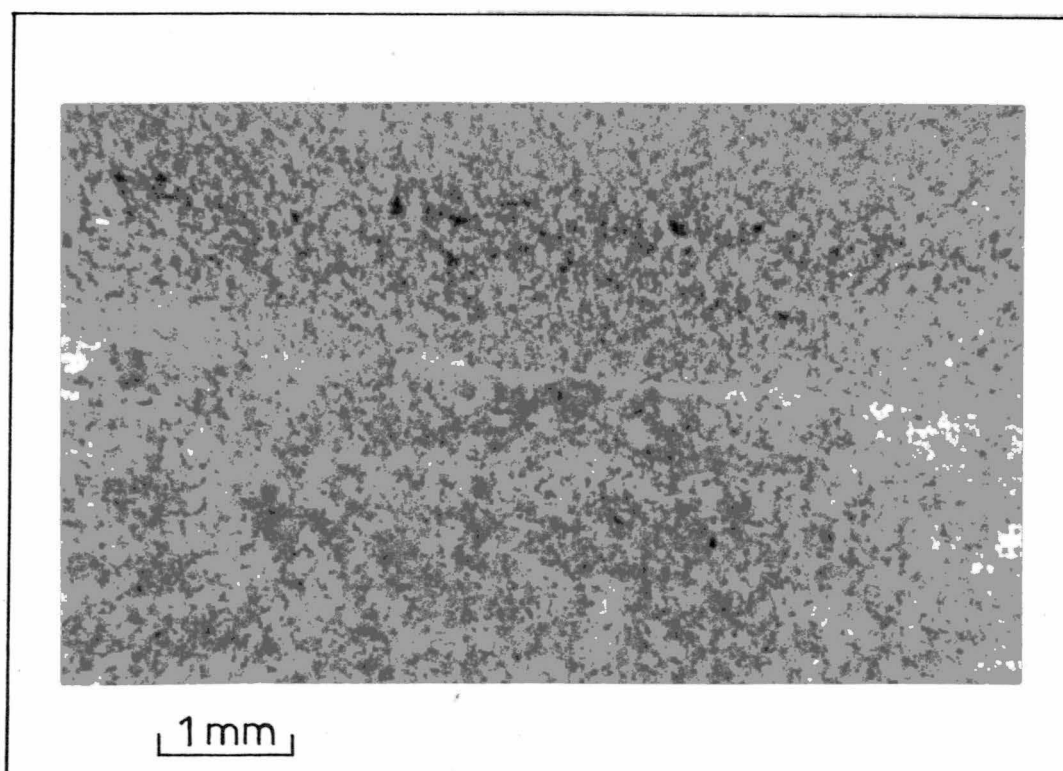


Fig. 3.10. Dismicrite overlain by dolomitized algal mat. The black material in dolomitic part is organic matter.

length. In some burrows, generation of spar has taken place, which resembles the fenestral fabrics of Tebutt *et al.* (1965).

These samples are interpreted to have formed in the subtidal and intertidal environments. In samples containing oolites, it is believed that they were probably transported from shoals existing off-shore.

6. Dismicrite or Disturbed Micrite

Folk (1962) defined "dismicrite" as a microcrystalline rock disturbed by burrowing organisms or by soft-sediment deformation, and containing less than 1% allochems. In this study, dismicrite is differentiated from "micrite" (described on p.28) by the presence of abundant birdseyes and from other allochem-bearing micrites by the absence of allochems (less than 1%).

The percentages of dismicrite samples in the studied sections are as follows: GPB = 23%, GPW = 5%, GPL = 3% and GPR = 7%. No dismicrite samples were observed in section GPD. The birdseyes commonly ranging up to 4 mm are of the bulbous type (see Figs. 3.8, 3.9 and 3.10) and occur randomly in a micrite matrix. Some birdseyes (as shown in Fig. 3.8) may partly have straight boundaries and rhombic or rectilinear outlines. According to Radke (1980) they suggest the former presence of evaporites. The dismicrites may alternate with micrite (Fig. 3.9) giving the appearance of being laminated. The laminae contain black organic matter and are believed to be algal laminations. Commonly the dismicrites are overlain by algal mats. Fig. 3.10 is a photomicrograph of one such sample showing birdseyes in micrite overlain by dolomite. The dolomite is faintly laminated and the presence of organic laminae indicates the former presence of algal mats, which have been dolomitized.

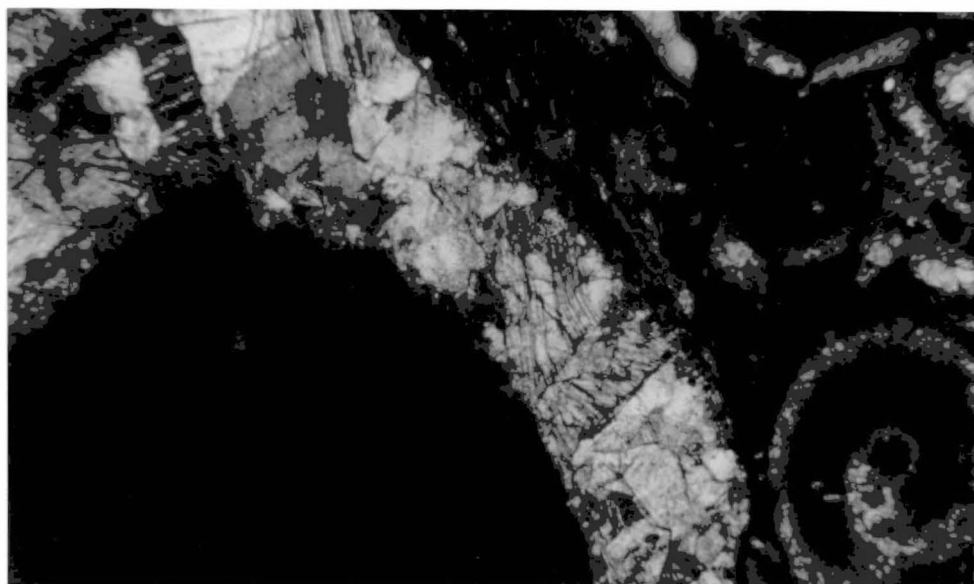
In addition to the abundant birdseyes, burrows of the random type are common in dismicrites, while vertical burrows are rare. Mudcracks may or may not be present.

According to Shinn (1968), escape of gases from sediments sub-aerially exposed and undergoing dessication results in open spherical voids, which may later fill with sparry calcite. Therefore birdseyes are considered to be significant indicators of subaerial exposure. Considering this observation together with the occurrence of mudcracks, upper intertidal to supratidal environments are believed to be the most likely depositional environments.

7. Biomicrite and Biosparite

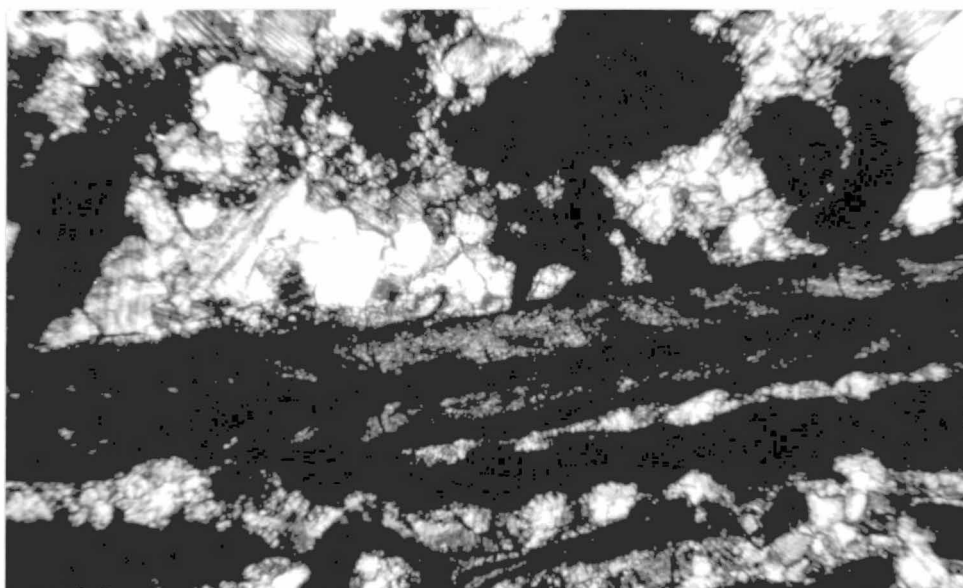
The carbonate rock types containing at least 10% fossils in a micrite matrix are defined as biomicrites. The fossils may be the only allochemical constituents or other allochems may also occur associated with them. Intraclasts, oolites and oncolites if present, must each be less than 20% (in this study, if they are above 20% they form carbonate rock types named after them (e.g. intramicrite). If both fossils and pellets are present, then following Folk (1959, p.62), the volume ratio of fossils to pellets must be greater than 3:1 in order to define that carbonate rock as a biomicrite. The grain to groundmass ratio in biomicrites is always greater than 1:9. In biosparites instead of micrite as the bonding agent, the allochems are bonded by a sparry calcite cement. The percentages of biomicrites/biosparites in the sections are GPB = 20%, GPW = 21%, GPL = 22%, GPD = 15% and GPR = 16%.

In section GPB, the biomicrites mostly contain intraclasts in addition to the fossils. The mean content of fossils is 15% and they range from 11 to 20%. Commonly the fossils have been broken into small unidentifiable fragments similar to those shown in Fig. 3.3. In samples containing recognizable forms, the most common are gastropods, although brachiopods, bryozoans and crinoids also occur. The intraclasts (ranging from 2 to 7%) are all composed of micrite and vary in shape



250 μ

Fig. 3.11. Gastropod biomicrite. The gastropods are recrystallized and filled with micrite (dark).



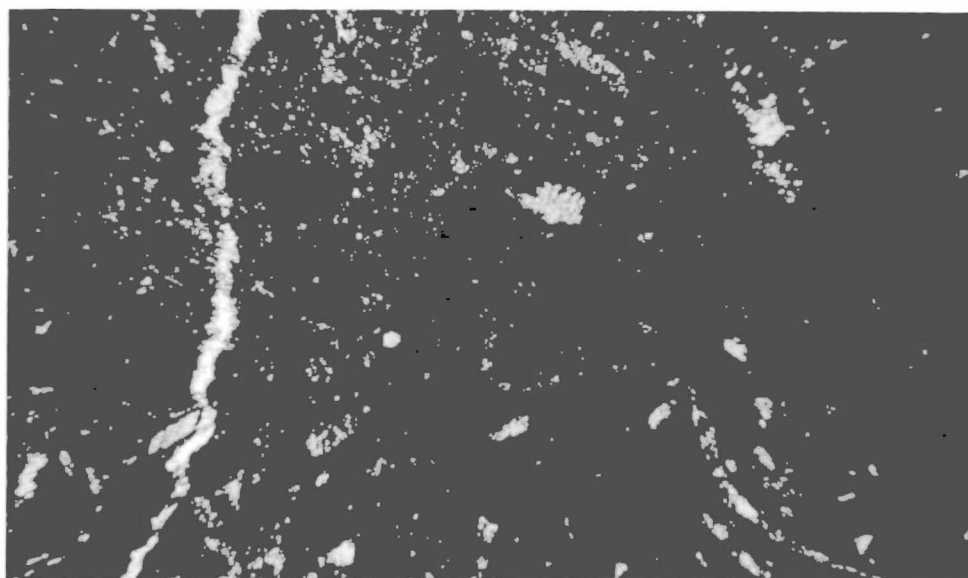
250 μ

Fig. 3.12. Biosparite. The moulds of gastropods are filled with micrite and the large bryozoan fragment is in a flat-lying position.

mostly from angular to subangular. Birdseyes are not always present, but nearly all show mudcracks. When present, vertical to random burrows are common.

The biomicrites in section GPW contain fossils from 11 to 56%, with a mean fossil content of 23%. About 42% of the total samples also contain 1 to 8% rounded to subrounded intraclasts composed of micrite or biomicrite. The fossils in biomicrites, which occur up to nearly 32 metres above the base of the section, are mostly brachiopods, bryozoans and gastropods. A few samples contain one fossil type only. The brachiopods may be randomly scattered or show orientation with their convex side up. The gastropods are quite abundant between 15 and 17 metres above the base. Fig. 3.11 is a photomicrograph of a gastropod biomicrite. The gastropods are of variable size and most of them show effects of recrystallization. The chambers in them are commonly filled with micrite. Although not shown in Fig. 3.11, a few show reverse grading with larger gastropods at the top. Towards the top of the section (above about 32 m), besides the above-mentioned fossils, the biomicrites contain calcareous algae, colonial corals, pelmatozoans, stromatoporoids and nautiloids. In some samples the fossils may be bounded by spar also, but generally micrite predominates over spar. Fig. 3.14 is a photomicrograph of a biosparite containing calcareous algae in addition to other unidentifiable forms. The fossils marked by the arrow is also a calcareous algae (transverse section). Only a few biomicrite/biosparite samples contain mudcracks and birdseyes ranging from rare to common. Vertical and random burrows ranging from rare to abundant are present in about half the total samples.

In section GPL, 41% of the biomicrite samples contain fossils as the only allochems, while the other samples also contain pellets or



250 μ

Fig. 3.13. Biomicrite with abundant pelmatozoan fragments. Note the micrite envelopes which are probably due to algal boring.



250 μ

Fig. 3.14. Biosparite with calcareous algae. Note dolomite crystals above erosional contact.

intraclasts or both. The mean content of fossils is 21% and they range up to 39%. The fossils vary in size from 0.01 mm to about 30 mm, but commonly they are in the form of small broken fragments and difficult to identify. Also, they are mostly recrystallized and lack any orientation. Recognizable forms include brachiopods, bryozoans, corals, crinoids, gastropods, pelecypods, and rarely ostracods and trilobite fragments. Fig. 3.12 shows moulds of gastropods filled with micrite and a large bryozoan in a flat-lying position. The pellets (ranging up to 10%, mean 4%) occur in 38% of the samples and are often difficult to distinguish from the micrite matrix. They commonly have a mean size of about 0.06 mm and are spherical in shape. More than half the samples containing pellets also contain intraclasts, and intraclasts also occur in samples lacking pellets. They range between 1 to 9% with a mean of about 4%. As in section GPW, they are composed of micrite or biomicrite and are commonly rounded to subrounded in shape. Birdseyes are present in 35% of the samples, while 46% show mudcracks. Vertical and random burrows are present in most of the samples.

The biomicrites in sections GPD and GPR do not contain any other allochems except fossils. The fossil content ranges up to 35% in section GPD, while in section GPR, in some cases a whole peel consists of a stromatoporoid. Other samples mostly contain bryozoans, pelmatozoans and trilobite fragments and rarely gastropods. Fig. 3.13 shows numerous pelmatozoan fragments with micrite envelopes. In the bottom right part of the photomicrograph are unidentified shell pieces, which occur only rarely. In addition, brachiopods, corals and pelecypods may occur. Birdseye structures and mudcracks are absent. Vertical and random burrows are present in most of the samples.

This microfacies is believed to have been deposited in a wide spectrum of environments. Most of the fossils recognized in the studied

sections (i.e. brachiopods, bryozoans, corals, echinoderms, trilobites etc.) are considered by Heckel (1972) to have lived in marine environments. The dominance of fragmented fossils, except bryozoans which although not broken are in a flat-lying position (see Fig. 3.12) and the occurrence of intraclasts in most of the samples suggests a shallow-water regime as the bottom would have to be shallow enough to be periodically affected by turbulence in order to cause intraclast formation. However, a preponderance of micrite over spar indicates that overall quiet conditions prevailed in the environment. Presence of bioturbation features in most of the samples suggests that besides wave action, biological activity may also have been responsible for the variety of sizes of the fossil grains. Samples with diverse fossil groups based on the presence or absence of birdseyes and mudcracks have been interpreted to have formed in the subtidal to intertidal environments. Brachiopod shells oriented with their convex side up are believed to be channel deposits. Samples containing gastropods only are envisaged as having been deposited in the intertidal to supratidal environment.

8. Pelmicrite and Pelsparite

The carbonate rock types containing at least 10% pellets in a micrite matrix are defined as pelmicrites, and if the pellets are bonded by spar they are defined as pelsparites. Pellets may be the only allochemical constituents or other allochems may also occur associated with them. If fossils are present, they must be less than 10% and following Folk (1962), the volume ratio of fossils to pellets must be less than 1:3. In this study, intraclasts, oolites and oncolites (if present) must each be less than 20%. The grain to groundmass ratio in pelmicrites and pelsparites is always greater than 1:9.

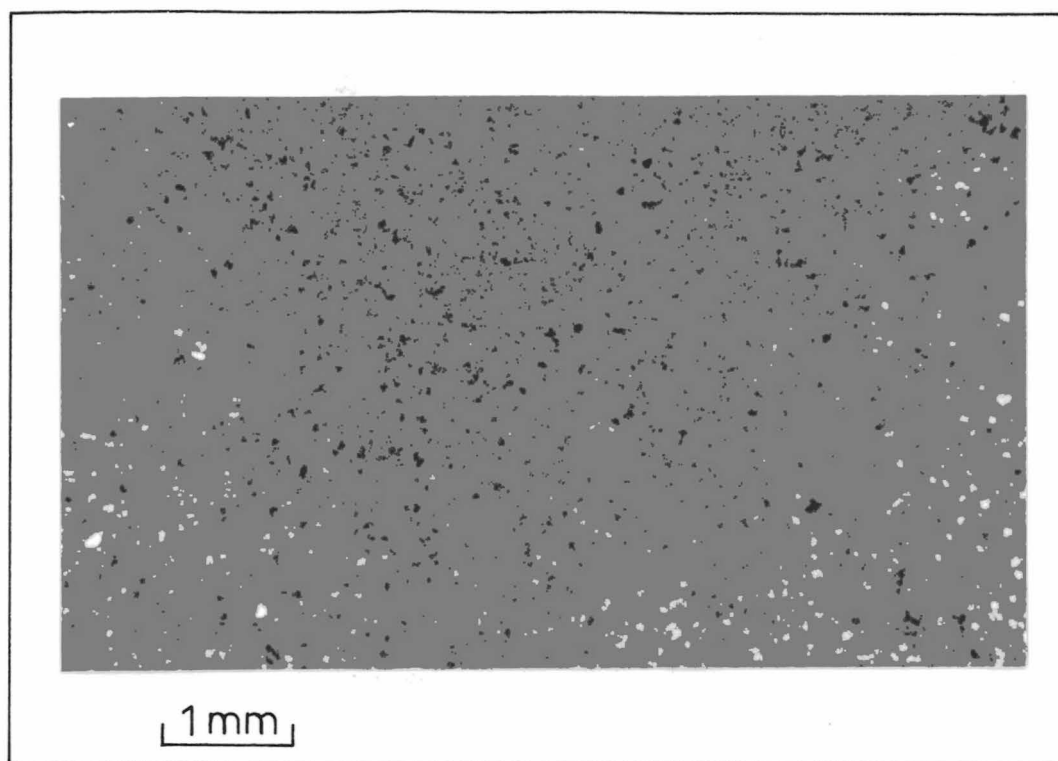


Fig. 3.15. Pelmicrite, faintly laminated and containing silt size quartz.

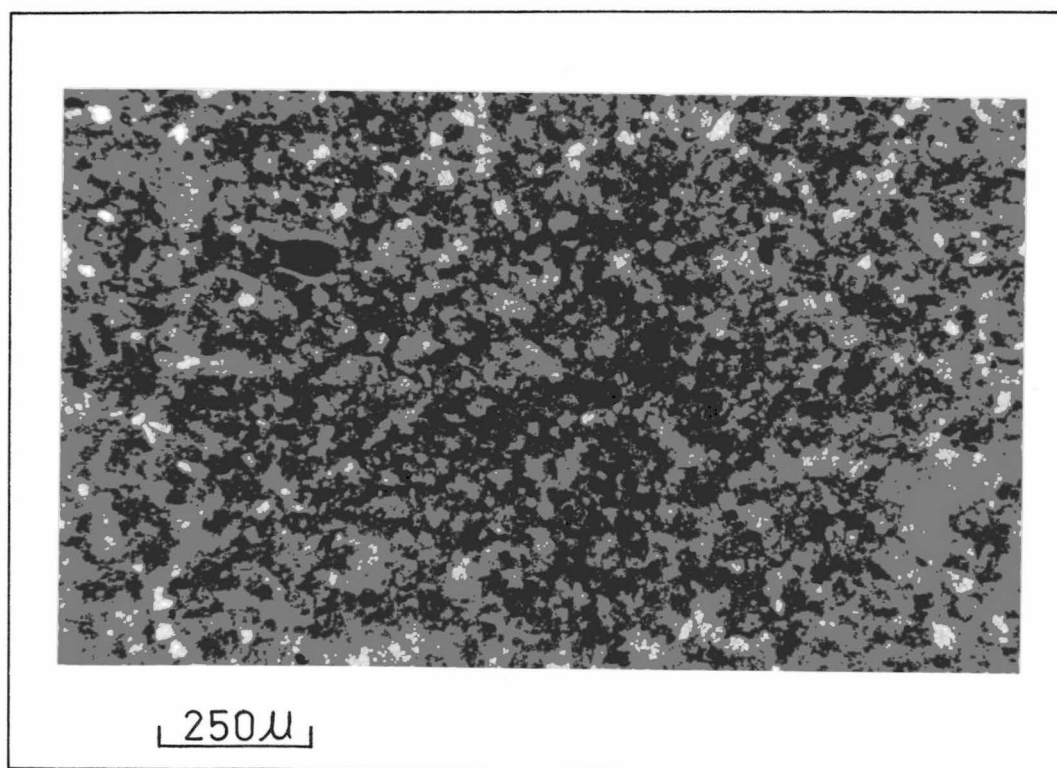


Fig. 3.16. Dolomitic pelmicrite with abundant quartz.

No pelmicrites/pelsparites were observed in section GPB and only one sample (49117) is a pelmicrite in section GPW. In the other sections their distribution is as follows: GPL = 2%, GPD = 21% and GPR = 24%.

The pellets are elliptical or ovoid in shape and commonly difficult to distinguish from the micrite matrix. In some samples they may not be clearly visible due to the presence of abundant quartz grains, some effects of recrystallization and occurrence of dolomite as in Fig. 3.16. Pellets bounded by spar have hazy boundaries and in some cases, gradations from pelmicrites to pelsparites were observed in a single sample. Certain samples as in Fig. 3.15 give the appearance of being laminated, which is more pronounced in areas where there is a greater concentration of silt size quartz.

Fossils and intraclasts may be present in addition to the pellets. The fossils are mostly small broken fragments, while the intraclasts composed of micrite vary in shape from subangular to rounded, the common shape being subrounded to rounded. One sample (49303) besides containing pellets and fossils, also has 17% oolites commonly with a recrystallized nucleus and core lining of fibrous calcite. Birdseyes ranging from rare to common are present in section GPL and about 20% of the samples from section GPR. Mudcracks are present in nearly 60% of the samples from section GPR. Rare to abundant, vertical or random burrows are present in most of the samples.

Folk (1962) regarded the pellets to be faecal in origin and now it is commonly believed that they are polygenetic in origin (e.g. Beales, 1965). In the study area it is difficult to assign a particular origin to the pellets. Some may be faecal, while others may have been formed by disintegration of lime mud and accumulated into piles. The breakup of lime mud may have been due to the activity of burrowing

organisms or due to the presence of weak currents or wave action. This probably was the case in samples containing skeletal grains concentrated together and is further borne out by the frequent association of sub-rounded to rounded intraclasts. In tidal flat deposits of Shark Bay, Woods and Brown (1975) have observed the frequent association of pellets and intraclasts in the intertidal zone and of pellets and fossil fragments in the sublittoral zone. They have also commented on the occurrence of fenestral fabrics in such sediments of the upper intertidal zone. Thus, following Woods and Brown (1965) this microfacies was probably deposited in subtidal to intertidal environments. The pelsparites could have been formed in the intertidal channels, where the moderate tidal currents wash them clean of lime mud.

9. Biopelmicrite and Pelbiomicrite

The carbonate rock types considered here contain both fossils and pellets in a micrite matrix. If fossils are greater than 10% and the volume ratio of fossils to pellets is less than 3:1, the carbonate rock containing them is defined as a biopelmicrite. In cases where pellets are the dominant allochems (greater than 10%) and the volume ratio of pellets to fossils is less than 3:1, the rock type is a pelbiomicrite. Other allochems (constituting less than 20% of the rock) may be present.

In the study area, the biopelmicrites and pelbiomicrites occur in sections GPL and GPR only, where they form 3% and 4% of the samples respectively.

The biopelmicrites in section GPL contain fossils ranging up to 12%, while the pellets form 4 to 8% of the allochemical content. In pelbiomicrites, the maximum contents of pellets and fossils are 32% and 10% respectively. The pellets in both carbonate rock types resemble the micrite matrix, while fossil types present include bryozoans, brachiopods

and gastropods. No birdseyes or mudcracks were observed. Commonly the burrows are of the random type and range from rare to abundant.

In section GPR, the maximum content of pellets in biopelmicrites is 6% and in pelbiomicrites is 22%. The maximum content of fossils in biopelmicrite is 18% and in pelbiomicrite is 9%. The fossils are mostly very small unrecognizable broken fragments scattered randomly. Pellets too are not closely packed. As in section GPL, no birdseyes and mudcracks are present, while random burrows ranging from rare to common are present in all the samples.

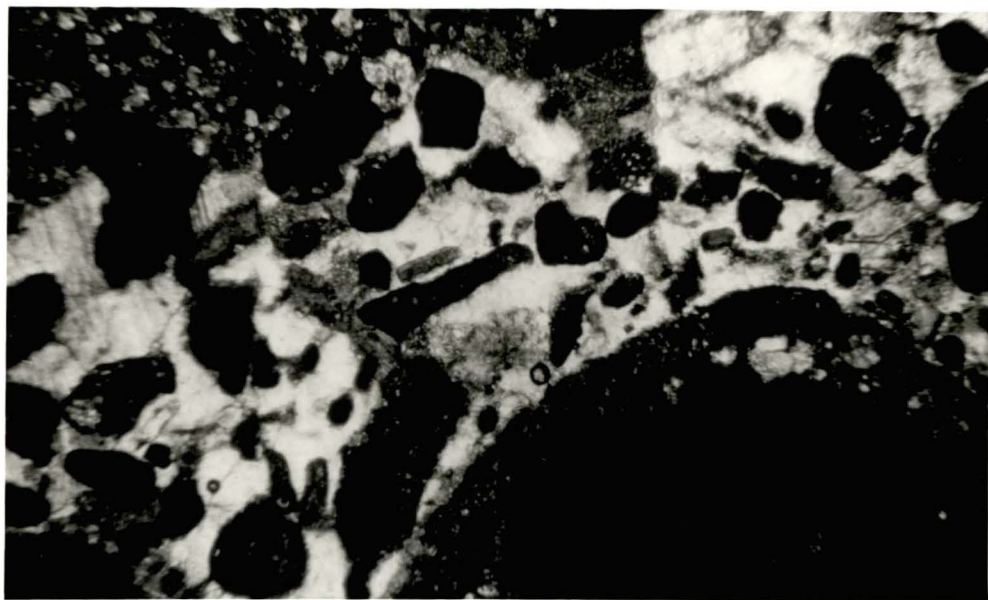
This microfacies is interpreted to have formed in the subtidal to lower intertidal environment.

10. Intramicrite and Intrasparite

In this study, the carbonate rock types containing at least 20% intraclasts in a micrite matrix are defined as intramicrites, while those bounded by spar are called intrasparites. Other allochems may occur associated with them. Oolites and oncolites, if present, must each be less than 20%, and the fossils and pellets each less than 10%. The grain to groundmass ratio is always greater than 2:8.

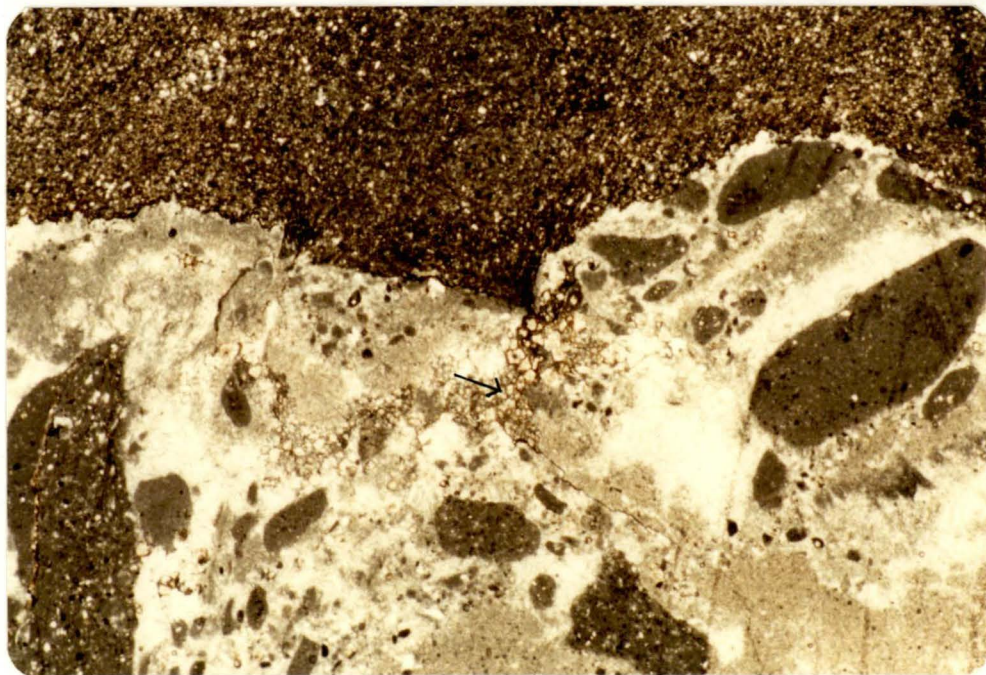
The intramicrites/intrasparites occur only in sections GPB, GPW and GPL, where they constitute 8%, 5% and 1% of the samples respectively.

The intraclasts are composed of micrite, although a few may contain some dolomite also. Fig. 3.18 shows intraclasts composed of micrite, but also containing dolomite. Note the intraclast at the top partly invaded by dolomite. Also spar has not completely obliterated the micrite although a few dolomite crystals (shown by arrow) have been replaced by spar. The shape of the intraclasts varies from angular to rounded and in some cases intraclasts of variable shape may characterize a single sample. Fig. 3.17 is a photomicrograph of an intraclast breccia grading upwards into dolomite. The presence of some rounded intraclasts with mostly



250 μ

Fig.3.17. Intrasparite grading upwards into dolomite.
Note the presence of both angular and rounded
intraclasts.



1 mm

Fig.3.18. Erosional contact between intrasparite and
dolomicrite(?algal). Some dolomite crystals have been
replaced by spar (shown by arrow).

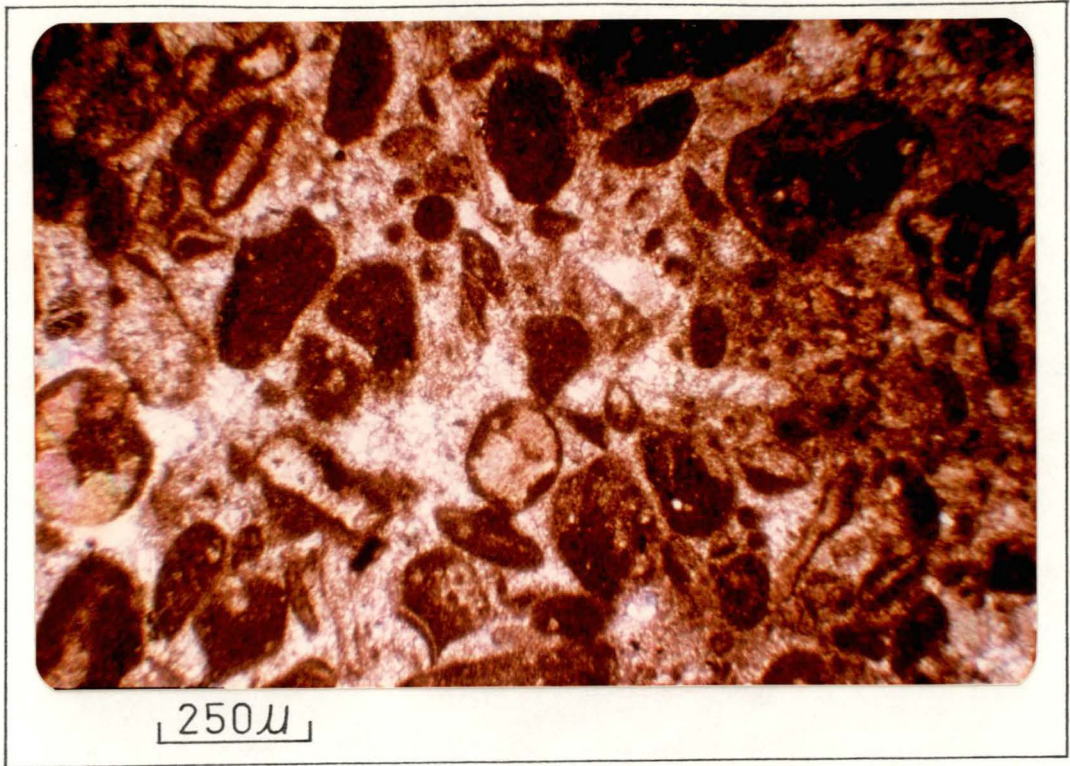


Fig.3.19.Oolitic Intrabiosparite with some intraclasts containing skeletal material.

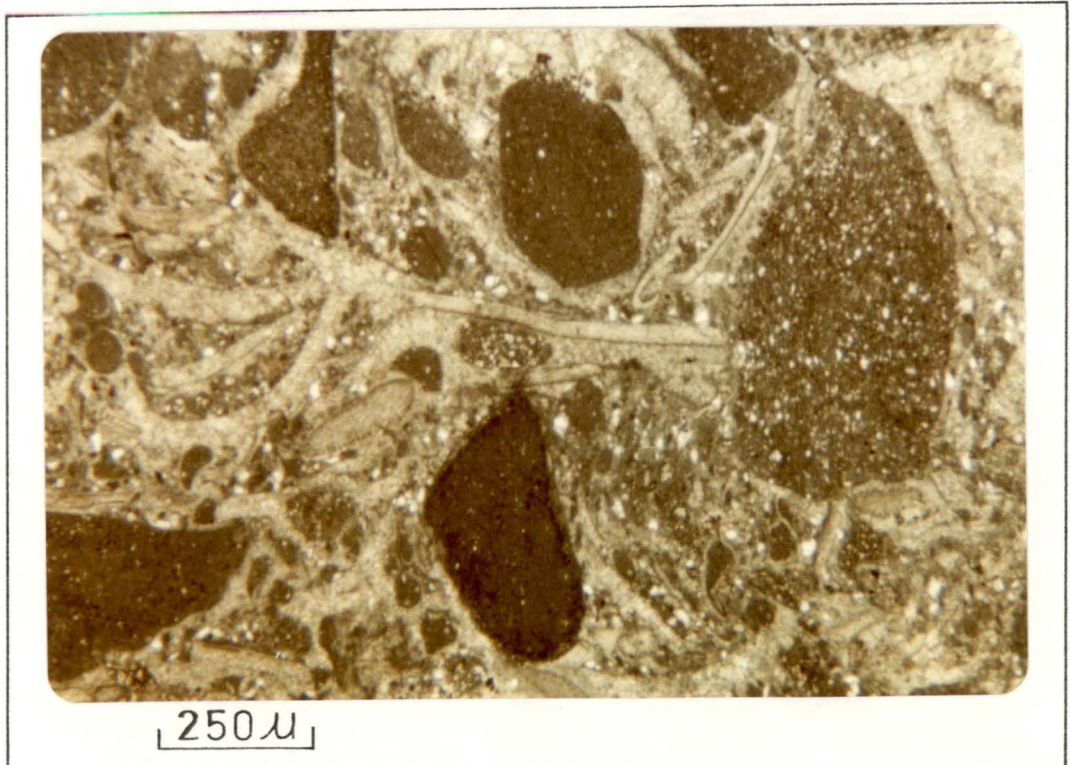


Fig.3.20. Intrabiosparite.The intraclasts are composed of micrite,dolomite and scattered quartz grains.

angular intraclasts suggests probable reworking of the breccia. Except for fossils in certain samples, no other allochems occur associated with the intraclasts. Birdseyes are rare. Intralaminar mudcracks, vertical and random burrows ranging from rare to common are mostly present.

The depositional environment of this microfacies is discussed below with other microfacies containing intraclasts as the major allochems.

11. Intrabiomicrite and Intrabiosparite

The carbonate rock type containing at least 20% intraclasts and 10% fossils is defined as an intrabiomicrite. If pellets are also present, the volume ratio of fossils to pellets must be greater than 3:1. The other allochems (oolites and oncolites), if present must each be less than 20%. The grain to groundmass ratio is greater than 3:7.

In the study area, both intrabiomicrites and intrabiosparites occur in sections GPB, GPL and GPD, where 10%, 3% and 10% of the samples respectively belong to this microfacies.

The intraclasts comprising up to 42% of the sample and of variable shape, are dominantly composed of micrite, except a few which may contain skeletal material (Fig. 3.19) or dolomite (Fig. 3.20). The fossils ranging up to 24%, in section GPB and GPL, are mostly broken unidentifiable forms, whereas in section GPD, pelmatozoans and trilobite fragments occur in addition to the unidentifiable forms (as in Fig. 3.20). Pellets ranging between 4 to 6% and bounded by spar may be present. Fig. 3.19 also shows the presence of some recrystallized well-rounded grains, which are considered to be oolites (following their description on p. 22). The spar content decreases laterally towards the right of the photomicrograph. Overall, in such samples, micrite is predominant and therefore they have been referred to as intrabiomicrites, unlike Fig. 3.19 which is an intrabiosparite. Rare to common birdseyes were observed only in section GPB. Mudcracks occur in section GPB and in some

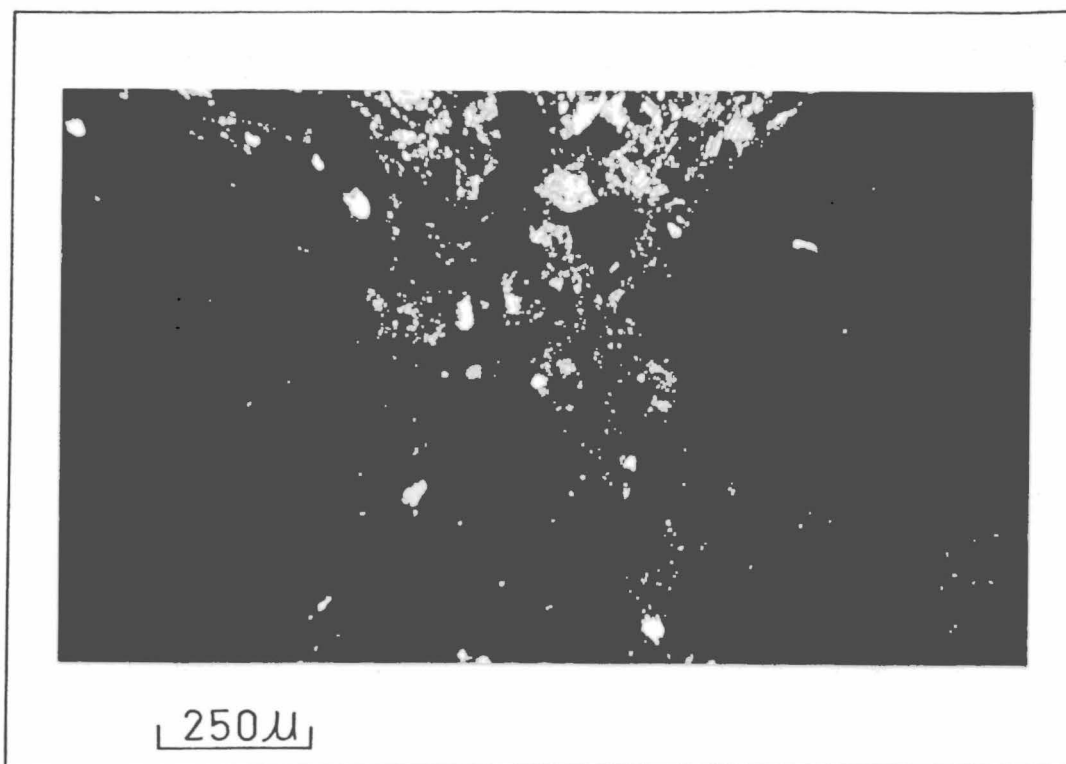


Fig.3.21.Intrapelsparite. The intracrysts are composed of micrite,few dolomite rhombs and scattered quartz.

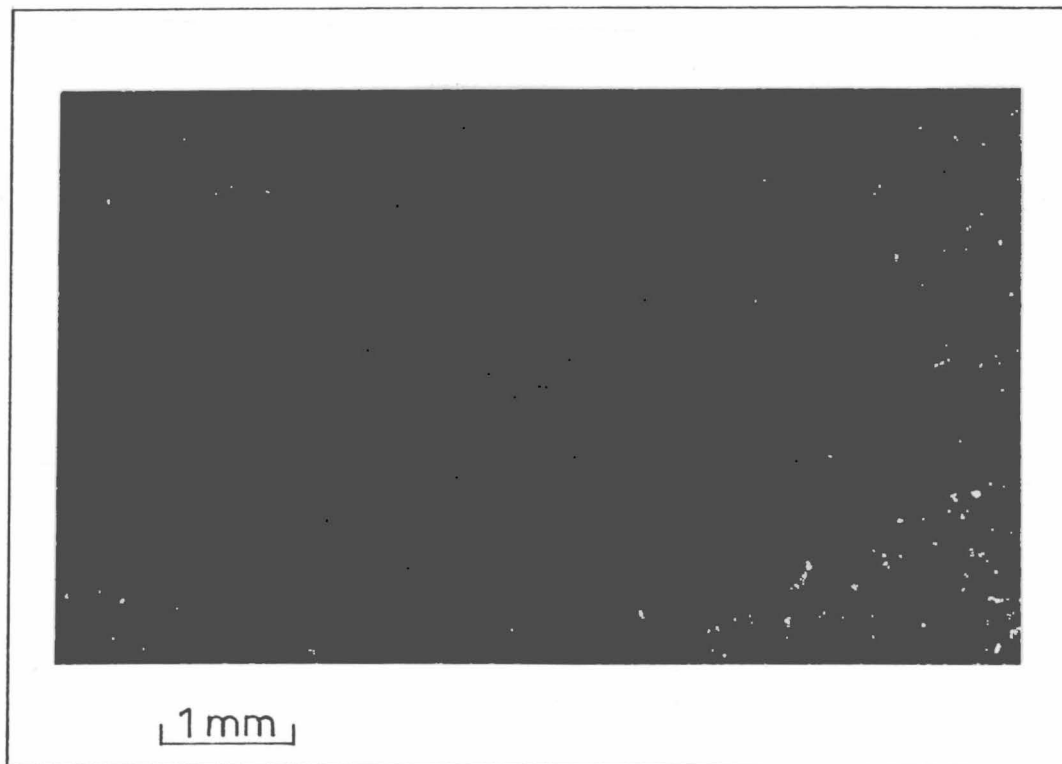


Fig.3.22.Intrapelsparite.Note the wide variation in grain size of intracrysts.

samples from GPD. Rare, vertical burrows are found in section GPB, while random burrows (rare to common) may occur in other sections.

The environment of deposition is discussed below with other major intraclast-bearing microfacies.

12. Intrapelsparites

The carbonate rock types containing at least 20% intraclasts and 10% pellets in a spar matrix are defined as intrapelsparites. If fossils are also present, the volume ratio of pellets to fossils must be greater than 3:1. The other allochems, if present, must each be less than 20%. The grain to groundmass ratio is greater than 3:7.

The intrapelsparites occur only in section GPR, where they constitute 7% of the samples. No intrapelmicrite is present. The intraclasts (range 20 to 30%, mean 25%) are bounded by spar (see Figs. 3.21, 3.22 and 3.23) and include the flat-pebble conglomerate (Figs. 3.22 and 3.23). They are predominantly composed of micrite, but a few (as in Fig. 3.21) may also contain dolomite and scattered quartz grains. Another feature observable in the photomicrograph (Fig. 3.21) is the transformation of micrite into spar along the intraclast boundaries. The intraclasts are commonly rounded and may have an erosional contact with the underlying rocks. This can be seen in Fig. 3.23, where an upward decrease in grain size is also noticeable. Figs. 3.22 and 3.23 are the only samples where a greater concentration of spar on the bottom side of intraclasts (gravitational cement) is observed and is believed to reflect vadose diagenesis. Also the pellets as seen in the figures are not of faecal origin, but seem to have been derived from the same material as the intraclasts.

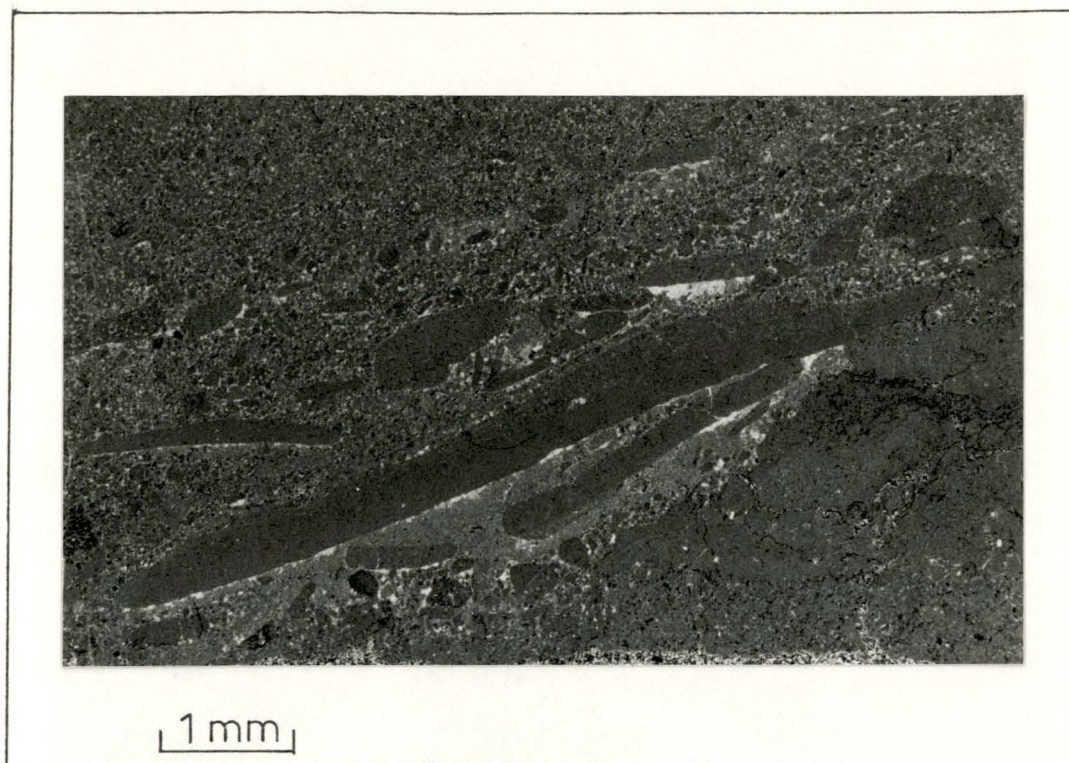


Fig.3.23. Intrapelsparite ----flat pebble conglomerate. Note upward decrease in grain size and erosional contact.

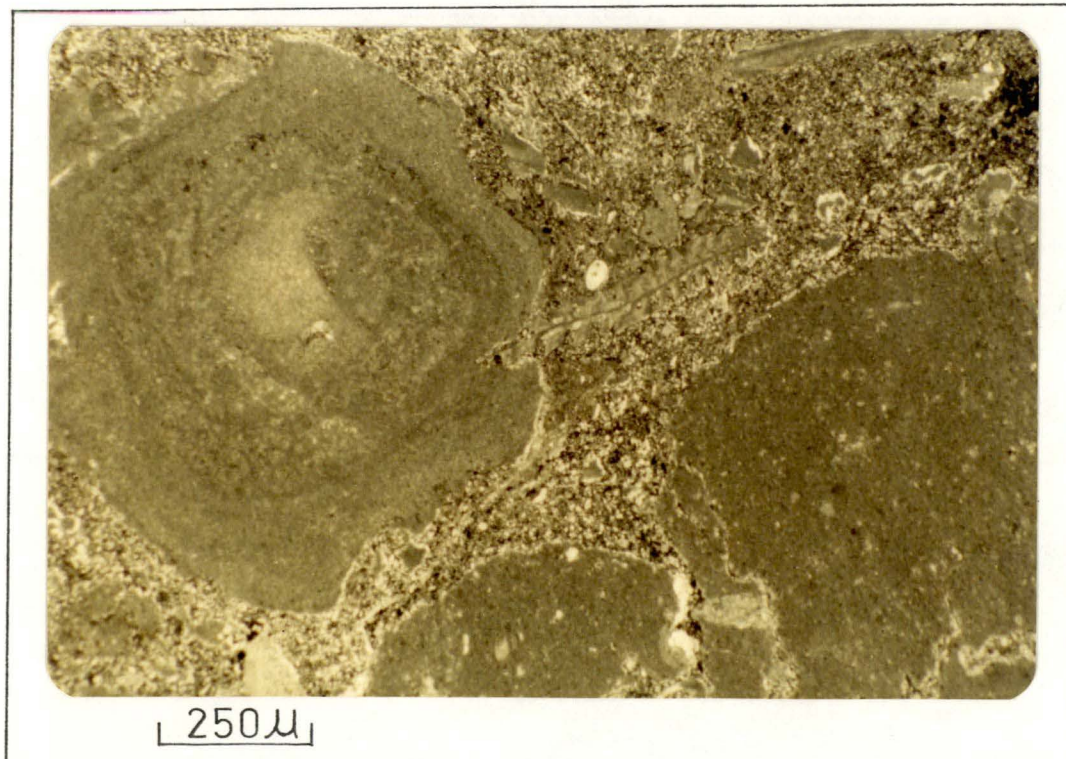


Fig.3.24. Dolomitic intraoncomicrite. Note skeletal fragment in core and irregular outline of oncolite. The bryozoan fragment partly overlies oncolite.

13. Intraoncomicrite

The carbonate rock types containing at least 20% intraclasts and 20% oncolites in a micrite matrix are defined as intraoncomicrites. Other allochems in subordinate amounts may occur.

The rock type occurs only in section GPL. Samples closely spaced (in the vertical sense) at about 21 metres above the base consisted of oncolites, intraclasts and a few skeletal fragments. Overall micrite predominates over spar, the latter only bounding a few intraclasts. The mean oncolite content is 25% and all have a irregular outline. Fig. 3.24 is a photomicrograph of an intraoncomicrite. The oncolite has a recrystallized fossil fragment in the centre and an abraded irregular outline. A bryozoan can be seen partly overlying the oncolite and both oncolite and the bryozoan are mostly surrounded by fine grained dolomite. The intraclasts are composed of micrite and are subangular to rounded in shape. No other structures were observed in these samples.

Microfacies containing intraclasts as the major allochems and described above are believed to have formed in a range of environments. It has already been mentioned while discussing the intraclast occurrences in other microfacies that the differences in roundness of the intraclasts is believed to reflect their abrasional history. The angular to subangular micritic intraclasts are interpreted to have formed in an environment where only periodic storms occurred. The association of mudcracks with these intraclasts plus occasional birdseyes indicates a supratidal environment. Samples with subangular to subrounded or rounded intraclasts with bioturbation features with or without mudcracks are considered as having formed in the intertidal environment. A similar environment is envisaged for the intrabiomicrite and intrapelsparite samples. The intraoncomicrites are believed to have formed in the shallow

subtidal to lower intertidal environments following Logan *et al.* (1964) and Buchanan *et al.* (1972). The conditions were agitating and the water movement probably more oscillatory than unidirectional.

Distribution of Microfacies and Depositional Environments

The distribution of the microfacies in the measured sections is shown in Table 3.2. These microfacies are predominantly micritic in composition. A predominance of micrite in Ordovician carbonates has been observed by many authors (e.g. Folk, 1973, p.128). However, Palaeozoic rocks usually contain abundant pellets (e.g. Beales, 1958, 1965) which, as seen in Table 3.2, are of rare occurrence in the studied sections. Either biological activity and abrasion (which have also commonly resulted in the reduction of the skeletal fragments to the smallest recognizable size) or diagenetic alteration may have made the pellets indistinguishable from the micrite matrix. Thus they may have been more abundant than now recognized.

The vertical distribution of the microfacies (lithologic succession), constituent allochems and structures together with the interpreted depositional environments in the measured sections are shown as Figs. 3.25, 3.26, 3.27, 3.28 and 3.29. Some of the beds are too thin to be represented individually and therefore are not shown in the figures. The allochems and structures observed in the figures have been discussed earlier. All these features indicate a shallow water regime for the Gunns Plains Limestone. Perusal of the literature (e.g. Laporte, 1969; Lucia, 1972; Ginsburg, 1975; Reineck and Singh, 1975; Multer, 1977) shows that a tidal-flat environment best fits the observed microfacies.

The vertical variation of the interpreted environments in the figures shows that carbonate sedimentation was cyclic. These cycles represent numerous alternations from subtidal conditions in the lower part of each cycle to intertidal and supratidal in the upper part.

Table 3.2

DISTRIBUTION (%) OF THE MICROFACIES IN THE STUDIED SECTIONS

Microfacies	Sections					Total Samples
	GPR	GPD	GPB	GPW	GPL	
Fossiliferous micrite	13	35	15	21	31	112
Intraclast-bearing fossiliferous micrite	11	14	8	21	25	88
Intraclast-bearing micrite	4	-	8	13	2	24
Micrite	4	-	-	-	-	3
Dismicrite	7	-	23	5	3	27
Biomicrite/biosparite	16	15	20	21	22	90
Biopelmicrite	3	-	-	-	1	4
Intramicroite	-	-	8	5	1	11
Intrabiomicrite/intrapelmicrite and intrapelsparite/intrabiopelmicrite	7	10	10	-	3	22
Intraoncosparite	-	-	-	-	2	4
Pelmicrite and/or pelsparite	24	21	-	1	2	34
Pelbiomicrite	4	-	-	1	2	8
Dolostone	6	5	8	10	-	21
Others	1	-	-	2	6	13
Number of samples	80	48	46	102	185	461

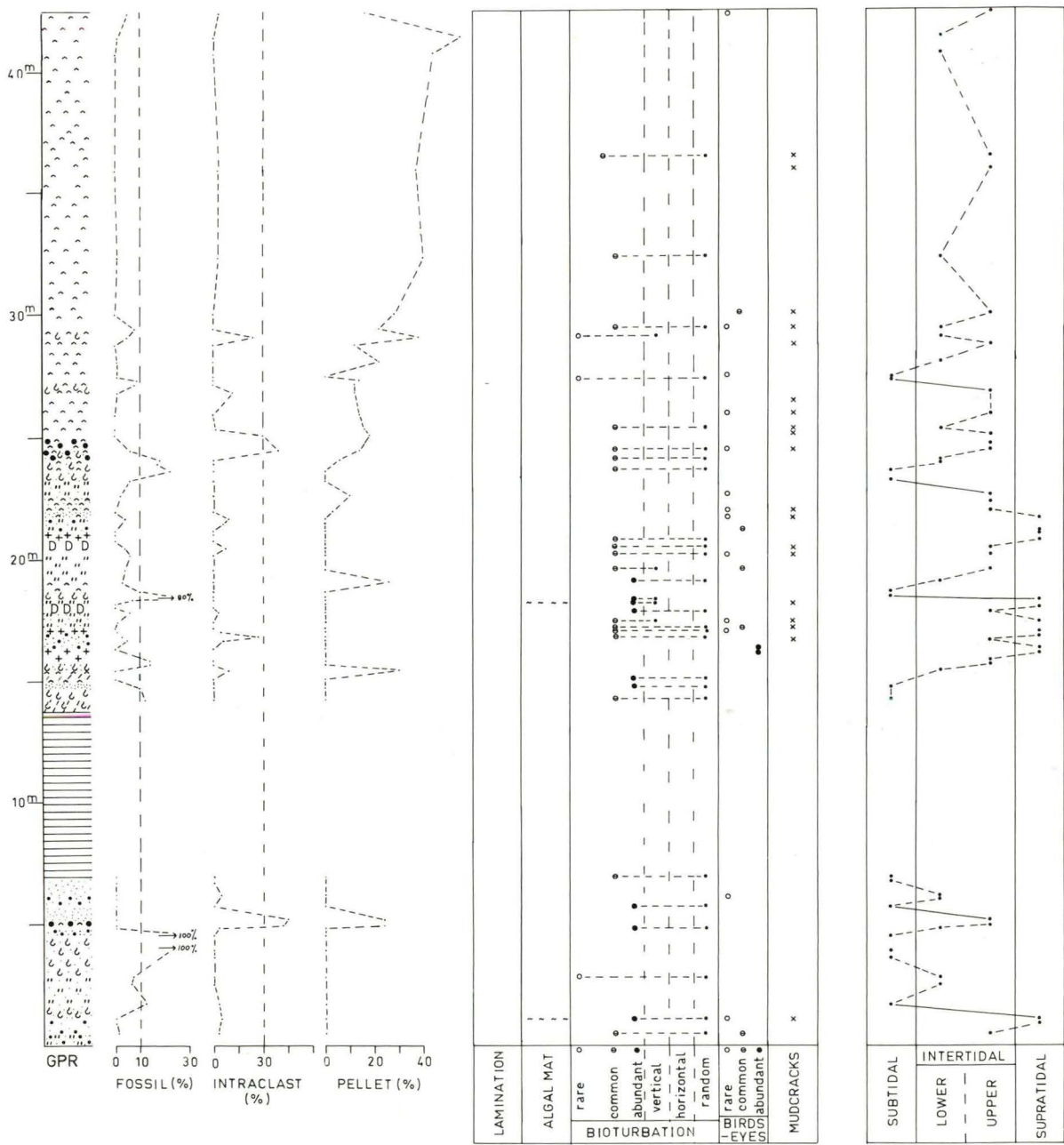


Fig. 3.25 Vertical distribution of the microfacies, constituent allochems, structures and depositional environments in section GPR. For symbols see p.72

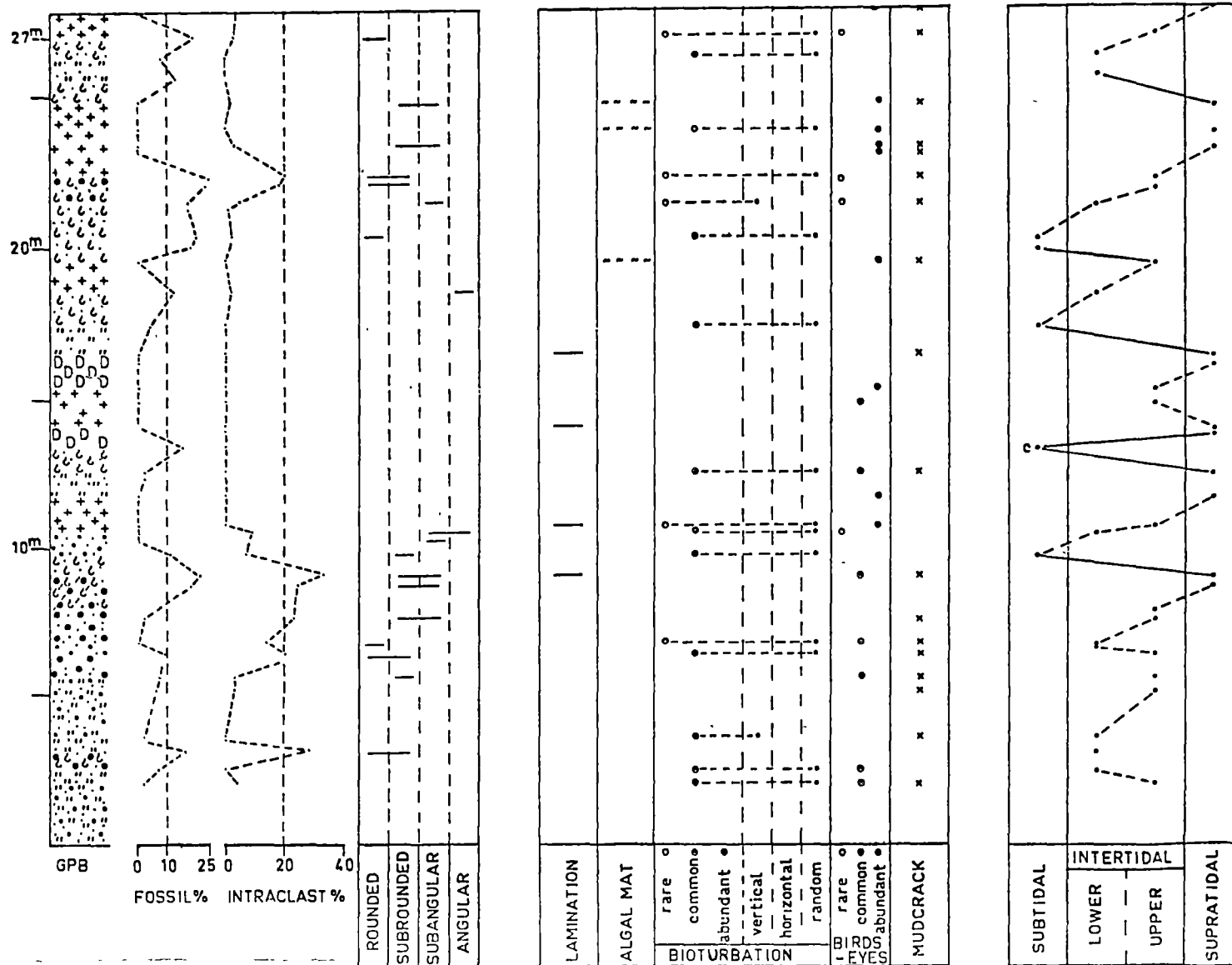


Fig. 3.27. Vertical distribution of the microfacies, constituent allochems structures and depositional environments in section GPB. For symbols see p.72.

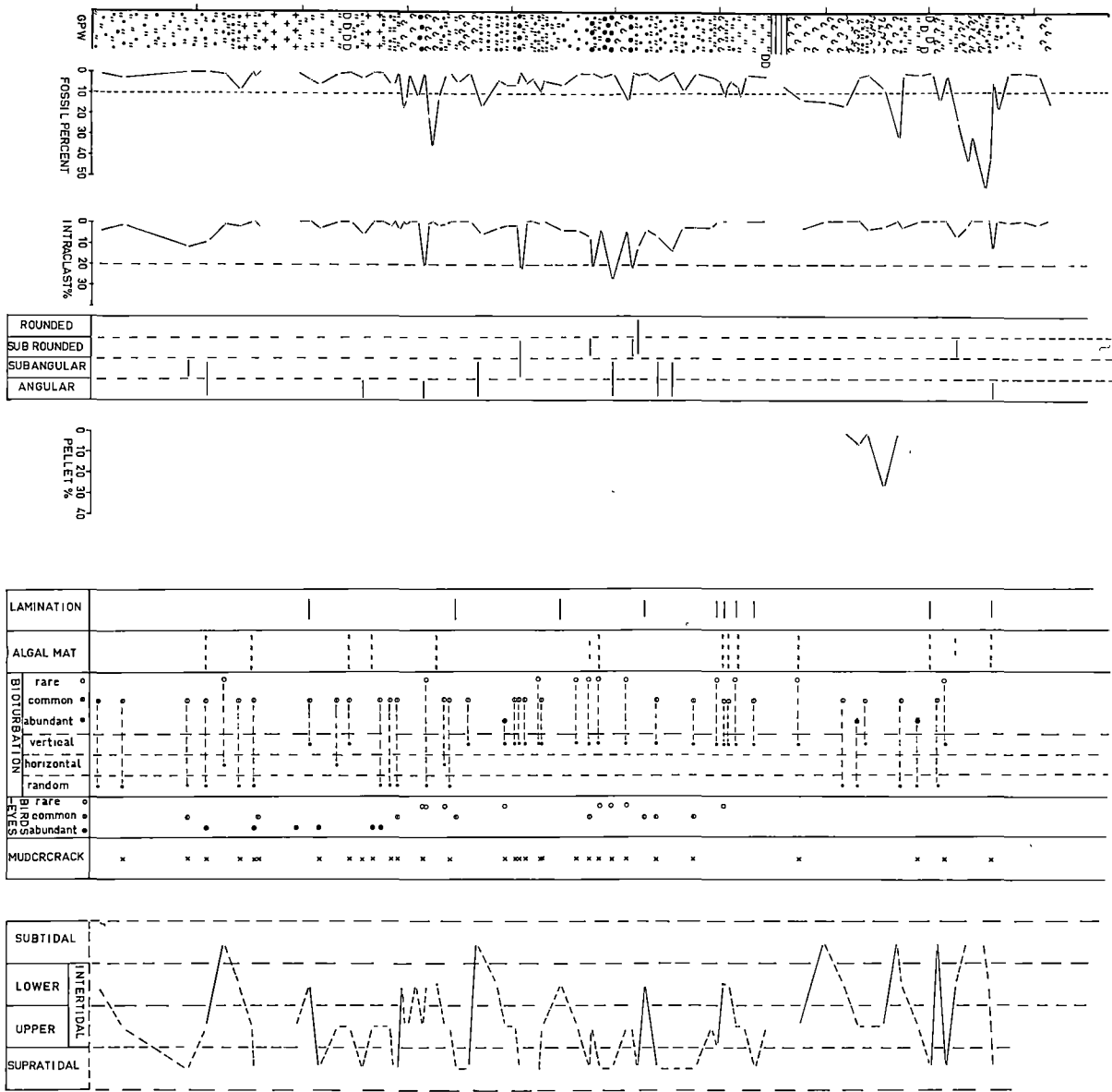
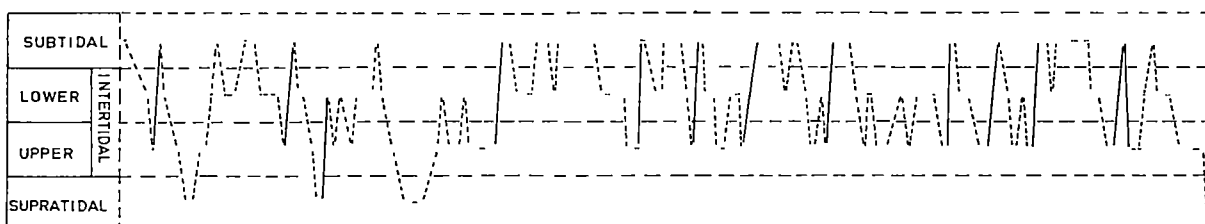
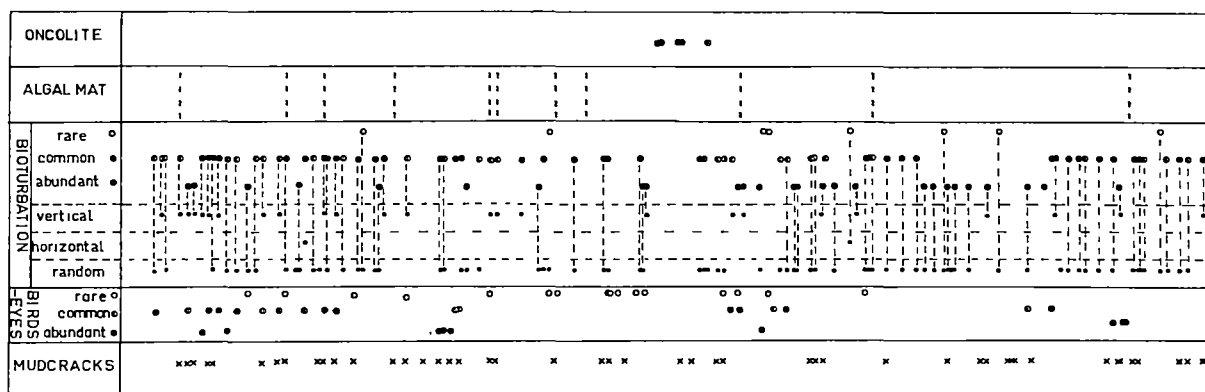
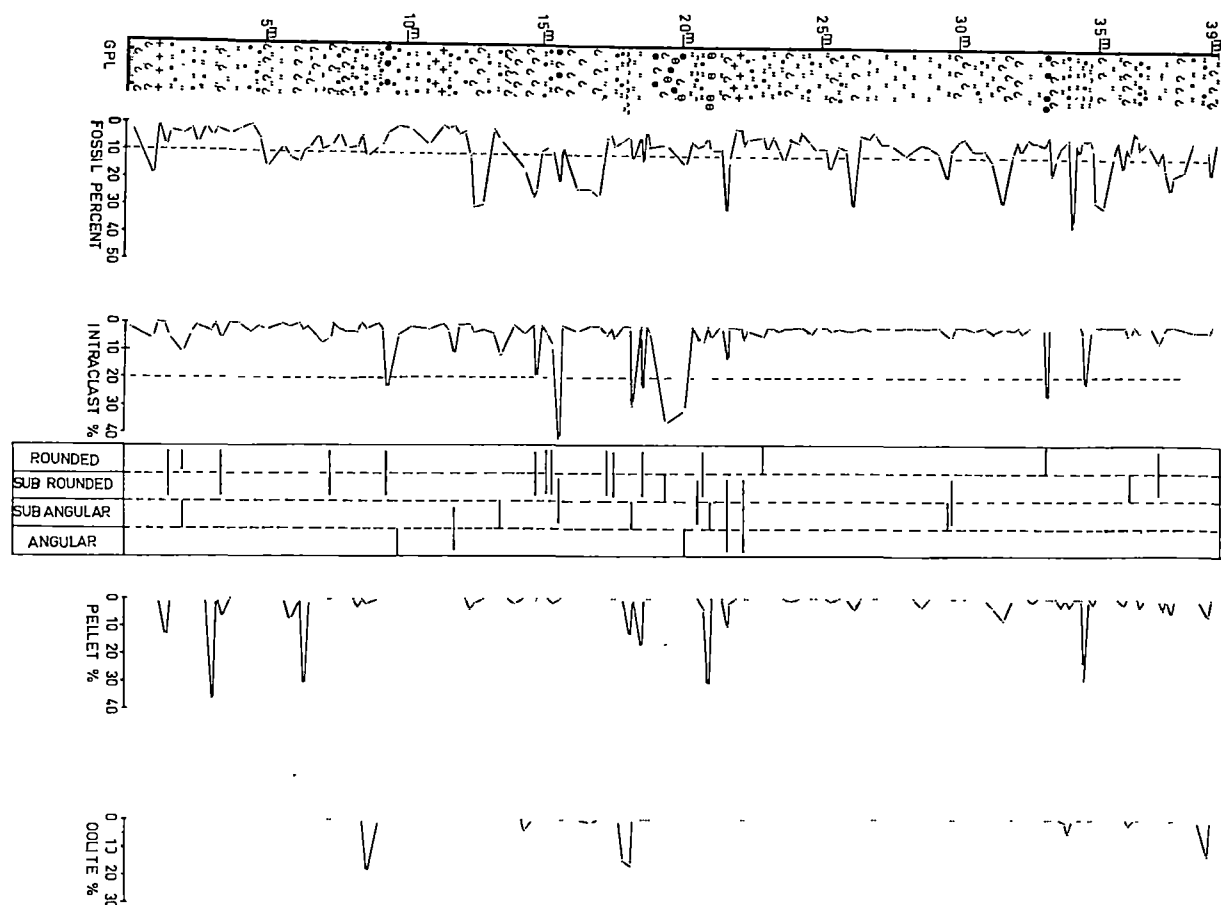


Fig. 3.28 Vertical distribution of the microfacies, constituent allochems, structures and depositional environments in section GPW. For symbols see p.72

Fig. 3.29 Vertical distribution of the microfacies and depositional environments in section GPL.



These depositional cycles range in thickness from about 1 m to approximately 6 m. Most of the supratidal or upper intertidal sequences are abruptly overlain by subtidal sequences which may contain reworked material from the basal beds. This abrupt transition denotes that the transgressions were rapid, while the subtidal to upper intertidal or supratidal sequences show that carbonate sedimentation mostly took place during regressions (also called offlap or regressive overlap). According to Curran (1964, p.198), depositional regressions in ancient carbonate rocks occur as a result of a seaward progradation of the shoreline by deposition. Thus except for a few interruptions, the vertical variation in the depositional environments suggest the existence of a number of progradational cycles.

The microfacies which have been recognized in the Gunns Plains Limestone have been grouped into three major facies - supratidal, intertidal and subtidal facies. Tables 3.3, 3.4 and 3.5 summarize the observed features of these major facies in the studied sections. Sixty-three percent of the samples as shown in the tables have been interpreted as belonging to the intertidal facies. Ginsburg (1975, p.234) has pointed out that the intertidal zone is the most commonly identified zone in ancient carbonate rocks because it has so many diagnostic structures. Such a bias exists in this study also.

Many models for carbonate sedimentation have been derived using the concepts of workers like Edie (1958), Shaw (1964) and Irwin (1965). Wilson (1975) has discussed ancient and modern models, and ways in which the individual worker can develop his own model.

The models pre-suppose broad epicontinental (epeiric) seas in the geologic past with a low gradient shelf hundreds of kilometres wide. Due to variations in water circulation, different zones are developed in these widespread, shallow seas. Irwin (1965) differentiated three hydraulic zones which directly affect depositional

Table 3.3
SUMMARY OF OBSERVED FEATURES IN SECTION GPR

	Subtidal	Intertidal		Supratidal
		Lower	Upper	
Sample Distribution (%)	24	24	35	17
FOSSILS	Percentage of samples containing fossils	83	67	61
	Maximum volume % of fossils	100	18	14
	Average volume % of fossils	28	6	5
	Type of fossil	Brachiopods, bryozoans, corals, gastropods, pelmatozoans, stromatoporoids and trilobites.	Mixture of unidentifiable and identifiable forms. Pelmatozoans, gastropods and trilobite fragments are common. Rarely brachiopod and bryozoans present.	Small, broken fragments. Recognizable forms include brachiopods and gastropods, and rarely bryozoan and pelmatozoan fragments.
INTRACLASTS	Percentage of samples containing intraclasts	8	50	56
	Maximum volume % of intraclasts	2	16	30
	Average volume % of intraclasts	2	5	10
	Shape of intraclasts	Rounded to subrounded	Subrounded - common Subangular - rare	Subangular to subrounded
PELLETS	Percentage of samples containing pellets	8	75	61
	Maximum volume % of pellets	14	55	37
	Average volume % of pellets	14	29	11
Birdseyes	-	Present in 15% of samples. Rare.	Present in 50% of samples. Mostly common.	Present in 66% of samples. Mostly rare to common.
Mudcracks	-	-	Present in 61% of samples. Common.	Present in 89% of samples. Common.
Bioturbation	Random - common.	Random - common to abundant.	Vertical - rare Random - common to abundant.	Vertical - common to abundant.
Average dolomite content (%)	< 10	< 10	11	17
Microfacies	Biomicrite/biosparite. Fossiliferous micrite. Burrowed micrite. Pelbiomicrite.	Pelmicrite/pelsparite. Intraclast-bearing micrite. Pelbiomicrite and biopelmicrite. Fossiliferous micrite.	Pelmicrite/pelsparite. Intrapelsparites. Intraclast-bearing fossiliferous micrite. Fossiliferous micrite. Other allochem-bearing micrite.	Dolostone. Intraclast-bearing fossiliferous micrite. Dismicrite. Intraclast bearing micrite.

Table 3.4

SUMMARY OF OBSERVED FEATURES IN SECTION GPD				
	Subtidal	Intertidal		Supratidal
		Lower	Upper	
Sample Distribution (%)	25	33	33	9
FOSSILS	Percentage of samples containing fossils	100	92	83
	Maximum volume % of fossils	35	10	21
	Average volume % of fossils	12	5	6
	Type of fossils	Mostly bryozoans, pelmatozoans and trilobites, rarely brachiopods and gastropods.	Recognizable forms include brachiopods, bryozoans, gastropods, rarely pelmatozoans and trilobite fragments.	Mostly broken and unidentifiable. Recognizable forms include brachiopods, gastropods, ostracods, and rarely pelmatozoan and trilobite fragments.
				Very fine skeletal material. Rarely gastropods recognized.
INTRACLASTS	Percentage of samples containing intraclasts	13	25	42
	Maximum volume % of intraclasts	4	22	26
	Average volume % of intraclasts	4	8	12
	Shape of intraclasts	Rounded to subrounded.	Subangular - common Rounded - rare	Subangular
PELLETS	Percentage of samples containing pellets	-	17	42
	Maximum volume % of pellets	-	65	48
	Average volume % of pellets	-	39	34
Mudcracks	-	-	Common	Common
Birdseyes	-	-	Rare	Rare
Bioturbation	Random - common	Random - common to abundant	Vertical - rare Random - common	Vertical - common
Average dolomite content (%)	<10	<10	24	36
Microfacies	Biomicrite/biosparite. Fossiliferous micrite.	Fossiliferous micrite. Pelmicrite. Intraclast-bearing fossiliferous micrite. Intrabiomicrite.	Pelmicrite. Fossiliferous micrite. Intrabiomicrite. Intraclast-bearing fossiliferous micrite.	Fossiliferous micrite.

Table 3.5

SUMMARY OF OBSERVED FEATURES IN THE LATERALLY

EQUIVALENT SECTIONS GPB, GPW AND GPL

	Subtidal			Intertidal						Supratidal		
				Lower			Upper					
	GPL	GPW	GPB	GPL	GPW	GPB	GPL	GPW	GPB	GPL	GPW	GPB
Sample distribution (%)	35	10	12	34	24	25	32	38	33	3	30	30
FOSSILS	Rel. sample %	100	100	96	88	67	93	66	64	100	58	22
	Range %	0-39	0-56	0-20	0-39	0-42	0-17	0-31	0-13	0-24	0-9	0-9
	Mean %	10	26	12	9	11	10	9	3	11	7	3
	Type of fossil	Diverse - algae, bryozoans, brachiopods, cephalopods, corals, gastropods etc. Stromatoporoids in section GPW only			Brachiopods, bryozoans, gastropods, trilobite fragments. Mostly individuals like gastropods abundant.			Mostly broken, shelly fauna.			Very small broken fragments.	
INTRACLASTS	Rel. sample %	38	42	33	39	61	67	61	61	64	86	63
	Range %	0-30	0-6	0-7	0-42	0-8	0-14	0-29	0-23	0-28	0-16	0-28
	Shape	Rounded to sub-rounded.			Subrounded common, rounded rare.			Subangular common, subrounded and angular rare.			Angular to subangular.	
PELLETS	Sample %	24	-	7	16	-	-	28	7	27	-	-
	Range %	0-32	-	0-6	0-32	-	-	0-37	0-27	0-6	-	-
COLLITES	Sample %	8	-	-	9	17	-	2	-	-	-	-
	Range %	0-5	-	-	0-33	0-8	-	0-13	-	-	-	-
Birdseyes	-	-	-	Rare			Abundant			Common		
Mudcracks	-	-	-	Rare			Abundant			Abundant		
Bioturbation	Random - common			Random - common to abundant			Random - rare to common; Vertical - common.			Vertical - common Random - present in section GPL.		
Dolomite (mean %)	< 10			17	24	< 10	20	25	21	34	44	32
Microfacies	Biomicrites/bio-sparites, fossiliferous micrite.			Biomicrites, biopelmicrite and pelbiomicrite, intraoncosparites, intramicrites and intra-sparites, intraclast-bearing fossiliferous micrite, intraclast-bearing micrite, fossiliferous micrite, minor allochem-bearing micrites and dismicrites.						Dismicrites, fossiliferous micrite, intraclast-bearing fossiliferous micrites, intraclast-bearing micrite, intramicrites.		

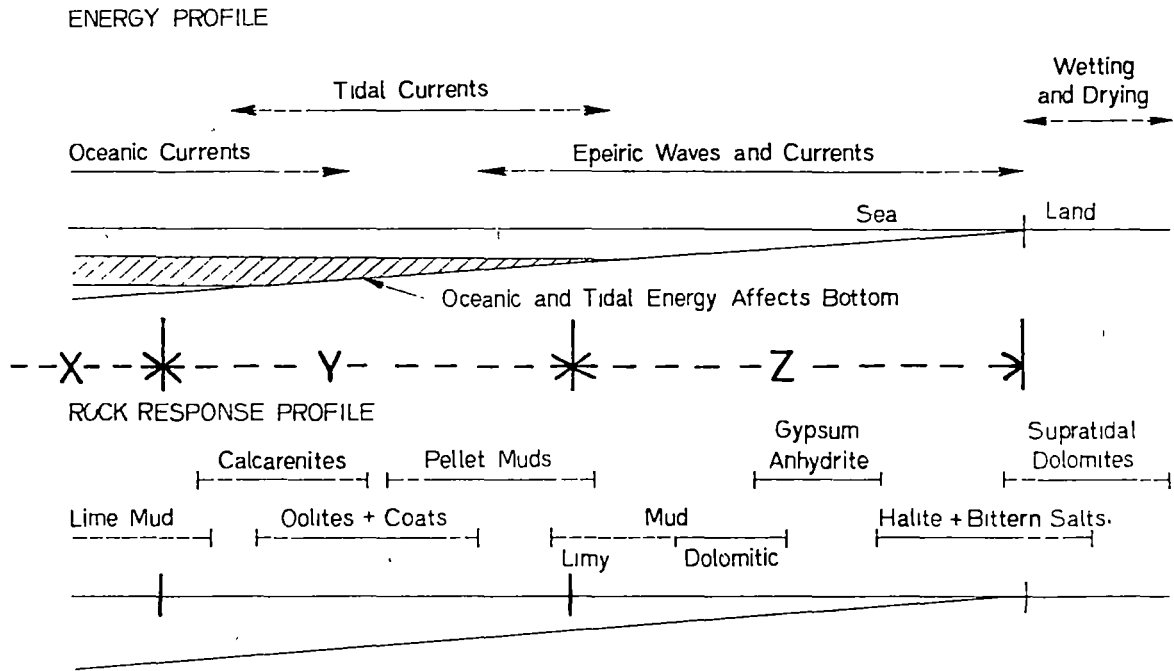


Fig.3.30. Simplified energy and rock response profiles across a stable cratonic shelf having no terrigenous input (reproduced from Horowitz and Potter, 1971; modified from Shaw, 1964, figs. 8.1 and 8.2). Irwin's (1965) three energy zones---X, Y, Z are also shown.

environments on the sea-floor: (1) the 'X' zone or the outer deeper parts of the shelf, where the sea-bottom is not influenced by the waves, (2) the 'Y' zone existing in a relatively narrow area where due to influence of waves on the sea-bottom, turbulent or high-energy conditions prevail, and (3) the 'Z' zone closer to the land, where the water movement is by winds and storms only.

An increase in the general depositional slope may cause the high energy zone to migrate shoreward restricting the extent of the near-shore low energy zone (Z zone) and if the wave, tidal and current energy is dissipated over a short distance a physical barrier may develop. In a barred-basin, the high energy conditions predominate near the opening of the basin due to funnelling of the currents and diminish basinward.

Fig. 3.30 which has been redrawn from Horowitz and Potter (1971) shows their interpretation of the energy and rock response profiles which develop across a stable cratonic shelf. These are based on Shaw's (1964) model to which have been added the energy zones of Irwin (1965).

The major facies recognized in the Gunns Plains Limestone may be related to the Z zone proposed by Irwin (1965) and shown in Fig. 3.30. Sections GPL, GPW and GPB, as has been mentioned in Chapter 2, are the lateral equivalents of each other. The observed features of these three sections, which are Blackriveran to Kirkfieldian in age are summarized in Table 3.5 and suggest the existence of more subtidal conditions in section GPL (north Gunns Plains) as compared to section GPW and GPB (south Gunns Plains). Probably a high energy Y zone existed north-east of section GPL (at least during Blackriveran to Kirkfieldian times) and is now covered by Tertiary basalts or has been eroded away. This inference is based on the presence of sparse oolites at some horizons in section GPL and GPW. The oolites are predominantly in amounts not sufficient to form a carbonate rock after Folk (1959, 1962) and appear to have been transported

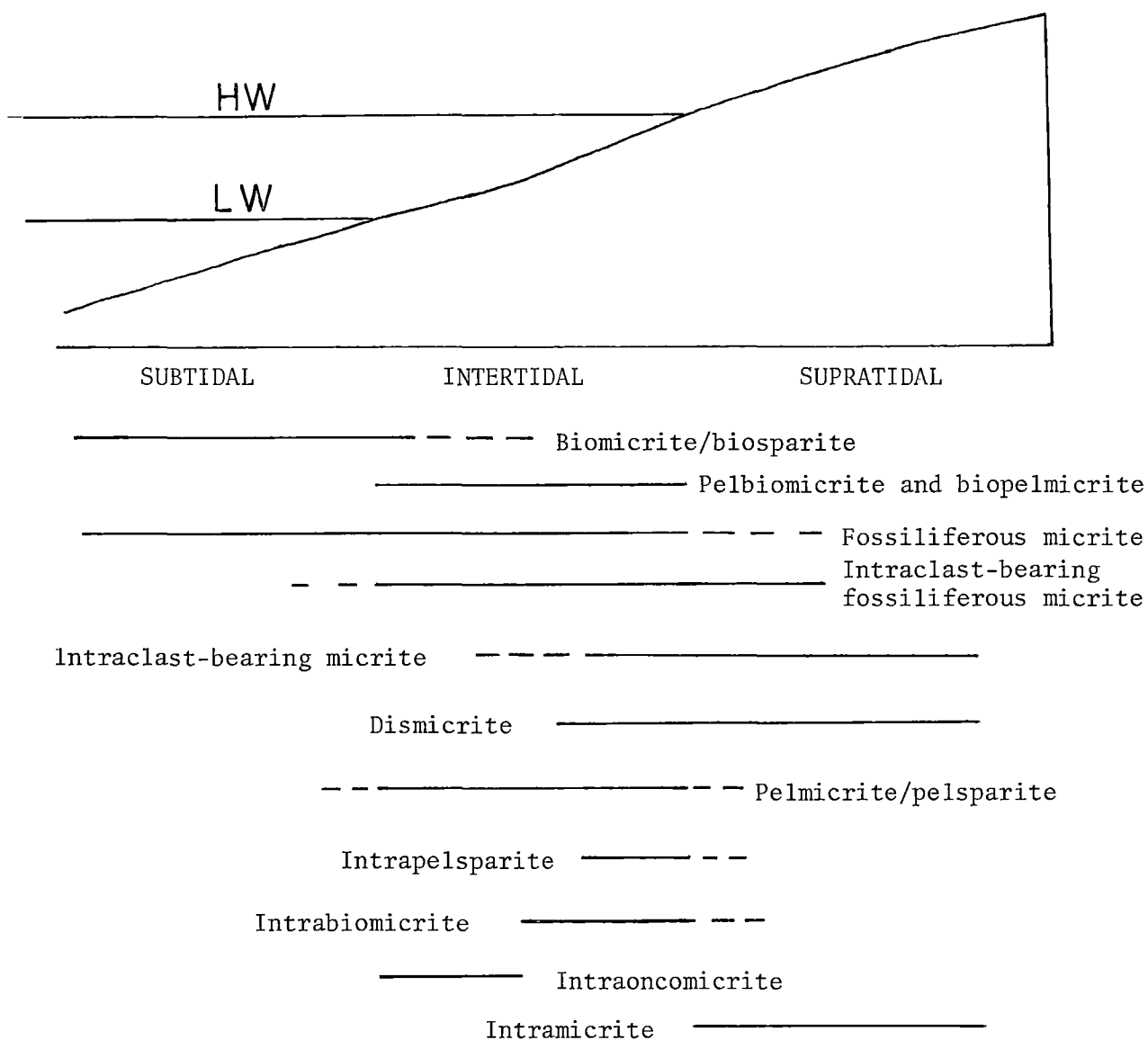
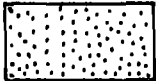



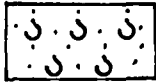
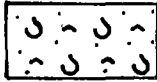
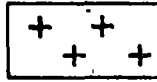




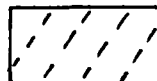


Fig. 3.31 A general model depicting the environments of deposition of the microfacies within the Gunns Plains Limestone (during any period of time).

from elsewhere (? the high energy Y zone). Further evidence is provided by intraclast roundness which as seen in Table 3.5 increases towards the subtidal and indicates an increase in the energy of the environment. Also the occurrence of oncolites with irregular outlines in section GPL suggests the existence of a high energy zone.

A general model depicting the environments of deposition during any period of time within the Gunns Plains Limestone is shown in Fig. 3.31. The shoreline was characterized by low energy and was extremely irregular with the depositional facies shifting landward and seaward. Migration of these tidal-flat deposits across subtidal deposits formed a facies mosaic of supratidal, intertidal and subtidal units. These facies patterns are believed to reflect eustatic sea-level changes, which in part could have been due to shelf subsidence and associated sedimentation.

1				
	Micrite	Fossiliferous micrite	Intraclast-bearing fossiliferous micrite	Intraclast-bearing micrite
2				
	Biomicrite	Biopelmicrite/ pelbiomicrite	Dismicrite	Dolostone
3				
	Intramicrite	Intrabiomicrite	Intrapelmicrite	Spar instead of micrite

Chapter 4

DOLOMITIZATION

INTRODUCTION

Recent shallow marine to hypersaline marine carbonates are characterized by aragonite and Mg-calcite with or without dolomite, whereas most ancient carbonate rocks commonly consist of calcite and/or dolomite. The factors affecting this carbonate equilibria are still in the process of being fully understood, and so far, attempts to synthesize (ideal) dolomite at near-surface temperatures and pressures have proved futile.

The field evidence of dolomite together with experimental work has led to the development of a large number of models that attempt to explain the dolomitization process. A popular hypothesis in areas of no evaporite formation suggests that the mixing zone between sea-water and fresh water is an important site for dolomitization (e.g. Hanshaw *et al.*, 1971; Land, 1973; Badiozamani, 1973; Folk and Siedlecka, 1974; Land *et al.*, 1975; Dunham and Olson, 1978). In many models the generation of hypersaline brines, in areas of evaporite mineral formation, is thought to be a prerequisite for dolomitization. The models vary from downward seepage refluxion (e.g. Adams and Rhodes, 1960; Deffeyes *et al.*, 1965) to upward movement by capillary concentration (Shinn *et al.*, 1965) or evaporitive pumping (e.g. Hsu and Siegenthaler, 1969; Hsu and Schneider, 1973) of the dolomitizing brines. Most of the dolomitized supratidal sequences are believed to have formed from such hypersaline brines and are also called sabkha dolomites by analogy with their occurrence in the arid surrounds of the Persian Gulf. Generally the source of Mg^{++} ions for the dolomitizing brines is believed to be sea-water.

Von der Borch *et al.* (1975, 1979) have described an analogue of the arid region sabkha dolomites from the humid Coorong area of South Australia. In these Coorong dolomites, minor amounts of evaporite minerals, precipitated during the summer are flushed out during the winter by refluxion of ground water (Muir *et al.*, 1979). The evaporation of ground water, in discharge areas, is believed to result in the formation of dolomite with the Mg^{++} ions being contributed by seaward flowing groundwaters.

There are many other models (e.g. Goodell and Garman, 1969), but despite the extensive literature on dolomites, the process is still not fully understood (for reviews, see Friedman and Sanders, 1967; Berner, 1971; Folk and Land, 1975; Bathurst, 1976; Meyers, 1980). There is, however, general agreement that environment of deposition makes it possible to distinguish between early and late diagenetic dolomites. The redistribution of trace elements is being investigated in order to provide some insight into the dolomitization process (e.g. Veizer *et al.*, 1977, 1978; Rao and Naqvi, 1977; Supko, 1977; Land *et al.*, 1975; Fritz and Katz, 1972).

This study adopts an integrated approach using facies distribution of dolomite and their geochemical characteristics to infer the process of dolomitization in the Gunns Plains Limestone.

PETROLOGY

Dolomite interlayered with limestone is of widespread occurrence in the Gunns Plains Limestone (see frontispiece). The dolomitic layers on weathered surfaces show positive relief and are coarser-grained than the limestones. Commonly the dolomite layers are yellowish-brown, laminated and less than 0.5 m thick. Burrows filled with dolomite are easily recognizable in the bioturbated units. V-shaped mudcracks are

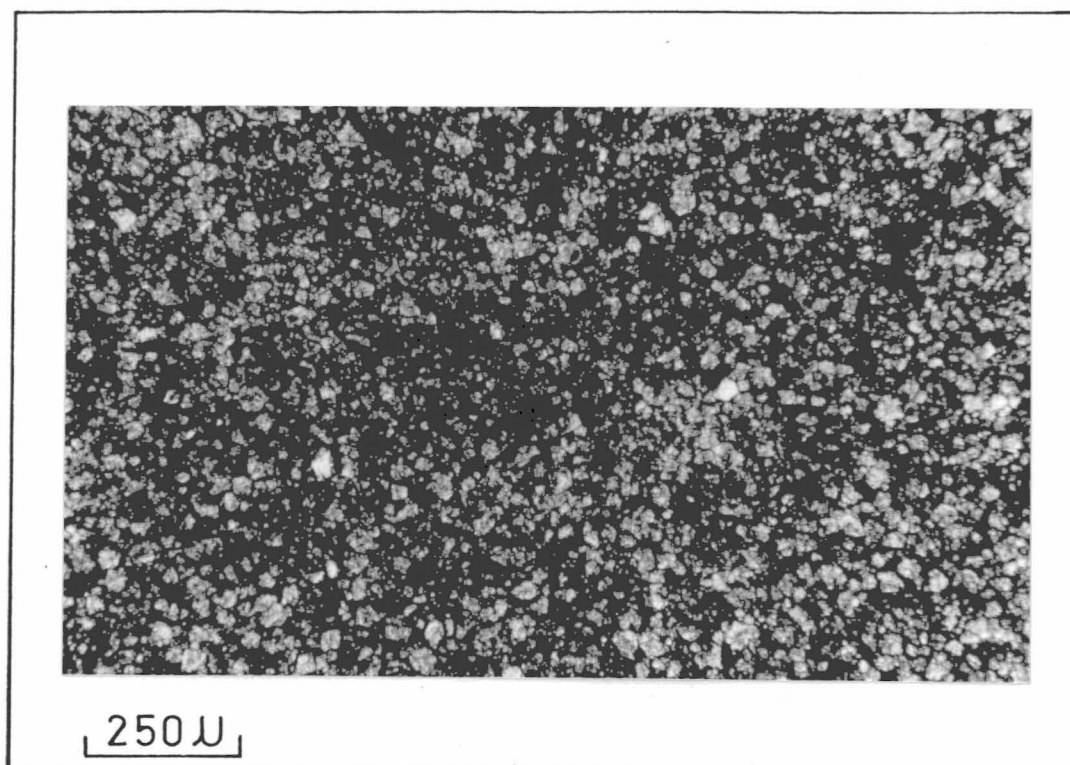


Fig. 4.1 Equigranular mosaic of finely crystalline euhedral to subhedral dolomite.

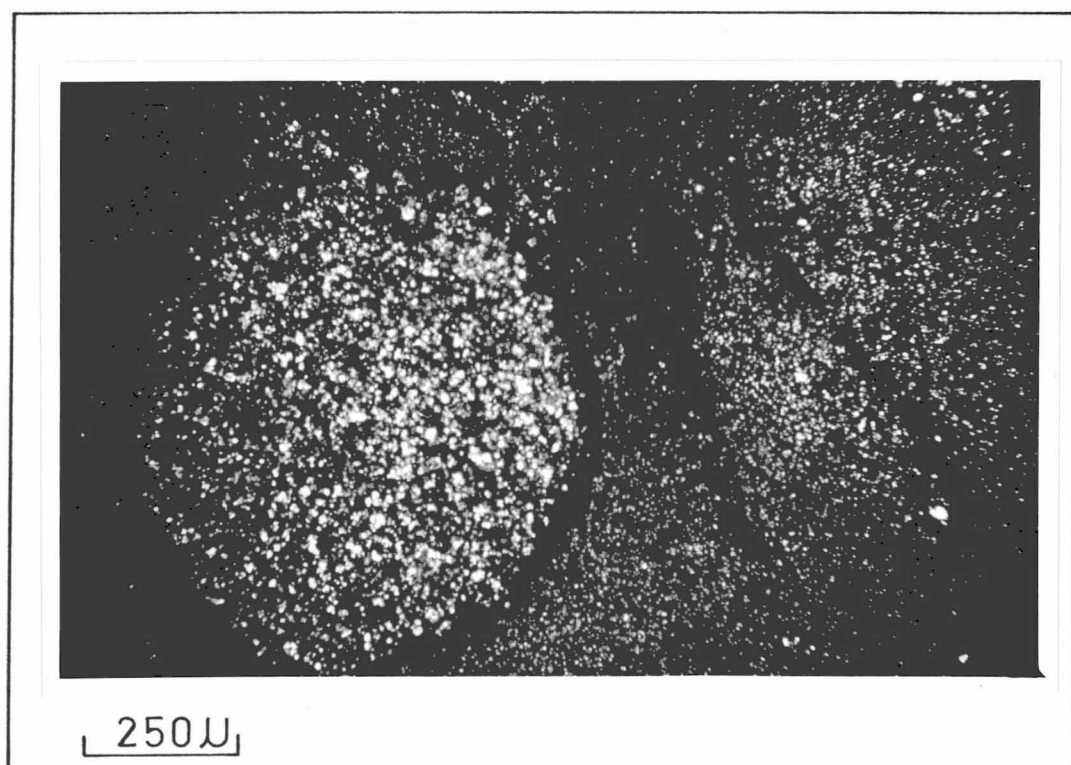


Fig. 4.2 Rounded intraclast composed of dolomite. The dolomite has also invaded the micrite matrix. X-nicols.

common, while the mudcracked polygons (about 4 cm across) surrounded by dolomite were only observed in section GPW. A similar type of dolomite occurrence in the Cretaceous Edwards Formation of Texas has been termed 'Stratal Dolomite' by Fisher and Rodda (1969).

Microscopic examination of peels and thin sections shows that the dolomite is brown or golden-yellow. The most abundant size of dolomite crystals ranges between 20 and 50 μ . Crystals as small as about 10 μ are common, while those ranging between 50 and 100 μ are rare. This finely crystalline dolomite typically is present as subhedral to euhedral crystals and these xenotopic to idiotopic dolomite crystals form an equigranular mosaic (Fig. 4.1).

No allochems, apart from intraclasts, are replaced by dolomite (see Figs. 3.5, 3.18, 3.20, 4.2). In such cases, the quartz silt present within the intraclasts may also be replaced. Dolomite is also commonly seen around the intraclasts and along the mudcrack margins (Fig. 3.6). In samples showing bioturbation features, the burrows have been selectively dolomitized (Figs. 3.1, 4.3). The variable amount of dolomite in the samples (0-86%) indicates that all stages of replacement of carbonate mud by dolomite exist. Other features replaced by dolomite are the wavy-laminated algal mats, containing scattered organic material (Fig. 3.10) or an anastomosing network of very fine, black, organic laminae (Fig. 5.5). In all the studied sections, dedolomitization (discussed in Chapter 5) has affected the dolomite fabric to various degrees.

X-ray diffractograms of some samples are shown as Fig. E.1 (in Appendix E). They show the presence of dolomite, calcite and minor quartz. The dolomite peaks observed at $2\theta = 30.92, 30.90$ and 30.82 give 'd' spacings between 2.89 and 2.90 Å, which corresponds to ideal and ferroan dolomites. No attempt has been made to make a quantitative estimate of the proportions of minerals present from the X-ray

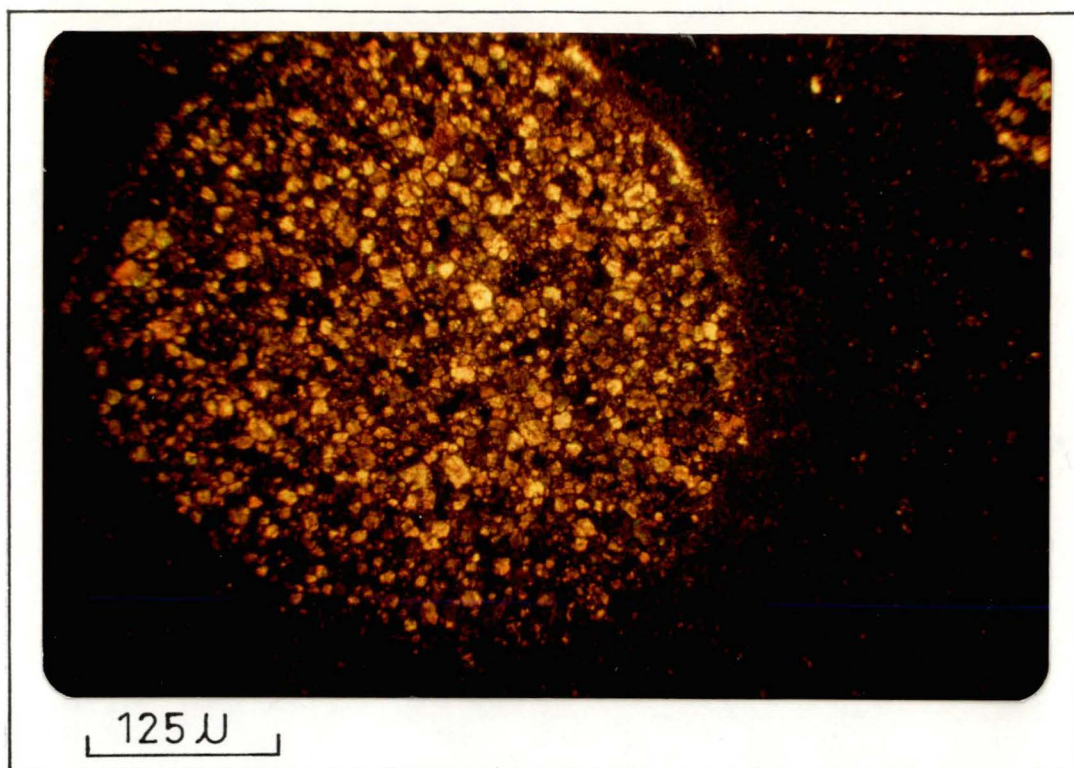


Fig. 4.3 Horizontal burrow filled with dolomite of variable size. X-nicols.

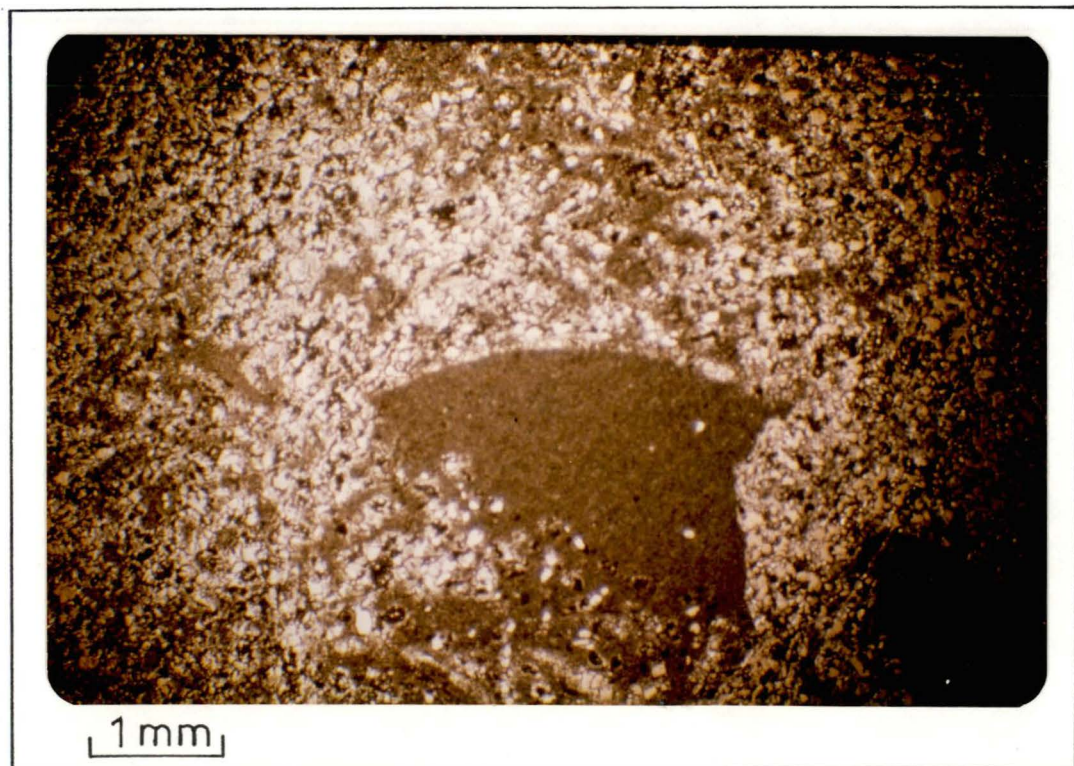


Fig. 4.4 Broken shell with convex side up. Note the unreplaced micrite beneath shell suggesting downward seepage of the dolomitizing brines. Note the primary fabric differences.

diffractograms. Lumsden (1979a, b) has pointed out the errors involved in making X-ray diffraction estimates of dolomite and instead recommends point count analysis as a reliable technique.

Ten peels and thin sections were counted for 500 points each, distributed to cover the whole area of the specimen, with the use of an integrating eyepiece (for details see Chayes, 1956; Galehouse, 1971). In all cases, the dolomite percentage obtained by point count analysis was slightly greater than the visual estimate of the dolomite content (see Table 4.1).

Table 4.1

COMPARISON OF THE VISUAL AND POINT COUNT ESTIMATES OF DOLOMITE PERCENTAGE

Sample Number	Dolomite %		Difference
	Visual	Point Count	
49146	32	40	8
49171	15	21	6
49239	33	42	9
49042	16	23	7
49064	17	23	6
49066	14	19	5
49070	26	32	6
49083	13	19	5
49090	35	41	6
49123	50	56	6
			64 total
			6.4 mean

$$\begin{aligned}
 \text{Correction factor} &= \frac{100 - 6.4}{100} \\
 &= 0.936
 \end{aligned}$$

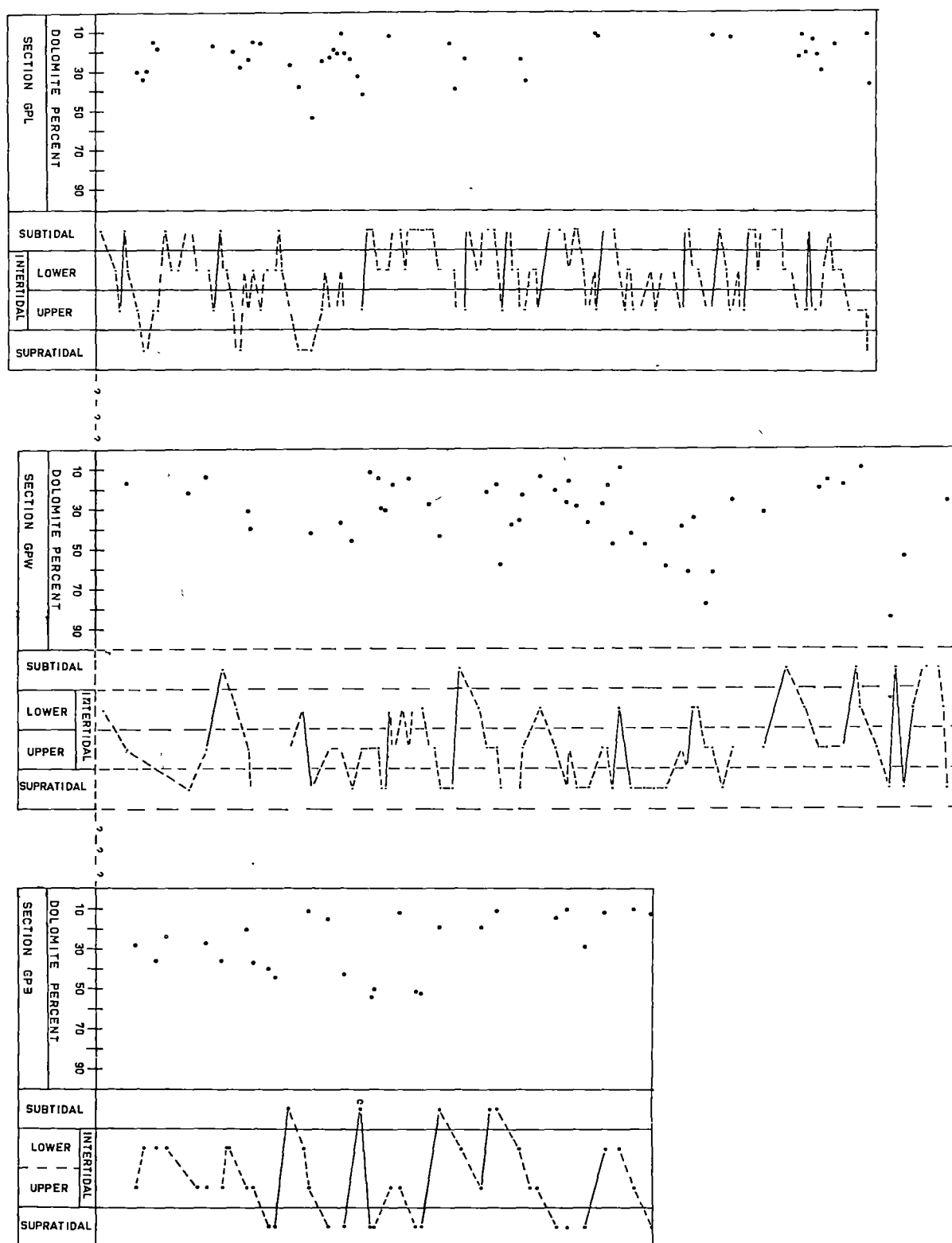


Fig. 4.5 Vertical variation of the dolomite content in the laterally equivalent sections GPL, GPW and GPB and the interpreted depositional environments. Samples containing less than 10% dolomite are not shown.

In spite of the visual estimates of dolomite being in good agreement with those obtained by point counting, a small correction factor obtained from Table 4.1 has been applied to all visual dolomite estimates. Another consideration worth mentioning and of importance in the discussion of dedolomitization (Chapter 5) is that the occurrence of dedolomitization textures has been ignored in the visual and point count estimates of dolomite. This has been done because the replacement of dolomite by calcite is on a very varied scale (from a small clot of calcite on dolomite to a whole dedolomitized rhomb, see Figs. 5.1 to 5.13) even in a single sample. Petrographic separation of the two for purposes of volumetric estimates is not only difficult, but also leads to significant error estimates of both dolomite and dedolomite. Thus the dolomite estimates of all samples include an unknown amount of dedolomite. The mean dolomite content in the studied sections is GPR = 14%, GPD = 7%, GPB = 21%, GPW = 20% and GPL = 11% indicating that the bulk of the samples are dolomitic limestones (10 to 50% dolomite).

VERTICAL DISTRIBUTION

Vertical distributions of the dolomite percentages in the studied sections, together with the interpreted depositional environments, are shown in Figs. 4.5 and 4.6. It can be observed that the dolomite content is very variable in all the stratigraphic sections. When compared with the depositional environments, the variation in the dolomite content appears to be related to the depositional cycles, generally being most abundant in the supratidal environment or, where supratidal is absent, in the upper intertidal environment of each cycle. The dolomite content decreases towards the subtidal environment, where it commonly occurs in amounts of less than 10%. Thus the supratidal facies contain

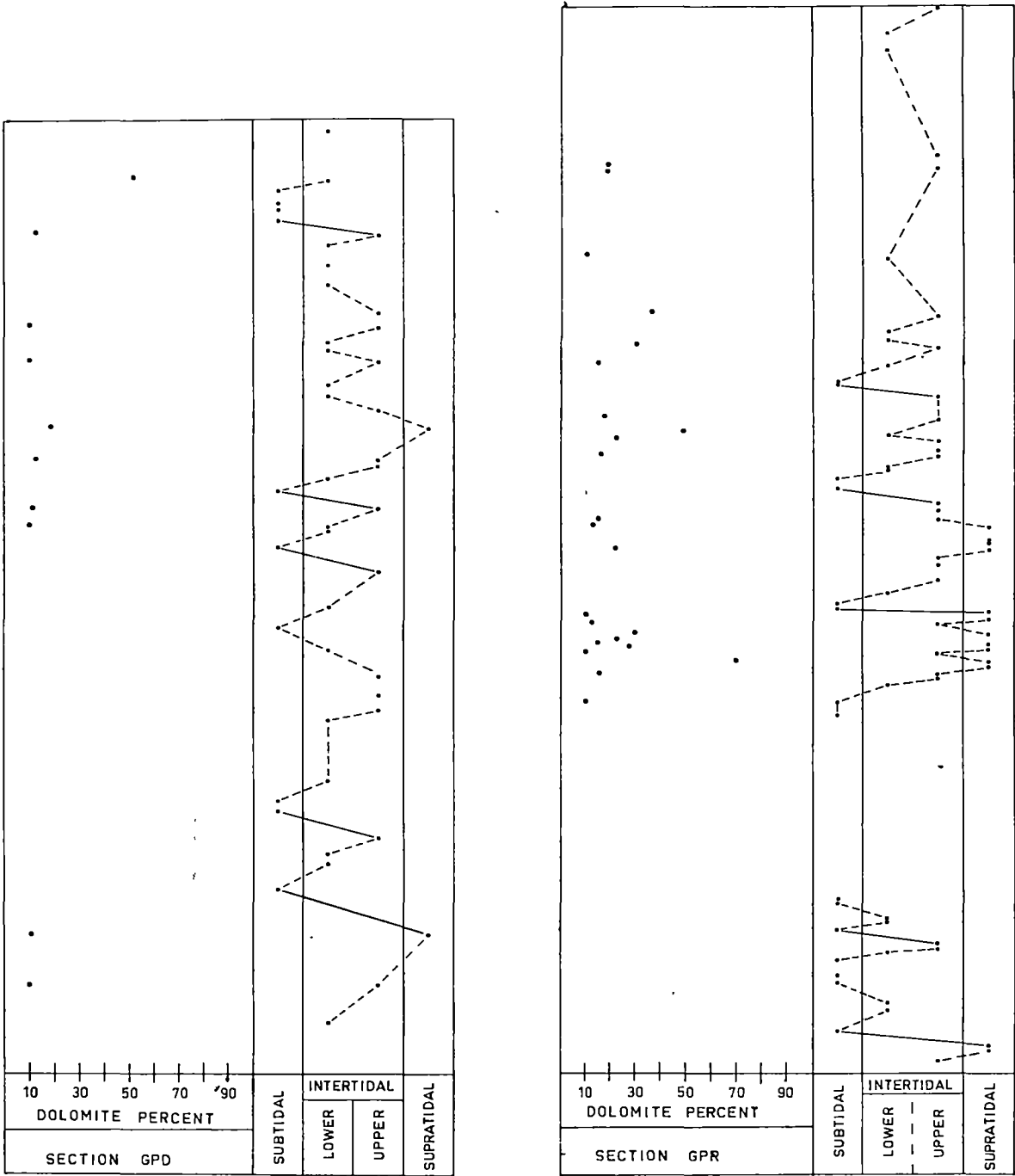


Fig. 4.6 Vertical variation of the dolomite content in sections GPR and GPD and the interpreted depositional environments. Samples containing less than 10% dolomite are not shown. Section GPD is lithostratigraphically above section GPR.

more dolomite than the subtidal facies (see also Tables 3.3, 3.4 and 3.5). This increase of dolomite in the supratidal facies and the variable amount of dolomite in the different depositional cycles indicates that dolomitization occurred in episodes of varying intensity during regressive phases of sedimentation, and that it was an early diagenetic process.

GEOCHEMISTRY

Aragonite and Mg-calcite, the carbonate phases stable in seawater, start diagenetic alterations to low Mg-calcite under the influence of meteoric water. The trace elements during this wet dissolution and reprecipitation process are also redistributed; the incorporation of cations in the precipitated phase being dependent on their partitioning through a liquid phase into the precipitate (e.g. Benson, 1974; for review of chemical partitioning see McIntire, 1963). The crystal size and habit of metastable and stable phases of CaCO_3 , among other factors, are also controlled by the Mg/Ca ratio and salinity (Folk, 1974), and these factors also control the crystallization of dolomite (Folk and Land, 1975). Thus the effect of dolomite formation on the trace element concentration in carbonate rocks may reflect important characteristics of the dolomite-forming solutions.

As the sequence of mineral transformation determined from textural studies also usually reflects the principal geochemical changes, it is possible to reconstruct the depositional and diagenetic changes by using the chemical characteristics along with petrographic criteria. Thus the whole rock (bulk) analyses of ancient carbonate rocks denote the sum of all geochemical changes that occurred in a rock.

In the present study, 217 samples from sections GPW and GPL (lateral equivalents of each other, Chapter 2) were used to understand

Table 4.2

CHEMICAL DATA OBTAINED BY X-RAY FLUORESCENCE

	Fe ₂ O ₃	MnO	TiO ₂	CaO	K ₂ O	P ₂ O ₅	SiO ₂	Al ₂ O ₃	MgO	Na ₂ O	S*	Ba	V	Ga	Rb
NO.	%											ppm			
49054	0.76	0.01	0.11	44.84	0.58	0.02	12.06	1.84	2.93	0.00	0.12	73	19	1.5	20
49057	0.68	0.01	0.10	45.23	0.66	0.03	10.97	1.76	1.98	0.00	0.11	73	23	1.7	23
49062	0.26	0.01	0.04	49.76	0.23	0.02	6.53	0.67	1.75	0.01	0.10	46	4	<1	8
49063	0.51	0.02	0.05	44.30	0.38	0.03	8.08	1.18	4.36	0.00	0.09	55	32	<1	16
49065	0.61	0.01	0.06	49.71	0.46	0.02	5.31	1.08	1.70	0.02	-	58	16	<1	12
49066	0.70	0.01	0.08	46.63	0.72	0.02	6.46	1.47	2.81	0.01	0.07	69	20	2.6	19
49069	0.72	0.01	0.11	46.79	0.83	0.02	8.79	1.94	2.70	0.00	0.03	108	32	1.1	24
49080	0.66	0.01	0.10	41.15	0.67	0.01	11.08	0.78	6.07	0.01	0.25	78	24	1.4	21
49082	0.78	0.01	0.11	44.28	0.70	0.01	8.51	1.87	4.10	0.00	-	81	23	1.8	24
49091	0.62	0.02	0.06	45.84	0.41	0.02	5.30	1.16	4.54	0.00	0.04	55	18	-	-
49110	0.56	0.03	0.02	44.39	0.13	0.01	12.51	0.39	2.65	0.00	-	57	<4	<1	9
49123	0.54	0.01	0.04	43.63	0.43	0.03	5.25	0.99	6.63	0.01	0.03	41	22	1.6	14
49140	0.69	0.01	0.08	48.07	0.63	0.02	6.76	1.75	1.59	0.01	0.08	60	24	1.6	21
49145	0.75	0.01	0.06	45.78	0.47	0.02	4.70	1.43	4.70	0.01	0.05	52	26	1.2	19
49146	0.70	0.01	0.03	46.36	0.27	0.01	3.22	0.08	5.61	0.01	0.07	34	13	1.7	11
49181	1.25	0.02	0.12	39.53	0.86	0.03	9.64	2.31	6.03	0.02	0.14	85	34	2.3	30
49212	0.72	0.02	0.05	44.57	0.33	0.02	4.72	0.99	3.73	0.00	0.04	46	12	0.0	13
49239	0.89	0.02	0.10	44.65	0.72	0.02	9.32	2.14	3.18	0.01	0.07	93	39	1.8	28
49273	0.66	0.02	0.07	47.68	0.53	0.02	6.09	1.59	2.12	0.02	0.06	62	31	<1	19
49280	0.41	0.02	0.03	51.28	0.24	0.02	3.43	0.89	1.57	0.03	0.09	30	19	0.0	10
49335	0.50	0.02	0.04	48.77	0.29	0.04	3.70	0.86	2.95	0.02	0.03	47	12	1.8	11

* semi-quantitative

Table 4.3

CORRELATION COEFFICIENTS FOR MAJOR AND MINOR ELEMENTS

	Ca*	S [§]	^x Rb	Ga	V	^x Ba	SiO ₂	K ₂ O	Al ₂ O ₃	TiO ₂	Na*	Mn*	Sr*	Fe*	Mg*
CaO	+0.81	-0.46	-0.57	-0.42	-0.36	-0.44	-0.57	-0.45	-0.46	-0.47	+0.49	-0.41	+0.41	-0.66	-0.75
Mg*	-0.61	+0.21	+0.19	+0.37	+0.18	-0.01	-0.02	+0.12	+0.09	+0.05	-0.25	+0.09	-0.35	+0.77	
Fe*	-0.70	+0.29	+0.29	+0.29	+0.13	+0.10	+0.29	+0.08	+0.17	+0.13	-0.37	+0.39	+0.09		
Sr*	+0.12	-0.18	-0.06	-0.13	-0.10	-0.32	-0.49	-0.09	+0.03	-0.12	+0.58	-0.61			
Mn*	+0.07	+0.34	-0.12	-0.18	-0.37	+0.12	+0.64	-0.23	-0.26	-0.15	-0.50				
Na*	+0.33	+0.09	-0.26	-0.12	-0.03	-0.38	-0.38	-0.17	-0.15	-0.25					
^x TiO ₂	-0.67	+0.44	+0.92	+0.56	+0.65	+0.88	+0.58	+0.94	+0.95						
- Al ₂ O ₃	-0.58	+0.37	+0.98	+0.59	+0.82	+0.82	+0.46	+0.97							
- K ₂ O	-0.66	+0.30	+0.94	+0.65	+0.75	+0.86	+0.43								
SiO ₂	-0.47	+0.63	+0.49	+0.15	+0.18	+0.68									
^x Ba	-0.61	+0.26	+0.84	+0.48	+0.60										
^x V	-0.53	+0.11	+0.82	+0.41											
Ga	-0.70	+0.11	+0.63												
^x Rb	-0.76	+0.28													
S [§]	-0.35														

§ semi-quantitative
* AAS

Table 4.4

ATOMIC ABSORPTION ANALYSES FROM DIFFERENT PARTS
OF THE SAME SAMPLE

No.	Mg %	Ca %	Sr	Mn	Na	Fe %
49156	1.46	33.22	640	81	161	0.174
	2.12	33.68	545	78	40	0.184
49294	0.86	36.94	649	67	117	0.101
	0.74	38.30	632	71	121	0.091
49303	0.73	36.71	806	80	77	0.081
	0.52	37.68	816	72	34	0.075
49309	1.03	37.17	925	75	90	0.082
	0.98	37.62	918	60	21	0.068
49322	1.18	30.59	455	93	0	0.134
	1.29	32.41	496	85	60	0.149

the trace element relationships. Sr, Mn, Fe, Na, Mg and Ca concentrations were determined in the soluble carbonate fraction using atomic absorption spectroscopy (AAS) (see Appendices B.1 to C.1). The chemical data are listed as Appendix C.2. Twenty-one samples from the same sections were analysed for SiO_2 , Al_2O_3 , K_2O , Fe_2O_3 , Ba, V, Ga, Rb, MgO and CaO by X-ray fluorescence (XRF) (Appendix D). The data obtained are shown in Table 4.2.

The concentrations of Rb (mean 18 ppm) and Ga (mean 2 ppm) reflect normal marine conditions (Degens *et al.*, 1958). The same holds for Ba (mean 62 ppm) concentrations (Friedman, 1969). These elements, like vanadium and titanium are associated with the clay minerals as indicated by the positive correlation coefficients with K_2O and Al_2O_3 (Table 4.3). It can also be seen from Table 4.3 that the trace elements (Sr, Mn and Na) in the soluble carbonate fraction have negative correlation coefficients with K_2O and Al_2O_3 suggesting their occurrence in the carbonate phase.

Robinson (1980), by using a similar method as in this study, has since demonstrated the leaching of some Fe from the alumino-silicate fraction, while showing that Sr, Mn and Na are in the carbonate fraction.

The major and minor element concentrations in the studied samples vary even within a single sample. This can be observed from Table 4.4 which shows 10 analyses of 5 samples (2 analyses from adjacent parts of each sample). This chemical variation is believed to be a result of the variable amount of dolomite and dedolomite in the different parts of the sample. Therefore in order to relate the chemical data to the petrographic observations, for example to the amount of dolomite, it is essential that the peels/thin sections and solutions for chemical analyses be made from the same parts of the samples.

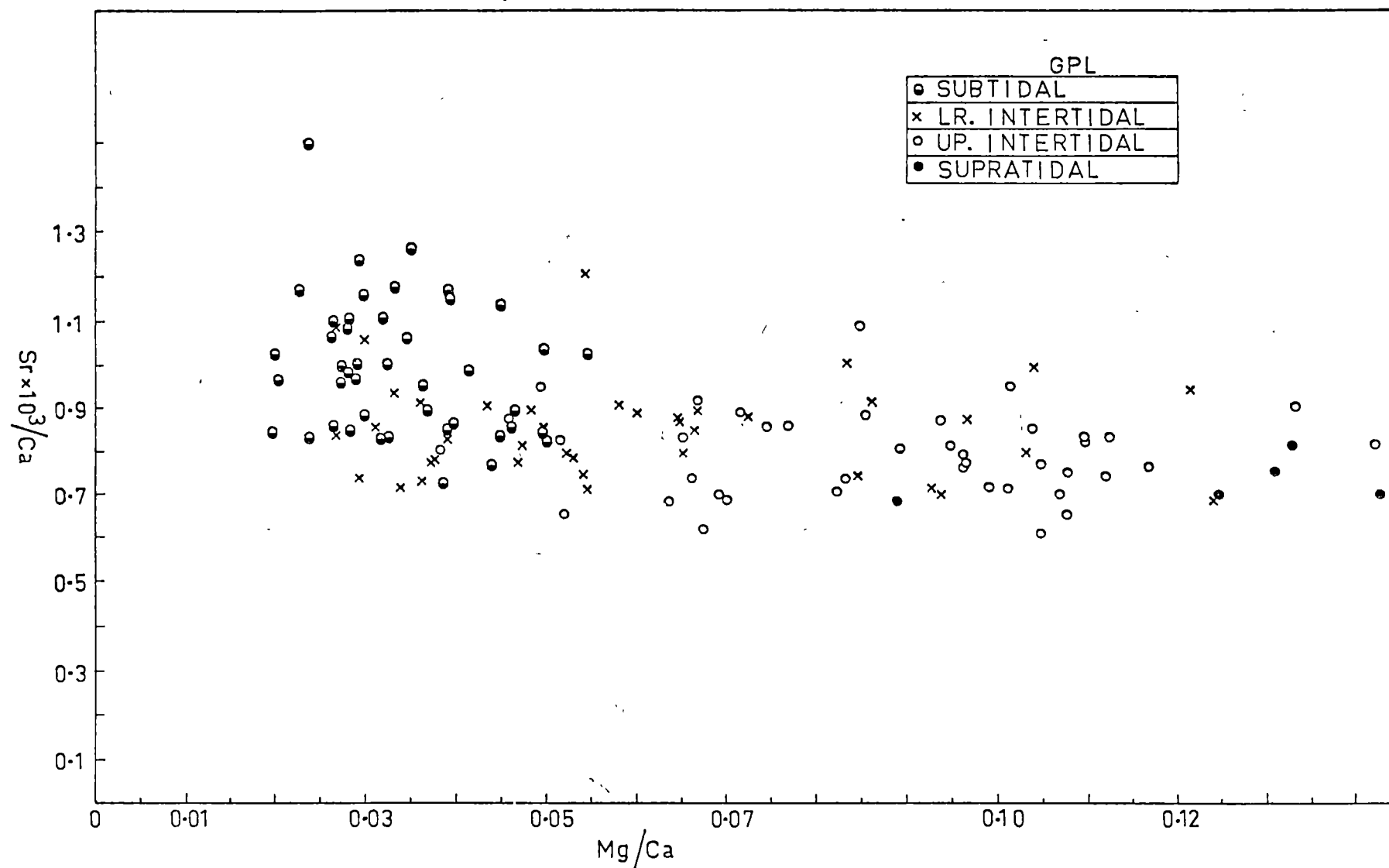


Fig. 4.7 Relationship of Sr/Ca molar ratio to Mg/Ca molar ratio in section GPL.

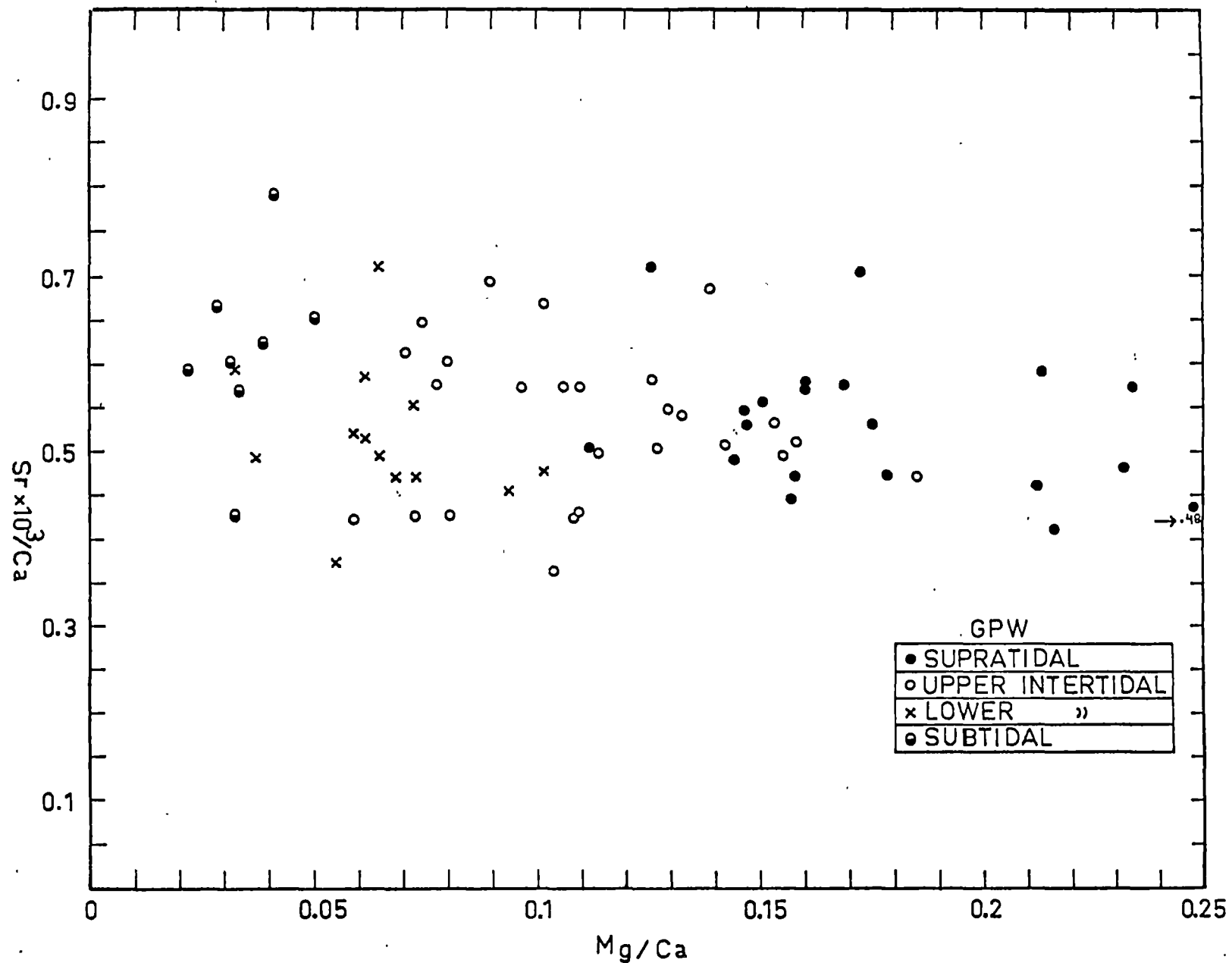


Fig. 4.8 Relationship of Sr/Ca molar ratio to Mg/Ca molar ratio in section GPW.

Strontium

The relationship of the Mg/Ca molar ratio, representing the dolomite content, to the Sr/Ca molar ratio in sections GPL and GPW is shown as Figs. 4.7 and 4.8. From these figures, the inverse relationship between the Sr/Ca ratio and the Mg/Ca ratio is apparent. It can also be seen that samples belonging to the subtidal facies (less than 10% dolomite) contain higher concentrations of Sr as compared to samples from the supratidal facies (up to 86% dolomite).

Strontium is the most extensively studied minor element in carbonate rocks. The strontium distribution in carbonate rocks and skeletons is reviewed by Kinsman (1969), Milliman (1974) and Bathurst (1976). Recent limestones contain variable amounts of Sr ranging up to 12500 ppm for pseudo-ooids from the Bahamas (Zellar and Wray, 1956). In contrast, the amount of Sr in recent, hypersaline, supratidal dolomites is about 660 ppm (Butler, 1973) or 620 to 640 ppm (Land and Hoops, 1973). According to Veizer and Demovic (1974), early diagenetic dolomites contain higher Sr concentrations compared to the late diagenetic dolomites. They related this to the partition of Sr between aragonite and dolomite (early diagenetic) and between calcite and dolomite (late diagenetic). The partition coefficient of Sr in dolomite is unknown because experiments to synthesize dolomite have proved unsuccessful. According to Behrens and Land (1972) a dolomite in equilibrium with calcite should contain about half the Sr of calcite (see also Jacobson and Usdowski, 1976), i.e.

$$(m_{\text{Sr}^{++}}/m_{\text{Ca}^{++}})_{\text{DOLomite}} = K_{\text{CALCITE}}^{\text{Sr}} \times \frac{1}{2}(m_{\text{Sr}^{++}}/m_{\text{Ca}^{++}})_{\text{SOLUTION}}$$

According to Kinsman (1969), the values of $K_{\text{CALCITE}}^{\text{Sr}}$ are 0.14 at 25°C and 0.08 at 100°C. The temperature of dolomite formation in the Gunns Plains Limestone is unknown. If the whole range of temperatures from 25°C to 100°C is assumed, then the Sr concentrations obtained for the

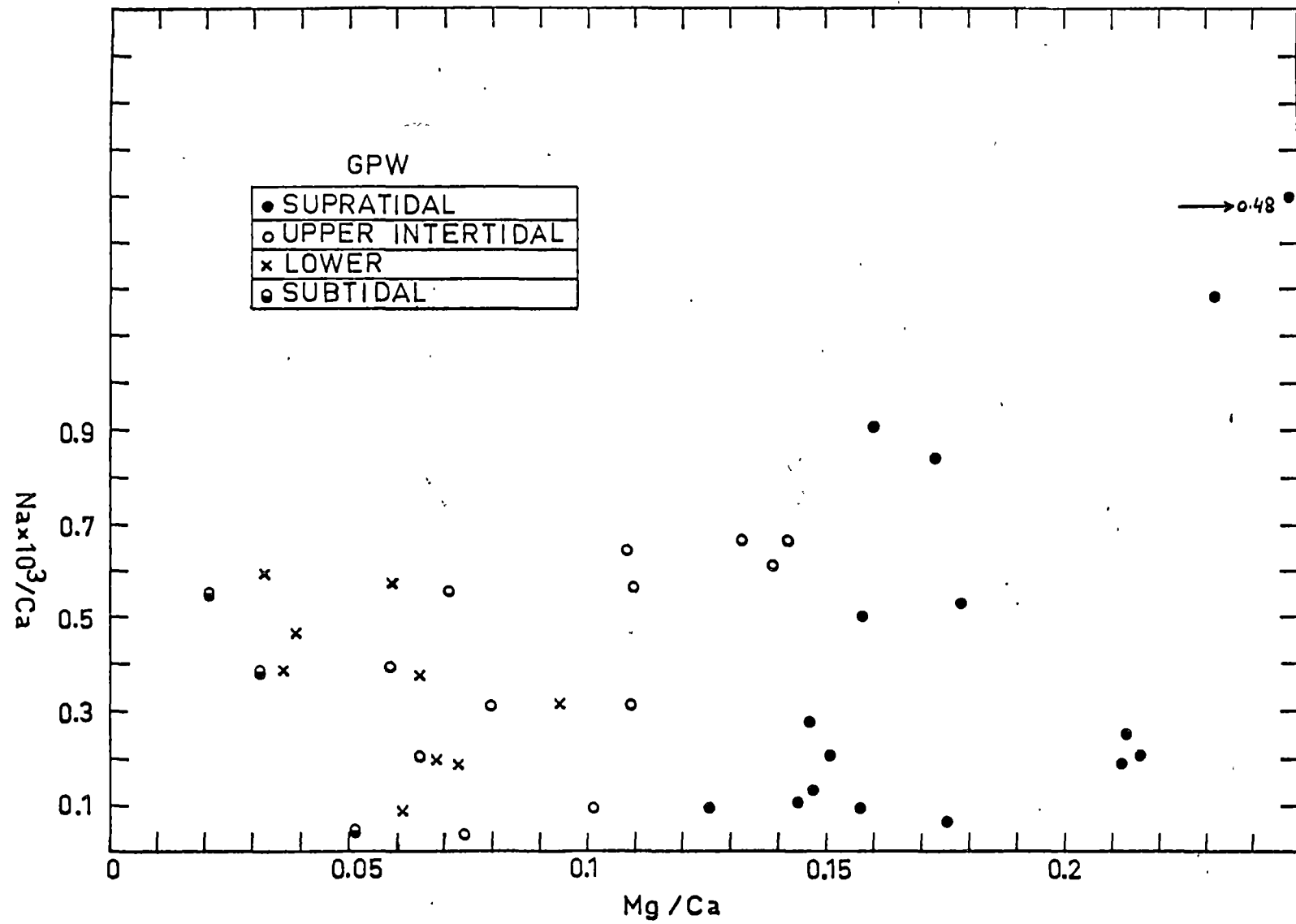


Fig. 4.9 Relationship of Na/Ca molar ratio to Mg/Ca molar ratio in section GPW.

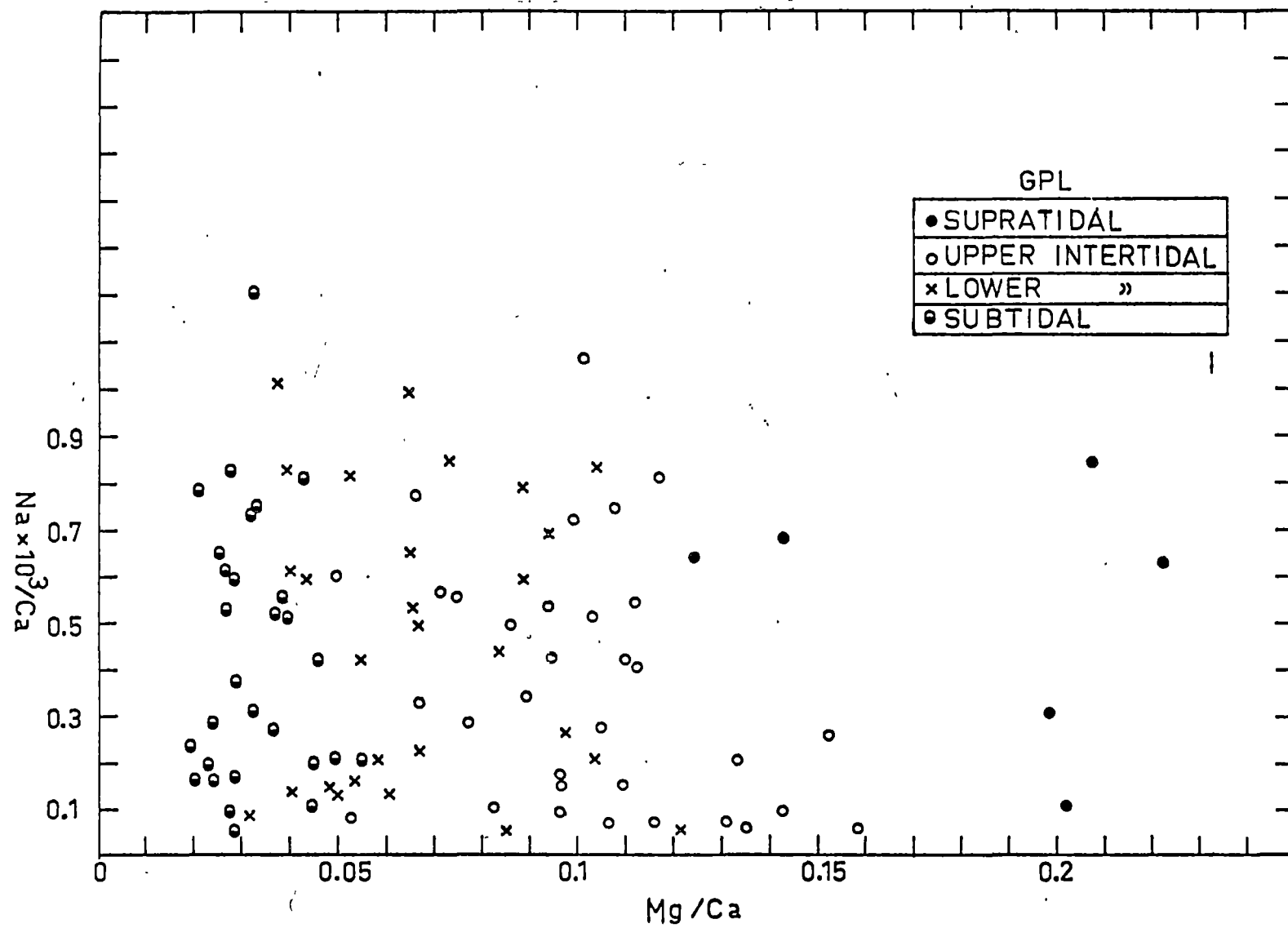


Fig. 4.10 Relationship of Na/Ca molar ratio to Mg/Ca molar ratio in section GPL.

the solutions based on the above relationship for dolostones (mean $\text{Sr/Ca} = 0.4816 \times 10^{-3}$) vary from 6000 ppm at 25°C to 10500 ppm at 100°C . These high Sr values suggest the presence of either aragonite or evaporites or both (e.g. Kinsman, 1969; Butler, 1973). Evaporitic moulds occur rarely in the study area. In either case, the early diagenetic origin of dolomites is indicated.

The above brief discussion is based on the inference that the Sr content in the dolomites has remained unchanged since dolomitization. As will be shown in the following chapter, the Sr concentrations underwent a loss during dedolomitization (approximate loss of Sr is believed to have been 66 ppm in the dolostones).

Sodium

The relationship of Mg/Ca to Na/Ca in sections GPW and GPL is shown in Figs. 4.9 and 4.10.

Na is considered to be a useful indicator of salinity (e.g. Fritz and Katz, 1972; Land and Hoops, 1973; Veizer, 1977, 1978). The wide variation of Na concentrations (Figs. 4.9 and 4.10) suggests either fluctuating salinities or dilution of trace elements during meteoric diagenesis (Land *et al.*, 1975).

The mean Na concentration in the dolostones is 42 ppm, std. dev. = 74 ppm. The standard deviation is higher than the mean because of the wide range from 0 to 205 ppm Na. This mean value of Na is far below the reported values in the literature. In the Junee Group elsewhere, Rao and Naqvi (1977) have reported mean Na values of 162 ppm Na for early diagenetic dolomites. It is believed that low Na values in the Gunns Plains Limestone are a result of dedolomitization (see Fig. 5.26). Samples containing high Na values are within the range reported by Rao and Naqvi (1977) and thus reflect the original concentration of hypersaline supratidal dolomites. In other cases, dedolomitization has completely removed the original traces of hypersaline conditions.

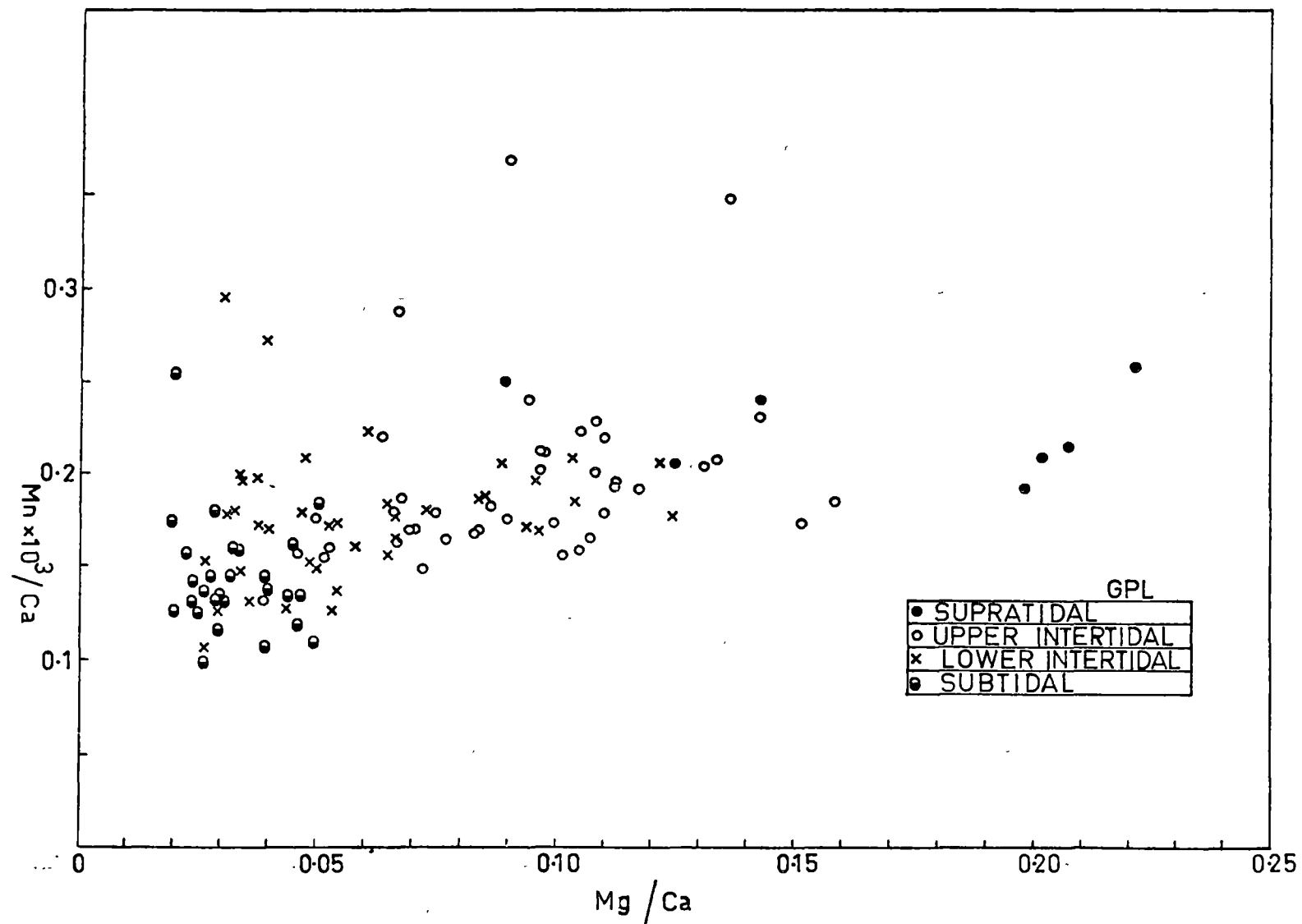


Fig. 4.11 Relationship of Mn/Ca molar ratio to Mg/Ca molar ratio in section GPL.

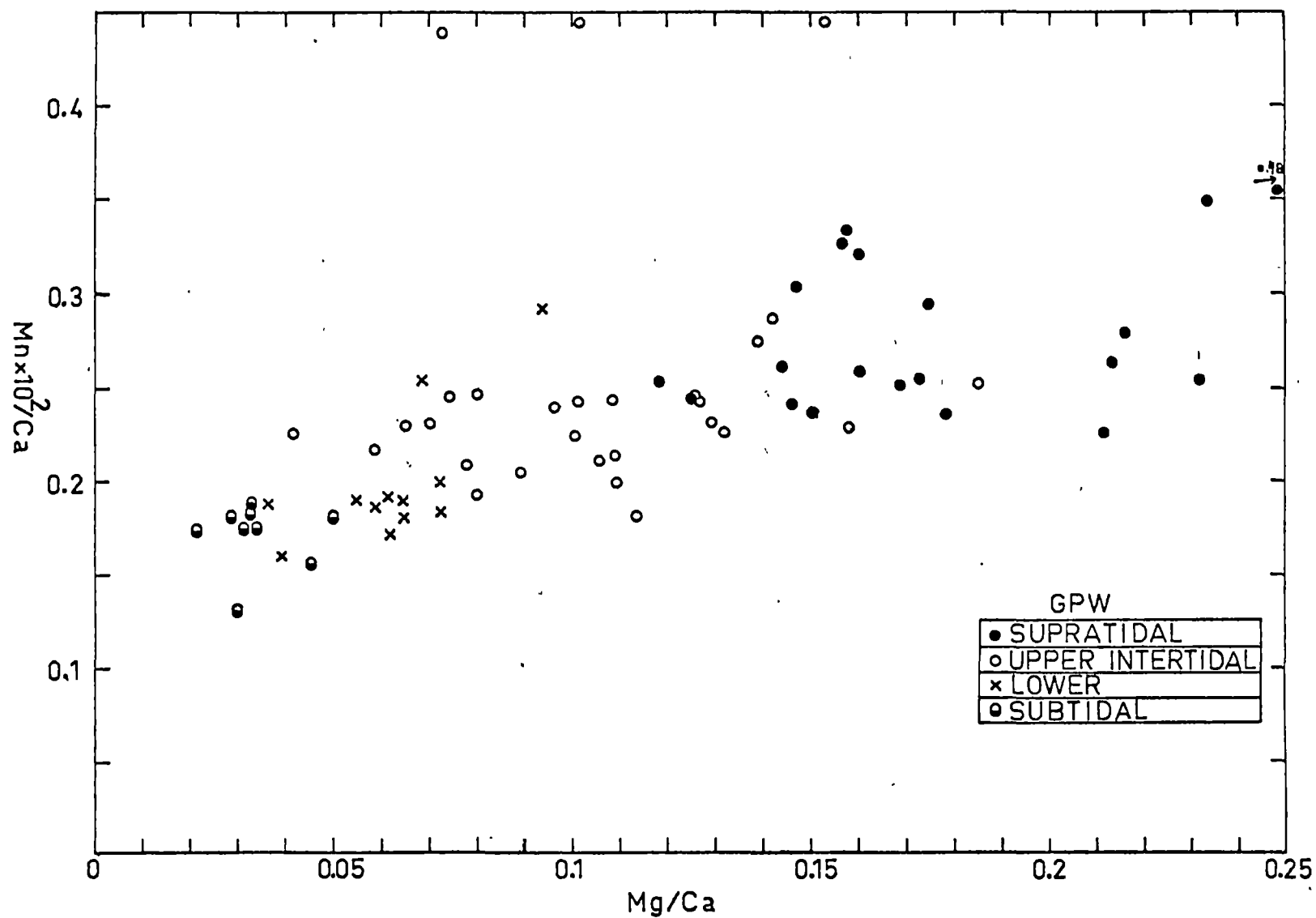


Fig. 4.12 Relationship of Mn/Ca molar ratio to Mg/Ca molar ratio in section GPW.

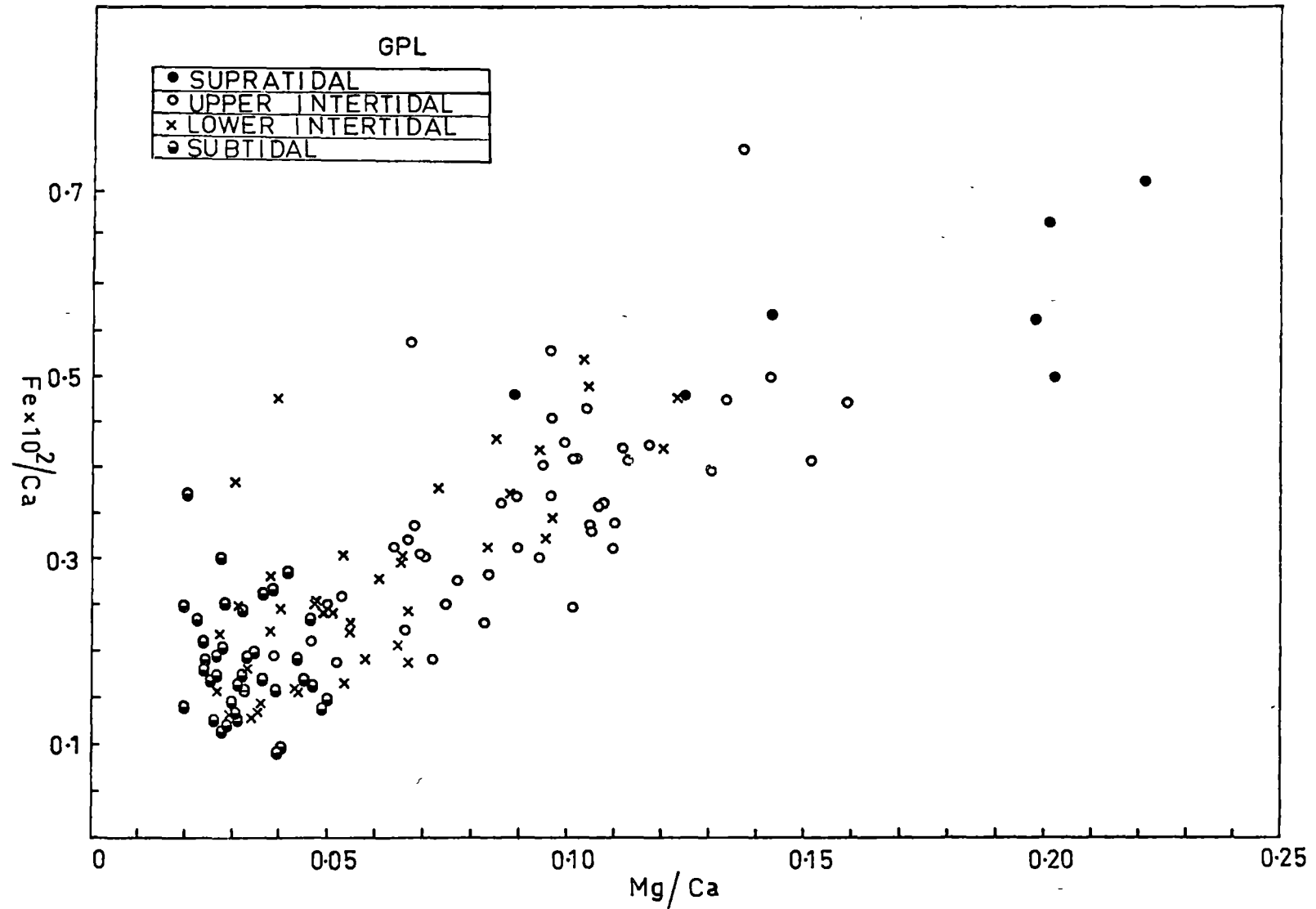


Fig. 4.13 Relationship of Fe/Ca molar ratio to Mg/Ca molar ratio in section GPL.

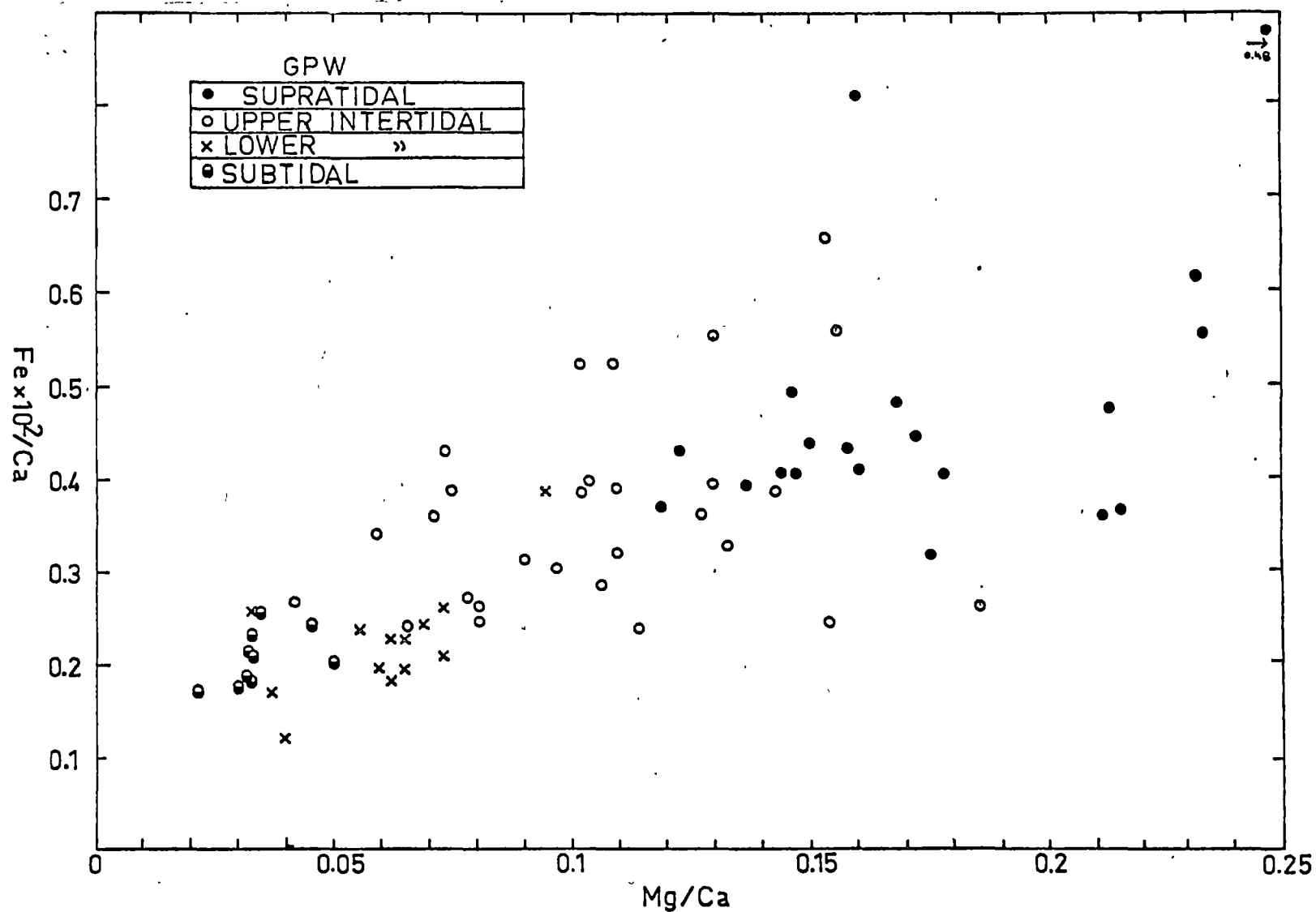


Fig. 4.14 Relationship of Fe/Ca molar ratio to Mg/Ca molar ratio in section GPW.

Iron and Manganese

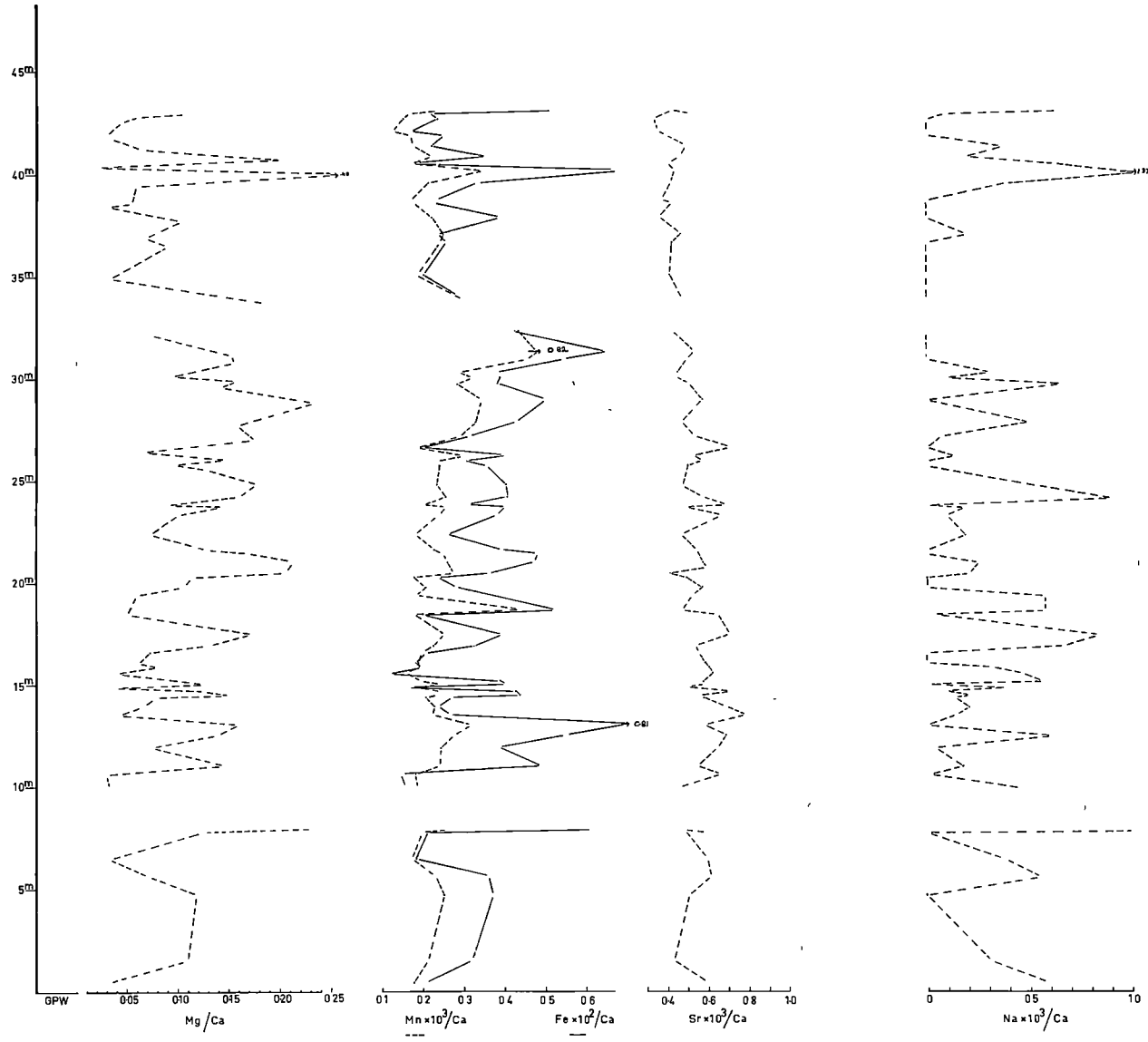
The relationship of Mg/Ca to Mn/Ca and Fe/Ca is shown in Figs. 4.11, 4.12, 4.13 and 4.14. The environmentally controlled variation of both Mn and Fe is very clearly evident from the figures with samples from the supratidal facies having a higher Mn and Fe content than samples from the subtidal facies. Similar observations were made by Cook (1973), who stated that manganization and ferruginization is related to supratidal dolomitization. In the case of iron, Land *et al.* (1975) observed a similar seaward decrease in the dolomites from the Eocene El Naqb Formation.

This increase of Mn and Fe in the supratidal facies suggests an external source for these elements during dolomitization.

Vertical Variation of Mg/Ca, Sr/Ca, Mn/Ca and Fe/Ca Molar Ratios

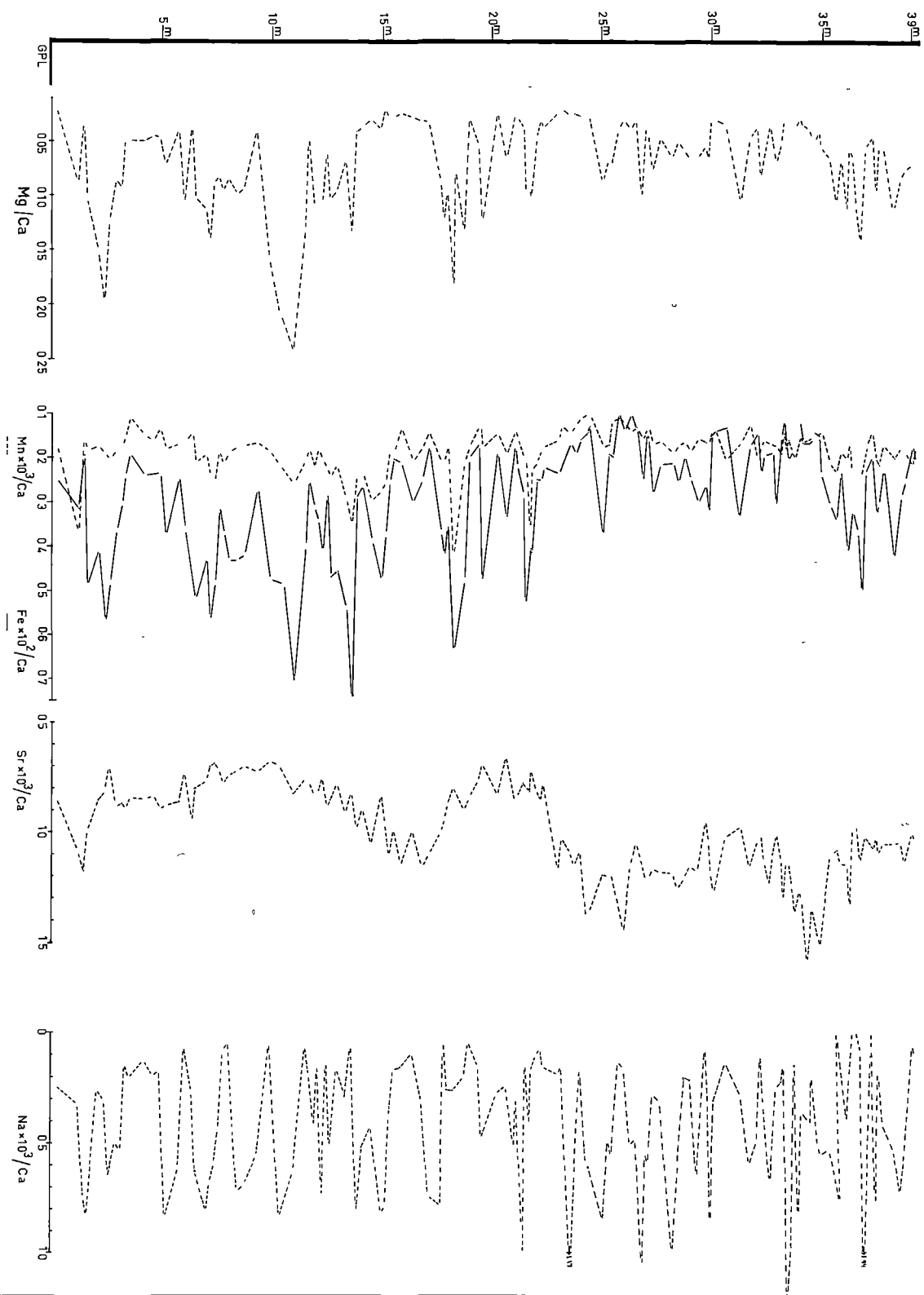
The vertical variation of Mg/Ca, Sr/Ca, Mn/Ca, Fe/Ca and Na/Ca in sections GPW and GPL is shown as Figs. 4.15 and 4.16 respectively. The similar relationship shown by Mn/Ca and Fe/Ca to Mg/Ca molar ratios and their increase in the supratidal facies compared to subtidal facies has already been mentioned. Figs. 4.15 and 4.16 show that this variation is related to the degree of dolomitization (amount of dolomite) in the different depositional cycles (see also Figs. 4.11 to 4.14). Thus different episodes of dolomitization of varying intensity have resulted in this distribution and have caused a corresponding decrease in the Sr/Ca molar ratios. Generally the subtidal facies of the different depositional cycles (containing less than 10% dolomite) have higher Sr/Ca molar ratios. The Na/Ca molar ratios are highly variable. In some depositional cycles, the subtidal samples contain more Na/Ca, whereas in other cycles higher values are more characteristic of the supratidal samples.

15
Fig. 4.14 Vertical variation of the major and minor elements
in section GPW.



SUBTIDAL			
INTERTIDAL	LOWER	UPPER	
SUPRATIDAL			

Fig. 4.16 Vertical variation of the major and minor elements
in section GPL.



INTERSTITIAL	SUBTIDAL	
	LOWER	
	UPPER	
SUPRATIDAL		

It must be kept in mind that the trends of increasing Mg, Mn and Fe and a corresponding decrease of Sr in the supratidal facies persist even if approximate increases of Mn and (?) iron, and losses of Sr during dedolomitization (Chapter 5) are taken into account. The Na values appear to have been the most modified in those cycles where dedolomitization has occurred.

Origin of Dolomites

Petrographic observations have demonstrated the early diagenetic, supratidal origin of dolomites in the study area. Fig. 4.4 is a photomicrograph showing a broken shell oriented with its convex side up. Micrite beneath the shell has remained unaffected, while elsewhere it has been replaced by dolomite. This evidence indicates that downward seepage of the dolomitizing brines took place. At the same time, other oriented shells were observed with no protected zones beneath them. Thus, besides the downward seepage, upward or lateral movement of the brines took place. The gradual decrease in the dolomite content towards the subtidal in the different cycles suggests a reflux type of mechanism. A general model for dolomitization in the Gunns Plains Limestone is shown as Fig. 4.17.

An increase in the Mn and Fe content in the supratidal facies (Fig. 4.15) compared to subtidal facies indicates influx of non-marine water during dolomitization. Strontium solution compositions indicate the presence of aragonite. Thus it seems likely that ground water passing through an aragonitic terrain could have been the agent responsible for bringing in Mn and Fe. Despite a loss of Na during dedolomitization (discussed in Chapter 5), high values of up to 205 ppm are still present in the dolomites suggesting the hypersaline character of the dolomitizing brines. It is believed that the mixing of ground water and marine water took place in an intermediate sabkha zone, similar to that reported by McKenzie *et al.* (1979) for the Abu Dhabi sabkhas in the Persian Gulf.

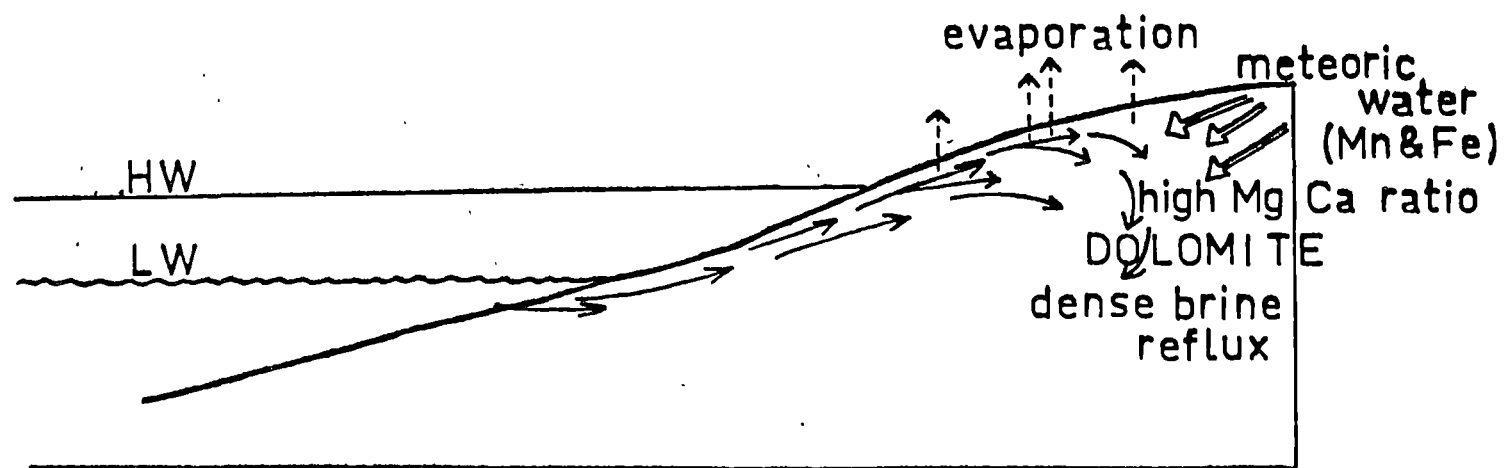


Fig. 4.17 A general model for dolomitization in the Gunns Plains Limestone.

Table 4.5

DISTRIBUTION (MEAN AND STANDARD DEVIATION OF MOLAR RATIOS)
RELATED TO INTERPRETED ENVIRONMENTS

GPL			GPW	
	Mean	Std.Dev.	Mean	Std.Dev.
<u>SUPRATIDAL</u>				
Mg/Ca	0.1736	0.0535	0.1875	0.0768
Sr x 10 ⁻³ /Ca	0.7417	0.0614	0.5344	0.0834
Mn x 10 ⁻³ /Ca	0.2213	0.0027	0.2768	0.0399
Na x 10 ⁻³ /Ca	0.5219	0.2656	0.3492	0.4136
Fe x 10 ⁻² /Ca	0.5682	0.1003	0.4716	0.1453
<u>UPPER INTERTIDAL</u>				
Mg/Ca	0.1028	0.0251	0.1115	0.0318
Sr x 10 ⁻³ /Ca	0.7749	0.0760	0.5382	0.0905
Mn x 10 ⁻³ /Ca	0.2078	0.0499	0.2485	0.0652
Na x 10 ⁻³ /Ca	0.2893	0.2506	0.1911	0.2570
Fe x 10 ⁻² /Ca	0.3919	0.1070	0.3586	0.1139
<u>LOWER INTERTIDAL</u>				
Mg/Ca	0.0810	0.0281	0.0715	0.0166
Sr x 10 ⁻³ /Ca	0.8038	0.0801	0.5024	0.1476
Mn x 10 ⁻³ /Ca	0.1988	0.0376	0.2141	0.0525
Na x 10 ⁻³ /Ca	0.3542	0.2491	0.1251	0.1536
Fe x 10 ⁻² /Ca	0.4009	0.1497	0.2712	0.0823
<u>SUBTIDAL</u>				
Mg/Ca	0.0346	0.0095	0.0348	0.0090
Sr x 10 ⁻³ /Ca	0.9975	0.1533	0.4471	0.1137
Mn x 10 ⁻³ /Ca	0.1533	0.0343	0.1706	0.0186
Na x 10 ⁻³ /Ca	0.4317	0.3271	0.1181	0.2124
Fe x 10 ⁻² /Ca	0.1848	0.0561	0.2101	0.0318

Table 4.5 summarizes the observed molar ratios of Mg/Ca, Sr/Ca, Mn/Ca, Fe/Ca and Na/Ca in the two laterally equivalent sections. Based on the greater amount of dolomite, Mg/Ca, Mn/Ca and Fe/Ca in section GPW (mostly supratidal and upper intertidal) compared to section GPL (mostly intertidal and subtidal), the generation of the dolomitization brines is believed to have been in the south (section GPW) and these brines moved northward (section GPL).

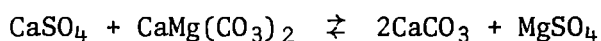
Chapter 5

DEDOLOMITIZATIONINTRODUCTION

The replacement of dolomite by calcite has been recognized since 1847, when Von Morlot coined the term "dedolomitization" for this process. Smit and Swett (1969), on valid grounds, objected to the use of this term and instead proposed "calcitization" as an appropriate name for this process. They used the term calcitization specifically for calcite after dolomite and not for other replacement processes such as the calcitization of anhydrite or gypsum, which may take place concurrently with the replacement of dolomite. As such it is a confusing term.

The term dedolomitization in spite of its limitations (Smit and Swett, 1969; Lippmann, 1973) is widely used (Shearman *et al.*, 1961; Folkman, 1969; Al-Hashimi and Hemingway, 1973; Longman and Mench, 1978; Hanshaw and Back, 1979; and many others), and sometimes dedolomitization and calcitization have been used synonymously (Friedman and Sanders, 1967; Lucia, 1961, 1972). In this study the term dedolomitization has been retained in the absence of a more suitable term.

According to many workers (citing Von Morlot, 1848), the process of dedolomitization is represented by the equation



The sulphate ions needed for the reaction are attributed to the dissolution of gypsum or anhydrite (Shearman *et al.*, 1961; De Groot, 1967; Lucia, 1972; Abbott, 1974; and many others), or the oxidation of pyrite (Evamy, 1963, 1969; Folkman, 1969). The process of dedolomitization can also take place in the absence of sulphate ions (Katz, 1968; Folkman, 1969; Al-Hashimi and Hemingway, 1973).

Dedolomitization is commonly considered to be a low temperature, low pressure, near-surface process (e.g. De Groot, 1967; Longman and Mench, 1978) resulting from physico-chemical changes in the depositional environment (Katz, 1971) or it may be late diagenetic (e.g. Folkman, 1969; Freeman, 1972). Different mechanisms have been proposed for dedolomitization and it is now believed that both fresh-water (e.g. Shearman *et al.*, 1961, 1969; Fritz, 1967; Goldberg, 1967; Lucia, 1972; Abbott, 1974; Jacka, 1977; Longman and Mench, 1978; Hanshaw and Back, 1979) and sea-water (Katz, 1971; Al-Hashimi and Hemingway, 1973; Al-Hashimi, 1976) can be the agents responsible for this important diagenetic process.

Most studies dealing with the elemental composition of carbonates as a function of diagenetic changes have not proceeded beyond the effects of dolomitization. It is considered that the trace element relationship inferred by different workers for dolomitization is not valid in cases where dedolomitization textures and fabrics have been recognized. This is based on the inference that as dedolomitization, like other diagenetic processes, results in changes in the texture, mineralogy and chemistry of the carbonate rocks, the trace elements in the dolomites (and dolomitic limestones) must surely have been affected. Therefore, in order to study the trace element geochemistry in limestones which have undergone dolomitization and dedolomitization, it is essential to take into consideration the changes due to dedolomitization. It is believed that for such an integrated study (dolomitization and dedolomitization), the first requirement is to overcome the problem of estimating the amount of dolomite affected by dedolomitization. The relationship of trace element concentrations to degree of dedolomitization can then be inferred. Only after considering the overprints of dedolomitization on the dolomites can trace element concentrations be ascribed to the process of dolomitization.

This leads subsequently to a fuller understanding of diagenetic and depositional changes in carbonate rocks. The different aspects of dedolomitization are discussed in this chapter.

PETROGRAPHY

Earlier works dealing with dedolomitization are in European languages other than English. The recognition and description of dedolomitization textures and fabrics (in English) are mostly the work of Shearman, Khoui and Taha (1961), Lucia (1961) and Evamy (1963, 1967). Prior to that Chilingar (1956) reviewed the Russian work of Tatarskiy (1949) and Yana'teva (1955).

Most studies dealing with carbonate diagenesis in ancient rocks show the presence of dedolomitization textures (some in photographs without mentioning the phenomenon explicitly). These dedolomitization features can be recognized in peels and thin sections (both stained and unstained). In unstained peels, as Braun and Friedman (1970) have pointed out, the identification of dedolomitization features and their differentiation from recrystallized ones requires the use of crossed-nicols. However, in stained peels and (stained and unstained) thin sections most of the dedolomitization features are visible both in plane-polarized light and under crossed-nicols. Some may require the use of slightly higher magnifications than used for identifying depositional textures.

Criteria for the petrographic recognition of dedolomites (the calcite which has replaced dolomite) and their occurrence in the Gunns Plains Limestone are shown in Table 5.1. Commonly more than one type of dedolomitization texture is present in a single sample. Also the degree to which the individual dolomite crystals are affected is highly variable.

Table 5.1

PETROGRAPHIC CRITERIA FOR RECOGNITION OF DEDOLOMITES

	GUNNS PLAINS LIMESTONE		
	Abundant	Common	Rare
Relics of incompletely replaced dolomite crystals (Shearman, <i>et al.</i> , 1961)	x	-	-
Ghosts (grain boundaries of earlier dolomite crystals) within the new generation of calcite (relict rims of Lucia, 1972; palimpsest texture of Shearman <i>et al.</i> , 1961)	-	x	-
Clots of finely crystalline calcite replacing dolomite	-	x	-
Syntaxial calcite borders on dolomite crystals (calcite rims of Zenger, 1973)	-	-	-
Clotted texture (Shearman <i>et al.</i> , 1961; Evamy, 1967)	-	-	-
Rhombohedral mosaics composed of equigranular anhedral calcite (composite calcite rhombohedra of Shearman <i>et al.</i> , 1961; Evamy, 1967)	-	x	-
Rhombohedral pores (Evamy, 1967)	-	x	-
Calcite crystals ranging from 0.1 to 1.0 mm and containing inclusions of dolomite (lacy calcite lenses of Lucia, 1961)	-	-	x
Coarse sparry calcite ranging from 0.25 to 5.0 mm and mimicking pore-filling calcite (pseudospar dedolomite currents of Moore, 1971)	-	-	x

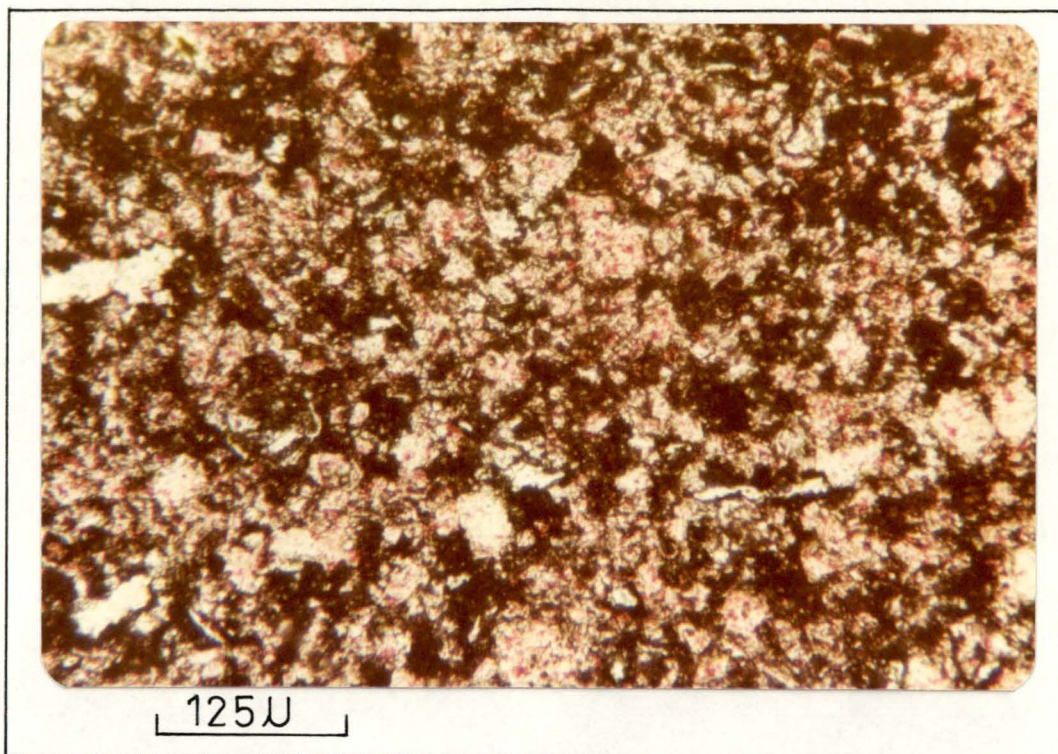


Fig.5.1.Clots of finely crystalline calcite(dedolomite) on dolomite.Sample treated with alizarin-redS and potassium ferri-cyanide.

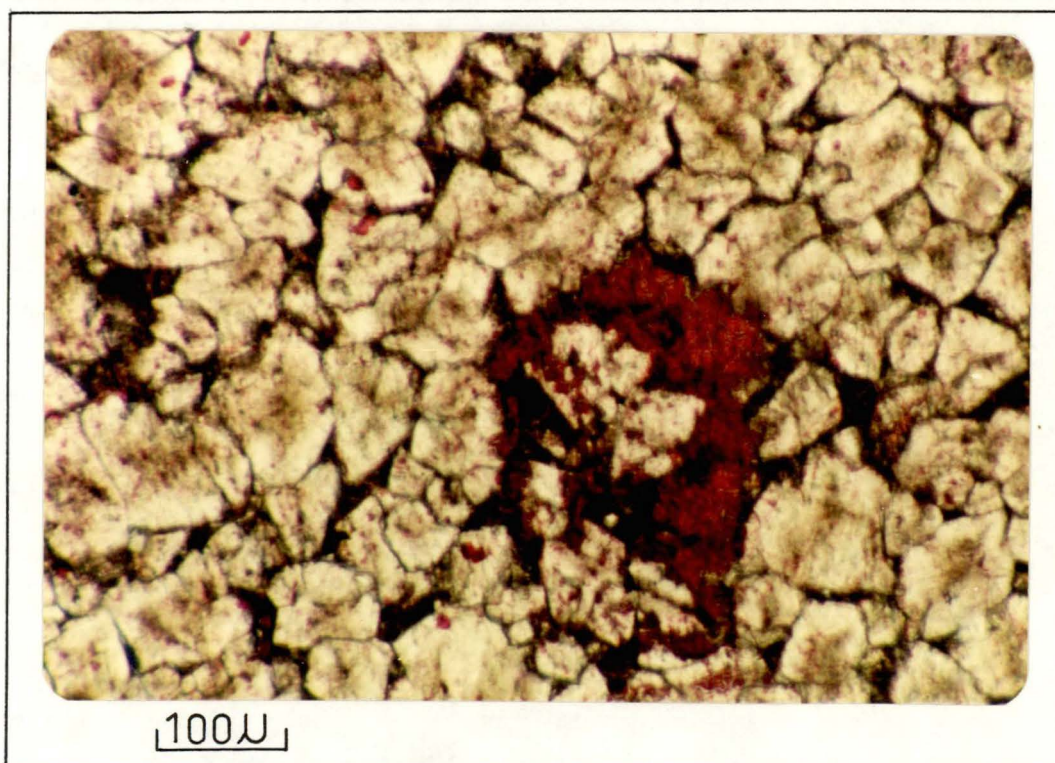


Fig.5.2.Clots of finely crystalline calcite on dolomite. Note the gradation of clots into a mosaic of anhedra calcite crystals(Composite calcite rhombohedra).Sample treated with alizarin-redS and potassium ferri-cyanide.

A dolomite crystal may exhibit only a small clot of calcite (dedolomite) or the whole crystal may be replaced by dedolomite (as in Fig. 5.2). As it is not possible to make a quantitative petrographic estimate of the dedolomite content, the following is only a general description of the features observed.

1. Clots of finely crystalline calcite replacing dolomite can only be seen in stained thin sections at magnifications above 6.5x.

However, partly or wholly replaced dedolomite rhombs occurring in the same sample and formed as a result of concentration of many small clots can be seen even at low magnifications. Figs. 5.1 and 5.2 are photomicrographs of stained samples showing clots of fine dedolomite as well as partly to wholly dedolomitized rhombs. The clots of fine dedolomite may occur on any part of the dolomite rhomb including the margins.

According to Evamy (1967), the relict inclusions occur universally in dolomite that has replaced calcite. That these clots are not relict calcite inclusions (pre-dolomitization calcite) is evidenced in samples where in a dense mosaic of dolomite crystals, a clot may be observed to continue from one rhomb across the rhombic margins into an adjacent rhomb.

2. Rhombs with well-defined boundaries and consisting of a mosaic of very small anhedral sparry calcite crystals are common in the Gunns Plains Limestone (Figs. 5.2, 5.3 and 5.4). These pseudomorphs of calcite after dolomite, termed "composite calcite rhombohedra" (Shearman *et al.*, 1961; Evamy, 1967), occur in rhombs less than 50 μ in size. As will be discussed later, the mosaics of anhedral crystals shown in Fig. 5.2 are believed to be a result of direct replacement, whereas those shown in Fig. 5.4 are considered to have formed after selective leaching following Evamy (1967, Fig. 1).

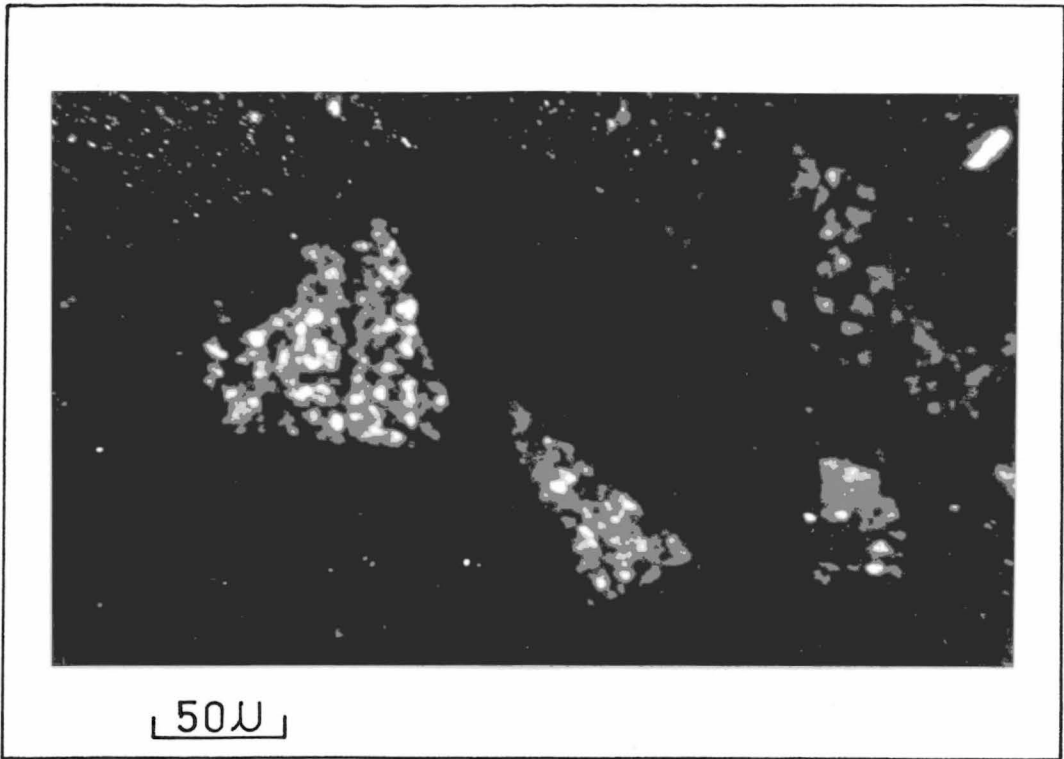


Fig.5.3.Composite calcite rhombohedra. X-nicols.

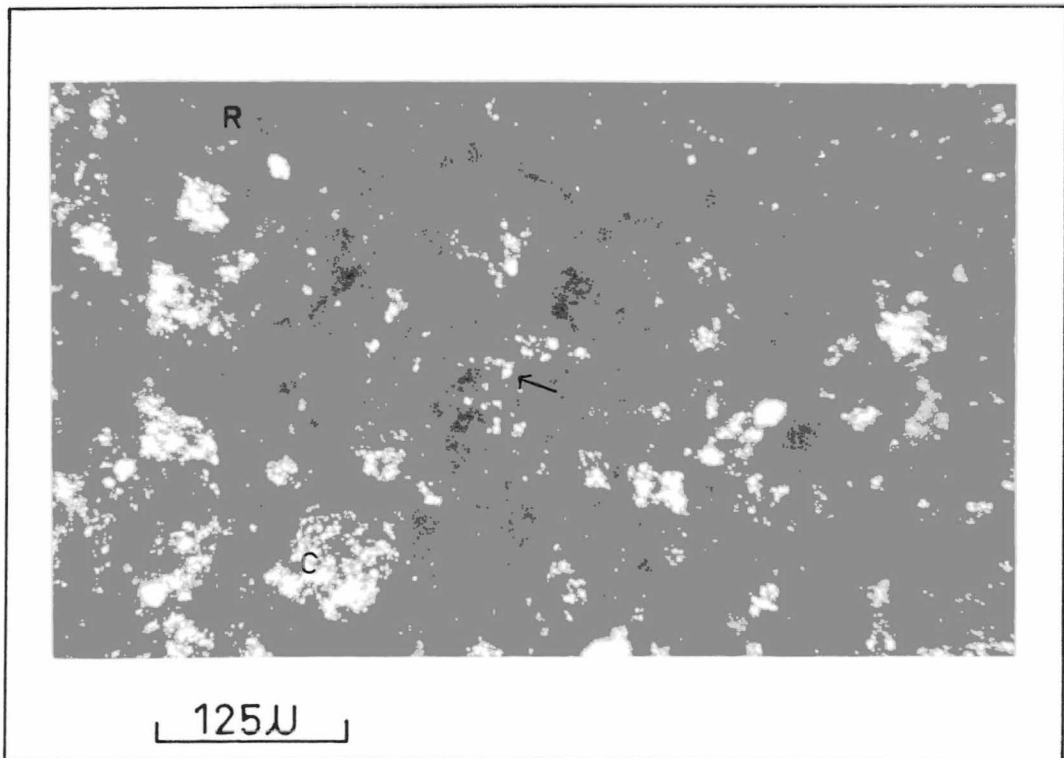


Fig.5.4.Composite calcite rhombohedra(C) and abundant rhombic pores(R).Note the presence of anhedral calcite crystals within rhombic pores(shown by arrow).X-nicols.

3. Sparry calcite (dedolomite) has replaced only the outer parts of the dolomite rhombs, while the centres have remained unaffected (Fig. 5.5). This is the most common type of dedolomitization observed in the Gunns Plains Limestone. The whole range from a dolomite rhomb replaced by dedolomite on only one side to a continuous dedolomite zone surrounding the dolomite core is found. The width of the dedolomite zone is usually fairly uniform in a single crystal, but in a whole sample the dedolomite zones are of variable width. Dedolomite may extend outwards from the rhombohedral boundaries into the intergranular pore space or micrite, while still retaining the rhombohedral shape with well-pronounced margins showing very small indentations and projections. The core generally consists of yellowish-brown dolomite and is commonly larger than the surrounding dedolomite zone, but rhombs with a bigger dedolomite zone and smaller core also exist. In some such cases, the dolomite in the core (Chilingar, 1956) is only just visible. Rhombs ranging up to 25μ in size appear to be more susceptible to dedolomitization in that they are commonly entirely replaced by dedolomite or show only dolomite "dust" in the core. The bigger rhombs, ranging between 25μ and 50μ mostly have continuous or discontinuous dedolomite zones about a dolomite core. In some dolomite rhombs of the same sample, the dedolomite instead of enclosing an entire rhomb may extend inwards from the margins on two or three sides only, the other sides remaining unaffected.

In the Gunns Plains Limestone (all measured sections), there are samples in which the dedolomite zones are breached in at least three or four places, but otherwise give the appearance of having been continuous envelopes (Fig. 5.6). In such cases, the dolomite is absent from the core, which is always larger in area than the dedolomite zone. Instead, dark calcite (micrite) similar to that occurring outside the rhombs is found in the core. A single sample is mostly characterized by rhombs of

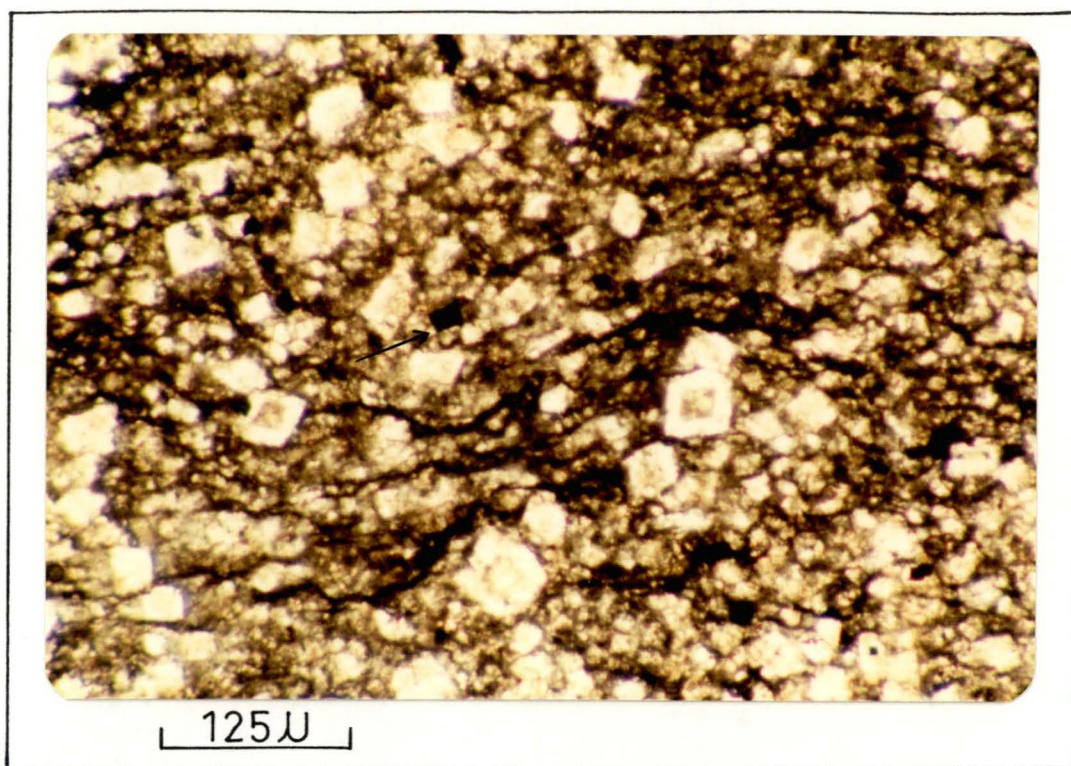


Fig.5.5. Partly to completely dedolomitized rhombs. Pyrite shown by arrow. The black organic laminae are believed to be algal mat.

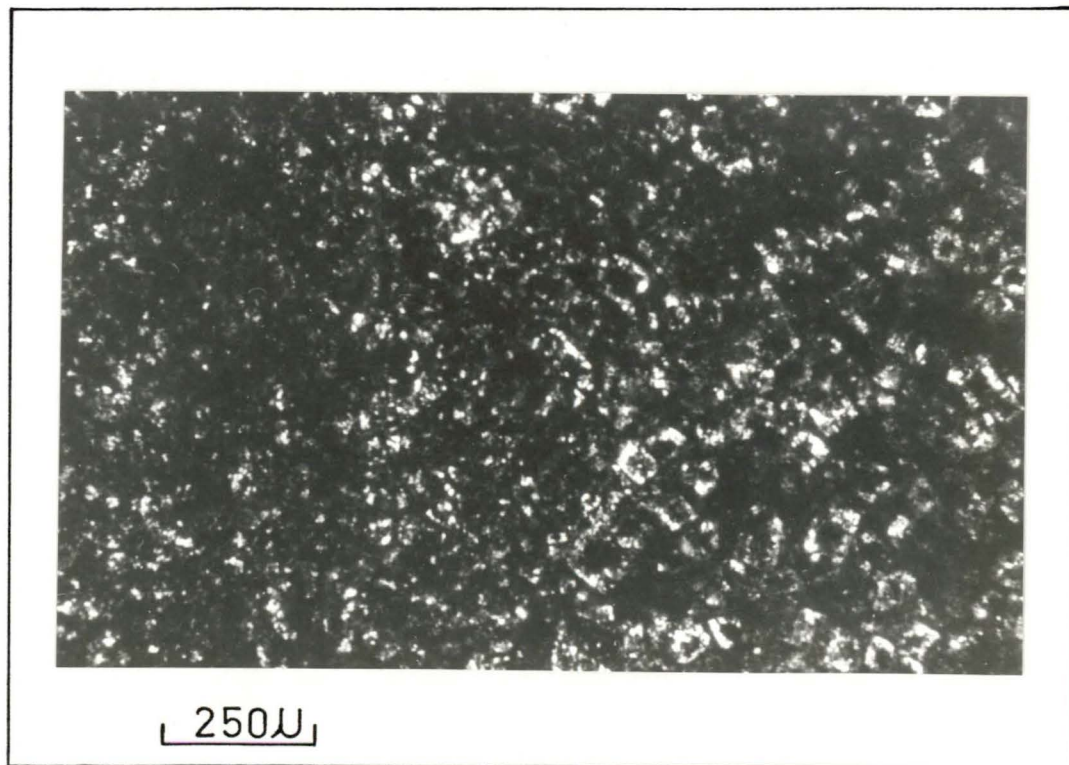


Fig.5.6. Breached dedolomite zones in a micrite matrix. Some are only faintly visible. X-nicols.



Fig.5.7. Patches of dedolomite. Note the well-defined crystal boundaries where dedolomitization has occurred.

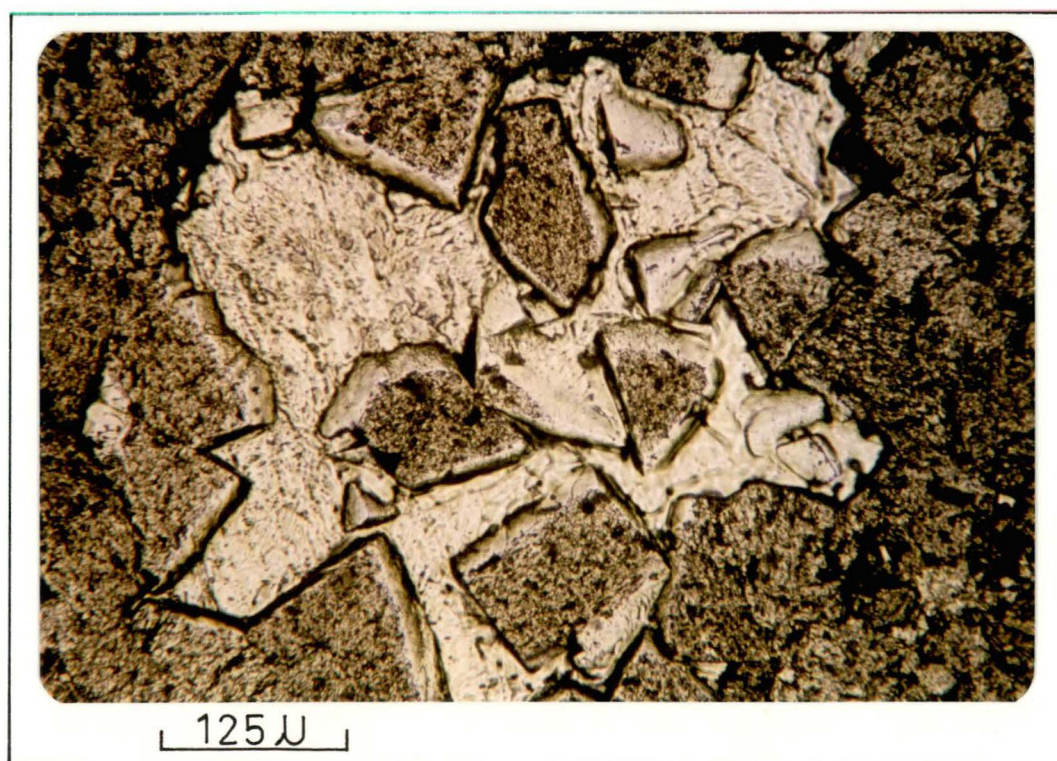


Fig.5.8. Enlarged view of one of the patches of dedolomite shown in Fig.5.7.

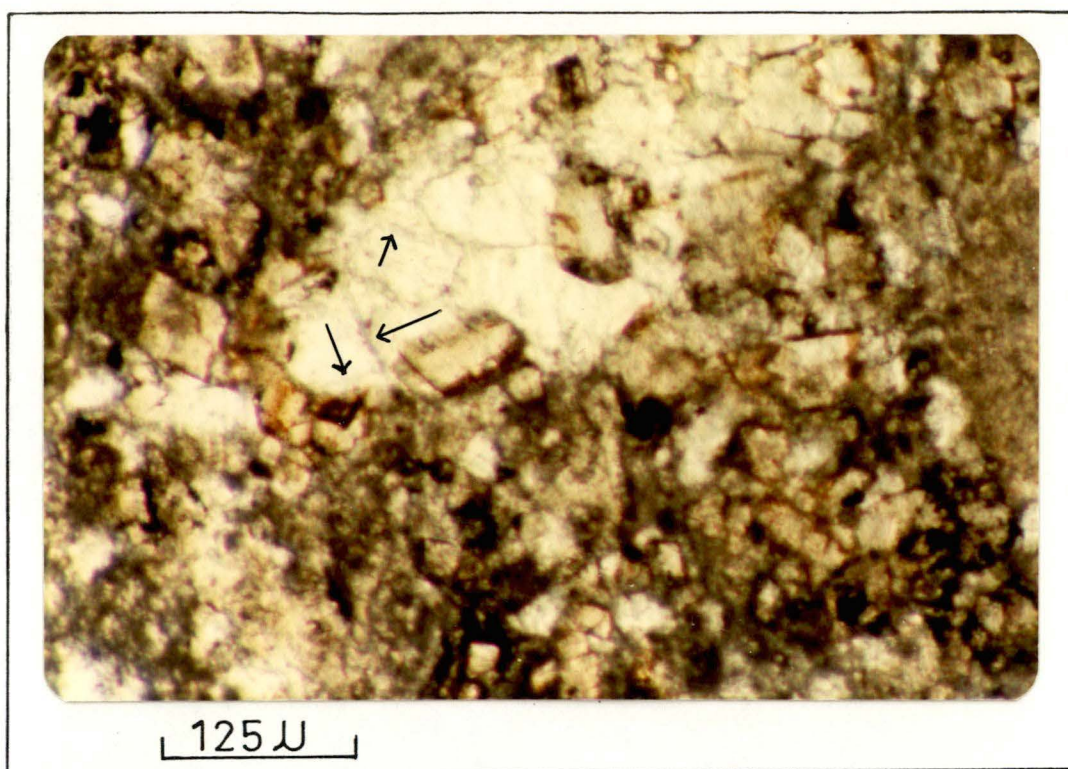


Fig. 5.9. Palimpsest texture. Arrows point to boundaries of former dolomite crystals. Iron oxide rims are also visible.

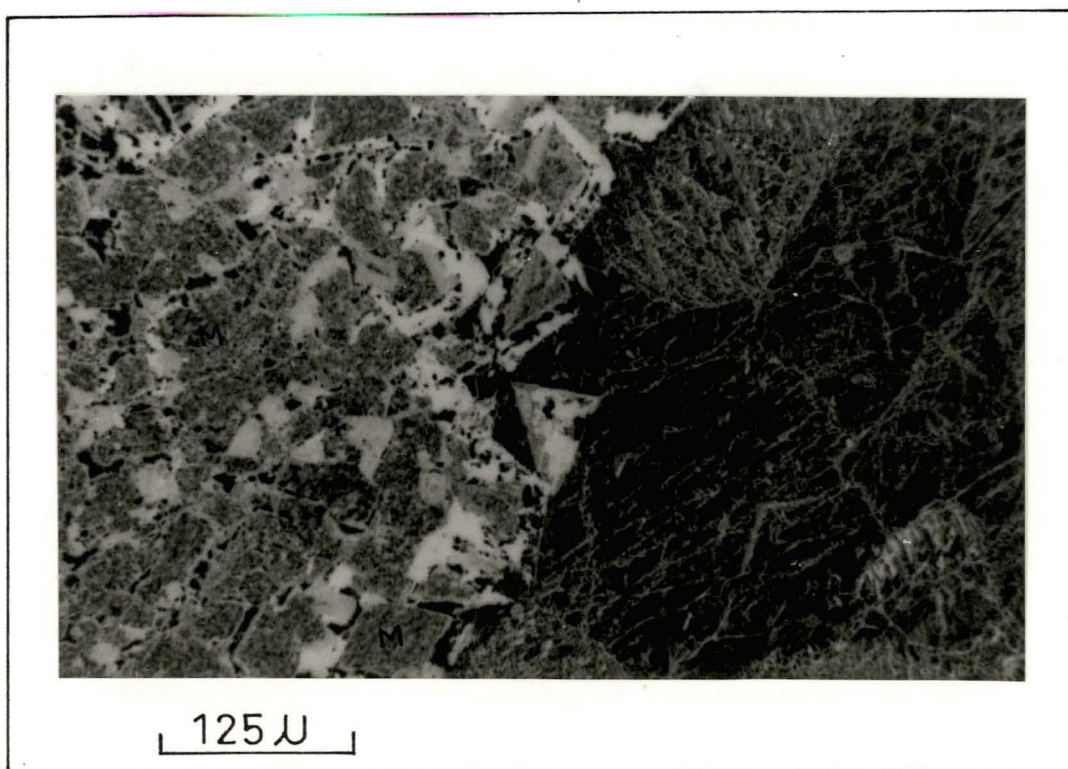


Fig. 5.10 Ghosts of earlier dolomite crystals (M) in a micrite matrix. Lacy calcite lenses (see text) to the right of centre in the photomicrograph. X - nicols.

similar size, the common size being 25 μ . It seems likely that the dolomite core and missing parts of the dedolomite zone have been dissolved away.

4. Certain samples in sections GPB and GPR contain a closely packed mosaic of dolomite crystals dominantly with mutual anhedral to subhedral boundaries (Figs. 5.7 and 5.8). The occurrence of dedolomite in these samples is restricted to small isolated patches similar to Plate 3A of Shearman *et al.* (1961). Commonly a single patch consists of seven to ten dolomite crystals which appear to have been dedolomitized.

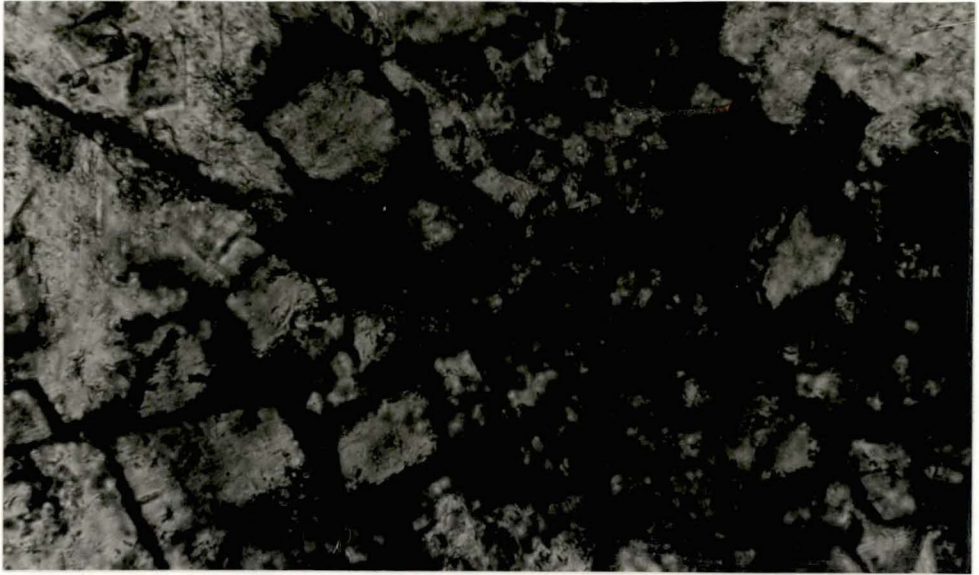
A notable feature of these patches is that the dolomite crystals (including those that have been completely replaced and are only observed as ghosts) have well-developed euhedral boundaries, in contrast to neighbouring dolomite unaffected by dedolomitization. In such cases, the dedolomite may be confined to only one side of the dolomite crystals or form continuous enveloping dedolomite zones similar to those described earlier. The width of the dedolomite zone is variable within a single crystal and may extend to the centre, resulting in a whole dedolomite crystal. Dedolomite may also occur between the closely-spaced rhombic margins, and this suggests an extension of the dedolomite zone even into the intergranular pore space.

5. The palimpsest texture described by Shearman *et al.* (1961) as a coarse-grained mosaic of calcite crystals enclosing a number of dolomite crystal ghosts occurs in some samples of the Gunns Plains Limestone. Shearman *et al.* (1961) described whole thin sections showing only palimpsest texture. In the studied samples, the granular mosaic of sparry calcite (dedolomite) has not replaced all the dolomite crystals within a single sample as can be seen in Fig. 5.9. All gradations from partly replaced to completely replaced dolomite rhombs can be observed within a

distance of less than 1 mm. The completely replaced dolomite rhombs in sparry calcite mosaics are mostly recognizable by their straight boundaries and by the fact that these faintly visible rhombohedral ghosts are of similar size to the adjacent unaffected or partly replaced rhombs. The unaffected dolomite rhombs mostly have a reddish-brown iron oxide-rich rim, which is only faintly visible or completely absent in dedolomitized rhombs.

6. In some micrites containing up to 50% dolomite, the equigranular mosaic of euhedral to subhedral dolomite crystals, within a single sample is observed to grade into calcite (micrite) containing only prominent, continuous or discontinuous brown (iron oxide) rhombic outlines similar to those shown in Fig. 5.10. These ghosts or grain boundaries of the earlier dolomite crystals ("relict rims" of Lucia, 1972; "pseudomorphs of calcite after dolomite" of Shearman *et al.*, 1961) are restricted in their occurrence, being confined to only a few millimetres in any sample.

In a very few cases, coarse sparry calcite occurs adjacent to the ghosts or relict rims of earlier dolomite crystals (Fig. 5.10). This coarse sparry calcite is not pore-filling calcite, but is similar to the lacy calcite lenses described and interpreted by Lucia (1961) as replacement calcite formed after the leaching of anhydrite or probably gypsum. Lacy calcite lenses not associated with relict rims also occur sparsely in the Gunns Plains Limestone and may contain "floating" rhombs of poikilitically enclosed dolomite about 10μ in size. The term "lacy calcite" (following Lucia, 1961) has been used for such textures in this study although a texture similar to the lacy calcite lenses has been described by Moore (1971) as "pseudospar dedolomite cements". These two different terms have probably been used for the same dedolomitization texture. The lacy calcite lenses and pseudospar dedolomite cements both



125 U

Fig.5.II.Dedolomitized rhombs with dark boundaries. Some show effects of leaching. X-nicols.



125 U

Fig,5.I2.Dolomite rhombs with calcite cores(dedolomite). Sample treated with alizarin-redS and potassium ferri-cyanide.

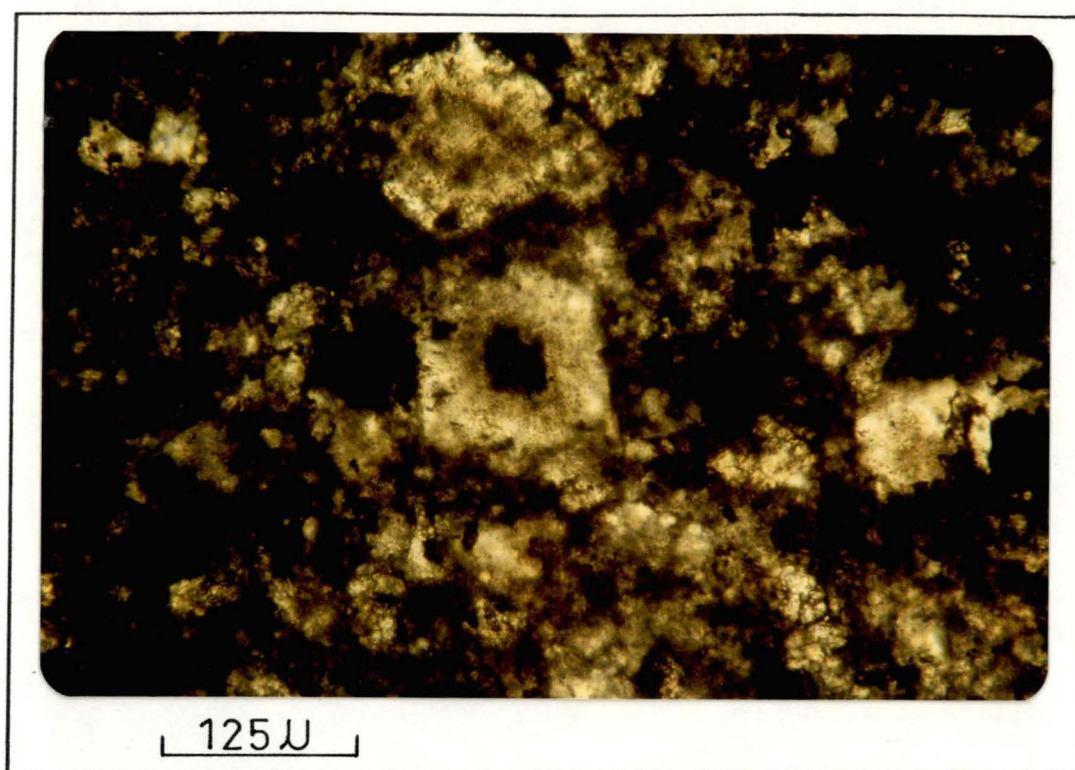


Fig.5.I3.Rhombic pores. X-nicols.

consist of calcite rhombohedrons with dolomite inclusions or tiny dolomite crystals and mimic pore-filling calcite. According to Lucia (1961), the calcite crystal size varies between 0.1 mm to 1.0 mm, while according to Moore (1971), the size of the crystals ranges between 0.25 mm to 5.0 mm. Except for this difference in crystal size, the descriptions are similar. Both authors suggest the leaching of anhydrite or gypsum to form this texture. Moore (1971) uses the term "cement", but at the same time reasons that they are not "true cements".

7. In section GPW, there are whole dedolomite rhombs with or without cloudy centres. They differ from other dedolomite rhombs in that they are bounded by narrow, dark zones containing no dedolomite (Fig. 5.11). These rhombic boundaries are straight, of uniform width and of low relief. Small fractures filled with dedolomite may occur perpendicular to the dark rhombic boundaries and extend inwards from the margins towards the centre. Dedolomite may also occur outside the distinct rhombohedral margins on one or more sides. In such cases, the fractures and dark boundaries disappear. The occurrence of these dedolomite rhombs in clusters results in the formation of a mosaic with rhombic outlines not visible or faintly visible. All of these textural varieties may be present in a single sample.

8. Rhombs with cores of calcite and an enveloping zone of dolomite

(Fig. 5.12) are of rare occurrence in the study area. They usually occur in samples which also contain rhombs with discontinuous enveloping zones of dedolomite and dolomite cores. The boundary between the calcite core and the dolomite zone is sharp and may be serrated. The dolomite zones may or may not be of uniform width. Commonly the larger rhombs (about 50 μ in size) show this texture.

9. Rhombic pores ranging from about 10μ to 50μ (Figs. 5.4 and 5.13)

occur in association with the dedolomitization textures described above. Commonly the rhombic pores have sharp and straight outlines, but rarely, curved or serrated outlines are observed. Usually the rhombic pores are randomly distributed, except in a few samples in section GPW where they occur in clusters adjacent to dolomite rhombs. The pores in the clusters may or may not contain anhedral calcite (Fig. 5.4). Bausch (1965) and others consider the rhombic pores to have formed as a result of solution of dolomite. Evamy (1967) concludes that the rhombic pores are formed by the selective leaching of high-Mg calcite or aragonite which may be the initial products of dedolomitization.

REGENERATION OF EARLIER TEXTURE DUE TO DEDOLOMITIZATION

Dedolomitization in certain cases is believed to result in the regeneration of the pre-dolomitization texture (Shearman *et al.*, 1961; Evamy, 1967; Wolfe, 1970).

In the Gunns Plains Limestone, the carbonate rock types are dominantly micritic (Chapter 3) and in such rocks, cementation mosaics seldom occur. Syntaxial overgrowths on echinoderm fragments occur in very few samples from section GPW, but rhombic zones [such as those described by Shearman *et al.* (1961) as occurring at the boundary of two secondary overgrowths with crystallographic continuity across the whole area] are not present. Evamy (1967) described the regeneration of the pre-dolomitization texture in pelletal and oolitic limestone due to dedolomitization. This too, was not observed in the studied samples. Wolfe (1970) recognized coccolith fragments (micrite) in the non-ferroan calcite cores of dolomite rhombs. He concluded that the original coccolith micrite had regenerated as a result of dedolomitization. Based on Evamy's (1967) reasoning that during dedolomitization the growth of

new calcite (dedolomite) is controlled by the orientation of the relict calcite inclusions in dolomite, Wolfe (1970) concluded that the dedolomite fabric depends on the orientation of the relict inclusions. He proposed that, if the relict inclusions had a single orientation then the dedolomitization fabric mimicked the dolomite, whereas if the calcite inclusions were randomly oriented (as they must have been in the coccolith micrite) then the dedolomitization fabric regenerated the pre-dolomitization fabric.

In the present study, the only dedolomitization texture which may be a result of regeneration of an earlier fabric are the micritic areas present in relict rims (described as type 5 dedolomitization texture). They consist of rhombic outlines in a micrite matrix and are interpreted to be the remnants of the former euhedral dolomite crystals. This is based on the observation that adjacent to these relict rims on one side are dolomite rhombs and the contact between them is gradational. Laterally no relict rims are visible in a micrite which is similar to that within the relict rims. This similarity of micrite both within and outside the relict rims indicates that the pre-dolomitization fabrics were also alike irrespective of the origin and mineralogy of the fabric. Otherwise, the two micrites would have had different textures as a result of different diagenetic histories.

TYPE OF DEDOLOMITIZATION

Shearman *et al.* (1961), on the basis of dedolomitization textures in carbonate rocks from the French Jura distinguished between centripetal and centrifugal dedolomitization. In centripetal dedolomitization the dolomite crystals are replaced from the outside by calcite extending inwards to the centre, while in centrifugal dedolomitization the dolomite

rhombs are replaced from the inside by calcite (the dedolomite extending outwards from the centre). Most later workers do not mention the type of dedolomitization involved although their photographs and discussion in the texts indicate that one or both types occur. Some workers (e.g. Fritz, 1967, Fig. 7; Evamy, 1967, Fig. 1; Al-Hashimi and Hemingway, 1973, Fig. 5) on the basis of observed dedolomitization textures have constructed diagrams to show dedolomitization effects on dolomite crystals and have implied centrifugal or centripetal dedolomitization.

In the Gunns Plains Limestone, the dolomite crystals have not been uniformly affected by dedolomitization with the result that partly to completely replaced dolomite rhombs commonly occur together in a single sample. Observation of these textures suggests that most have formed as a result of the centripetal type of dedolomitization. The only textures in the study area, which can be ascribed to centrifugal dedolomitization are the rarely occurring dolomite rhombs with calcite cores (described as type 8).

The clots of finely crystalline calcite on dolomite (as in Figs. 5.1 and 5.2) appear to have been randomly generated. Therefore, they are different from the centripetal and centrifugal type of dedolomitization. It is proposed that such types be called the random type of dedolomitization. Shearman *et al.* (1961) considers the complete to partly formed composite calcite rhombohedra (described as type 2) to have formed by centrifugal dedolomitization. In the study area, the occurrence of clots of finely crystalline calcite in association with partly to wholly formed mosaics of anhedral calcite crystals in composite calcite rhombohedra (Fig. 5.2) is observed. This seems to indicate that the mosaics of anhedral calcite crystals (in composite calcite rhombohedra) are formed as a result of formation of many clots on dolomite. Thus, they have not originated due to centrifugal dedolomitization as originally proposed by Shearman *et al.*

(1961), but as a result of random type of dedolomitization. On the other hand, mosaics of anhedral calcite crystals formed in rhombic pores as in Fig. 5.4 may or may not have resulted due to centrifugal dedolomitization.

TYPE OF DOLOMITE (affected by dedolomitization)

In the present study, only a few samples chosen at random were subjected to X-ray Diffraction (XRD). The non-carbonate minerals present are illite and quartz, while the carbonate minerals present are calcite and dolomite. No protodolomite was detected. The dolomite peaks were observed at $2\theta = 30.92, 30.90$ and 30.82 giving "d" spacings between 2.89 and 2.90 \AA (see Fig. E.1 in Appendix E), and corresponding to ideal dolomites and ferroan dolomites. In further discussion, the dolomites (in spite of iron substituting in some of them) are assumed to be ideal dolomites.

Katz (1968, 1970) in his study of the Jurassic Mahmal Formation (Israel) concluded that calcian dolomites were preferentially dedolomitized (compared to ideal dolomite) during the growth of the dolomite crystals. Lippmann (1973) postulated that although it is hard to prove the higher solubility of calcian dolomites, they are more soluble than dolomite. As such, what is known as the process of dedolomitization may actually be the dissolution of calcian dolomites accompanied by the reprecipitation of calcium carbonate. However, Wolfe (1970), Scholle (1971), and Al-Hashimi and Hemingway (1973) demonstrated that ferroan dolomites can become dedolomitized and Rao and Naqvi (1977) observed dedolomite fabrics in ideal dolomites. Thus, it follows that any type of dolomite can be dedolomitized.

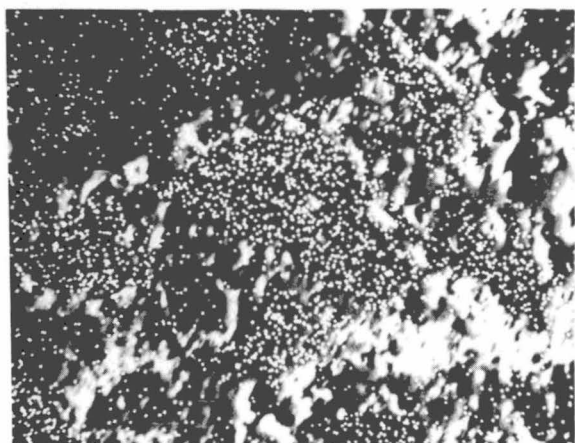
CHEMICAL EVIDENCE FOR DEDOLOMITIZATION

It is widely accepted that the Mg present in ancient carbonate rocks is a measure of the dolomite content. Therefore, the replacement of dolomite by calcite should result in a loss of Mg. De Groot (1967) in his experimental work on dedolomitization has demonstrated the removal of Mg ions from an ideal dolomite and precipitation of a Mg-free calcite. Other workers (e.g. Scholle, 1971; Katz, 1971; Basnayake, 1975) have used electron-probe analysis (Ca and Mg scans across dolomite crystals) to demonstrate dedolomitization.

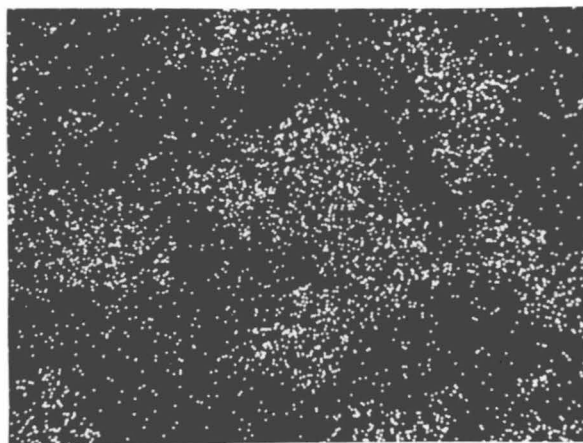
In the present study, five samples were selected for electron-probe analysis (see Appendix F). The secondary electron images and Ca and Mg X-ray distribution maps of dolomite crystals which have been partly dedolomitized (the most common type of dedolomitization in the Gunns Plains Limestone) are shown in Figs. 5.14, 5.15 and 5.16. The higher Ca (with little or no Mg) towards the margins of the crystals in Figs. 5.14 and 5.15 clearly demonstrates centripetal dedolomitization.

Chemical evidence for dedolomitization can also be obtained from atomic absorption spectroscopy. Prior to relating the chemical data to the petrographic observations, it is essential that the peels/thin sections and solutions for chemical analyses (Appendix C.1) be made from the same parts of the samples, as the Mg/Ca molar ratio can vary even within a single sample. This can be observed in Table 4.4, where 10 analyses of ~~six~~ ^{five} samples (two analyses from adjacent parts of each sample) show variable values of Mg/Ca.

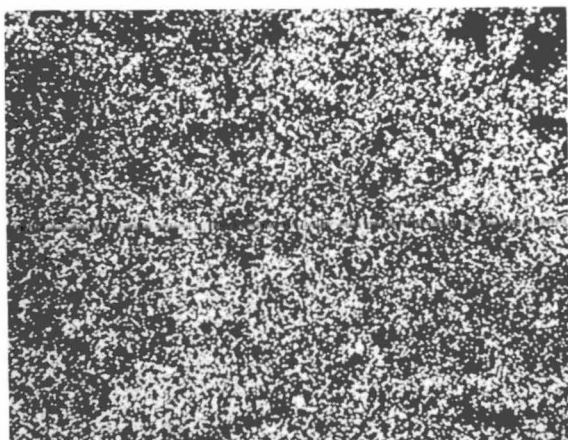
Dolomite rhombs which now appear as dedolomite rhombs were also included in the point counting and visual estimates of the dolomite content (Chapter 4, p. 78). Those samples in which it was difficult to make a distinction between pore-filling calcite and dedolomite fabric



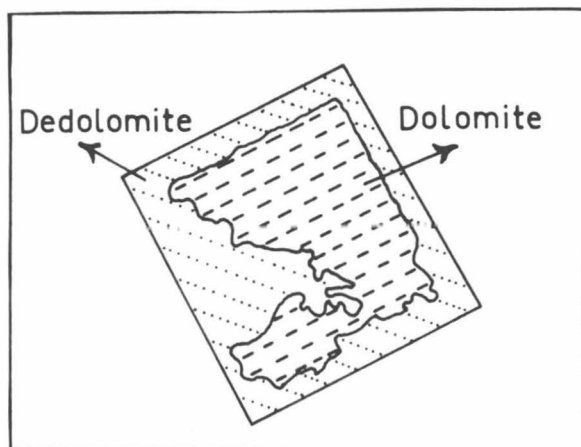
(a)



(b)

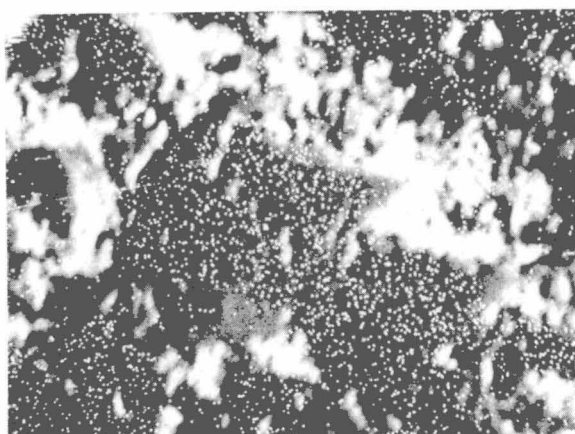


(c)

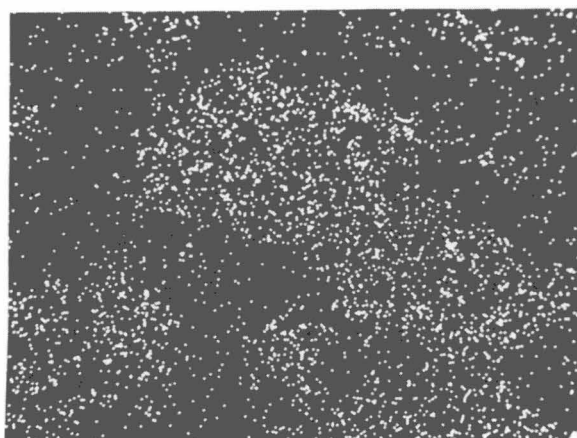


(d)

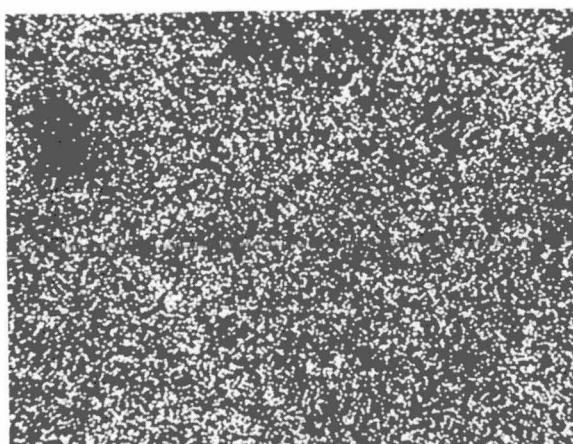
Fig. 5.14. Electron microprobe scans of a partly dedolomitized rhomb of dolomite. (a) Back scattered electron image and X-Ray distribution map of Mg. (b) and (c) are X-Ray distribution maps of Mg and Ca respectively. (d) Reconstruction of the dolomite rhomb showing areas replaced by dedolomite. Intensity of individual patterns do not reflect absolute or relative abundances of elements. Sample 49043.



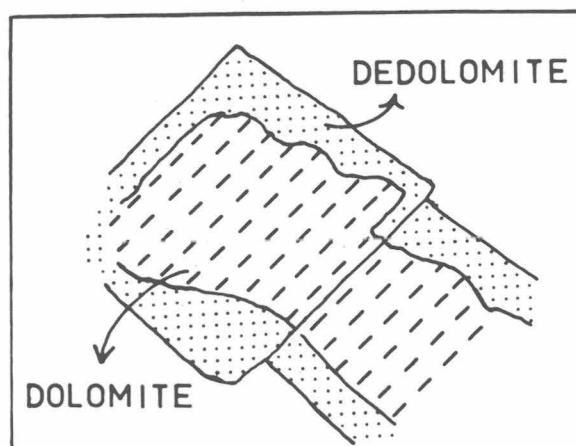
(a)



(b)

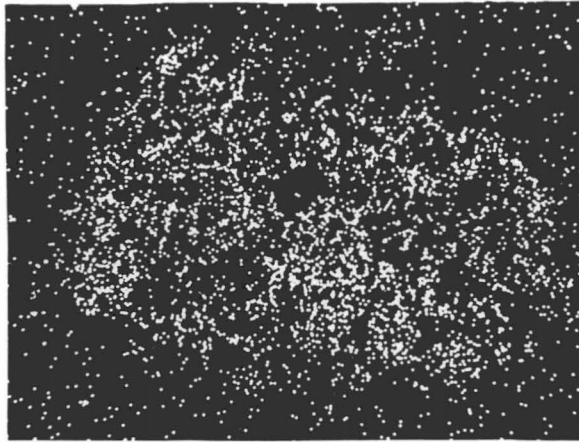


(c)

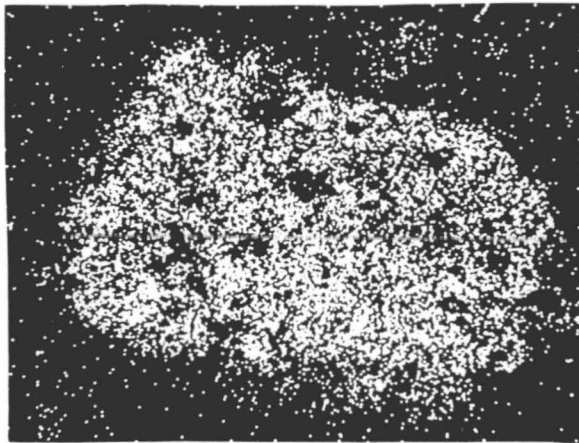


(d)

Fig. 5.15. Electron microprobe scans of a partly dedolomitized rhomb of dolomite. (a) Back scattered electron image and X-Ray distribution map of Mg. (b) and (c) are X-Ray distribution maps of Mg and Ca respectively. (d) Reconstruction of the dolomite rhomb showing areas replaced by dedolomite due to centripetal dedolomitization. Intensity of individual patterns do not reflect absolute or relative abundances of elements. Sample 49077.



(a)



(b)

Fig.5.16. X- Ray distribution maps of (a) Magnesium and
(b) Calcium in a dolomite crystal with irregular
outlines. Petrographic observations showed clots
of dedolomite within the crystal. Sample 40043.

were excluded. Also excluded were samples in which silica had replaced dolomite. A plot of petrographic estimates of the dolomite content against the Mg/Ca ratios of the dissolved rocks is shown in Fig. 5.17 (see also explanation p. 131). Data for samples in which there has been no dedolomitization should plot on the line for ideal dolomite ($\text{Mg:Ca} = 1$, molar) or very close to it. For samples which do not plot on that line, dedolomitization is implied, i.e. the petrographic volume-estimate of dolomite content must also be including variable amount of dedolomite to cause deviation of sample points from the ideal dolomite line.

ESTIMATION OF THE DEDOLOMITE CONTENT

Previous studies, except that of Al-Hashimi (1976, p.370), dealing with diagenesis have not attempted to quantify the observed dedolomite fabrics. He found the degree of dedolomitization in the Carboniferous carbonate rocks of England to vary from a few weight percent to more than 90 wt.%, but the method employed to estimate dedolomitization is not mentioned.

In the study area, petrographic observations have shown that generally the dolomite rhombs in a single sample are not replaced uniformly by dedolomite, which may vary from a small clot to a whole dedolomitized rhomb. This complex nature of occurrence of the dedolomite fabrics is the main obstacle in making a quantitative petrographic estimate of the dedolomite content (excluding, of course, the case of a whole sample which may have become dedolomitized).

However, a combination of both petrographic and chemical data can be utilized in solving the problem of estimating the dedolomite content. It has been mentioned earlier that the visual estimate of the dolomite content (confirmed by point counting) includes the dedolomitized parts

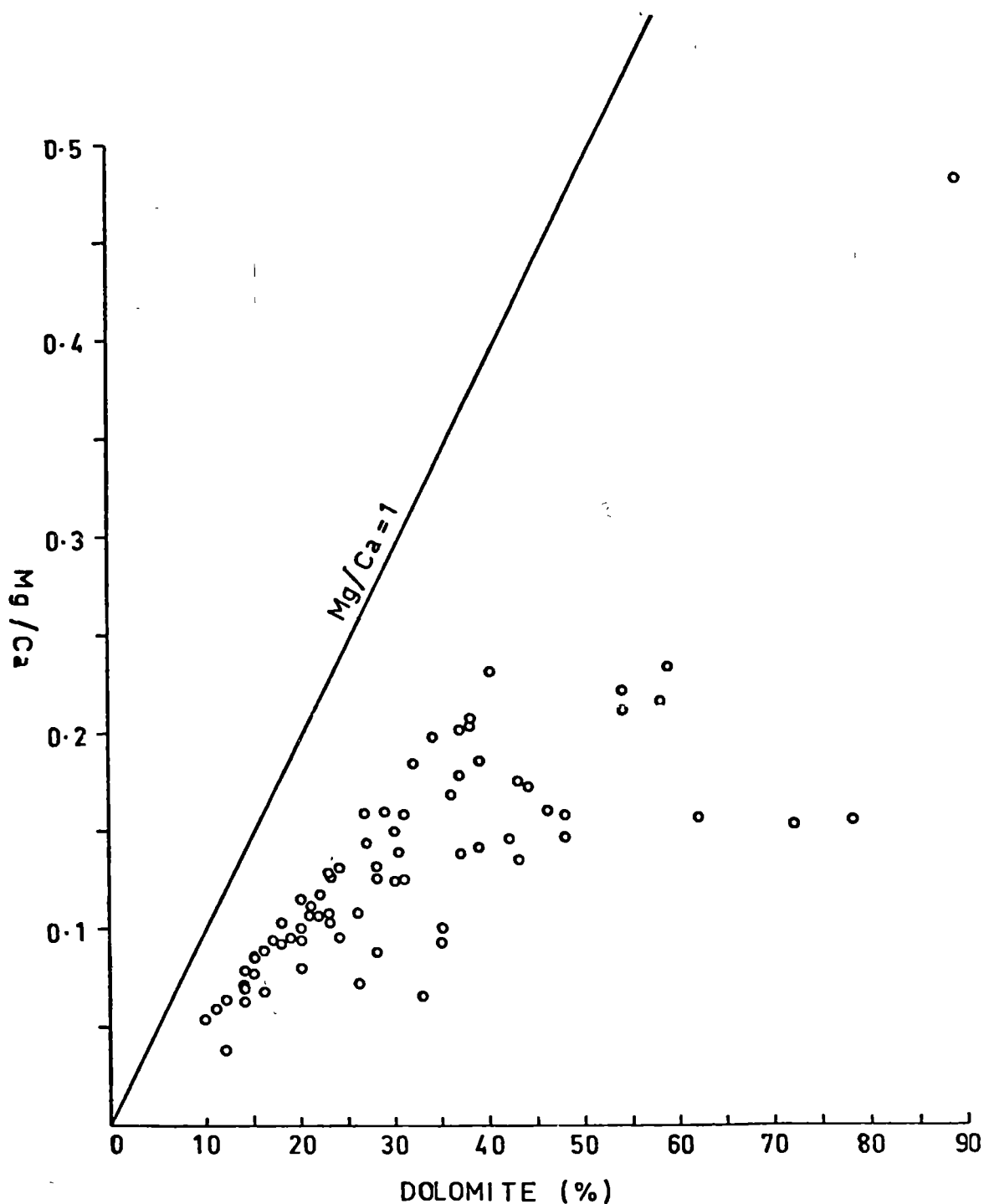


Fig.5.I7. Plot of Mg/Ca molar ratios against the dolomite percent (volumetric estimate). The straight line ($Mg/Ca=1$) representing the ideal dolomite has been drawn taking e.g. Mg/Ca 0.5, 0.3, 0.2 = 50%, 30% and 20% dolomite respectively.

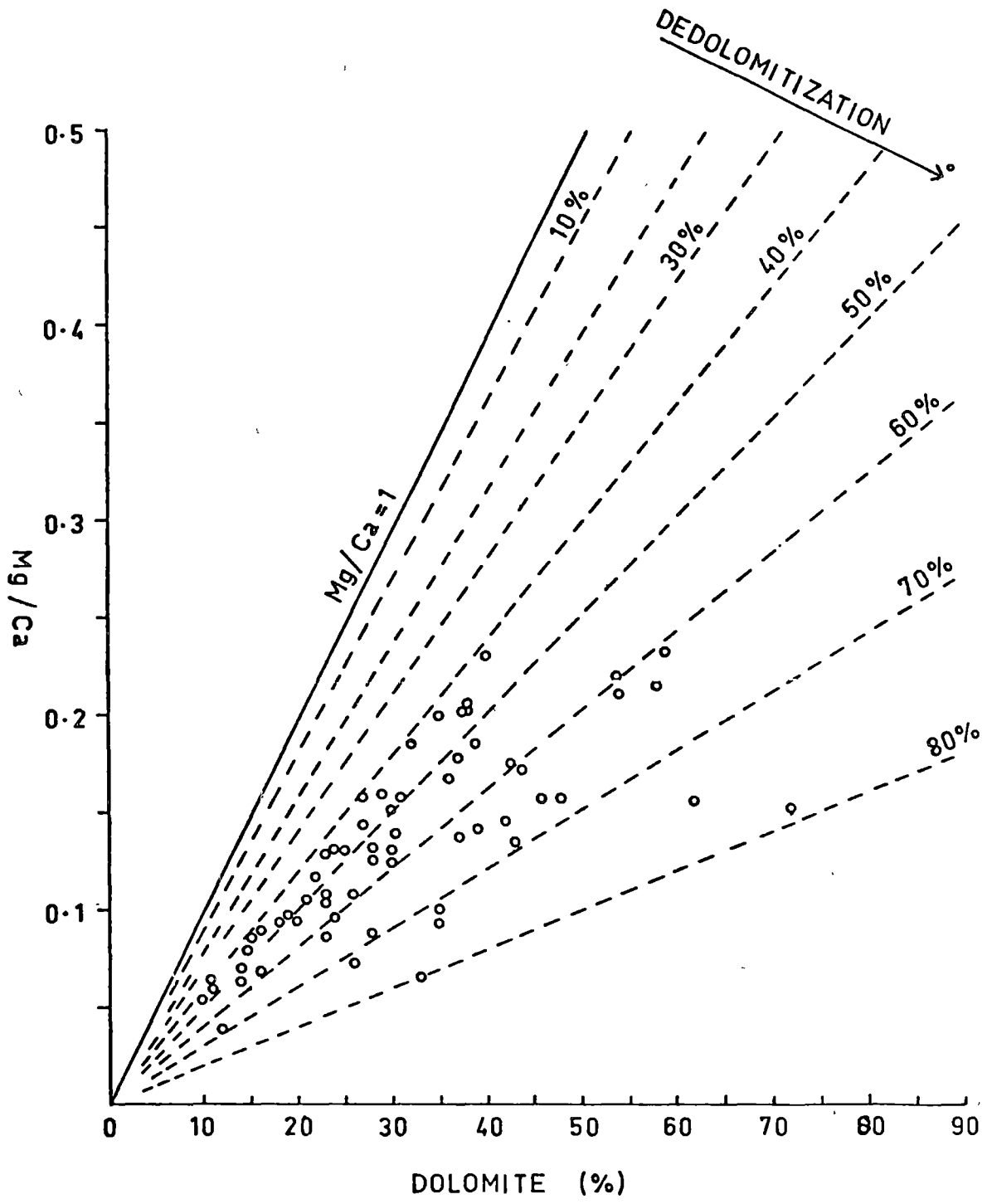


Fig.5.18. Plot of Mg/Ca molar ratios against the dolomite percent(volumetric estimate).The area between Mg/Ca=1 line(zero percent dedolomitization) and X-axis has been divided to represent different percentages of dedolomitization.

of rhombs also, i.e. when making dolomite estimates, dedolomitization was ignored. This estimated dolomite content (including dedolomite) in the samples and the Mg/Ca molar ratios do not correspond to the ideal dolomite line (Mg/Ca = 1) in Fig. 5.17 because of the presence of some unknown amount of dedolomite. In other words, samples (ideal dolomites) with no included dedolomite (i.e. zero percent dedolomitization), whatever their dolomite content, should plot on the line Mg/Ca = 1. Similarly a wholly dedolomitized sample (no matter how much dolomite was originally present) should plot on the x-axis of Fig. 5.17. Thus, the area within these two extremes from 0 to 100 represents the various degrees or percentages of dedolomitization. In Fig. 5.18 a subdivision of this area by lines denoting the various percentages are shown and data for samples with known Mg/Ca and dolomite percentages are plotted. The dedolomite percentage obtained varies from 38 to 80%.

The straight lines in Fig. 5.18 were calculated without taking into account the differences in density and the molecular weight of calcite and dolomite. These factors have been used (see below) in the construction of Fig. 5.19. Fig. 5.18, however, gives answers which differ by a maximum of ~25%.

The first consideration for drawing the curves in Fig. 5.19 is that the estimate of dolomite (including dedolomite) is a volume estimate, made in samples containing a proportion of calcite. The expression for this relationship would be:

$$\text{volume ratio} = \frac{\text{volume of dolomite}}{\text{total volume}}$$

$$\begin{aligned} \text{or} \quad n &= \frac{V_d}{V_c + V_d} \\ &= \frac{1}{(V_c + V_d)/V_d} \\ &= \frac{1}{1 + (V_c/V_d)} \end{aligned}$$

Where V_d = volume of dolomite, V_c = volume of calcite and n = volume ratio.

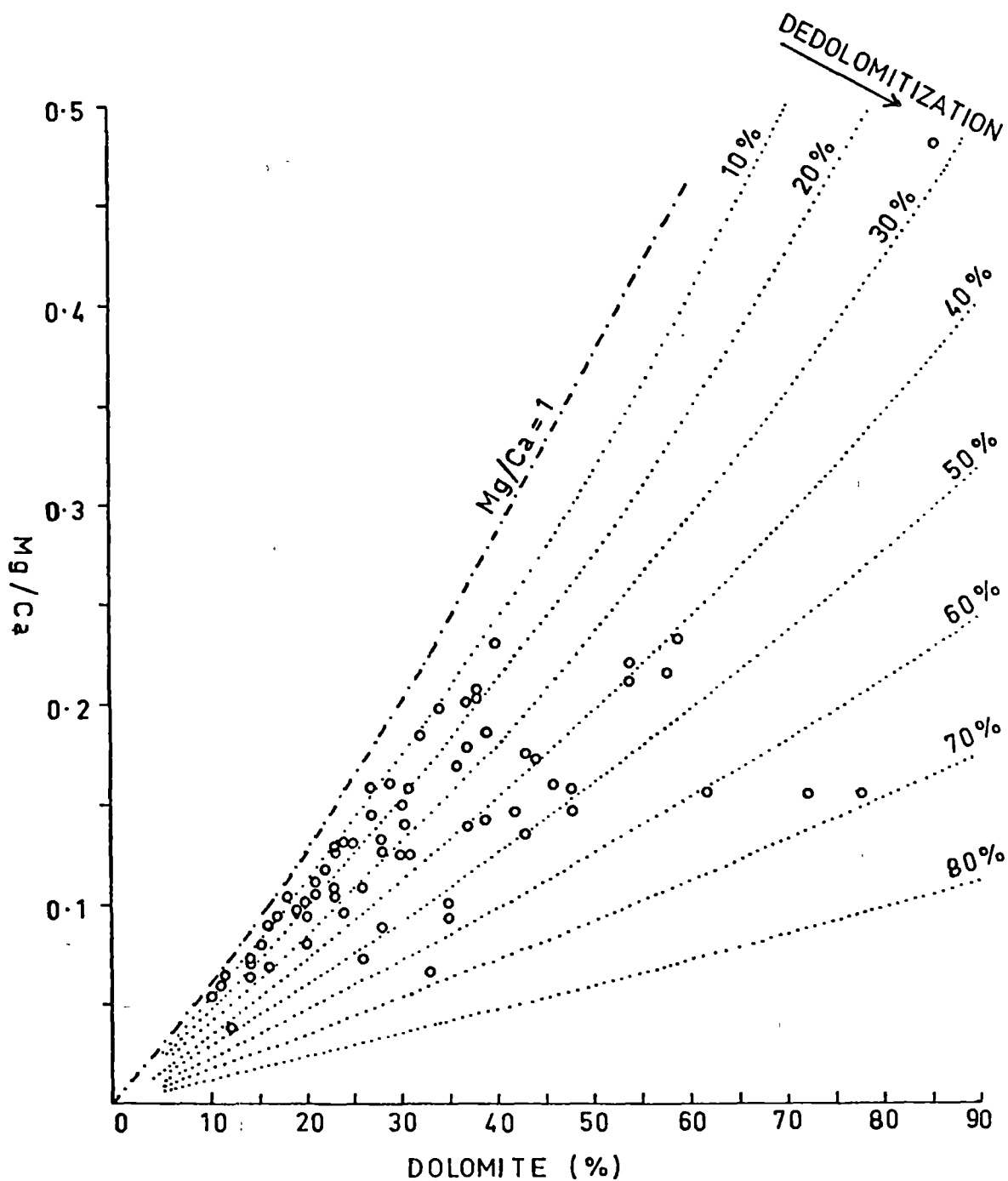


Fig.5.I9. Plot of Mg/Ca molar ratios against the dolomite percent (volumetric estimate). See text for dedolomite percentages curves.

In other words,

$$\frac{V_c}{V_d} = \frac{1-n}{n} \quad \text{or} \quad \frac{V_d}{V_c} = \frac{n}{1-n} \quad \dots (1)$$

The molar ratio of dolomite to calcite (for 100% dolomite by volume) would be

$$\begin{aligned} \frac{M_d}{M_c} &= \frac{(V_d \times P_d)/\text{MW of dolomite}}{(V_c \times P_c)/\text{MW of calcite}} \\ &= \frac{V_d}{V_c} \times \frac{2.85}{2.71} \times \frac{100}{184} \end{aligned}$$

where M = moles, MW = molecular weight, P_c and P_d denote the densities of dolomite and calcite respectively.

From expression (1) we know that

$$\frac{V_d}{V_c} = \frac{n}{1-n}$$

Substituting we get

$$\frac{M_d}{M_c} = \frac{n}{1-n} \times 0.57 \quad \dots (2)$$

The mole fraction of dolomite $[M_d/(M_c + M_d)]$ is also the molar ratio of Mg to Ca, so that

$$\begin{aligned} \frac{M_{Mg}}{M_{Ca}} &= \frac{1}{(M_c + M_d)/M_d} \\ &= \frac{1}{1 + (M_c/M_d)} \end{aligned}$$

From expression (2), substituting the value of M_d/M_c , we get

$$\frac{M_{Mg}}{M_{Ca}} = \frac{1}{1 + (1-n/0.57n)}$$

or

$$\begin{aligned} \frac{M_{Mg}}{M_{Ca}} &= \frac{1}{[0.57n + (1-n)]/0.57n} \\ &= \frac{0.57n}{1-n(1-0.57)} \end{aligned}$$

$$\frac{M_{Mg}}{M_{Ca}} = \frac{0.57n}{1 - 0.43n} \quad \dots (3)$$

Thus, for no dedolomitization, i.e. 100% dolomite, the $Mg/Ca = 1$ curve is obtained from equation (3), where n = volume ratio as defined above.

Suppose now that 100x% of the dolomite has been dedolomitized (i.e. x = the percent dedolomitization).

The volume estimates must be adjusted as follows:

	petrographic estimate	actual value
dolomite	V_d	$V_d(1-x)$
calcite	V_c	$V_c + xV_d$

The actual ratio becomes

$$\frac{V'_d}{V'_c} = \frac{V_d(1-x)}{V_c + xV_d} = \frac{1-x}{(V_c/V_d) + x}$$

Substituting for V_c/V_d from equation (1),

$$\frac{V'_d}{V'_c} = \frac{1-x}{(1-n)/n + x}$$

$$\therefore \frac{M'_d}{M'_c} = 0.57 \times \frac{V'_d}{V'_c}$$

and

$$\begin{aligned} \frac{M'_{Mg}}{M'_{Ca}} &= \frac{1}{1 + (M'_c/M'_d)} = \frac{1}{1 + (V'_c/V'_d \times 0.57)} \\ &= \frac{1}{1 + (1/0.57) \left(\frac{(1-n)/n + x}{1-x} \right)} \end{aligned}$$

which may be simplified to

$$\frac{M'_{Mg}}{M'_{Ca}} = \frac{0.57n(1-x)}{1 - 0.43n(1-x)} \quad \dots (4)$$

For $x = 0$, the equation (4) reduces to the result already derived in equation (3).

Thus, for each value of x , a curve relating M'_{Mg}/M'_{Ca} to n can now be calculated, e.g. to draw a curve for 40% dedolomitization (i.e. $x = 0.4$), knowing the estimated dolomite to be 20% ($n = 0.2$). Substituting in equation (4),

$$\begin{aligned}\frac{Mg}{Ca} &= \frac{0.57 \times 0.2(1-0.4)}{1 - 0.43 \times 0.2(1-0.4)} = \frac{0.114 \times 0.6}{1 - 0.0516} \\ &= 0.0721\end{aligned}$$

which would be the point on the 40% dedolomitization curve for a sample with 20% dolomite. Similarly a series of points for different degrees of dedolomitization in 20% dolomite are obtained. Joined together, they represent the curve for 40% dedolomitization.

Likewise, curves representing other percentages of dedolomitization are drawn. Samples with known Mg/Ca molar ratios and estimated dolomite percent are also plotted. The percentage of dedolomite can be read directly from the figure. The dedolomite percentage was not determined in samples containing less than 10% dolomite because of the very closely situated curves in this region (Fig. 5.19). Small errors in the dolomite estimates would lead to significant errors in the results for dedolomite. Excluding these samples, the dedolomite percentages obtained range up to 69%.

VERTICAL DISTRIBUTION

Vertical distributions of the dolomite percent and dedolomite percentage in sections GPL and GPW, together with the interpreted depositional environments of the samples containing dedolomite are shown in Figs. 5.20 and 5.21. (The complete vertical distribution of environments for these two sections is shown in Figs. 3.28 and 3.29.) It can be observed that

Fig. 5.20 Vertical distribution of the dolomite and dedolomite percentages in section GPL.

Fig. 5.21 Vertical distribution of the dolomite and dedolomite percentages in section GPW.

the dedolomite content is very variable in both the stratigraphic sections. When compared with the depositional environments in Figs. 3.28 and 3.29, the variation in the dedolomite content appears to be related to the depositional cycles, generally being most abundant in the supratidal environment or, where supratidal is absent, in the upper intertidal environment of each cycle. Dedolomitization decreases towards the lower intertidal environment. All subtidal samples contained less than 10% dolomite and for reasons mentioned previously, the dedolomite content was not determined in them. This increase of dedolomitization towards the supratidal suggests that dedolomitizing solutions were derived from a landward source. The variable amount of dedolomite in the different depositional cycles indicates that dedolomitization occurred in episodes of various intensity at the end of each cycle, i.e. it was an early diagenetic process.

RELATIONSHIP OF TRACE ELEMENTS TO DEDOLOMITIZATION

Strontium

Strontium is the most commonly studied minor element in carbonate rocks. The strontium distribution in sections GPL and GPW is shown in Figs. 4.15 and 4.16. There is little, if any, relationship between strontium and the clay content, as indicated by a very small correlation coefficient (+0.03) of strontium with Al_2O_3 (Table 4.3). This shows that the bulk of the strontium occurs in the lattices of the carbonate minerals.

In the dedolostones (samples with more than 50% dolomite originally, but now having undergone 28 to 69% dedolomitization), the mean Sr/Ca molar ratio is 0.4816×10^{-3} (422 ppm Sr), std. dev. = 0.0583×10^{-3} . These dedolostones, like most of the other studied samples, underwent a decrease in their Sr content during dedolomitization. This is indicated

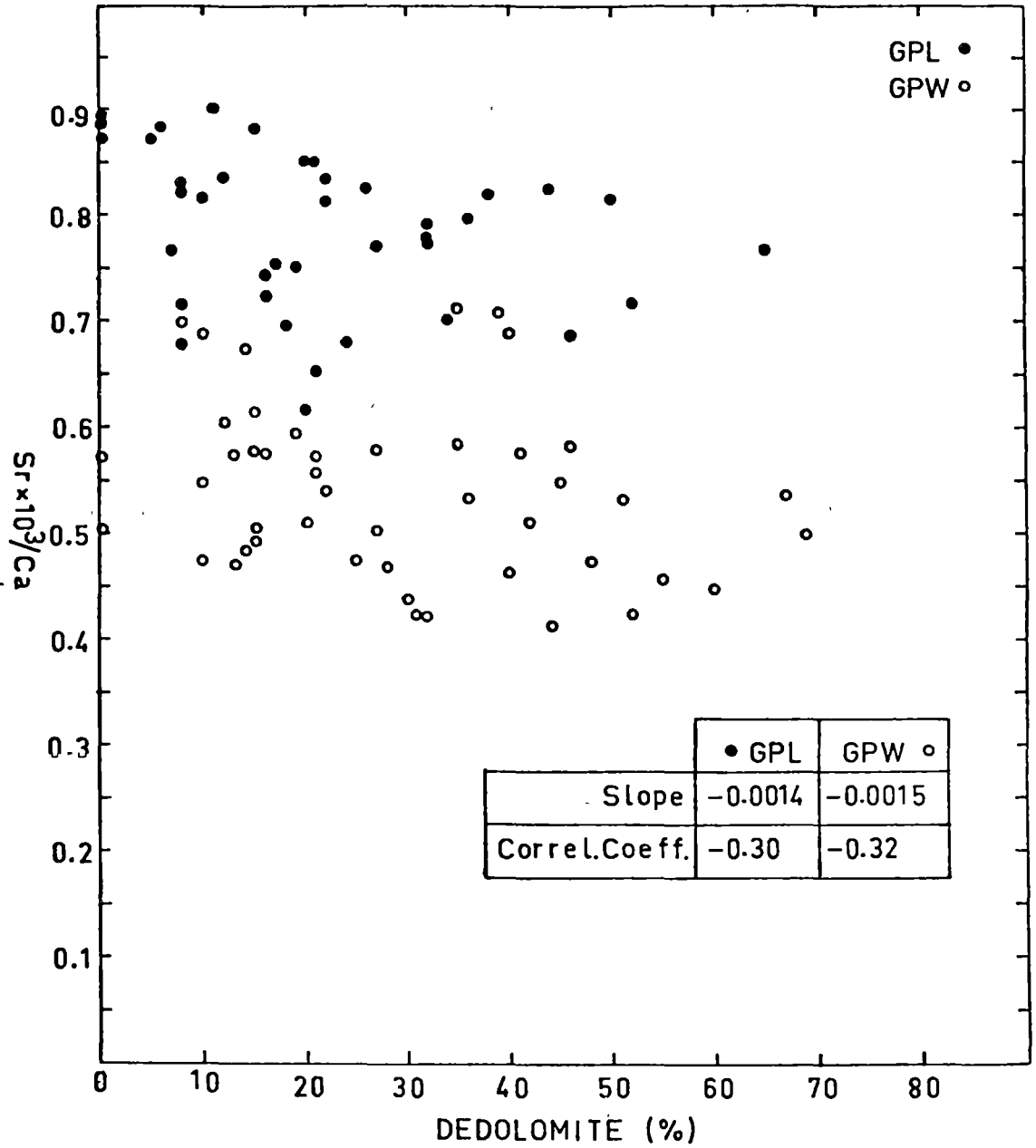


Fig. 5 22. Plot of Sr/Ca molar ratio against the dedolomite percent in sections GPL and GPW.

by a negative correlation in a plot of Sr against the dedolomite percentage (Fig. 5.22). This loss of Sr during dedolomitization has also been demonstrated in the French Jura (Shearman and Shirmohammadi, 1969) and in Carboniferous rocks in England (Al-Hashimi, 1976) by applying methods different from those used in the present study.

The amount of Sr contained in the dedolomites (calcites) is directly dependent on the composition of the dedolomitizing solutions and is related to the distribution coefficient (partition coefficient) of Sr between the solution and calcite. Kinsman and Holland (1969) experimentally determined the partition coefficient for calcite to be 0.14 at 25°C and 0.08 at 100°C. In a closed system, according to Katz *et al.* (1972), the experimentally determined (K_{Sr}) calcite is 0.055 at 40°C and 0.058 at 90°C. For further details and discussion the reader is also referred to Holland *et al.* (1964), Holland (1966), Kinsman (1969) and Ichikuni (1973).

Following Al-Hashimi (1976), if it is assumed that the dedolostones were formed by water containing CO₂ only or by meteoric water whose Ca and Sr were derived only from the dissolving dolostones, then the dissolution of the dolostones would have continued until the solution became just supersaturated with respect to dedolostones (calcite). Thus, if the (K_{Sr}) calcite and the Sr/Ca molar ratio of the solution, which during the dissolution would have been identical to the Sr/Ca of the dissolving dolostones is known, then the Sr content in the forming dedolostones can be determined from the relationship

$$(m_{Sr^{++}}/m_{Ca^{++}})_{SOLID} = (K_{Sr})_{SOLID} \times (m_{Sr^{++}}/m_{Ca^{++}})_{SOLUTION}$$

As the dolostones have undergone a loss in their Sr content during dedolomitization, the present Sr concentrations need to be adjusted for changes during dedolomitization. The approximate Sr content in

the samples prior to dedolomitization can be found from Fig. 5.22 by using the equation:

$$\text{Sr}_{(\text{before dedolomitization})} = \text{Sr}_{(\text{in sample})} - (\text{slope} \times \text{dedolomite percentage})$$

The mean Sr/Ca obtained for dolostones (containing no dedolomite) is 0.5564×10^{-3} (488 ppm Sr), std. dev = 0.0689×10^{-3} .

In the relationship mentioned above $(m_{\text{Sr}^{++}}/m_{\text{Ca}^{++}})_{\text{SOLUTION}}$ would be equal to the Sr/Ca in the dolostones, i.e. 0.5564×10^{-3} . De Groot (1967) has experimentally shown that dedolomitization is a near-surface process. Therefore taking $(K_{\text{Sr}})_{\text{calcite}}$ as 0.14 at 25°C and using the relationship $(m_{\text{Sr}^{++}}/m_{\text{Ca}^{++}})_{\text{SOLID}} = K_{\text{Sr}}^{\text{SOLID}} (m_{\text{Sr}^{++}}/m_{\text{Ca}^{++}})_{\text{SOLUTION}}$, the forming dedolostone should have contained

$$\begin{aligned} (m_{\text{Sr}^{++}}/m_{\text{Ca}^{++}})_{\text{DEDOLOSTONE}} &= 0.14 \times 0.5564 \times 10^{-3} \\ &= 0.0779 \times 10^{-3} \end{aligned}$$

$$[\text{Sr}] = 68 \text{ ppm}$$

The actual Sr concentration (mean 422 ppm, $\text{Sr}/\text{Ca} = 0.4816 \times 10^{-3}$) in the dedolostones is much higher than the predicted value of 68 ppm Sr, suggesting that the dedolomitizing solutions were not completely dependent on the dissolving dolostones for their Sr content.

As the actual concentration of Sr in the dedolostones is known, the Sr/Ca in the solution can be determined.

$$\begin{aligned} 0.4816 \times 10^{-3} &= 0.14 \times (m_{\text{Sr}^{++}}/m_{\text{Ca}^{++}})_{\text{SOLUTION}} \\ (m_{\text{Sr}^{++}}/m_{\text{Ca}^{++}})_{\text{SOLUTION}} &= \frac{0.4816 \times 10^{-3}}{0.14} \\ &= 3.44 \times 10^{-3} \end{aligned}$$

$$\text{Whence } [\text{Sr}] = 3014 \text{ ppm in the solution.}$$

Likewise, as the Sr concentration of the dedolomitic limestones (samples containing 10 to 50% dolomite, but now having undergone up to

55% dedolomitization) is known (mean Sr/Ca = 0.5526×10^{-3} , std. dev. = 0.0833×10^{-3} in section GPW; and mean Sr/Ca = 0.7879×10^{-3} , std. dev. = 0.0725×10^{-3} in section GPL), the Sr concentration in the solution can be obtained and is found to be 3459 ppm and 4931 ppm for sections GPW and GPL respectively. These concentrations of Sr indicate a dedolomitizing solution highly enriched in Sr. According to Badiozamani (1977, p.977), secondary calcite (including dedolomite) can form from high Sr ground waters.

Presently forming shallow-water marine carbonates have Sr contents ranging from 2000 ppm for carbonate mud from British Honduras (Matthews, 1966) to 12,500 ppm for pseudo-oooids from the Bahamas (Zellar and Wray, 1956). Also, see Bathurst (1976, fig. 225), who has summarized some Sr concentrations in marine carbonates obtained by different workers. According to Stehli and Hower (1961), high strontium values (2700 to 4600 ppm) occur in the lime muds of Florida Bay. On alteration to stable calcite, during the wet dissolution and reprecipitation process, these lime muds would lose most of their Sr to the diagenetic solutions. Such a process may also have occurred in the carbonates at Gunns Plains, thus providing the Sr-enriched solutions which brought about dedolomitization. In this case, it is implied that metastable phases were present at the time of dedolomitization in the carbonate terrain. In other words, the transformation to stable calcite had not been completed.

On the other hand, presence of celestite, gypsum and anhydrite can also account for high Sr solutions (e.g. Kinsman, 1965; Butler, 1973). In the present study, no celestite was observed and calcitized evaporitic moulds occur only rarely. So far, other studies of the Junee Group (e.g. Weldon, 1974; Basnayake, 1975; Burrett, 1978; Rao and Naqvi, 1977), to which the Gunns Plains Limestone belongs, have revealed the presence of only calcitized evaporitic moulds.

Manganese

The manganese distribution in sections GPL and GPW is shown in Figs. 4.15 and 4.16 . The small negative correlation coefficient (-0.26) between the manganese and Al_2O_3 content (Table 4.3) indicates that manganese is not related to the clay content. Therefore it is probably associated with the carbonate phase.

The Mn/Ca molar ratio in the dedolostones ranges from 0.2260×10^{-3} to 0.4596×10^{-3} with a mean of 0.3317×10^{-3} (182 ppm Mn), std. dev. = 0.0788×10^{-3} . In the dedolomitic limestones, the mean Mn/Ca is 0.2468×10^{-3} (135 ppm Mn), std. dev. = 0.0459×10^{-3} in section GPW and 0.2118×10^{-3} (116 ppm Mn), std. dev. = 0.0548×10^{-3} in section GPL. There are no other published data on the Mn content of dedolomites.

An increase of Mn during dedolomitization is indicated in plots of Mn against the dedolomite percentage (Figs. 5.23 and 5.24). This increase during dedolomitization is further considered below, in terms of the partitioning of Mn at the time of dedolomite formation.

There is no agreement on the partition coefficient of Mn in calcite, although in all cases it is higher than the partition coefficient of Mn in aragonite (0.86 at 30° to 60°C - Brimblecombe and Raiswell, 1977). Bodine *et al.* (1965) determined the partition coefficient as 16.2 ± 2.0 at 40°C . Michard (1968) experimentally determined it to be 5.4 ± 0.3 at 25°C and 12.5 at 175°C . Ichikuni (1973) determined it as 10 and 18 at 40°C in two travertine samples. Pingitore (1978) considered a partition coefficient of 15 to be appropriate for conditions of surficial carbonate diagenesis.

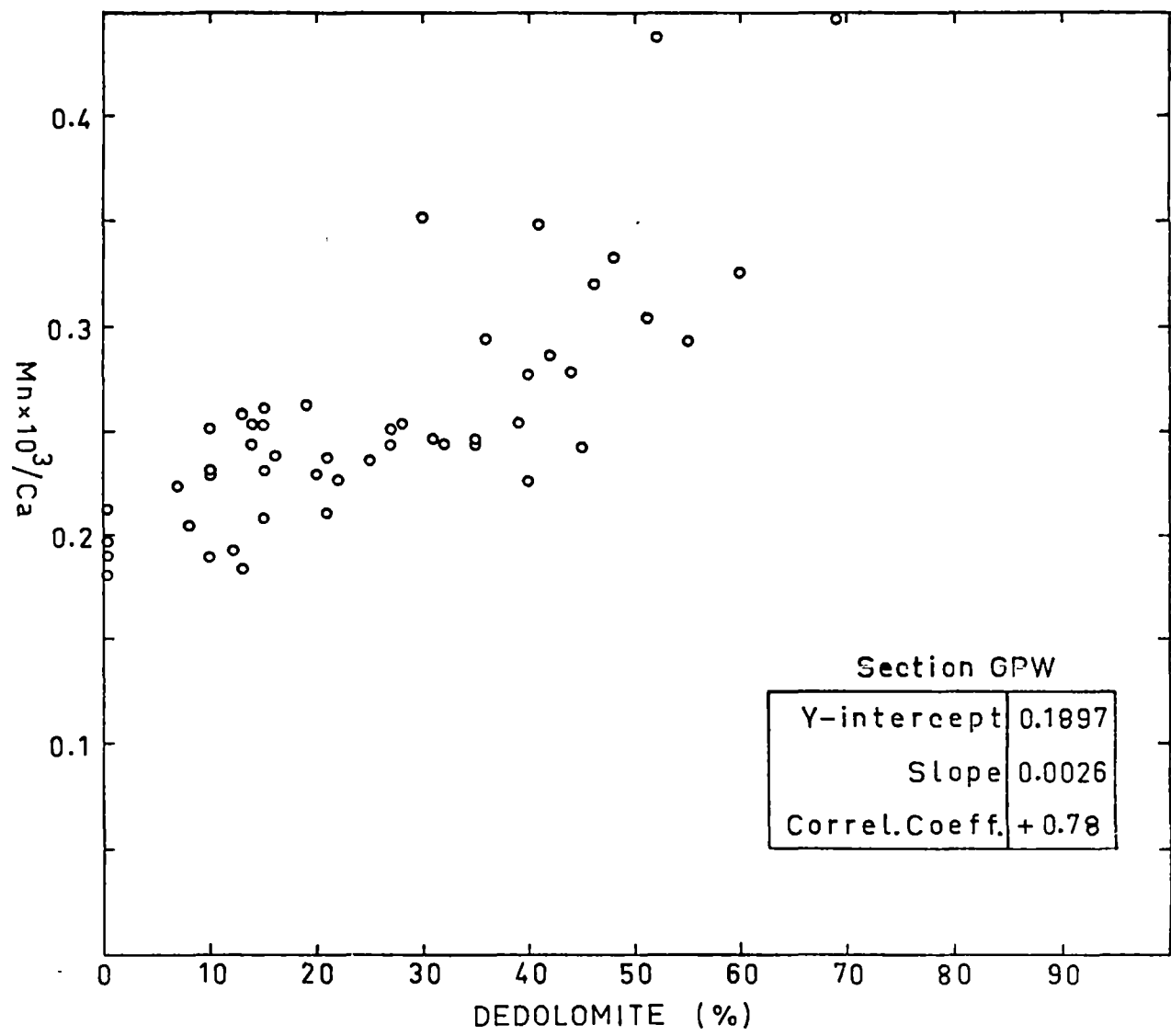


Fig. 5.23. Plot of Mn/Ca molar ratio against the dedolomite percent in section GPW

If it is assumed that all the Mn of the dedolomitizing solution were derived from sea-water, then

$$(m_{\text{Mn}^{++}}/m_{\text{Ca}^{++}})_{\text{SEA WATER}} = (m_{\text{Mn}^{++}}/m_{\text{Ca}^{++}})_{\text{SOLUTION}}$$

Morgan (1967) has shown that Mn in sea-water is in Mn^{++} form and the Mn/Ca in sea-water is about 3.6×10^{-6} (Gross, 1972). The forming dedolostones should have contained

$$\begin{aligned} (m_{\text{Mn}^{++}}/m_{\text{Ca}^{++}})_{\text{DEDOLOSTONE}} &= K_{\text{DEDOLOSTONE}}^{\text{Mn}} \times (m_{\text{Mn}^{++}}/m_{\text{Ca}^{++}})_{\text{SOLUTION}} \\ &= 16.2 \times 3.6 \times 10^{-6} \\ &= 58.32 \times 10^{-6} \\ [\text{Mn}] &= 32 \text{ ppm} \end{aligned}$$

If partition coefficients of 15 and 5.4 are used, then the forming dedolostones should have contained 30 and 11 ppm respectively. The actual concentration of 182 ppm Mn (mean) in the dedolostones is about 5 to 16 times higher (depending on the partition coefficient used) than the predicted values. Similarly the mean Mn/Ca in the dedolomitic limestones is also higher than the predicted values, suggesting some other source of Mn.

Surface waters have Mn/Ca ranging from 2×10^{-4} to 3×10^{-3} (Garrels and Mackenzie, 1972; Hem, 1959). Assuming these values in the dedolomitizing solution results in Mn/Ca ratios which are 3 to 146 times higher (depending on the partition coefficient used) than the actual ratios in the dedolostones.

In the same way as the Sr content prior to dedolomitization was determined (p.141), the Mn concentration can be found. In the dolostones (before dedolomitization), the approximate mean Mn/Ca obtained is 0.2095×10^{-3} (115 ppm Mn), std. dev. = 0.0666×10^{-3} . If it is assumed that all the Mn in the dedolostones was derived from the dissolution of

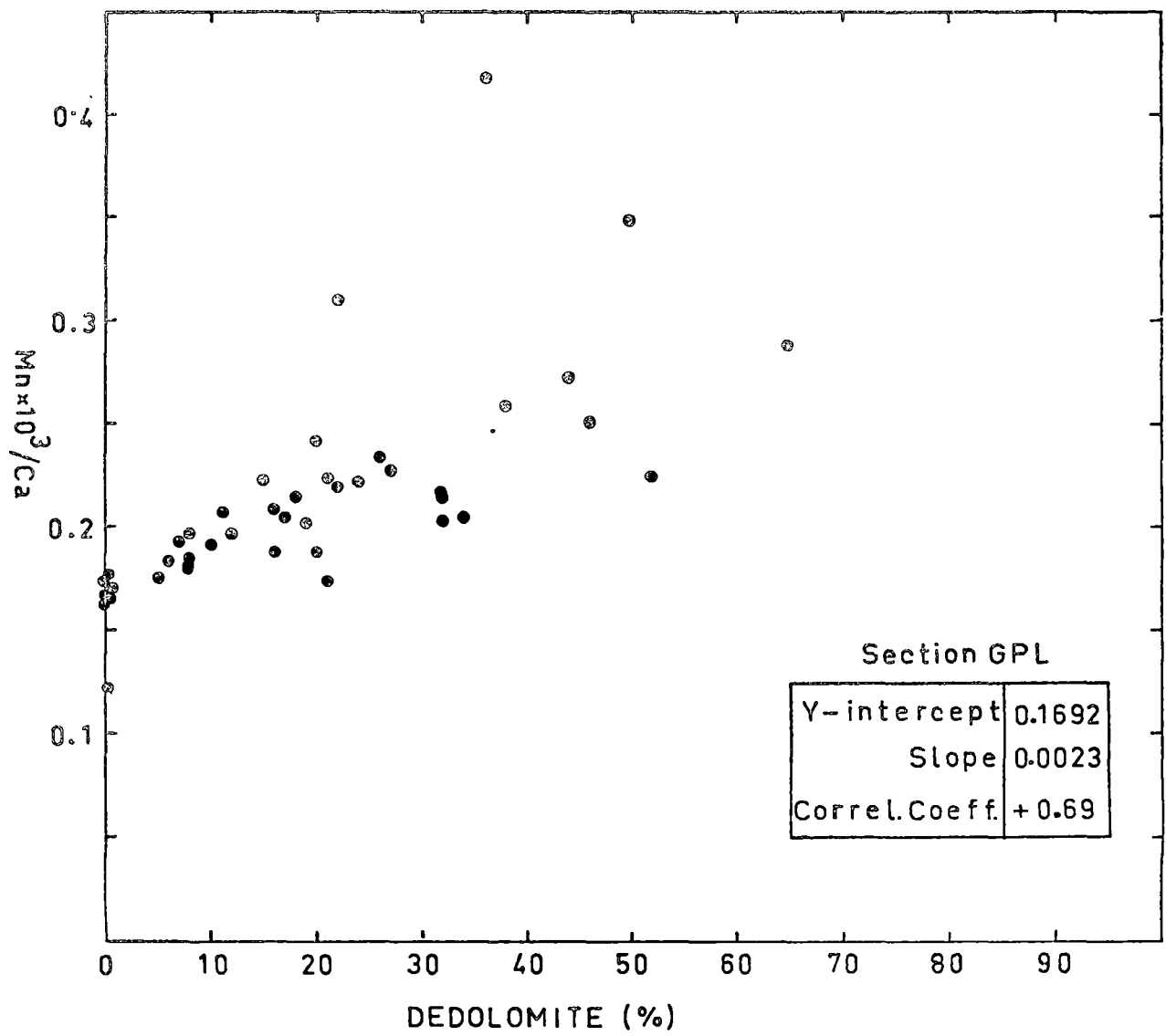


Fig. 5.24. Plot of Mn/Ca molar ratio against the dedolomite percent in section GPL.

the dolostones; then the Mn/Ca in the solution (as discussed for Sr concentrations, p. 140) would have been similar to the Mn/Ca in the dolostones (0.2095×10^{-3}) and the forming dedolostone should have contained 622 ppm, 1726 ppm and 1865 ppm Mn, given partition coefficients of 5.4, 15 and 16.2 respectively. All these values are much higher than the actual concentration in the dedolostones (182 ppm Mn) suggesting that probably only part of the Mn was derived from the dissolution of the dolostones. Another possibility is that the Mn of the dolostones was completely removed and the dedolostones derived their Mn later from another source.

The concentration of manganese believed to have been present in the dedolomitizing solution, based on the actual concentration in dedolostones (mean Mn/Ca = 0.3317×10^{-3}), is 11 ppm, 12 ppm and 33 ppm given partition coefficients of 16.2, 15 and 5.4 respectively. According to data from dedolomitic limestones, the Mn concentrations in solutions would be

25 ppm at $K = 5.4$, 8 ppm at $K = 16.2$ in section GPW

21 ppm at $K = 5.4$, 7 ppm at $K = 16.2$ in section GPL.

Stehli and Hower (1961), Friedman (1968, 1969) and others have shown that in recent mostly aragonitic sediments, the Mn content is very low (ranging up to 50 ppm). According to Thompson (1972), the amount of Mn present in shallow-marine carbonates is controlled by the carbonate mineralogy, aragonite containing about 20 ppm and calcite up to a few percent. Low Mn concentrations in ancient carbonate rocks (like the 182 ppm Mn in dedolostones) are thus believed to reflect the original carbonate phase, mainly aragonite (e.g. Bencini and Turi, 1974). The values obtained in this study for the Mn concentrations of dedolomitizing solutions, based on actual concentrations in the dedolostones and dedolomitic limestones, are similar to those present in recent aragonitic sediments.

On the basis of the vertical distribution of the dedolomite content and Sr concentrations, it has been suggested that dedolomitization was an early diagenetic process. The Mn concentrations of aragonitic composition obtained for the dedolomitizing solution provide additional evidence, implying the presence of aragonite at the time of dedolomitization. Waters transforming aragonite into calcite could have taken up Mn from the aragonite, thus accounting for the concentrations in the dedolostones and dedolomitic limestones. This is in agreement with the environmentally controlled variation of dedolomite content (Figs. 5.20 and 5.21).

Iron

The Fe/Ca molar ratio in the dedolostones ranges from 0.3620×10^{-2} to 0.8895×10^{-2} with a mean of 0.5329×10^{-2} (0.3% Fe), std. dev. = 0.1914×10^{-2} . In the dedolomitic limestones, the mean Fe/Ca is 0.3747×10^{-2} (0.21% Fe), std. dev. = 0.1169×10^{-2} in section GPW and 0.4178×10^{-2} (0.23% Fe), std. dev. = 0.1262×10^{-2} in section GPL.

In Table 4.3, the positive correlation coefficient of Fe with Al_2O_3 (+0.17) and with Rb (+0.29) and Ga (+0.29), the two other elements commonly associated with the clay minerals, suggests leaching of Fe from the clays during the laboratory acid treatment of the samples (see Appendix B.1). Robinson (1980) has subsequently demonstrated the leaching of iron from the clays when using HCl of similar strength. However, the positive correlation coefficient (+0.39) of Fe with Mn, the element present in the carbonate phase (discussed on p.143) and with Mg (+0.77) representing the dolomite content, suggests that not all iron has been derived from the clays. Some Fe must also be present in the carbonate phase.

Fig. 5.25 shows the relationship of Fe/Ca to dedolomitization. The trend of increasing iron with dedolomitization is not very apparent from

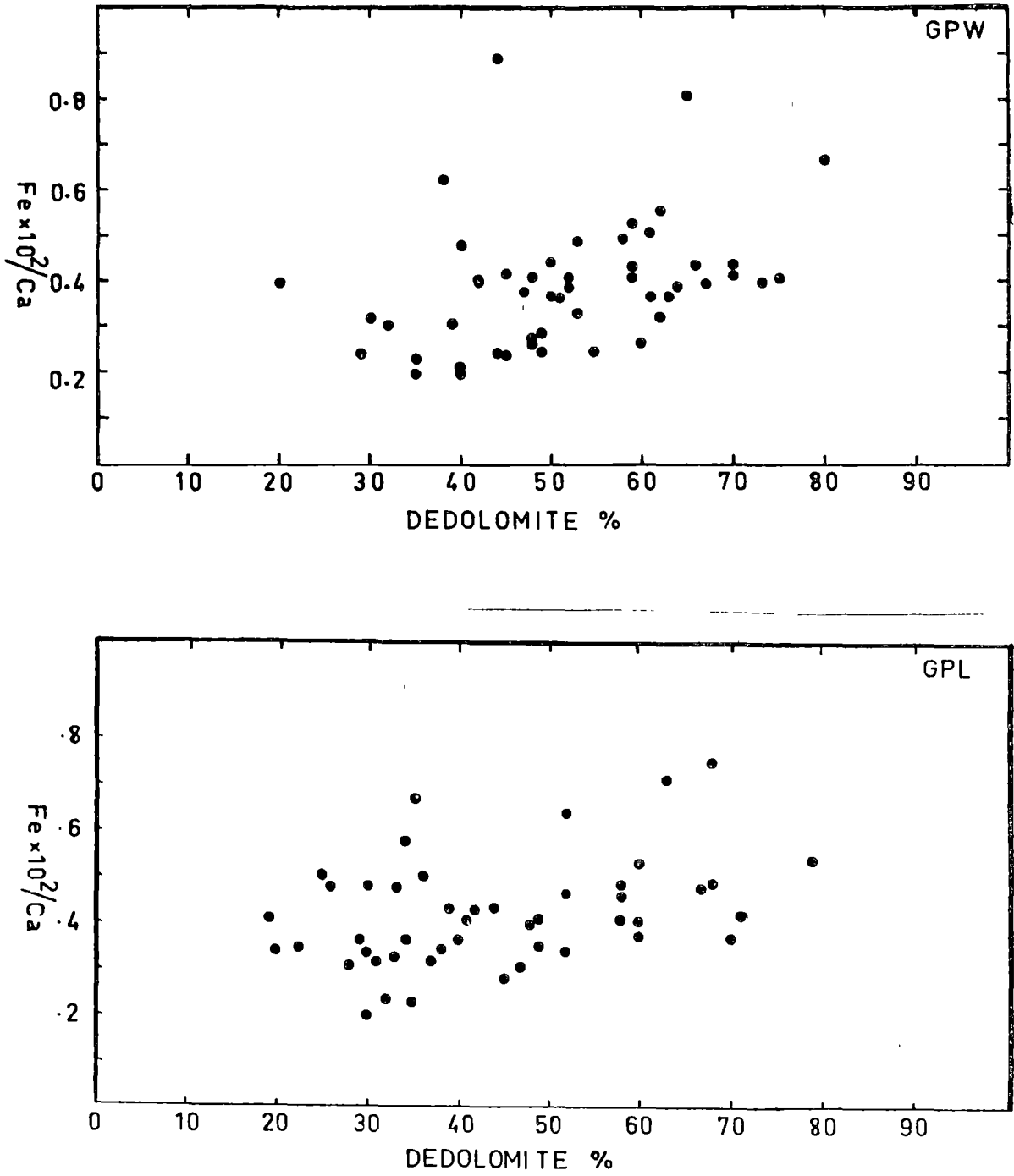


Fig. 5.25. Plot of Fe/Ca molar ratio against the dedolomite percent in sections GPL and GPW.

Fig. 5.25, but is suggested by the positive correlation coefficients (+0.47 in section GPW, and +0.56 in section GPL). However, as Robinson (1980, p.138) states, "Acid-soluble Fe results should be treated with caution."

The possibility of an increase in iron content during dedolomitization is suggested especially by the occurrence of iron-rich relict rims (Fig. 5.10). Conversely, Fig. 5.9 (see description of palimpsest texture) has shown that the iron-rich rims are generally absent from dedolomitized rocks. Furthermore, there are other textures like the mosaic of anhedral calcite in rhombohedra (described on p.109), in which staining has shown no iron enrichment. Thus, the probability of both an increase and loss of iron during dedolomitization exists. It is now known that Mn and Fe may behave differently (e.g. Hem, 1970, p.126), i.e. the demonstrated Mn increase during dedolomitization (Figs. 5.23 and 5.24) may not necessarily also correspond with an increase in Fe. Similar observations were made by Meyers (1974), who distinguished cements with five different combinations of Fe and Mn.

In the present study, the exact relationship of Fe to dedolomitization remains uncertain due to the presence of some unknown amount of Fe leached from the clays. Thus, the limitations imposed on the data, permit discussion in general terms only.

Veizer (1977) states that a calcite in equilibrium with sea-water should contain about 70 ppm Fe (for a partition coefficient of 21). If this is correct, then the concentrations in the dedolostones and dedolomitic limestones (in the present study) argue against the formation of dedolomites from sea-water. Further, Meyers (1974, p.858) points out that nearly all the iron in sea-water is present as Fe^{+++} and therefore the ferroan calcites (determined by staining with potassium ferri-cyanide) cannot precipitate out of normal marine waters.

According to Hem (1970), in cases where the bicarbonate activity does not exceed 61 mg/l, the ground waters may carry as much as 50 mg/l of ferrous iron at a pH between 6 and 8. He also reports that in many areas, the occurrence of 1 to 10 mg/l of iron is common. Thus, if iron content increased during dedolomitization, then reducing conditions prevailed as according to Evamy (1969) reducing conditions seem to enable iron to enter the calcite (dedolomite) lattice.

Except for two samples (Figs. 3.22 and 3.23), no other vadose cements were observed in the study area. The iron-rich relict rims are believed to form in a phreatic environment with low Eh (Richter and Fuchtbauer, 1978, p.856). Evamy (1969) had earlier proposed a similar origin for calcite cements that contained ferrous iron. Those dedolomitization textures which show no iron enrichment could also have been formed by phreatic waters according to Petta (1977), who states that "the absence of ferrous iron does not imply that the cement was precipitated in the vadose zone, but only that phreatic waters did not have a low Eh or that little dissolved iron was available."

Sodium

The small negative correlation coefficient of Na with Al_2O_3 (-0.15) in Table 4.3 indicates that Na is not related to the clay content. This shows that the bulk of the Na occurs in the lattices of the carbonate minerals.

The Na/Ca molar ratio in the dedolostones ranges from 0 to 1.3796×10^{-3} with a mean of 0.2675×10^{-3} (62 ppm Na), std. dev. = 0.4984×10^{-3} . In the dedolomitic limestones, the mean Na/Ca is 0.2461×10^{-3} (57 ppm Na), std. dev. = 0.3023×10^{-3} in section GPW and 0.3609×10^{-3} (83 ppm Na), std. dev. = 0.2701×10^{-3} in section GPL.

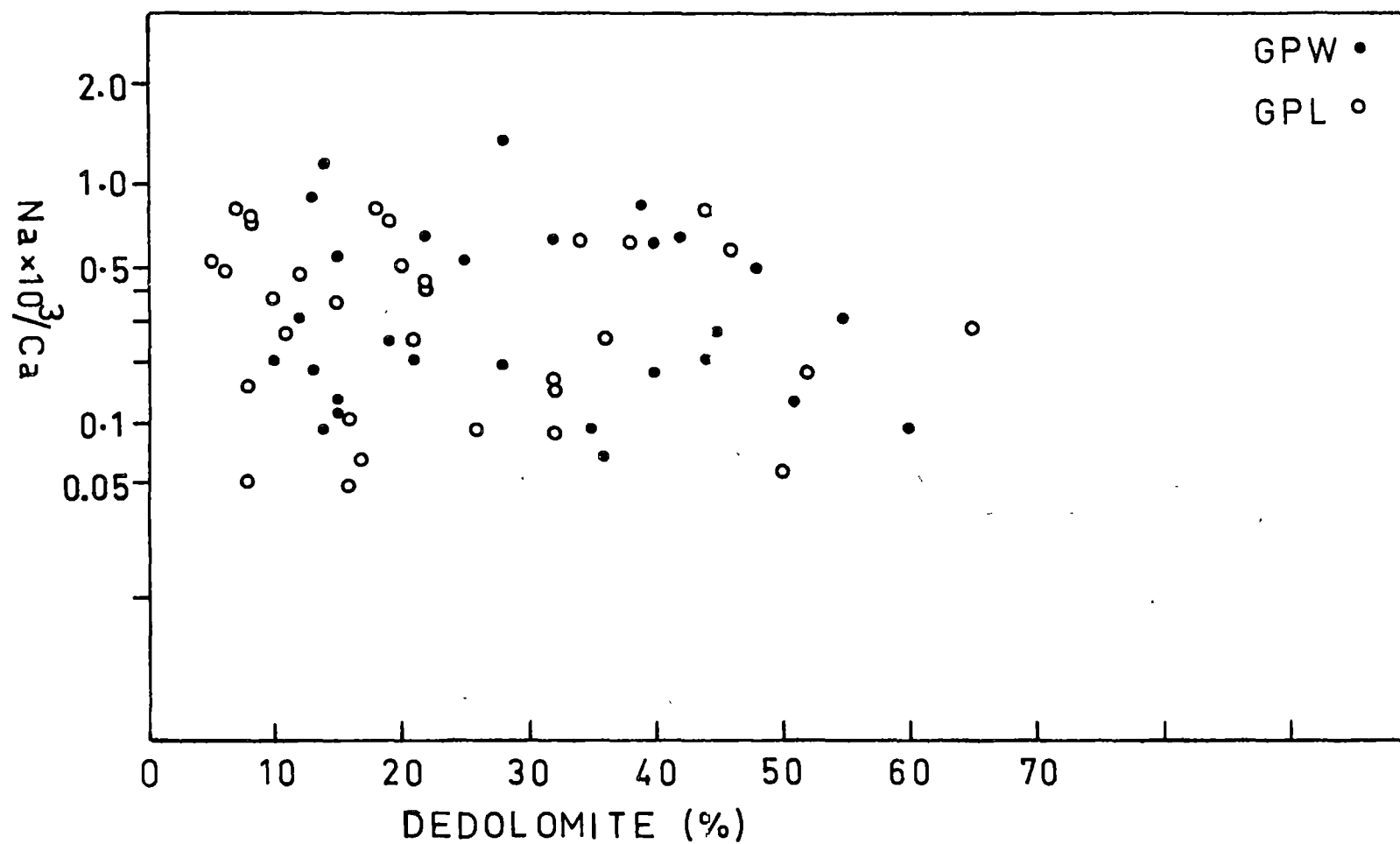


Fig. 5.26 Plot of Na/Ca molar ratio against the dedolomite percentage in sections GPW and GPL.

A decrease in Na during dedolomitization is indicated in a plot of Na against the dedolomite percentage (Fig. 5.26). Further evidence is provided by the vertical variation of Na/Ca in Figs. 4.15 and 4.16. Most of the supratidal and upper intertidal samples (in spite of their containing early diagenetic dolomites) have little or no Na in comparison with the other samples. This is in contrast to the observations made elsewhere in Junee Group carbonates by Basnayake (1975), and Rao and Naqvi (1977). They found higher concentrations of Na in dolomitized (early diagenetic) supratidal samples (without dedolomite) as compared to samples from other environments. It has already been suggested (p. 138) that dedolomitizing solutions were derived from a landward source during regressive phases. Thus, it is to be expected that Na loss due to dedolomitization would be more pronounced in the supratidal than elsewhere.

Na concentrations in carbonate rocks are considered to indicate the salinity and reflect the chemistry of the diagenetic solutions (Fritz and Katz, 1972; Land and Hoops, 1973; Land *et al.*, 1975; Rao and Naqvi, 1977; Veizer *et al.*, 1977, 1978; and others). Decreases in Na due to meteoric diagenesis in Recent and Pleistocene carbonate sediments have been observed by Land and Hoops (1973). According to Veizer *et al.* (1978), a calcite in equilibrium with sea-water contains a little over 200 ppm Na, whereas a calcite in equilibrium with meteoric water contains about 25 ppm Na. The present values in the dedolostones and dedolomitic limestones are closer to the meteoric calcites suggesting that dedolomitization occurred in a fluid medium with markedly different salinity from the original marine water.

Natural waters have a wide range of Na concentrations ranging from 1 ppm (in rain water) to 100,000 ppm in closed brines (Hem, 1970).

The experimental Na distribution in calcites is pH controlled (White, 1978). Because of this, without putting a constraint on the pH at the time of dedolomitization, the experimental data of White cannot be utilized to derive the composition of the dedolomitizing solutions.

ORIGIN OF DEDOLOMITES

Dedolomites may form by the action of sea-water (Katz, 1971; Al-Hashimi and Hemingway, 1973; Al-Hashimi, 1976) or of fresh water (Shearman and Shirmohammadi, 1969; Fritz, 1967; Goldberg, 1967; Abbott, 1974; Longman and Mench, 1978; and others).

In the Gunns Plains Limestone, based on the vertical distribution of the dedolomite content and abundance of dedolomite fabrics in the supratidal and upper intertidal zones of the different depositional cycles (see p. 138) implies that dedolomitization was brought about by influx of solutions from a landward source during early diagenesis. Solution compositions in terms of Sr and Mn have indicated the presence of metastable phases thereby implying that the transformation to stable calcite had not been completed. Low Na concentrations in the dedolomitized rocks are probably due to the non-saline character of the dedolomitizing solutions.

The above inference of landward derived solutions is further substantiated by the trace element concentrations in the two laterally equivalent sections shown as Table 5.2.

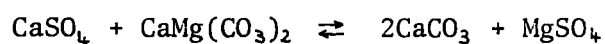
Table 5.2

DISTRIBUTION (MEAN) OF TRACE ELEMENTS IN SECTIONS GPL AND GPW
DEDOLOMITIZATION

Section	GPL		GPW	
Depositional environment	Mostly intertidal and subtidal		Mostly supratidal and upper intertidal	
	<u>Mean</u>	<u>Std.Dev.</u>	<u>Mean</u>	<u>Std.Dev.</u>
Sr $\times 10^{-3}/\text{Ca}$	0.7879	0.0725	0.5422	0.0827
Mn $\times 10^{-3}/\text{Ca}$	0.2129	0.0540	0.2572	0.0567
Fe $\times 10^{-2}/\text{Ca}$	0.4178	0.1262	0.3969	0.1384
Na $\times 10^{-3}/\text{Ca}$	0.3609	0.2701	0.2516	0.3330
Dedolomite (mean) percentage	22		29	

It has been demonstrated that during dedolomitization loss of Mg, Sr and Na together with increase of Mn takes place. Under certain conditions an increase of Fe also takes place. As seen in Table 5.2, the effect of dedolomitization (in terms of trace element concentrations) is more pronounced in section GPW (mostly supratidal and upper intertidal) as compared to section GPL (mostly intertidal and subtidal). A general model of dedolomitization in the Gunns Plains Limestone is shown as Fig. 5.27.

The formation of dedolomite is believed by many authors to be represented by the equation:



The sulphate ions needed for the reaction are attributed to the dissolution of gypsum or anhydrite (De Groot, 1967; Goldberg, 1967; Abbott, 1974; and others) or the oxidation of pyrite (Evamy, 1969; Folkman, 1969).

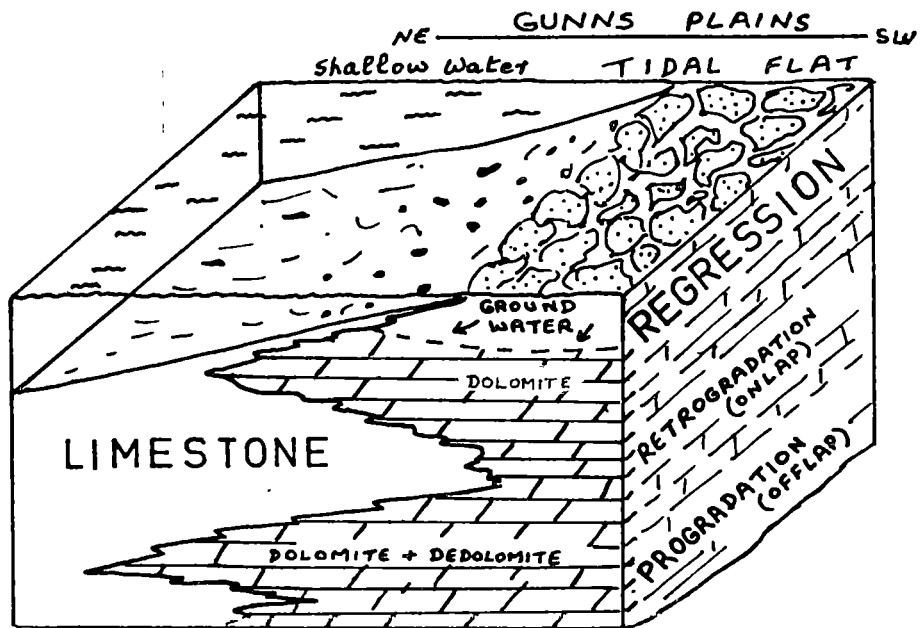
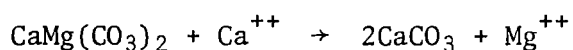


Fig.5.27. A general model for dedolomitization due to influx of ground water during regressive phases in the Gunns Plains Limestone.

In the study area, evaporitic moulds although present are not common. Pyrite is even less common than the evaporitic moulds. However, the possibility of sulphate ions being derived from the dissolution of evaporite minerals cannot be over-ruled. Perhaps, they were in greater abundance than now suggested in areas now eroded away (marginal to the tidal flats, south-east of section GPW).

The process of dedolomitization can also take place in the absence of sulphate ions (Katz, 1968; Folkman, 1969; Al-Hashimi and Hemingway, 1973). According to Lippmann (1973), Hanshaw and Back (1979), dolomite may convert to CaCO_3 in the presence of calcium-rich solutions according to the reaction:



According to Abbott (1974), dedolomitization can proceed in a ground-water system where the Ca/Mg activity ratio is greater than 1 and this ratio is initially determined by the type of rocks in the ground-water source terrain. Meteoric ground-water passing through a carbonate terrain (in this study metastable carbonates) can account for high Ca/Mg ratios. According to Land (1967), fresh waters that may be undersaturated with respect to CaCO_3 remove Mg^{++} from magnesian calcite by exsolution or incongruent dissolution and congruently dissolve aragonite. At a low P_{CO_2} , dolomite dissolves incongruently (Yana'teva, 1955; De Groot, 1967). Extensive flushing by fresh water may remove the Mg as Longman and Mench (1978) have proposed. At the same time, abundant Ca^{++} ions may be derived from the dissolution of aragonites in the recharge area to raise the Ca/Mg ratio of the pore waters and cause calcite to replace dolomite.

Chapter 6

STABLE-ISOTOPE STUDIES

INTRODUCTION

Petrographic and geochemical studies indicate that the limestones at Gunns Plains have undergone early diagenetic supratidal dolomitization and dedolomitization. At times of dolomitization, mixing with the dolomitizing brines of small amounts of water from a landward source took place, but this did not alter the (?hypersaline) fundamental marine character of the dolomitizing brines. A greater influx of non-saline ground water resulted in dedolomitization of the dolomitic rocks.

The isotopic composition of carbonate rocks depends not only on the environment at the time of deposition, but also on isotopic exchange processes since deposition, i.e. diagenesis (Land and Epstein, 1970). Therefore, besides the petrographic and geochemical evidence, additional insight into the nature of depositional and diagenetic changes (limestone → dolomitic limestone → dedolomitic limestone) may be gained by isotopic analysis.

With this in view, 32 limestones, dolomitic limestones and dolostones, and dedolomitic limestones were analyzed for oxygen and carbon isotopic abundances.

SAMPLE PREPARATION AND ANALYTICAL PROCEDURE

Three different series of samples were selected for isotope analysis:

1. About 40 mg of powdered limestone samples (containing less than 10% dolomite) were reacted with 100% phosphoric acid at 25°C following the method described by McCrea (1950). The CO₂ extracted after three hours reaction has been taken as coming from the calcitic parts.

TABLE 6.1

159

Series 1: Isotope Analyses

UTGD Number	$\delta^{18}\text{O}$ ‰		$\delta^{13}\text{C}$ ‰	Rock Type
	PDB	SMOW	PDB	
49041	-6.5	+24.2	+0.1	Intraclast bearing micrite
49051	-6.9	+23.7	-0.4	Dismicrite
49062	-6.7	+24.0	-0.7	Biomicrite
49065	-7.3	+23.3	-0.3	Biomicrite
49112	-8.3	+22.3	-0.7	Biomicrite
49115	-8.3	+22.3	-0.8	Pelbiomicrite
49112	-8.6	+22.0	-0.7	Biomicrite
49126	-6.4	+24.3	0.0	Biosparite
49143	-6.0	+24.6	-0.6	Pelbiomicrite

TABLE 6.2

Series 2: Isotope Analyses

UTGD Number	Limestone (calcite+dedolomite)			Dolomite			Rock Type
	$\delta^{18}\text{O}$ ‰		$\delta^{13}\text{C}$ ‰	$\delta^{18}\text{O}$ ‰		$\delta^{13}\text{C}$ ‰	
	PDB	SMOW	PDB	PDB	SMOW	PDB	
49053	-6.8	+23.9	+0.7	-4.4	+26.3	+1.3	Intraclast bearing fossiliferous micrite
49072	-5.4	+25.3	+1.6	-3.1	+27.7	+1.8	Fossiliferous micrite
49078	-6.5	+24.2	+0.5	-4.2	+26.5	+0.8	Intramicroite
49080	-5.7	+25.0	+1.4	-3.2	+27.6	+1.1	Fossiliferous micrite
49121	-6.4	+24.3	+1.1	-3.1	+26.4	+1.7	Dolomicroite
49181	-	-	-	-4.4	+26.3	+0.7	Intraclast bearing fossiliferous micrite
49164	-7.1	+23.5	-1.5	-5.1	+25.6	-0.7	" "
49090	-7.0	+23.6	-1.0	-5.6	+25.0	0.0	Intramicroite

TABLE 6.3

Series 3: Isotope Analyses

UTGD Number	Dedolomite			Dolomite			Rock Type
	$\delta^{18}\text{O}$ ‰		$\delta^{13}\text{C}$ ‰	$\delta^{18}\text{O}$ ‰		$\delta^{13}\text{C}$ ‰	
	PDB	SMOW	PDB	PDB	SMOW	PDB	
49080	-4.0	+26.7	-0.4	-	-	-	Fossiliferous micrite
49055	-	-	-	-2.6	+28.2	0.0	Micrite
49076	-4.5	+26.2	-0.6	-3.0	+27.8	-0.4	Intraclast bearing fossiliferous micrite
49061	-5.0	+25.7	+0.2	-2.2	+28.6	+0.1	Intraclast bearing micrite
49111	-4.2	+26.5	-0.4	-2.1	+28.7	+1.7	Intraclast bearing biomicrite

2. In dolomitic limestones (10 to 50% dolomite) and dolostone (>50% dolomite), no separation of the dolomitic and calcitic parts was attempted. About 50 mg of the powdered samples were permitted to react with the phosphoric acid. The CO₂ extracted after three hours reaction was taken as coming from the calcitic parts. Further reaction was allowed to proceed and the CO₂ collected after 18 to 20 hours was taken as coming from the dolomitic parts. (This is essentially the procedure followed by Sheppard and Schwarz, 1970.)
3. In samples with a dense mosaic of dolomite, as revealed by microscopic examination, about 50 mg of the central part of these mosaics was removed with the help of a vibrator drill. (Extreme care is required in this operation, so as not to include any surrounding micritic calcite.) The CO₂ obtained after three hours reaction of this fraction with the acid is considered to represent the dedolomites, while that obtained after 18 to 20 hours is taken to represent the dolomite.

It must be kept in mind that for series 1 and 2 analyses, any dedolomite that might have been present would now be included in the limestone (calcite) part. [See discussion below.] The dolomite $\delta^{18}\text{O}$ and $\delta^{13}\text{C}$ values obtained in series 2 and 3 are for pure dolomites without any dedolomites in them. As shown in Table 6.3, the values obtained for the dedolomites in series 3 analyses are distinct from those of limestones (calcites) shown in Tables 6.1 and 6.2.

Cylinder CO₂, calibrated against TKL (Tekviti Limestone, New Zealand) was used as a working mass spectrometer standard. Isotopic measurements of the CO₂ gas were made on a VG Micromass 602D mass spectrometer with ^{13}C and ^{18}O expressed in the δ -terminology, as parts per mil (‰) deviation relative to the PDB standard (= *Belemnitella americana* from the Pee Dee Formation of South Carolina), where

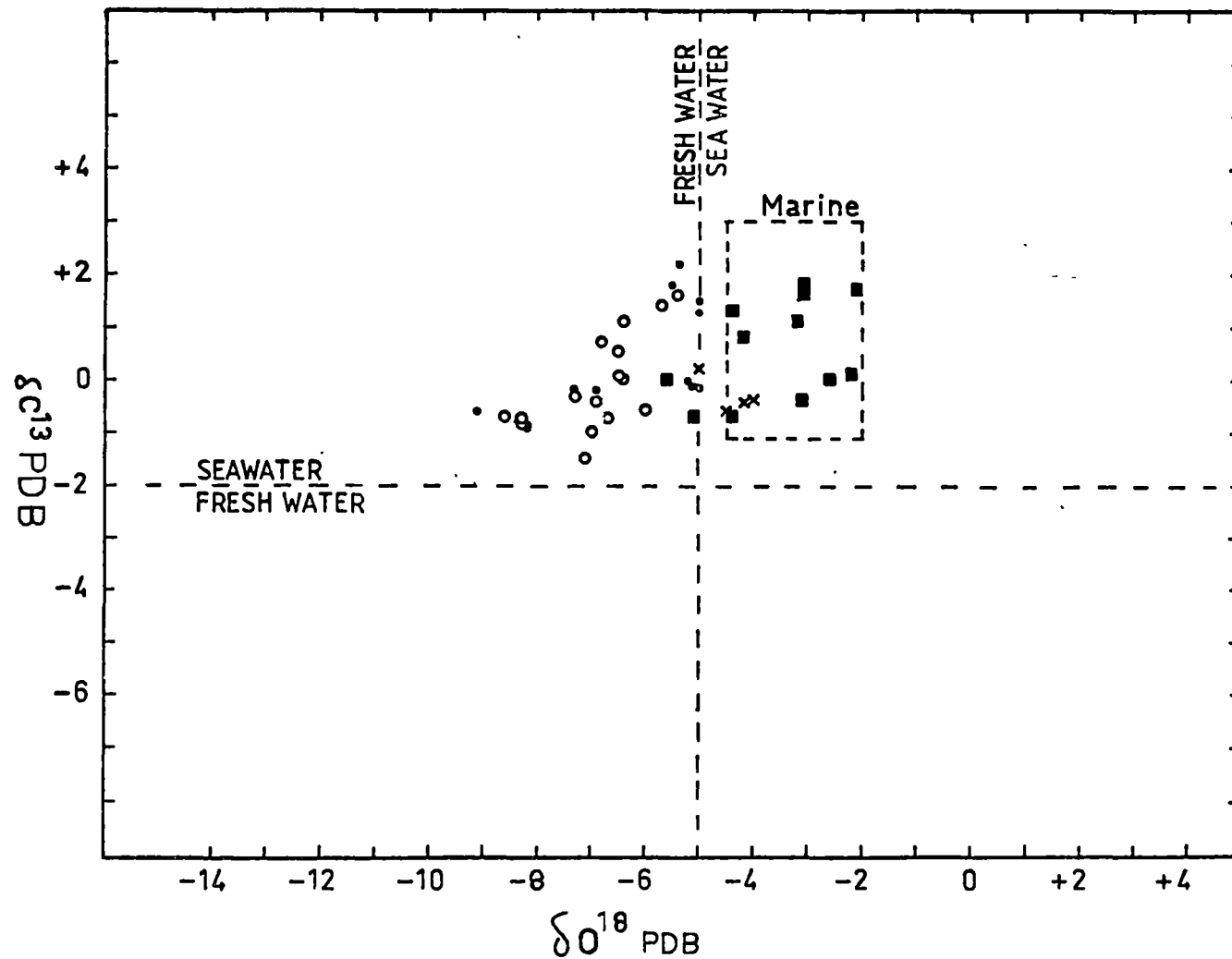


Fig.6.1. Plot of δC^{13} and δO^{18} data. Open circle: limestone; closed circle: Veizer and Compston (1974) data for Gordon Limestone Subgroup; cross: dedolomite; square: dolomite. Line separating fresh water and seawater samples after Keith and Weber (1964). About 84 % of marine limestones analysed by Keith and Weber fall in box labelled marine.

$$\delta^{13}\text{C} \text{ or } \delta^{18}\text{O} \text{ ‰} = \frac{R_{\text{sample}} - R_{\text{standard}}}{R_{\text{standard}}} \times 1000$$

where R = isotope ratio for either element.

The oxygen isotope data have also been expressed relative to Standard Mean Ocean Water (SMOW) using the following expression of Friedman and O'Neil (1977):

$$\delta^{18}\text{O}_{\text{SMOW}} = \delta^{18}\text{O}_{\text{PDB}} \times 1.03086 + 30.86$$

RESULTS

All results of oxygen and carbon isotopic analyses are listed in Tables 6.1, 6.2 and 6.3. Figure 6.1 shows the $\delta^{18}\text{O}$ values plotted against the $\delta^{13}\text{C}$ values.

In order to use the isotopic composition of the analysed samples, it must be decided whether these analyses reflect the original depositional composition or whether the samples have undergone exchange reactions since deposition resulting in changes to the isotopic composition.

Dedolomites

During dedolomitization, the dolomite crystals are partly or totally replaced by calcite (dedolomite). The resultant effect of dedolomitization in the limestone part of a sample is revealed in microscopic studies by the occurrence of relict rims (see Chapter 5). This microscopic evidence of a transition from dedolomites to limestone (micrite) indicates (by itself) that the isotopic composition of the limestone part could have been affected by the dedolomitization process. On this basis, it is reasonable to assume that the limestone values in Tables 6.1 and 6.2 could reflect some degree of re-equilibration in their isotopic composition during dedolomitization.

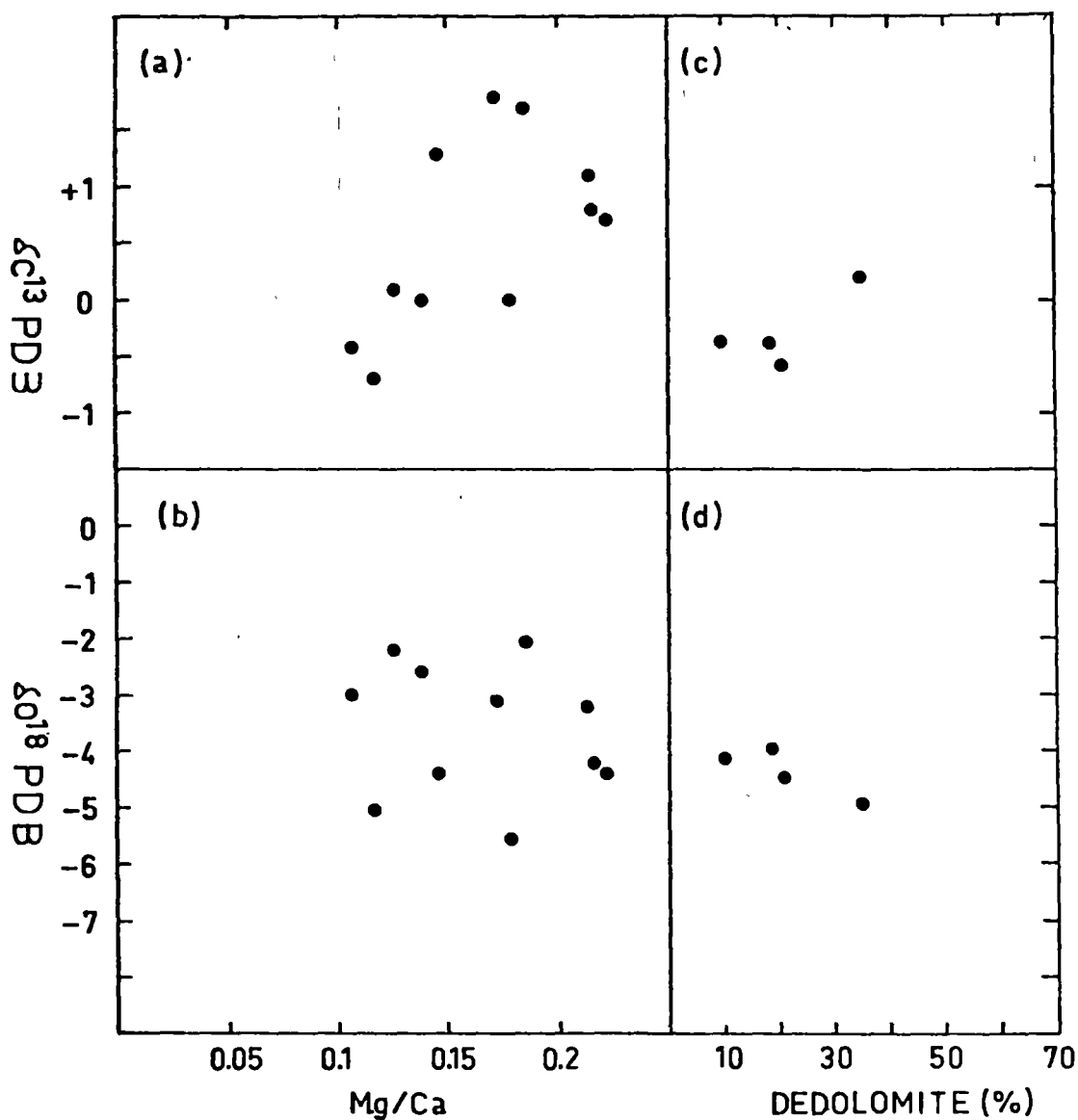


Fig.6.2. Relationship of Mg/Ca molar ratio representing the dolomite content with (b) $\delta^{18}\text{O}$ and (a) $\delta^{13}\text{C}$. Relationship of dedolomite with $\delta^{13}\text{C}$ and $\delta^{18}\text{O}$ shown in (c) and (d) respectively.

The dedolomites have $\delta^{18}\text{O}$ values ranging from -4.0 to $-5.0\text{‰}_{\text{PDB}}$ ($+26.7$ to $+25.7\text{‰}_{\text{SMOW}}$) and $\delta^{13}\text{C}$ values from $+0.2$ to $-0.6\text{‰}_{\text{PDB}}$.

Fig. 6.1 shows that the $\delta^{18}\text{O}$ values of the dedolomites are within the limits given by Keith and Weber (1964) for marine limestones. If dedolomitization proceeded under marine conditions, then the earlier conclusion drawn in Chapter 5 regarding an influx of non-marine water from a landward source during dedolomitization would be in doubt. However, the following discussion will show that sea-water is unlikely to have been responsible for dedolomitization.

A plot of the dedolomite content and the $\delta^{18}\text{O}$ and $\delta^{13}\text{C}$ content is shown as Figs. 6.2c and 6.2d. These samples are from three different cycles and were the only ones from which dedolomite could be extracted without risk of contamination from original calcite (micrite). [See sample preparation, p. 160.] Thus within the limitations imposed by the small number of suitable dedolomites, the samples plotted in Fig. 6.2d show a tendency towards a depletion in ^{18}O with increasing dedolomite content. The $\delta^{13}\text{C}$ values obtained for dedolomites are similar to those of dolomites and limestones. No clear relationship of $\delta^{13}\text{C}$ with the dedolomite content is evident from Fig. 6.2c. However in sample 49080, isotopic analyses for limestone (calcite + dedolomite), dolomite and dedolomite gave $\delta^{13}\text{C}$ values of $+1.4$, $+1.1$ and -0.4‰ . This light $\delta^{13}\text{C}$ value of -0.4‰ in dedolomite compared to the calcite + dedolomite fraction suggests depletion of ^{13}C during dedolomitization.

The $\delta^{18}\text{O}$ values in dedolomites would depend on the amount of dedolomitizing solution, its isotopic composition and temperature. The isotopic composition of the carbonate must also have been controlled by the ratio between the quantity of dedolomitizing solution and amount of dedolomite formed, i.e. the water to rock ratio. For one sample (49080), isotopic analysis was performed on three separate fractions: limestone (calcite + dedolomite), dolomite and dedolomite. The $\delta^{18}\text{O}$ values

are -5.7‰, -3.2‰ and -4.0‰_{PDB} respectively. The dedolomite $\delta^{18}\text{O}$ value of -4.0‰ probably reflects a decrease in the ^{18}O content of the sample during dedolomitization, but as compared to the limestone ^{18}O value (-5.7‰), the dedolomite is heavier in its oxygen content. According to Fritz (1967, p.1263), if only a small amount of fresh water is available (for dedolomitization), it will change its isotopic composition during the process of solution (of limestone) and reprecipitation of carbonate (dedolomite). Thus, as the fresh water dissolves mainly marine carbonates it becomes gradually enriched in ^{18}O and therefore one finds a consequent progressive enrichment in heavy isotopes in the newly formed calcite (dedolomite).

Further argument to negate the possible sea-water origin of dedolomites proceeds in three steps:

- a) Calculation of the present value of $\delta^{18}\text{O}$ of the original calcite (formed from aragonite?) of the limestones, including the cumulative effects of diagenesis on $\delta^{18}\text{O}$.
- b) The establishment of a relationship between the water to rock ratio the $\delta^{18}\text{O}$ values of dedolomitizing solution and calcite prior to dedolomitization.
- c) Use of known limits of isotopic composition of marine carbonates with the results of step (a) and (b) to delineate all possible paired values of water to rock ratios and $\delta^{18}\text{O}$ of dedolomitizing solution in order to compare that water with sea-water.

The following symbols will be used:

R = whole rock	D = dolomite	C = calcite	Dd = dedolomite
Ca ⁰ = original carbonate fraction	X = mole fraction		
W/R = water to rock ratio (molar)			

$\delta^{18}\text{O}$ of Original Carbonate Plus Effects of Diagenesis

It has already been mentioned in the earlier discussion (p.162) that the isotopic composition of the limestones may have been affected by the dedolomitization process. The series 1 and 2 analyses sampled $\delta\text{C} + \text{Dd}$ in the first CO_2 fraction and δD in the second fraction of series 2. It has also been mentioned previously that in one sample (49080) it was possible to separate a fraction of D and Dd uncontaminated by C. Thus, for this case alone, the following data exists:

$$\text{R} = \text{C} + \text{D} + \text{Dd}$$

<u>Volume est.</u>	<u>Molar proportions</u>	<u>$\delta^{18}\text{O}_{\text{PDB}}$</u>
64% C = 64%	0.71	?
36% D = 22%	0.13	-3.2 (+27.6 _{SMOW})
40% Dd = 14%	0.16	-4.0 (+26.7 _{SMOW})

$$\text{and } \text{C} + \text{Dd} = -5.7\%$$

In the C + Dd fraction

$$\delta(\text{C}+\text{Dd}) = \delta\text{C} \cdot \text{XC} + \delta\text{Dd} \cdot \text{XDd} \quad (\text{X} = \text{mole fraction with respect to total calcite only})$$

$$\text{XC} = \frac{64}{64 + 14} = 0.82$$

$$\text{XDd} = \frac{14}{64 + 14} = 0.18$$

$$-5.7 = (\delta\text{C} \times 0.82) + (-4.0 \times 0.18)$$

$$\delta\text{C} = \frac{-5.7 + 0.72}{0.82} = -6.1\% \text{ PDB} \quad (\text{or } +24.0\% \text{ SMOW})$$

Thus $-6.1\% \text{ PDB} = \delta\text{Ca}^0 + \text{effects of diagenesis}$, where δCa^0 refers to the $\delta^{18}\text{O}$ value of the original carbonate at the time of deposition, i.e. prior to diagenesis. It must be kept in mind that the above mass balance calculations depend on the correct estimation of the dolomite and dedolomite content (discussed in the previous chapters).

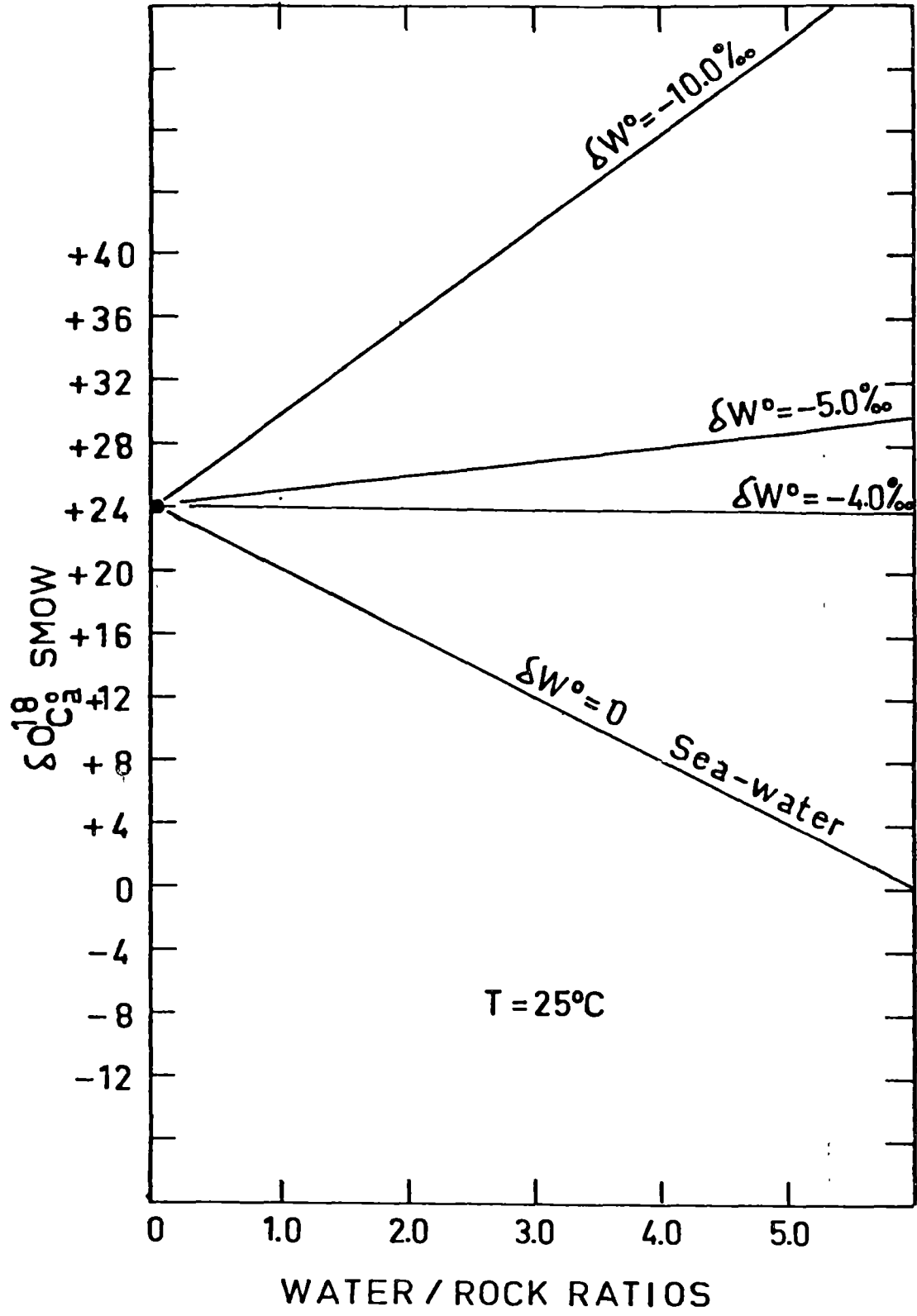


Fig.6.3. Relationship between δC_a° and W/R ratio. The W/R ratio is based on Taylor (1974) equation for closed system. See discussion in text.

Relationship Between W/R, $\delta\text{Ca}^{\text{O}}$ and $\delta^{18}\text{O}$ Content of the Dedolomitizing Solution

Suppose that all subsequent changes in $\delta\text{Ca}^{\text{O}}$ can be ascribed to dedolomitization. [Changes due to dolomitizing fluids, which were fundamentally marine, and therefore already in isotopic equilibrium with original calcite can be ignored.]

The W/R ratios can be calculated by using the equation given in Taylor (1974) assuming complete equilibration during dedolomitization.

$$W/R = \frac{\delta_{\text{Rock}}^f - \delta_{\text{Rock}}^i}{\delta_{\text{H}_2\text{O}}^i - (\delta_{\text{Rock}}^f - \Delta)}$$

where i = initial value

f = final value after exchange

$\Delta = \delta_{\text{Rock}}^f - \delta_{\text{H}_2\text{O}}^f$ fractionation factor

For the present case, considering only the calcite and dedolomite in the rock, which form 87% of the total rock (see step a), the relationship can be expressed as:

$$W/R = \frac{\delta\text{C} - \delta\text{Ca}^{\text{O}}}{\delta\text{W}^{\text{O}} - (\delta\text{C} - \Delta)}$$

where Δ = calcite-water fractionation factor

$\delta\text{W}^{\text{O}} = \delta^{18}\text{O}$ value of the dedolomitizing solution

The temperature at which dedolomitization occurred in the Gunns Plains limestone is not known. Dedolomitization is considered to be a near-surface process. Experimental work (e.g. De Groot, 1967; Al-Hashimi and Hemingway, 1973) has shown that the process is even operative at room temperatures. Therefore, assuming a temperature of 25°C and using the Epstein *et al.* (1953) equation for calcite-water fractionation, the Δ value obtained is $+28.0\text{‰}_{\text{SMOW}}$. The value of δC from step (a) is known

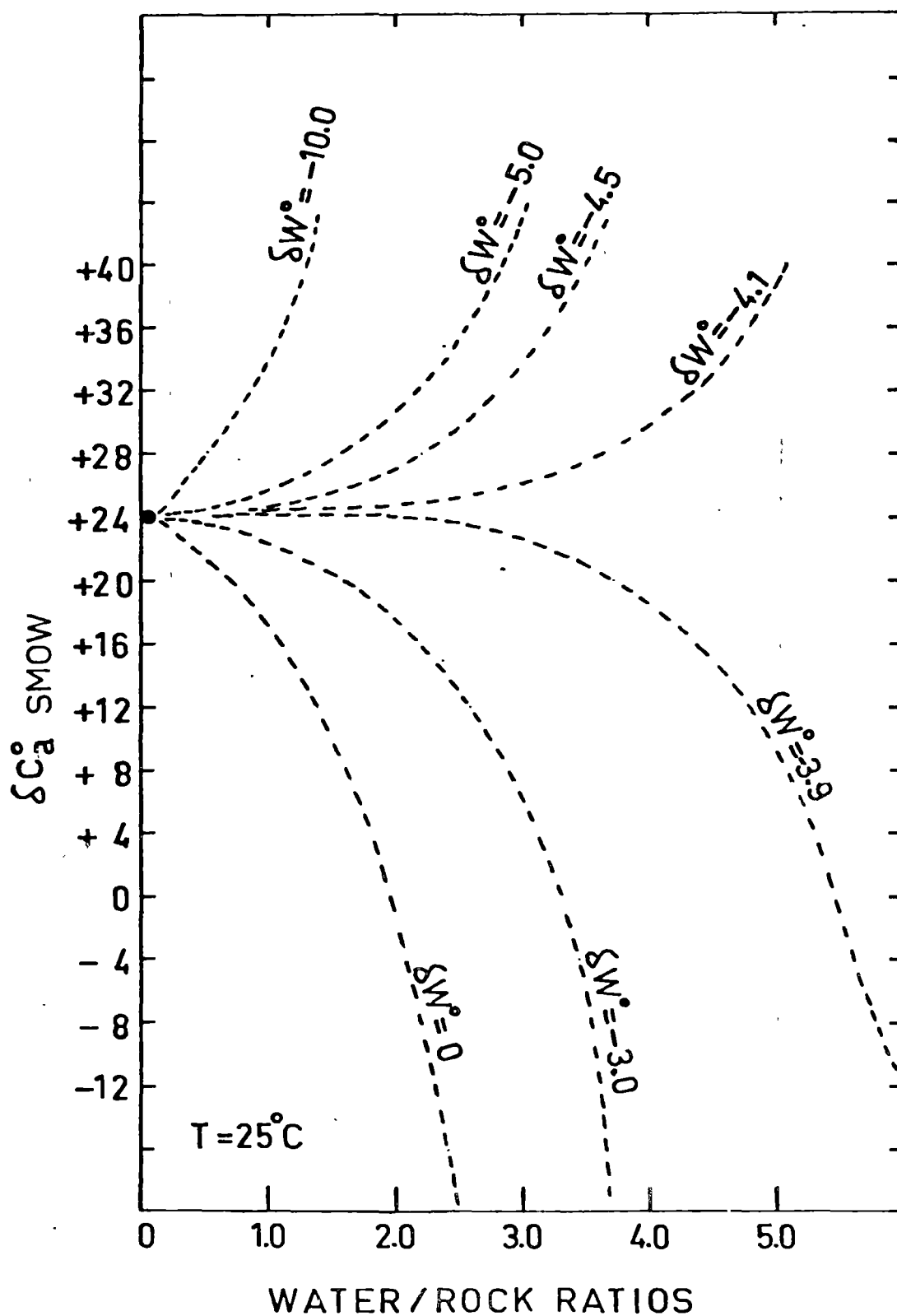


Fig.6.4. Relationship between δC_a and W/R ratio derived from Taylor (1977) equation for open system.

to be +24.0‰_{SMOW} (-6.1‰_{PDB}). Substituting in the above relationship,

$$W/R = \frac{+24.0 - \delta Ca^O}{\delta W^O - (24.0 - 28.0)} = \frac{24 - \delta Ca^O}{\delta W^O + 4}$$

For chosen values of δW^O (0, -4.0, -5.0 and -10.0‰_{SMOW}), values of δCa^O and W/R have been plotted in Fig. 6.3. The point shown on the Y-axis of the figure is the δC value. From this figure, it is seen that if $\delta W^O = < -4.0$, $\delta Ca^O > \delta C$. If dedolomitizing waters were of this isotopic composition, then, original carbonate would have become isotopically lighter during dedolomitization, regardless of W/R ratio.

According to Taylor (1977, p.524), the above relationship for determining W/R ratios applies to systems in which continuous recirculation and cyclic re-equilibration of the water takes place with insignificant loss. In a system (open) where each increment of water makes only a single pass, the equation for determining W/R ratio is

$$W/R = \log_e \frac{\delta_{H_2O}^i + \Delta - \delta_{Rock}^i}{\delta_{H_2O}^i - (\delta_{Rock}^f - \Delta)}$$

Based on this relationship, for chosen values of δW^O (0, -3.0, -3.9, -4.1, -4.5, -5.0 and -10.0‰), the δCa^O and W/R have been plotted in Fig. 6.4. Again, it can be seen that if $\delta W^O = < -4.0$, $\delta Ca^O > \delta C$.

Delineation of Paired Values of W/R Ratios and $\delta^{18}O$ of Dedolomitizing Solution

The above discussion has not been able to place enough constraints to determine whether or not sea-water was involved in dedolomitization. To investigate this, extra data must be invoked.

According to the data of Keith and Weber (1964), 85% of their samples contained $\delta^{18}O$ in the range of about -4.5 to -2.0‰_{PDB}, or +26.2 to +28.8‰_{SMOW}. Assuming that the Ordovician marine carbonates of the study area were also of this composition, i.e.

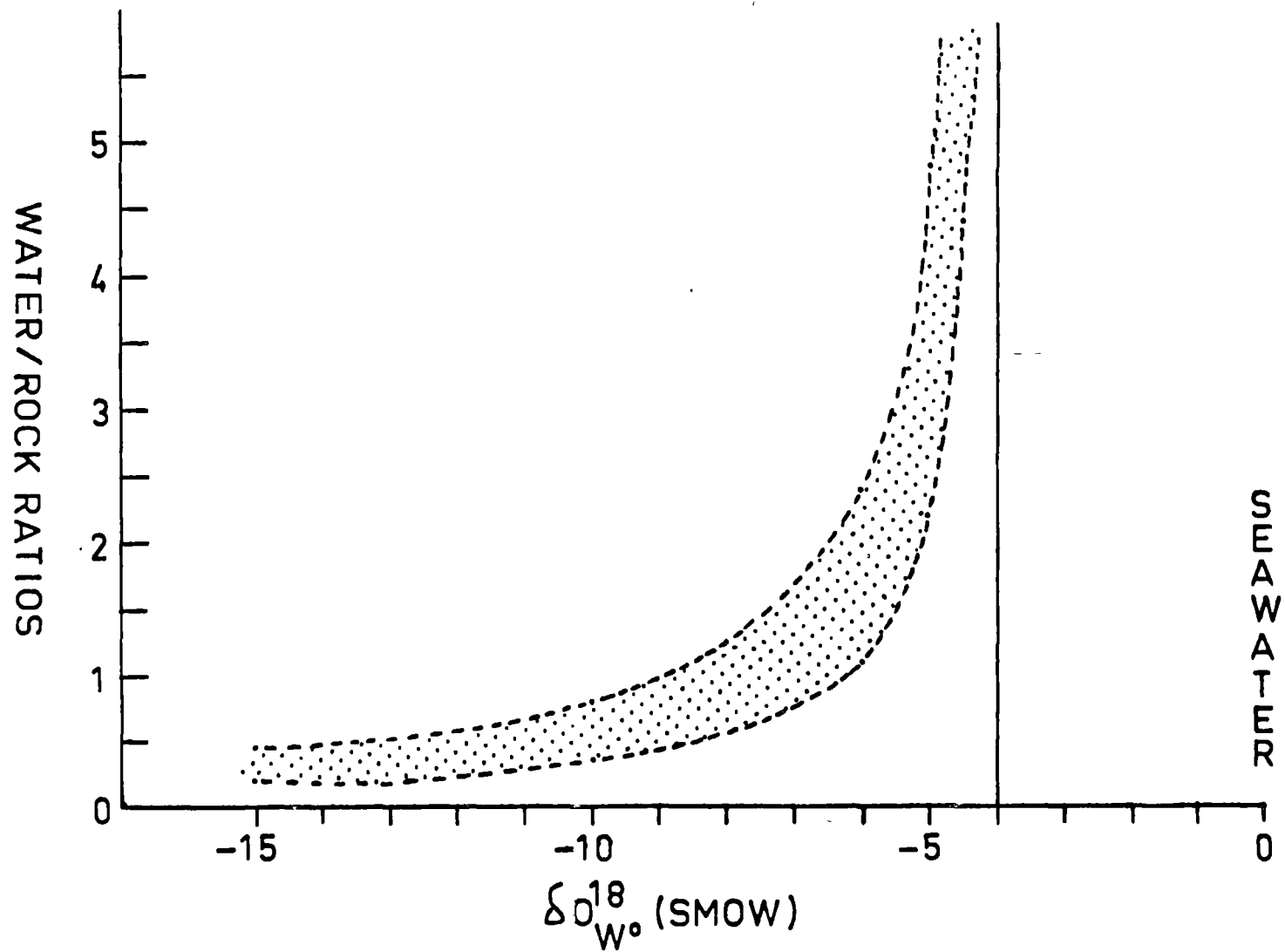


Fig.6.5. Permissible values of dedolomitizing solution and W/R ratio. The field lies away from seawater of present day composition, thus ruling it out as the agent of dedolomitization.

$$26.2 < \delta\text{Ca}^{\text{O}} < 28.8\text{‰}$$

$$\text{or } 26.2 < 24.0 - W/R (\delta\text{W}^{\text{O}}+4) < 28.8$$

$$2.2 < -W/R (\delta\text{W}^{\text{O}}+4) < 4.8$$

For any chosen value of $\delta\text{W}^{\text{O}}$, the range of W/R can be calculated,

e.g. if $\text{W}^{\text{O}} = 0$,

$$2.2 < -4 W/R < 4.8$$

$$-0.55 > W/R > 1.2$$

Since negative values of W/R are not valid, it can be seen that only values of $\delta\text{W}^{\text{O}} < -4.0$ give reasonable solutions. The field of such solutions is plotted in Fig. 6.5.

e.g. for $\delta\text{W}^{\text{O}} = -5.0$, $2.2 < -W/R (-1) < 4.8$

for $\delta\text{W}^{\text{O}} = -6.0$, $2.2 < -W/R (-2) < 4.8$

for $\delta\text{W}^{\text{O}} = -10.0$, $2.2 < -W/R (-6) < 4.8$

A more precise estimate of $\delta\text{W}^{\text{O}}$ now depends on estimating W/R . In any case, it is seen that $\delta\text{W}^{\text{O}}$ cannot be 0‰_{SMOW}, i.e. sea-water of present day composition is ruled out as the agent of dedolomitization. However, the possibility of isotopically lighter sea-water during the Palaeozoic has also been advanced (e.g. Fritz, 1971; Perry and Tan, 1972; Veizer, 1977). In addition, Knauth and Epstein (1976) favour higher temperatures (av. 34°C) for the early Palaeozoic. At present the isotopic composition and maximum temperature of the Palaeozoic oceans remain uncertain (Hudson, 1977, p.645).

Dolomites

Perusal of the literature shows that stable isotope determinations have yielded contradictory results. According to O'Neil and Epstein (1966) the penecontemporaneous dolomites are enriched in their ^{18}O content by 5.0 to 7.0‰ relative to calcite (syngenetic). Other $\delta^{18}\text{O}$ enrichment values reported range from 0.5 to 10‰ (see Weber, 1964; Gross and Tracey, 1966; Fritz, 1967; Hall and Friedman, 1969; Sheppard and Schwarz, 1970). $\delta^{18}\text{O}$ values isotopically lighter than coexisting calcites are also known (e.g. Fritz, 1967; Bausch and Hoefs, 1972).

The isotopic fractionation of oxygen in the dolomite-water system at low temperature is not well known and the above-mentioned enrichment of 5.0 to 7.0‰ is obtained by extrapolation of oxygen isotope fractionation from high temperature experiments. Matthews and Katz (1977) observed nearly zero enrichment in ^{18}O between synthetic hydrothermal dolomite and its precursor calcite. To explain the variation in observed fractionation many workers have concluded that enrichment only occurs under equilibrium conditions, but Fritz and Smith (1970) have shown experimentally that protodolomites (believed to form under non-equilibrium conditions) were enriched by approximately 3 to 4‰ relative to pure calcite. Evaporation is also believed to result in higher ^{18}O values (e.g. Epstein and Mayeda, 1953) and has led to suggestions that dolomites isotopically heavier than coexisting calcite form in the presence of hypersaline brine which is enriched in ^{18}O by evaporation (e.g. Berner, 1965; Gross and Tracey, 1966). In ancient carbonates, the interpretation of isotopic data is further complicated by the inference that past oceans had a lower ^{18}O content than the present day oceans (e.g. Fritz, 1971; Friedman, in Ross *et al.*, 1975).

The above brief discussion shows the state of controversy regarding the isotopic data interpretation of dolomites. It is within these overall limitations that the isotopic data of dolomites in the present study is discussed.

The $\delta^{18}\text{O}$ values in dolomite are believed to be prone to diagenetic exchange processes (e.g. Land and Epstein, 1970; Land *et al.*, 1975). According to Gross (1964) and Land *et al.* (1975) the general trend during diagenesis is a depletion in ^{13}C and ^{18}O from marine carbonate minerals as a result of re-equilibration with meteoric water. On the other hand, it is believed that marine environments can be differentiated from fresh water environments (e.g. Keith and Weber, 1964). Thus there are two extreme models:

1. The $\delta^{18}\text{O}$ content of the dolomite remained unchanged at the time of dedolomitization, i.e. the dolomite, which formed under marine conditions did not undergo isotopic exchange with non-marine water at the time of early diagenetic dedolomitization.
2. The $\delta^{18}\text{O}$ content of dolomite changed during dedolomitization, i.e. dolomite underwent isotopic exchange and came into isotopic equilibrium with the newly formed calcite (dedolomite).

In the present study, the $\delta^{18}\text{O}$ values in the dolomites range from -2.1 to -5.6‰ PDB (+28.7 to +25.0‰ SMOW). All dolomites are heavier in their $\delta^{18}\text{O}$ content compared to calcites analyzed from the same samples (see Table 6.2). The degree of enrichment relative to calcite in sample 49090 is 1.4‰, while in others it ranges from 2.0 to 3.3‰. It must be kept in mind that this ^{18}O enrichment in dolomites is relative to those calcites which are believed to have undergone isotopic exchange during the process of dedolomitization (see previous discussion). As the dolomites may have also undergone isotopic exchange during dedolomitization, the initial relative enrichment resulting from dolomitization may have been significantly different.

According to the experimental work of Tarutani *et al.* (1969), Mg-rich calcites are enriched in ^{18}O relative to pure calcite. Supko (1977) observed a trend of ^{18}O enrichment with increasing mol % MgCO_3 in dolomites. In the present study, a plot of $\delta^{18}\text{O}$ against the Mg/Ca molar ratios, representing the dolomite content (Fig. 6.2b) shows a random relationship. However, the $\delta^{13}\text{C}$ values of dolomites show a trend of more positive $\delta^{13}\text{C}$ values with increasing Mg/Ca (Fig. 6.2a). According to Rothe, Hoefs and Sonne (1974, p.392), shells of *Hydrobia* feeding on algae have high Mg. As this high Mg is chlorophyll-derived, the $\delta^{13}\text{C}$ values are low because ^{12}C is enriched in plant tissues and therefore high Mg contents should correlate with low $\delta^{13}\text{C}$ values. It is believed that a trend similar to that of Rothe *et al.* (1974) would have been present in dolomites, if the Mg in these dolomites had been derived from algal mats.

At this stage, the interpretation of the isotopic data is equivocal. The situation cannot be resolved without a better understanding of the process of dolomite formation at low temperature.

Limestones

The limestones (calcites) have $\delta^{18}\text{O}$ values ranging from -5.4 to -8.6‰ PDB (+25.3 to +22.0‰ SMOW) and $\delta^{13}\text{C}$ values ranging from +1.6 to -1.5‰ PDB. The only other previous isotopic analyses of the Gordon Limestone Subgroup have been done by Veizer and Hoefs (1976). They analyzed 12 limestone samples from different localities (mostly from the Florentine Valley type area; see also Veizer and Compston, 1974) and reported $\delta^{18}\text{O}$ values ranging from -5.0 to -9.1‰ PDB, and $\delta^{13}\text{C}$ values ranging from +2.2 to -0.8‰ PDB. These values have also been plotted in Fig. 6.1 together with the values obtained in this study. Considering the widespread locations covered by Veizer and Hoefs (1976), their

reported values are quite similar to those obtained in the present study.

Both petrographic studies and the discussion of the isotopic data of dedolomites (p.162) have shown that the limestones have been affected by dedolomitization. Veizer and Compston (1974) have also stated that their values probably reflect partial diagenetic equilibration, although they do not mention the time at which this re-equilibration may have taken place. Green *et al.* (1980) have analyzed rain water and cave seepage samples from Tasmania in order to study their effects on diagenesis. Green (pers. comm., 1980) reports $\delta^{18}\text{O}$ values for waters from near the study area (Mole Creek) to be -6.0 to -8.0‰ SMOW . These values based on the calcite-water fractionation factor of +28.0 at 25°C (Epstein *et al.*, 1953) result in values of +34.0 to +36.0‰ for the calcite. Comparison with the measured $\delta^{18}\text{O}$ values in the present study (see Tables 6.1 and 6.2) shows that no re-equilibration with present day waters has taken place. Thus a similar spread of values in the Florentine Valley (Veizer and Compston, 1974) as in the present study suggests possible re-equilibration during early diagenesis.

According to Keith and Weber (1964), samples with $\delta^{13}\text{C}$ heavier than -2.0‰ PDB are of marine origin. The analyzed samples (see Table 6.1) fall within this range. According to Degens and Epstein (1964), the $\delta^{13}\text{C}$ in carbonates is more resistant to depletion than $\delta^{18}\text{O}$ due to a larger reservoir of carbon in the marine sediments relative to the HCO_3^- in the diagenetic solution. Hudson (1975) believes that ancient limestones with $\delta^{13}\text{C}$ values in the marine range were not affected by near-surface fresh water diagenesis, but by burial diagenesis. The opposite view is held by Allan and Matthews (1977, p.18), who state that negative values are rare in ancient limestones not because subaerial diagenesis was less important, but because highly negative values are only produced near the subaerial exposure surface. In other words,

deeper vadose or phreatic samples would not have negative values.

In the present study, it is believed that the $\delta^{13}\text{C}$ values in the limestones, like the $\delta^{18}\text{O}$ content, must have undergone re-equilibration during early diagenesis.

Chapter 7

SUMMARY AND CONCLUSIONS

In this study the Ordovician Gordon Subgroup at Gunns Plains is represented by a 450+ m thick carbonate sequence named the Gunns Plains Limestone.

Skeletal debris followed by intraclasts are the most common allochemical constituents. Pellets, in significant amounts, occur only in sections GPR and GPD and are believed to have been more abundant than now recognised. This is based on the observations that pellets are often difficult to differentiate from the micrite matrix or patchy recrystallization and dolomitization may be seen obliterating the pellet texture. Oolites are noticeably absent from the Gunns Plains Limestone, occurring sparsely in section GPL. Oncolites occur very sparsely and only in section GPL.

The carbonate rock types (microfacies) recognized in the Gunns Plains Limestone are dominantly micritic in composition and based on their interpreted environments, have been grouped into three major facies - supratidal, intertidal and subtidal. Sixty-three percent of the total samples have been interpreted as belonging to the intertidal facies. Microfacies observed are (a) subtidal - sparse and packed biomicrites: biosparites, pelbiomicrites, fossiliferous micrites and micrites; (b) intertidal - sparse biomicrites, biopelmicrites and pelbiomicrites, pelmicrites and pelsparites, intrapelosparites, intrabiomicrites, intra-oncosparites, intramicrites and intrasparites, intraclast-bearing micrites, intraclast-bearing fossiliferous micrites, fossiliferous micrites, other minor allochem-bearing micrites and dismicrites; (c) supratidal - dismicrites, fossiliferous micrites, intraclast-bearing fossiliferous micrites, intraclast-bearing micrites and intramicrites.

Abundant mudcracks, birdseyes, and vertical and random burrows characterize the supratidal and intertidal facies, while diverse fossil types and random bioturbation features are characteristic of the subtidal facies. The intraclast shapes commonly vary from angular to subangular in the supratidal facies, and rounded to subrounded in the subtidal facies. The observed microfacies are believed to represent a tidal-flat environment.

Vertical distribution of the interpreted environments shows that carbonate sedimentation was cyclic. These asymmetric cycles range in thickness from about 1 m to 6 m, and represent numerous alternations from subtidal conditions in the lower part to intertidal and supratidal in the upper part, indicating that carbonate accumulation mostly took place during regressions and that these depositional regressions represent progradation of the supratidal sequences. The supratidal sequences are mostly immediately overlain by the subtidal sequences, such abrupt transitions denoting that the transgressions were rapid.

Microfacies variation based on the laterally equivalent sections GPB, GPW and GPL suggest supratidal conditions in the south and subtidal conditions in the north of the study area. The microfacies may be related to the Z zone proposed by Irwin (1965). A high energy Y zone probably existed in the north of the studied area during Blackriveran to Kirkfieldian times (i.e. at the time of sections GPL, GPW and GPB deposition) as evidenced by the presence of transported (sparse) oolites, mostly rounded intraclasts and rare oncolites with irregular outlines in section GPL.

Dolomite is of widespread occurrence in the Gunns Plains Limestone and fits the description of "stratal dolomites" as proposed by Fisher and Rodda (1969). The brown or golden-yellow dolomite ranges in grain size from about 10 to 100 μ , the most common range being from 20 to 50 μ . This finely crystalline dolomite, present as subhedral to euhedral crystals, forms an

equigranular mosaic of idiotopic to xenotopic crystals. The dolomite occurs in and around intraclasts, in burrows and around mudcrack margins. No attempt has been made to estimate the dolomite content from X-ray diffractograms. Point count estimates and visual estimates are in good agreement.

Vertical distribution of the dolomite content in the studied sections indicate that there were different episodes of dolomitization, of varying intensity, during regressions. The dolomite content in the different cycles is generally most abundant in the supratidal environment or, where supratidal is absent, in the upper intertidal environment of each cycle. The subtidal environments commonly contain less than 10% dolomite. This early diagenetic dolomite represents tidal flats undergoing sabkha diagenesis.

The Mg/Ca molar ratios, representing the dolomite content, show an inverse relationship with Sr/Ca molar ratios. Samples belonging to the subtidal facies have a higher Sr concentration compared to the supratidal facies. Sr solution compositions are similar to those of aragonite. Na/Ca molar ratios are highly variable. Some Na values are within the range reported from elsewhere in the Junee Group for hypersaline supratidal dolomites (Rao and Naqvi, 1977). The positive relationship of Mn/Ca and Fe/Ca to Mg/Ca, and the higher concentrations of Mn and Fe in the supratidal samples suggests an external source for these elements. The molar ratio variation (except Na/Ca) is related to the degree of dolomitization (amount of dolomite) in the different depositional cycles. These trends persist despite modifications in the trace element concentrations during dedolomitization.

Evidence suggests that besides the downward seepage of the dolomitizing brines, upward or lateral movement also took place. It is believed that ground water passing through an aragonitic terrain mixed with seawater in an intermediate sabkha zone similar to that reported by McKenzie

et al. (1979) for the Abu Dhabi sabkhas during dolomitization in a reflux type of mechanism.

Dedolomitization textures are easily recognized in the Gunns Plains Limestone. Both petrographic and chemical studies demonstrate dedolomitization. The degree to which the individual dolomite crystals within a single sample are affected is highly variable, ranging from a small clot to a whole dedolomitized rhomb. Observation of these textures suggests that most have formed as a result of a centripetal type of dedolomitization. The clots of dedolomite are believed to have been randomly generated and thus the term "random dedolomitization" is proposed in addition to the centrifugal and centripetal types proposed by Shearman *et al.* (1961).

Perusal of the literature shows that all types of dolomite can be affected by dedolomitization, in contrast to the proposal made by Lippmann (1973) that only calcian dolomites are affected.

The complex nature of the dedolomite fabrics has been the main obstacle in making a quantitative petrographic estimate of the dedolomite content. This is the first study to propose a method for estimating the dedolomite content. The volumetric estimates of (ideal) dolomite are plotted against their Mg/Ca molar ratios. Taking into consideration the differences in density and molecular weights of calcite and dolomite, curves representing different percentages of dedolomitization are constructed with the Mg/Ca = 1 curve corresponding to zero percent dedolomitization. The dedolomite percentage obtained for each sample can be read directly from the graph, which in the present study ranges up to 69%.

In the different depositional cycles, the dedolomite is generally most abundant in the supratidal environment or where supratidal is absent, in the upper intertidal environment. This increase of dedolomitization in the supratidal and the variable amount in the different depositional cycles indicates that dedolomitization occurred in episodes of varying

intensity during regressive phases (i.e. early diagenetic process) and that the dedolomitizing solutions were derived from a landward source.

Most studies dealing with the elemental composition of carbonates as a function of diagenetic changes have not proceeded beyond the effects of dolomitization. In this study, the relationship of trace elements to dedolomitization shows losses of Sr, Na and Mg, and a gain in Mn. The relationship of iron to dedolomitization is not clear.

Sr and Mn concentrations obtained for the dedolomitizing solutions are similar to those of aragonite, suggesting that the transformation of aragonite to calcite had not been completed. Na values are similar to those of meteoric calcites reported by Veizer *et al.* (1978) indicating that dedolomitization occurred in a fluid medium with markedly different salinity from the marine water. It is believed that meteoric ground water passing through a (metastable) carbonate terrain resulted in dedolomitization. The movement of this water was from the south to the north.

The $\delta^{18}\text{O}$ values of the dedolomites (-4.0 to -5.0‰ PDB , $+26.7$ to $+25.7\text{‰ SMOW}$) are within the limits given by Keith and Weber (1964) for marine carbonates. The samples show a tendency towards a depletion in ^{18}O with increasing dedolomite content. Calculation of the $\delta^{18}\text{O}$ of the calcite including the cumulative effects of diagenesis on $\delta^{18}\text{O}$; the relationship between the water to rock ratio (open and closed system), and $\delta^{18}\text{O}$ values of the dedolomitizing solution and calcite prior to dedolomitization; the combination of the above and use of known limits of marine carbonates in order to delineate paired values of water to rock ratios and $\delta^{18}\text{O}$ of dedolomitizing solutions show that sea-water could not have been the agent for dedolomitization.

The $\delta^{18}\text{O}$ values in the dolomites range from -2.1 to -5.6‰ PDB . These values are heavier compared to calcites analyzed from the same sample.

It is believed that the initial enrichment prior to dedolomitization in dolomites must have been significantly different. At present, interpretation of isotopic data is equivocal and will remain so, until the fractionation of oxygen in the dolomite-water system at low temperatures is known.

The $\delta^{18}\text{O}$ values in limestones (-5.4 to -8.6‰) reflect re-equilibration. Comparison with recent rain and cave waters from near the study area shows that this re-equilibration most probably took place sometime after deposition.

According to the data of Keith and Weber (1964), the $\delta^{13}\text{C}$ values in dedolomites (+0.2 to -0.6‰_{PDB}), dolomites (+1.8 to -0.7‰_{PDB}) and limestones (+1.6 to -1.5‰_{PDB}) are of marine origin. In the present study, it is believed that like the ^{18}O content, the ^{13}C content must have also undergone re-equilibration during early diagenesis.

This study has demonstrated the changes in the trace element concentrations during dedolomitization. It is proposed that, in cases where the dedolomite fabrics have been recognized, the trace element concentrations for dolomitization may not be valid. Only after considering the overprints of dedolomitization on the dolomites can trace elements be ascribed to the process of dolomitization. This leads subsequently to a fuller understanding of diagenetic changes in carbonate rocks.

REFERENCES

- ABBOTT, P.L., 1974: Calcitization of Edwards Group dolomites in the Balcones fault zone aquifer, south-central Texas. *Geology*, 2, 359-362.
- ADAMS, J.E., & RHODES, M.L., 1960: Dolomitization by seepage reflexion. *Bull. Am. Assoc. Pet. Geol.*, 44, 1912-1940.
- AITKEN, J.D., 1967: Classification and environmental significance of cryptalgal limestones and dolomites, with illustrations from the Cambrian and Ordovician of southwestern Alberta. *J. Sedim. Petrol.*, 37, 1163-1178.
- AL-HASHIMI, W.S., 1976: Significance of strontium distribution in some carbonate rocks in the Carboniferous of Northumberland, England. *J. Sedim. Petrol.*, 46, 369-376.
- AL-HASHIMI, W.S., & HEMINGWAY, J.E., 1973: Recent dedolomitization and the origin of the rusty crusts of Northumberland. *Jour. Sedim. Petrol.*, 43, 82-91.
- ALLAN, J.R., & MATTHEWS, R.K., 1977: Carbon and oxygen isotopes as diagenetic and stratigraphic tools: Surface and subsurface data, Barbados, West Indies. *Geology*, 5, 16-20.
- BADIOZAMANI, K., 1973: Dorag dolomitization model, Ordovician, Wisconsin. *Jour. Sedim. Petrol.*, 43, 965-984.
- BANKS, M.R., 1956: The Middle and Upper Cambrian series (Dundas Group and its correlates) in Tasmania. In *El Sistema Cambrico*, 2, *Int. geol. Congr.*, 20, Mexico; 165-212.
- BANKS, M.R., 1957: The stratigraphy of Tasmanian limestones. In *Limestones in Tasmania*. (Ed. T.D. Hughes). *Geol. Surv. Min. Resour. No.10*, Tas. Dept. Mines.
- BANKS, M.R., 1962: The Ordovician System. In *The Geology of Tasmania* (Eds. Spry, A.H. & Banks, M.R.). *J. geol. Soc. Aust.*, 9, 2, 147-176.
- BANKS, M.R., 1962: The Cambrian System. *Ibid.*, 127-146.
- BASNAYAKE, S.B., 1975: Geochemistry and petrography of Ordovician Gordon Limestone, Mole Creek area. Thesis (B.Sc. Hons.). Geol. Dept., Univ. Tasm (unpubl.).
- BATHURST, R.G.C., 1976: *Carbonate sediments and their diagenesis*. Elsevier Publishing Co., 658p.
- BAUSCH, W.M., 1965: Dedolomitizierung und Recalcitisierung in frankischen Malmkalken. *Neues Jahrb. Miner.*, 75-82.

- BAUSCH, W., & HOEFS, J., 1972: Die Isotopenzusammensetzung von Dolomiten und Kalken aus dem süddeutschen Malm. *Contr. Mineral. Petrol.*, 37,
- BEALES, F.W., 1958: Ancient sediments of Bahaman type. *Bull. Am. Assoc. Petrol. Geol.*, 42, 1845-1880.
- BEALES, F.W., 1965: Diagenesis in pelleted limestones. In Pray, L.C. & Murray, C. (eds.), *Dolomitization and limestone diagenesis. Spec. Publ. Soc. Econ. Paleont. Miner.*, 13, 49-70.
- BEHRENS, E.W. & LAND, L.S., 1972: Subtidal Holocene dolomite, Baffin Bay, Texas. *Jour. Sed. Petrol.*, 42, 155-161.
- BENCINI, A., & TURI, A., 1974: Manganese distribution in the Mesozoic carbonate rocks from Lima Valley, North Appennines. *Jour. Sed. Petrol.*, 44, 774-782.
- BENSON, L.V., 1974: Transformation of a polyphase sedimentary assemblage into a single phase rock: A chemical approach. *Jour. Sed. Petrol.*, 44, 123-135.
- BERNER, R.A., 1965: Dolomitization of the mid-Pacific atolls. *Science*, 147, 1297-1299.
- BERNER, R.A., 1971: *Principles of chemical sedimentology*. McGraw-Hill, New York, 240p.
- BODINE, M.W., HOLLAND, H.D. & BORCSIK, M., 1965: Coprecipitation of manganese and strontium with calcite. In Symposium on problems of postmagmatic ore deposition, II. Prague, 401-406.
- BRADLEY, J., 1954. The geology of the West Coast Range of Tasmania, Part I. *Pap. Proc. roy. Soc. Tasm.*, 88, 193-243.
- BRAUN, M. & FRIEDMAN, G.M., 1970: Dedolomitization fabric in peels: a possible clue to unconformity surfaces. *J. Sed. Petrol.*, 40, 417-419.
- BRIMBLECOMBE, P. & RAISWELL, R., 1977: The partition of Mn into aragonite between 30° and 60°C. *Chem. Geol.*, 19, 145-151.
- BUCHANAN, H., STREETER, S. & GEBELEIN, C.D., 1972: Possible living algal-foraminiferal consortia in nodules from modern carbonate sediments of the Great Bahama Bank. *Am. Assoc. Petrol. Ann. Meeting*, 56, 606.
- BURNS, K.L., 1957: Geology of the Nook-Gunns Plains area. Thesis (B.Sc. Hons.), Geology Dept., Univ. Tasm. (unpubl.).
- BURNS, K.L., 1963: The tectonic history of the Dial Range area. Ph.D. thesis, Geology Dept., Univ. Tasm. (unpubl.).
- BURNS, K.L., 1964: One Mile Geological Map Series K/55-6-29, Devonport. *Explan. Rep. geol. Surv. Tasm.*

- BURRETT, C.F., 1978: Middle and Upper Ordovician conodonts and stratigraphy of the Gordon Limestone Sub-group, Tasmania. Ph.D. thesis, Geology Dept., Univ. Tasm. (unpubl.).
- BUTLER, G.P., 1973: Strontium geochemistry of modern and ancient calcium sulphate minerals. In Purser, B.H. (ed.), *The Persian Gulf*. Springer-Verlag, New York, 324-452.
- CAREY, S.W. & BANKS, M.R., 1954: Lower Palaeozoic unconformities in Tasmania. *Pap. Proc. roy. Soc. Tasm.*, 88, 245-269.
- CHAYES, F., 1956: *Petrographic modal analysis*. John Wiley and Sons, 113p.
- CHILINGAR, G.V., 1956: Dedolomitization: A review. *Am. Assoc. Petrol. Geol. Bull.*, 40, 762-764.
- COOK, P.J., 1973: Supratidal environment and geochemistry of some Recent dolomite concretions, Broad Sound, Queensland, Australia. *Jour. Sed. Petrol.*, 43, 998-1011.
- CORBETT, K.D. & BANKS, M.R., 1974: Ordovician stratigraphy of the Florentine synclinorium, south-west Tasmania. *Pap. Proc. roy. Soc. Tasm.*, 107, 207-238.
- CURRAY, J.R., 1964: Transgressions and regressions. In Miller, R.L. (ed.), *Papers in Marine Geology*, Shepard commemorative volume. The Macmillan Co., New York, 531p.
- DEFREYES, K.S., LUCIA, F.J. & WEYL, P.K., 1965: Dolomitization of Recent and Plio-Pleistocene sediments by marine evaporitic waters on Bonaire, Netherland Antilles. In Pray, L.C. and Murray R.C. (eds.), *Dolomitization and limestone diagenesis*. *Spec. Publ. Soc. Econ. Paleont. Miner.* 13, 71-88.
- DEGENS, E.T., WILLIAMS, E.G. & KEITH, M.L., 1958: Environmental studies of Carboniferous sediments. Part II: Application of geochemical criteria. *Bull. Am. Assoc. Petrol. Geol.*, 42, 981-997.
- DUNHAM, J.B. & OLSON, E.R., 1978: Diagenetic dolomite formation related to Paleozoic paleogeography of the Cordilleran miogeocline in Nevada. *Geology*, 6, 556-559.
- EDIE, R.W., 1958: Mississippian sedimentation and oil fields in south-eastern Saskatchewan. *Bull. Am. Assoc. Petrol. Geol.*, 42, 94-125.
- EPSTEIN, S., BUCHSBAUM, R., LOWENSTEIN, H.A. & UREY, H.C., 1953: Revised carbonate-water isotopic temperature scale. *Bull. Geol. Soc. Am.*, 64, 1315-1326.
- EPSTEIN, S. & MAYEDA, T., 1953: Variation of O^{18} content of waters from natural sources. *Geochim. Cosmochim. Acta*, 4, 213-224.
- EVAMY, B.D., 1967: Dedolomitization and the development of rhombohedral pores in limestones. *Jour. Sed. Petrol.*, 37, 1204-1215.
- EVAMY, B.D., 1969: The precipitational environment and correlation of some calcite cements deduced from artificial staining. *J. Sed. Petrol.*, 39, 787-793.

- EVAMY, B.D. & SHEARMAN, D.J., 1965: The development of overgrowths from echinoderm fragments. *Sedimentology*, 5, 211-233.
- FERAY, D.E., HEUER, E. & HEWATT, W.G., 1962: Biologic, genetic and utilitarian aspects of limestone classification. In Ham, W.E. (ed.), *Am. Assoc. Petrol. Geol. Mem.1*, 279.
- FISHER, W.L. & RODDA, P.U., 1969: Edwards Formation (Lower Cretaceous), Texas: Dolomitization in a carbonate platform system. *Bull. Am. Assoc. Petrol. Geol.*, 53, 55-72.
- FOLK, R.L., 1959: Practical petrographic classification of limestones. *Bull. Am. Assoc. Petrol. Geol.*, 43, 1-38.
- FOLK, R.L., 1962: Spectral subdivision of limestone types. In Ham, W.E. (ed.), *Classification of carbonate rocks. Mem. Am. Assoc. Petrol. Geol.*, 1, 62-84.
- FOLK, R.L., 1973: Carbonate petrology in the post-Sorbian age. In Ginsburg, R.N. (ed.), *Evolving concepts in sedimentology. Johns Hopkins University Studies in Geology No.21*, Johns Hopkins University Press, Baltimore, 191p.
- FOLK, R.L. & LAND, L.S., 1975: Mg/Ca ratio and salinity. Two controls over crystallization of dolomite. *Bull. A. Assoc. Petrol. Geol.*, 59, 60-68.
- FOLK, R.L. & SIEDLECKA, A., 1974: The "schizohaline" environment. Its sedimentary and diagenetic fabrics as exemplified by late Paleozoic rocks of Bear Island, Svalbard. *Sed. Geol.*, 11, 1-15.
- FOLKMAN, Y., 1969: Diagenetic dedolomitization in the Albian-Cenomanian Yagur dolomite on Mount Carmel (N. Israel). *Jour. Sed. Petrol.*, 39, 380-385.
- FREEMAN, T., 1972: Sedimentology and dolomitization of Muschelkalk carbonates (Triassic), Iberian Range, Spain. *Bull. Am. Assoc. Petrol. Geol.*, 56, 434-453.
- FRIEDMAN, G.M., 1969: Trace elements as possible environmental indicators in carbonate sediments. In Friedman, G.N. (ed.), *Depositional environments in carbonate rocks. Soc. Econ. Paleont. & Mineral., Spec. Publ. No.4*, 193-200.
- FRIEDMAN, I. & O'NEIL, J.R., 1977: Compilation of stable isotope fractionation factors of geochemical interest. *U.S. Geol. Surv. Prof. Pap. 440-KK*.
- FRIEDMAN, G.M. & SANDERS, J.E., 1967: Origin and occurrence of dolostones. In Chilingar, G.V., Bissell, H.J. & Fairbridge, R.W. (eds.), *Carbonate rocks, origin, occurrence and classification*. Elsevier, Amsterdam, 267-348.

- FRITZ, P., 1967: Oxygen and carbon isotopic composition of carbonates from the Jura of Southern Germany. *Ca. J. Earth Sci.*, 4, 1247-1266.
- FRITZ, P., 1971: Geochemical characteristics of dolomites and the O^{18} content of Middle Devonian oceans. *Earth Planet. Sci. Letters*, 11, 277-282.
- FRITZ, P. & KATZ, A., 1972: The sodium distribution of dolomite crystals. *Chem. Geol.*, 72, 170-194.
- FRITZ, P. & SMITH, D.G.W., 1970: The isotopic composition of secondary dolomites. *Geochim. Cosmochim. Acta*, 34, 1161-1173.
- GALEHOUSE, J.S., 1971: Point counting. In Carver, R.E. (ed.), *Procedures in sedimentary petrology*. Wiley, New York, 385-407.
- GARRELS, R.M. & MACKENZIE, F.T., 1971: *Evolution of sedimentary rocks*. W.W. Norton & Co., Inc., New York, 383p.
- GINSBURG, R.N. (ed.), 1975: *Tidal deposits - a casebook of recent examples and fossil counterparts*. Springer-Verlag, New York, 428p.
- GOLDBERG, M., 1967: Supratidal dolomitization and dedolomitization in Jurassic rocks of Hamakhtesh Haqatan, Israel. *J. Sed. Petrol.*, 37, 760-773.
- GOODELL, H.G. & GARMAN, R.K., 1969: Carbonate geochemistry of Superior deep test well, Andros Island, Bahamas. *Bull. Am. Assoc. Petrol. Geol.*, 53, 513-536.
- GREEN, D.C., GOEDE, A., & HARMON, R., 1980: Light stable isotope ratios in Tasmanian precipitation. *Prog. and Abstracts 4th Aust. Geol. Convention, Hobart. Geol. Soc. Aust.*, 60.
- GROOT, K. de, 1967: Experimental dedolomitization. *Jour. Sed. Petrol.*, 37, 1216-1220.
- GROSS, M.G., 1964: Variations in the O^{18}/O^{16} and C^{13}/C^{12} ratios of diagenetically altered limestones in Bermuda Island. *J. Geol.*, 72, 170-194.
- GROSS, M.G., 1972: *Oceanography - a view of the earth*. Prentice-Hall, New Jersey, 503p.
- GROSS, M.G. & TRACEY, J.I., Jr., 1966: Oxygen and carbon isotopic composition of limestones and dolomites. Bikini and Eniwetok Atolls. *Science*, 151, 1082-1084.
- GUBLER, Y., BERTRAND, J.P., MATTAVELLI, L., RIZZINI, A. & PASSEGA, R., 1967: Petrology and petrography of carbonate rocks. In Chilingar, G.V., Bissell, H.J. & Fairbridge, R.W. (eds.), *Carbonate rocks. Developments in Sedimentology*, 9A. Elsevier, Amsterdam, 471p.

- HALL, W.E. & FRIEDMAN, I., 1969: Oxygen and carbon isotopic composition of ore and host rock of selected Mississippi Valley deposits. *U.S. Geol. Surv. Prof. Paper* 650-C, C140-C148.
- HANSHAW, B.B. & BACK, W., 1979: Major geochemical processes in the evolution of carbonate-aquifer systems. *Jour. Hydrology*, 43, 287-312.
- HANSHAW, B.B., BACK, W & DEIKE, R.E., 1971: A geochemical hypothesis for dolomitization by ground water. *Econ. Geol.*, 66, 710-724.
- HECKEL, P.H., 1972: Recognition of ancient shallow marine environments. *Spec. Publs. Soc. Econ. Paleont. Miner.*, No.16, 226-286.
- HEM, J.D., 1970: Study and interpretation of the chemical characteristics of natural water. *U.S. Geol. Surv. Prof. Paper* 1473.
- HOLLAND, H.D., HOLLAND, H.J. & MUNOZ, J.L., 1964: The coprecipitation of cations with CaCO_3 . II. The coprecipitation of Sr^{2+} with calcite between 90° and 100°C . *Geochim. Cosmochim. Acta*, 28, 1287-1301.
- HOROWITZ, A.S. & POTTER, P.E., 1971: *Introductory petrography of fossils*. Springer-Verlag, Berlin, 302p.
- HSU, K.J. & SCHNEIDER, J., 1973: Progress report on dolomitization-hydrology of the Abu Dhabi sabkha, Arabian Gulf. In Purser, B.H. (ed.), *The Persian Gulf*. Springer-Verlag, New York, 409-471.
- HSU, K.J. & SIEGENTHALER, C., 1969: Preliminary experiments on hydrodynamic movement induced by evaporation and their bearing on the dolomite problem. *Sedimentology*, 12, 11-25.
- HUDSON, J.D., 1975: Carbon isotopes and limestone cement. *Geology*, 3, 19-22.
- HUDSON, J.D., 1977: Stable isotopes and limestone lithification. *Jour. Geol. Soc.*, 133, 637-660.
- HUGHES, T.D., 1957: The Ordovician Limestone. In Limestones in Tasmania. *Geol. Surv. Min. Resour.* 10. Tasm. Dept. Mines.
- ICHIKUNI, M., 1973: Partition of strontium between calcite and solution: effect of substitution by manganese. *Chem. Geol.*, 11, 315-319.
- IRWIN, M.L., 1965: General theory of epeiric clear water sedimentation. *Bull. Am. Assoc. Petrol. Geol.*, 49, 445-459.
- JACKA, A.D., 1977: Deposition and diagenesis of the Fort Terrett Formation (Edwards Group) in the vicinity of Junction, Texas. In Bebout, D.G. & Loucks, R.G. (eds), *Cretaceous carbonates of Texas and Mexico*. *Bur. Econ. Geol. and Uni. Texas Rep.* 89, 182-200.

- JACOBSON, R.L. & USDOWSKI, H.E., 1976: Partitioning of strontium between calcite, dolomite and liquids. *Contr. to Mineral. & Petrol.*, 59, 171-185.
- JAGO, J.B., 1973: Paraconformable contacts between Cambrian and June Group sediments in Tasmania. *J. geol. Soc. Aust.*, 20, 373-377.
- JAGO, J.B., 1976: Late Middle Cambrian Agnostid trilobites from Gunns Plains area, north-western Tasmania. *Pap. Proc. roy. Soc. Tasm.*, 110, 1-18.
- JAGO, J.B., COOPER, J.A. & CORBETT, K.D., 1977: First evidence for Ordovician igneous activity in the Dial Range Trough, Tasmania. *J. geol. Soc. Aust.*, 24, 81-86.
- JENNINGS, I.B., BURNS, K.L., MAYNE, S.J. & ROBINSON, R.G., 1959: Geological atlas 1 mile series. Zone 7, Sheet 37. Sheffield. *Explan. Rep. geol. Surv., Tasm.*
- JENNINGS, I.B., 1963: Middlesex. *Explan. Rep. geol. Surv., Tasm.* 151p.
- KATZ, A., 1968: Calcian dolomites and dedolomitization. *Nature*, 217, 439-440.
- KATZ, A., 1971: Zoned dolomite crystals. *J. Geol.*, 79, 38-51.
- KATZ, A., SAAS, E., STARINSKY, A. & HOLLAND, H.D., 1972: Strontium behaviour in the aragonite-calcite transformation: an experimental study at 40-90°C. *Geochim. Cosmochim. Acta*, 36, 481-496.
- KEITH, M.L. & WEBER, J.N., 1964: Carbon and oxygen isotopic composition of selected limestones and fossils. *Geochim. Cosmochim. Acta*, 28, 1787-1816.
- KINSMAN, D.J.J., 1969: Interpretation of Sr^{++} concentrations in carbonate minerals and rocks. *Jour. Sed. Petrol.*, 39, 486-508.
- KINSMAN, D.J.J. & HOLLAND, H.D., 1969: The co-precipitation of cations with CaCO_3 . IV. The co-precipitation of Sr^{++} with aragonite between 16°C and 96°C. *Geochim. Cosmochim. Acta*, 33, 1-17.
- KNAUTH, L.P. & EPSTEIN, S., 1976: Hydrogen and oxygen isotope ratios in nodular and bedded cherts. *Geochim. Cosmochim. Acta*, 40, 1095-1108.
- LAND, L.S., 1973: Holocene meteoric dolomitization of Pleistocene limestones, north Jamaica. *Sedimentology*, 20, 411-424.
- LAND, L.S. & HOOPS, G.K., 1973: Sodium in carbonate sediments and rocks. A possible index to the salinity of diagenetic solutions. *Jour. Sed. Petrol.*, 43, 614-617.
- LAND, L.S. & EPSTEIN, S., 1970: Late Pleistocene diagenesis and dolomitization, north Jamaica. *Sedimentology*, 14, 187-200.

- LAND, L.S., SALEM, M.R.I. & MORROW, D.W., 1975: Paleohydrology of ancient dolomites: geochemical evidence. *Am. Assoc. Petrol. Geol. Bull.*, 59, 1602-1625.
- LAPORTE, L.F., 1969: Recognition of a transgressive carbonate sequence within an epeiric sea : Helderberg Group (Lower Devonian) of New York State. In Friedman, G.M. (ed.), *Spec. Publ. Soc. Econ. Paleont. Miner.* 14, 98-119.
- LIPPMANN, F., 1973: *Sedimentary carbonate minerals*. Springer, Berlin, 228p.
- LOBO, C.F. & OSBORNE, R.H., 1973: The American Upper Ordovician Standard XVIII: Investigation of micrite in typical Cincinnati limestones by means of scanning electron microscopy. *J. Sed. Petrol.*, 43, 478-483.
- LOGAN, B.W., REZAK, R. & GINSBURG, R.N., 1964: Classification and environmental significance of algal stromatolites. *J. Geol.*, 72, 68-83.
- LONGMAN, M.W. & MANCH, P.A., 1978: Diagenesis of Cretaceous limestones in the Edwards aquifer system of south-central Texas: a scanning electron microprobe study. *Sedim. Geol.*, 21 (4), 241-276.
- LUCIA, F.J., 1961: Dedolomitization in the Tansill (Permian) Formation. *Bull. Geol. Soc. Am.*, 72, 1107-1109.
- LUCIA, F.J., 1972: Recognition of evaporite-carbonate shoreline sedimentation. In Recognition of ancient sedimentary environments. *Spec. Publ. Soc. Econ. Paleont. Miner.* 16, 160-191.
- LUMSDEN, D.N., 1979a: Discrepancy between thin-section and X-ray estimates of dolomite in limestone. *Jour. Sed. Petrol.*, 49, 429-436.
- LUMSDEN, D.N., 1979b: Error in X-ray diffraction estimates of dolomite in carbonate rocks - causes and cures. *Abstr., Am. Assoc. Petrol. Geol.-Soc. Econ. Paleont. Miner. Annual Convention*, 124.
- MATTHEWS, R.K., 1966: Genesis of recent lime mud in southern British Honduras. *Jour. Sed. Petrol.*, 36, 428-454.
- MATTHEWS, A. & KATZ, A., 1977: Oxygen isotope fractionation during the dolomitization of calcium carbonate. *Geochim. Cosmochim. Acta*, 41, 1431-1438.
- MCCREA, J.M., 1950: On the isotopic chemistry of carbonates and a paleotemperature scale. *Jour. Chem. Physics*, 18, 849-857.
- McINTIRE, W.L., 1963: Trace element partition coefficients - a review of theory and applications to geology. *Geochim. Cosmochim. Acta*, 27, 1209-1264.
- McKEE, E.D. & GUTSCHICK, R.C., 1969: History of the Redwall Limestone of northern Arizona. *Mem. Geol. Soc. Am.*, 114, 726p.

- McKENZIE, J.A., HSU, K.J. & SCHNEIDER, J., 1979: Movement of subsurface waters under Sabkha, Abu Dhabi, United Arab Emirates, and its relation to dolomite genesis. *Abstracts, Am. Assoc. Petrol. Geol.-Soc. Econ. Paleont. Miner. Annual Convention, Houston*, 132.
- MEYERS, W.J., 1974: Carbonate cement stratigraphy of the Lake Valley Formation (Mississippian), Sacramento Mts., New Mexico. *Jour. Sed. Petrol.*, 44, 837-861.
- MEYERS, W.J., 1980: Carbonate geology - SEPM research group state-of-the-art summaries. *Jour. Sed. Petrol.*, 50, 310-311.
- MEYERS, W.J. & LOHMANN, K.C., 1978: Microdolomite-rich syntaxial cements: Proposed meteoric-marine mixing zone phreatic cements from Mississippian limestones, New Mexico. *J. Sed. Petrol.*, 48, 475-488.
- MICHARD, G., 1968: Coprecipitation de l'ion manganeux avec le carbonate de calcium. *Comptes Rendus Acad. Sci., Paris*, 267, 1685-1688.
- MILLIMAN, J.D., 1974: *Marine carbonates*. Springer-Verlag, New York, 375p.
- MOORE, C.H., Jr., 1971: Pseudospar dedolomite "cements" of evaporite solution collapse breccias. In Bricker, O.P. (ed.), *Carbonate cements*. Johns Hopkins Univ. Press.
- MORGAN, J.J., 1967: Chemical equilibria and kinetic properties of manganese in natural waters. In Faust, S.J. & Hunter, J.V. (eds), *Principles and applications of water chemistry*. John Wiley & Sons, New York, 561-624.
- MUIR, M., LOCK, D. & VON DER BORCH, C.C., 1979: Coorong model for penecontemporaneous dolomite formation in Middle Proterozoic McArthur Group, Northern Territory, Australia. *Abstracts, Am. Assoc. Petrol. Geol.-Soc. Econ. Paleont. Miner. Annual Convention, Houston*, 136.
- MULTER, H.G., 1977: *Field guide to some carbonate rock environments, Florida Keys and western Bahamas*. Kendall/Hunt Publishing Co., Iowa, 415p.
- NORRISH, K. and CHAPPELL, B.W., 1967: X-ray fluorescence spectrography. In Zussman, J. (ed.), *Physical Methods in Determinative Mineralogy*. Academic Press.
- NORRISH, K. and HUTTON, J.T., 1969. An accurate X-ray spectrographic method for analyses of a wide range of geological samples. *Geochim. Cosmochim. Acta*, 33, 431-453.
- O'NEIL, J.R. & EPSTEIN, S., 1966: Oxygen isotope fractionation in the system dolomite-calcite-carbon dioxide. *Science*, 152, 198-201.
- PERRY, E.C., Jr. & TAN, F.C., 1972: Significance of oxygen and carbon isotope variations in Early Precambrian cherts and carbonate rocks of southern Africa. *Bull. Geol. Soc. Am.*, 83, 647-664.

- PETTA, T.J., 1977: Diagenesis and geochemistry of a Glen Rose patch reef complex, Bandera County, Texas. In Bebout, D.G. & Loucks, R.G. (eds), *Cretaceous carbonates of Texas and Mexico. Bur. Econ. Geol. and Univ. Texas Rep. 89*, 138-167.
- PINGITORE, N.E., Jr., 1978: The behaviour of Zn^{2+} and Mn^{2+} during carbonate diagenesis: theory and applications. *J. Sed. Petrol.*, 48, 799-814.
- RADKE, B.M., 1980: Carbonate textures after Cambro-Ordovician Sabkha deposits. *Prog. and Abstracts 4th Aust. Geol. Convention, Hobart. Geol. Soc. Aust.*, 74.
- RAO, C.P. & CAROZZI, A.V., 1971: Application of computer techniques to the petrographic study of oolitic environments, Ste. Genevieve Limestone (Mississippian), southern Illinois and eastern Missouri. *Arch. Sc. Geneve*, 24, 17-55.
- RAO, C.P. & NAQVI, I.H., 1977: Petrography, geochemistry and factor analysis of a Lower Ordovician subsurface sequence, Tasmania, Australia. *Jour. Sed. Petrol.*, 47, 1036-1055.
- REINECK, H.E. & SINGH, I.B., 1975: *Depositional sedimentary environments*. Springer-Verlag, New York, 439p.
- RICHTER, D.K. & FUCHTBAUER, H., 1978: Ferroan calcite replacement indicates former magnesium calcite skeletons. *Sedimentology*, 25, 843-860.
- ROBINSON, P., 1980: Determination of calcium, magnesium, manganese, strontium, sodium and iron in the carbonate fractions of limestones and dolomites. *Chem. Geol.*, 28, 135-146.
- ROTHER, P., HOEFS, J. & SONNE, V., 1974: The isotopic composition of Tertiary carbonates from the Mainz Basin: an example of isotopic fractionations in 'closed basins'. *Sedimentology*, 21, 373-395.
- SCHOLLE, P.A., 1971: Diagenesis of deep-water carbonate turbidites, Upper Cretaceous Mount Antola Flysch, Northern Apennines, Italy. *J. Sed. Petrol.*, 41, 251-260.
- SHAW, A.B., 1964: *Time in stratigraphy*. McGraw-Hill, New York, 365p.
- SHEARMAN, D.J., KHOURI, J. & TAHA, S., 1961: On the replacement of dolomite by calcite in some Mesozoic limestones from the French Jura. *Proc. Geol. Assoc. Lond.*, 72, 1-12.
- SHEARMAN, D.J. & SHIRMOHAMMADI, N.H., 1969: Distribution of strontium in dedolomites from the French Jura. *Nature*, 223, 606-608.
- SHEPPARD, S.M.F. & SCHWARCZ, H.P., 1970: Fractionation of carbon and oxygen isotopes and magnesium between coexisting metamorphic calcite and dolomite. *Contr. Mineral. Petrol.*, 26, 161-198.
- SHINN, E.A., 1968: Practical significance of birdseye structures in carbonate rocks. *J. Sed. Petrol.*, 38, 215-223.

- SHINN, E.A., GINSBURG, R.N. & LLOYD, R.M., 1965: Recent supratidal dolomite from Andros Island, Bahamas. *In* Pray, L.C. & Murray, C. (eds), Dolomitization and limestone diagenesis. *Soc. Econ. Paleont. Miner. Spec. Publ.* 13, 112-123.
- SMIT, D.E. & SWETT, K., 1969: Devaluation of dedolomitization. *J. Sed. Petrol.*, 39, 379-380.
- SPRY, A.H., 1962. The Precambrian rocks. *In* Spry, A.H. and Banks, M.R. (eds), The Geology of Tasmania. *Jour. geol. Soc. Aust.*, 9 (2). 107-129.
- STEHLI, F.G. & HOWER, J., 1961: Mineralogy and early diagenesis of carbonate sediments. *J. Sed. Petrol.*, 31, 358-371.
- SUPKO, P.R., 1977: Subsurface dolomites, San Salvador, Bahamas. *J. Sed. Petrol.*, 47, 1063-1077.
- SWETT, K., 1965: Dolomitization, silicification and calcitization patterns in Cambro-Ordovician oolites from northwest Scotland. *J. Sed. Petrol.*, 35, 928-938.
- TARUTANI, T., CLAYTON, R.N., & MAYEDA, K., 1969: The effect of polymorphism and magnesium substitution on oxygen isotope fractionation behaviour between calcium carbonate and water. *Geochim. Cosmochim. Acta*, 33, 987-996.
- TAYLOR, H.P., Jr., 1974: The application of oxygen and hydrogen isotope studies to problems of hydrothermal alteration and ore deposition. *Econ. Geol.*, 69, 843-883.
- TAYLOR, H.P., Jr., 1977: Water/rock interactions and the origin of H₂O in granitic batholiths. *Jour. Geol. Soc.*, 133, 509-558.
- TEBBUTT, G.E., CONLEY, C.D. & BOYD, D.W., 1965: Lithogenesis of a distinctive carbonate rock fabric. *Contr. to Geology, Univ. Wyoming*, 4, 1-13.
- THOMPSON, G., 1972: A geochemical study of some lithified carbonate sediments from the deep-sea. *Geochim. Cosmochim. Acta*, 36, 1237-1253.
- TWELVETREES, W.H., 1909: Gunns Plains, Alma and other mining fields, north-west coast. *Bull. Geol. Surv. Tasm.* 5.
- VEIZER, J., 1977: Diagenesis of prequaternary carbonates as indicated by tracer studies. *J. Sed. Petrol.*, 47, 565-581.
- VEIZER, J. & COMPSTON, W., 1974: Sr⁸⁷/Sr⁸⁶ composition of seawater during the Phanerozoic. *Geochim. Cosmochim. Acta*, 38, 1461-1484.
- VEIZER, J. & DEMOVIC, R., 1974: Strontium as a tool in facies analysis. *J. Sed. Petrol.*, 44, 93-115.
- VEIZER, J. & HOEFS, J., 1976: The nature of O¹⁸/O¹⁶ and C¹³/C¹² secular trends in sedimentary carbonate rocks. *Geochim. Cosmochim. Acta*, 40, 1387-1395.

- VEIZER, J., LEMIEUX, J., JONES, B., GIBLINGS, M.R. & SAVELLE, J., 1977: Sodium: Paleosalinity indicator in ancient carbonate rocks. *Geology*, 5, 177-179.
- VEIZER, J., LEMIEUX, J., JONES, B., GIBLING, M.R. & SAVELLE, J., 1978: Paleosalinity and dolomitization of a Lower Paleozoic carbonate sequence, Somerset and Prince of Wales Islands, Arctic Canada. *Can. Jour. Earth Sci.*, 15, 1448-1461.
- VON DER BORCH, C.C., 1976: Stratigraphy and formation of Holocene dolomitic carbonate deposits of the Coorong area, South Australia. *J. Sed. Petrol.*, 46, 952-966.
- VON DER BORCH, C.C. & LOCK, D., 1979: Geological significance of Coorong dolomites. *Sedimentology*, 26, 813-824.
- VON DER BORCH, C.C., LOCK, D.E. & SCHWEBEL, D., 1975: Ground-water formation of dolomite in the Coorong region of South Australia. *Geology*, 3, 283-285.
- WEBER, J.N., 1964: Carbon isotope ratios in dolostones: some implications concerning the genesis of secondary and 'primary' dolostones. *Geochim. Cosmochim. Acta*, 28, 1257-1265.
- WELDON, B.D., 1974: Ordovician Gordon Limestone Subgroup, Florentine Valley. Thesis (B.Sc. Hons.), Geol. Dept., Univ. Tasm. (unpubl.).
- WHITE, A.F., 1978: Sodium coprecipitation in calcite and dolomite. *Chem. Geol.*, 23, 65-72.
- WILLIAMS, E. & TURNER, N.J., 1974: Geological atlas 1:250 000 series. Sheet No. Sk-55/3 Burnie. *Explan. Rep. geol. Surv. Tasm.*
- WILLIAMS, E., 1976: Tasman fold belt system in Tasmania. *Explan. Notes 1:500 000 Structural map pre-Cambrian rocks of Tasmania*. Tasm. Dept. Mines.
- WILSON, J.L., 1975: *Carbonate facies in geologic history*. Springer-Verlag, Berlin, 471p.
- WOLFE, M.J., 1970: Dolomitization and dedolomitization in the Senonian chalk of Northern Ireland. *Geol. Mag.*, 107, 39-49.
- WOODS, P.J. and BROWN, R.E., 1975: Carbonate sedimentation in an arid zone tidal flat, Nilemah Embayment, Shark Bay, Western Australia. In Ginsburg, R.N. (ed.), *Tidal deposits*. Springer-Verlag, 223-232.
- YANAT'EVA, O.K., 1955: Effect of aqueous solutions of gypsum on dolomite in the presence of CO₂. *Akad. Nauk. SSSR, Doklady*, 101, 911-912.
- ZELLAR, E.J. & WRAY, J.L., 1956: Factors influencing precipitation of calcium carbonate. *Bull. Am. Assoc. Petrol. Geol.*, 40, 140-152.
- ZENGER, D.H., 1973: Syntaxial calcite borders on dolomite crystals, Little Falls Formation (Upper Cambrian), New York. *J. Sed. Petrol.*, 43, 118-124.

I REFERENCE NO. T S NO. LOCATION D H. NO.
CAT. NO. STRATIGRAPHIC UNIT DEPTH

II NAME OF ROCK

III MEGASCOPIC DESCRIPTION

IV MICROSCOPIC DESCRIPTION

(A) Colour: 1. light grey 2 dark grey 3. alternating 1 & 2 4. red 5 other

(B) Texture: (a) Terrigenous material%

1. Fundamental end-members (b) Allochemical material%
All % volumetric
None: leave blank (c) Orthochemical material %

2. General homogeneity 1. homogeneous 2 inter-layered 3 irregular
4 wavy 5. wispy 6. disrupted 7 brecciated

3. Grain Size: mm (use size class symbols)

(a) Entire sediment:	Median	Sorting Index
	% Median	Roundness Sphericity
(b) Gravel fraction		
(c) Sand fraction		
(d) Mud fraction		

4. Textural maturity: 1. immature 2. submature 3. mature 4. supermature
5. inversion

5. Bonding agents: 1. micrite 2. spar 3. dolomite 4. silica 5. silt-clay
6 other

6. Grain-groundmass ratio: Grns:Gm = 1. 1:9 2 1:9 to 1:1 3. 1:1 to 9:1
4. 9:1

7 Spar Type: 1 passive, equant mosaic filling 2. passive bladed
filling 3. very coarse (>100μ) blocky without dolomite
inclusions and initial finer spar 4. displacive with
dolomite inclusions 5 passive (1-3) and displacive
6. pseudospar (>25μ) very irregular margins (micrite
clots) 7. Recrystd. intraclasts

8. Micrite type: 1. minimicrite <1μ 2. normal micrite (2-3μ)
3. microspar (5-10μ subrhombic)

(C) Grain Composition

1. Terrigenous materials Note heavy mineral type

Quartz%	Chert%	Feldspar%	Clay %	Pyrite%	Org. mat %
Rock frag. %	M%	I%	V%	Clast. sed %	Heavy 1 2 3 Min
Quartz type	Poly. %	MU%	MNU%		

2 Allochemical materials

Fossils%	Oolites%	Pellets (<0.2mm, structureless)%
Intra. (>0.2mm)%	Onco. %	A. Mat. %
		Algal species

3. Algal Mat. - stromatolites

Thickness:
1. <1mm 2 1-2mm 3. 2-5mm 4 5mm-1cm 5. >1cm
Type
3. tufted 4. convoluted 1. smooth 2 pal-sade 5. LLH-S 6. LLH-C 7. SH-C 8. SH-V

4. Type of allochems

(a) Relative percent of fossils (b) Intraclast (>0.2mm)
Compn: > 50%

Rivulites	
Brachiopods	
Bryozoans	
Cephalopods	
Corals	
Echinoderms	
Gastropods	
Ostracods	
Sponges	
Stromatopora	
Trilobites	

1. Algal
 2. Micrite
 3. oomicrite
 4. oosparite
 5. pelmicrite
 6. pelsparite
 7. intramicrite
 8. intrasparite
 9. biomicrite
 10. biosparite
 11. dolomite
 12. breccia
- (to 11 add 1 to 11 to indicate composition)

APPENDIX A

PHOTOGRAPH

Film No

Frame No

Magnification

196a

V STRUCTURE

1. Sed. unit thickness	
1. v.t. laminated (1-2mm) 2. t. laminated (2-5mm) 3. laminated (5mm-1cm) 4. v.t. bedded (1-2 cm) 5. t. bedded (2-4cm) 6. bedded (>4cm)	
2. Birdseye abundance	
1. rare 4. common 8. abundant	
Type	
1. laminar 2. bulbous 3. tabular	
3. Mudcrack - dessication	
1. ter. cracks 2. V-shape 3. concave 4. intralaminar	
4. Bioturbation	
1. rare 4. common 8. abundant	
Type	
1. vertical 2. horizontal 3. random	
5. Other structures	
1. Cross-bedding 2. graded-bedding 3. current oriented grains	
6. Deformation	
1. undeformed 2. slightly deformed 3. moderately deformed 4. deformed 5. highly deformed	
7. Stylolites	
1. rare 4. common 8. abundant	
Note: a. Pattern no. 1. fibrous displacive spar specific zones throughout 2. colour 3. dolomite 4. clay, bit. and quartz	

REMARKS:

PHASE CONTRAST FLUORESCENCE.

VI DIAGENESIS

1. Dolomite	
(a) Colour:	%
1. colourless 2. colourless, water clear, mirror-like 3. golden yellow 4. dark brown 5. rose pink 6. lots of inclusions (add colour code to 5)	Abundant Common
(b) Size:	Abundant
1. <20µ 2. 20-50µ 3. 50-150µ 4. 150-300µ 5. >300µ	Common
(c) Shape:	Abundant
1. Anhedral 2. Subhedral 3. Euhedral 4. Zones (add 1 - 3 to indicate shape)	Common
(d) Fabric:	
1. equigranular 2. porphyrotopic 3. poikilotopic	
(e) Deodolomites:	
1 rare 4. common 8. rhombic pores 9. rhombic pores, spar filled	
2. Vanished evaporites	
1. leached nodules or molds. 2. collapse breccia (in dolomitic matrix) 3. calcitized pseudomorphs 4. silicified pseudomorphs 5. length slow chalcedony 6. displacive nodules and crystals with crenulations 7. collective evidence (to 6 add other evidences)	
3. Chert	
1. bedded 2 nodular	
Type	
1. amorphous 2. crystalline 3. length slow chalcedony	

VII EVOLUTION OF PERMEABLE POROSITY

1. Porosity est. %	
2. Basic Porosity type	
Refer sheet, list dominant type; note compd. types	
3. Pore shape	
1. irregular 2. equant 3. tabular 4. platy	
4. Size of regular pores	
1. micropores (<1/16 mm) 2 mesopores (1/16-4mm) 3. megapores (4-256mm)	

VIII GEOCHEMISTRY

AAS - carbonate fraction

I	Res. %	Ca %	Mg %	Sr	Mn	Na	Fe	Mg/Ca	Sr/Ca	Mn/Ca	Na/Ca	Fe/Ca	Fe/Mn

XRF - bulk rock

SiO ₂	Al ₂ O ₃	Fe ₂ O ₃	MgO	CaO	K ₂ O	TiO ₂	MnO	Ba			

Appendix A.1

SAMPLE LOCATIONS AND DESCRIPTIONS

Catalogue numbers: 48878 to 48948 are samples from section GPR

48949 to 48997	"	GPD
48998 to 49040	"	GPB
49041 to 49139	"	GPW
49140 to 49339	"	GPL

The sample codes denote the following:

R - hand specimen
 AP - acetate peel/thin section
 CA - chemical analysis (AAS)
 D - X-ray disc
 P - X-ray pill.

Catalogue Number	Field Number	Description	Sample Code
48878	254	Intraclast bearing fossiliferous micrite	R,AP
48879	254a	Intraclast bearing micrite	R,AP
48880	253	"	R,AP
48881	252	Biomicrite	R,AP
48882	252a	Fossiliferous micrite	AP
48883	251	"	R,AP
48884	251	Biomicrite	R,AP
48885	251a	"	R,AP
48886	250	"	R,AP
48887	249	"	R,AP
48888	248	Intraclast bearing micrite	R,AP
48889	248a	Intrapelsparite	R,AP
48890	247	"	R,AP
48891	246	Micrite	R,AP
48892	246a	Intraclast bearing micrite	R,AP
48893	245	"	R,AP
48894	245a	Micrite	R,AP
48895	244	"	R,AP
48896	243	Biosparite	R,AP
48897	242	Biomicrite	R,AP
48898	241	Micrite	R,AP
48899	240	Pelmicrite to pelsparite	R,AP
48900	240a	Biomicrite	R,AP
48901	239	"	R,AP
48902	239a	Dismicrite	R,AP
48903	238	"	R,AP
48904	237	Intraclast bearing fossiliferous micrite	R,AP

Catalogue Number	Field Number	Description	Sample Code
48905	236	Intraclast bearing fossiliferous micrite	R,AP
48906	235	"	R,AP
48907	234	Dismicrite	R,AP
48908	233	Fossiliferous micrite	R,AP
48909	232	"	R,AP
48910	231	"	R,AP
48911	230	"	R,AP
48912	229	Biomicrite	R,AP
48913	228	"	R,AP
48914	227	Pelmicrite	R,AP
48915	226	Fossiliferous micrite	R,AP
48916	226a	"	R,AP
48917	225	"	R,AP
48918	224	Intraclast bearing fossiliferous micrite	R,AP
48919	223	Dolomicrite	R,AP
48920	222	Dismicrite	R,AP
48921	222a	Intraclast bearing fossiliferous micrite	R,AP
48922	221	"	R,AP
48923	220	Pellet bearing micrite	R,AP
48924	220a	Pelmicrite	R,AP
48925	219	"	R,AP
48926	218	Fossiliferous micrite	R,AP
48927	217	Biomicrite	R,AP
48928	217a	Biopelmicrite	R,AP
48929	216	"	R,AP
48930	215	"	R,AP
48931	215a	Intrapelsparite	R,AP
48932	214	"	R,AP
48933	213	Pelmicrite	R,AP
48934	212	"	R,AP
48935	211	"	R,AP
48926	211a	Pelbiomicrite	R,AP
48937	210	"	R,AP
48938	209	Fossiliferous micrite	R,AP
48939	208	Pelmicrite	R,AP
48940	207	Pelmicrite	R,AP
48941	206	"	R,AP
48942	206a	Pelbiomicrite	R,AP
48943	205	"	R,AP
48944	204	Pelmicrite	R,AP
48945	203	"	R,AP
48946	202	"	R,AP
48947	201	"	R,AP
48948	200	"	R,AP
48949	100	Fossiliferous micrite	R,AP
48950	101	"	R,AP
48951	101a	"	R,AP
48952	102	"	R,AP
48953	103	Biomicrite	R,AP
48954	103a	Intraclast bearing fossiliferous micrite	AP
48955	104	"	R,AP

Catalogue Number	Field Number	Description	Sample Code
48956	105	Fossiliferous micrite	R,AP
48957	105a	Biomicrite	?
48958	106	"	R,AP
48959	107	Fossiliferous micrite	R,AP
48960	108	Pelsparite	R,AP
48961	108a	"	R,AP
48962	109	"	R,AP
48963	109a	"	AP
48964	110	"	R,AP
48965	111	Biosparite	R,AP
48966	112	Pelsparite	R,AP
48967	113	Intraclast bearing fossiliferous micrite	R,AP
48968	114	Pelsparite	R,AP
48969	115	Fossiliferous micrite	R,AP
48970	115a	Intrabiomicrite	R,AP
48971	116	"	R,AP
48972	117	Intraclast bearing fossiliferous micrite	R,AP
48973	118	Biomicrite	R,AP
48974	119	Fossiliferous micrite	R,AP
48975	119a	Pelmicrite	?
48976	120	"	R,AP
48977			
48978	121	Fossiliferous micrite	R,AP
48979	122	Pelmicrite	R,AP
48980	122a	Fossiliferous micrite	R,AP
48981	127a	"	R,AP
48982	123	"	R,AP
48983	124	Intrabiomicrite	R,AP
48984	124a	"	R,AP
48985	125	"	R,AP
48986	126	Fossiliferous micrite	R,AP
48987	127	"	R,AP
48988	128	"	R,AP
48989	129	Intraclast bearing fossiliferous micrite	R,AP
48990	129a	"	R,AP
48991	130	"	R,AP
48992	131	Fossiliferous micrite	R,AP
48993	131a	Biomicrite	R,AP
48994	132	"	R,AP
48995	133	"	R,AP
48996	134	Fossiliferous micrite	R,AP
48997	135	"	R,AP
48998	801	Intraclast bearing fossiliferous micrite	R,AP
48999	802	Fossiliferous micrite	R,AP
49000	803	Intrabiomicrite to intrabiosparite	R,AP
49001	803a	Fossiliferous micrite	R,AP
49002	804	"	R,AP
49003	804a	Intraclast bearing fossiliferous micrite	R,AP
49004	805	"	R,AP

Catalogue Number	Field Number	Description	Sample Code
49005	805a	Intramicrorite	R,AP
49006	806	"	R,AP
49007	806a	Intraclast bearing micrite	R,AP
49008	807	"	R,AP
49009	807a	Intramicrorite	R,AP
49010	807b	"	R,AP
49011	807c	Intrabiomicrite to intrabiosparite	R,AP
49012	808	"	R,AP
49013	809	Biomicrite	R,AP
49014	809a	Intraclast bearing micrite	R,AP
49015	810	"	R,AP
49016	811	Dismicrorite	R,AP
49017	812	"	R,AP
49018	812a	Fossiliferous micrite	R,AP
49019	813	"	R,AP
49020	814	Biomicrite	R,AP
49021	814a	Dolostone	R,AP
49022	815	"	R,AP
49023	815a	Dismicrorite	R,AP
49024	816	"	R,AP
49025	817	Dolostone	R,AP
49026	818	Fossiliferous micrite	R,AP
49027	819	Biomicrite	R,AP
49028	820	Dismicrorite	R,AP
49029	821	Biomicrite	R,AP
49030	822	"	R,AP
49031	822a	Intrabiomicrite	
49032	823	"	R,AP
49033	823a	Dismicrorite	
49034	824	"	R,AP
49035	825	"	R,AP
49036	826	"	R,AP
49037	827	Biomicrite	R,AP
49038	828	Fossiliferous micrite	R,AP
49039	829	Biomicrite	R,AP
49040	830	Dismicrorite	R,AP
49041	600	Intraclast bearing fossiliferous micrite	R,AP,CA
49042	601	"	R,AP,CA
49043	602	"	R,AP,CA
49044	603	Intraclast bearing micrite	
49045	604	Intraclast bearing fossiliferous micrite	R,AP,CA
49046	605	Oolite, intraclast bearing fossiliferous micrite	R,AP
49047	606	Dismicrorite	R,AP,CA
49048	617	Fossiliferous micrite	R,AP
49049	608	"	R,AP,CA
49050	609	Intraclast bearing micrite	R,AP
49051	610	Dismicrorite	R,AP,CA
49052	611	Fossiliferous micrite	R,AP,CA
49053	612	Intraclast bearing fossiliferous micrite	R,AP,CA
49054	613	Fossiliferous micrite	R,AP,CA,D,P

Catalogue Number	Field Number	Description	Sample Code
49055	614	Fossiliferous Micrite	R,AP,CA
49056	615	"	R,AP,CA
49057	616	Dismicrite	R,AP,CA,D,P
49058	617	"	R,AP,CA
49059	618	Intraclast bearing fossiliferous micrite	R,AP,CA
49060	619	Fossiliferous micrite	R,AP,CA
49061	620	Intraclast bearing micrite	R,AP,CA
49062	621a	Biomicrite	R,AP,CA,D,P
49063	621b	"	R,AP,CA,D,P
49064	622	Fossiliferous micrite	R,AP,CA
49065	623	Biomicrite	R,AP,CA,D,P
49066	624	Intramicroite	R,AP,CA,D,P
49067	625	Biomicrite	R,AP,CA
49068	633	"	R,AP,CA
49069	627	Biomicrite	R,AP,CA,D,P
49070	628	Intraclast bearing fossiliferous micrite	R,AP,CA
49071	629	Fossiliferous micrite	R,AP
49072	630	"	R,AP,CA
49073	631	"	R,AP
49074	632	Biomicrite	R,AP,CA
49075	634	Oolite, intraclast bearing fossiliferous micrite	R,AP,CA
49076	635	Intraclast bearing fossiliferous micrite	R,AP,CA
49077	636	"	R,AP,CA
49078	637	Intramicroite	R,AP,CA
49079	638	Fossiliferous micrite	R,AP
49080	639	"	R,AP,CA,D,P
49081	640	Intraclast bearing fossiliferous micrite	R,AP,CA
49082	641	Fossiliferous micrite	R,AP,CA,D,P
49083	642	Intraclast bearing fossiliferous micrite	R,AP,CA
49084	643	Intraclast bearing micrite	R,AP
49085	644	"	R,AP,CA
49086	645	"	R,AP
49087	646	"	R,AP,CA
49088	647	Intramicroite	R,AP,CA
49089	648	Intraclast bearing fossiliferous micrite	R,AP,CA
49090	649	Intramicroite	R,AP,CA
49091	650	Biomicrite	R,AP,CA,D,P
49092	651	Intramicroite	R,AP,CA
49093	652	Intraclast bearing fossiliferous micrite	R,AP,CA
49094	653	Intraclast bearing micrite	R,AP,CA
49095	654	Intraclast bearing fossiliferous micrite	R,AP,CA
49096	655	Intraclast bearing micrite	R,AP,CA
49097	656	Intraclast bearing fossiliferous micrite	R,AP
49098	657	Dolostone	R,AP,CA

Catalogue Number	Field Number	Description	Sample Code
49099	658	Intraclast bearing fossiliferous micrite	R,AP,CA
49100	659	Dolostone	R,AP,CA
49101	660	Biomicrite	R,AP,CA
49102	661	Fossiliferous micrite	R,AP
49103	662	"	R,AP
49104	663	"	R,AP
49105	664	Dolostone	R,AP,CA
49106	665	Fossiliferous micrite	R,AP
49107	666	Dolostone	R,AP,CA
49108	667	Fossiliferous micrite	R,AP
49109	668	"	R,AP
49110	669	"	R,AP,CA,D,P
49111	670	Biomicrite	R,AP,CA
49112	671	"	R,AP,CA
49113	672	"	R,AP
49114	673	"	R,AP
49115	674	Pelbiomicrite	R,AP,CA
49116	675	Intraclast bearing fossiliferous micrite	R,AP,CA
49117	676	Pelmicrite to pelsparite	R,AP,CA
49118	677	Biomicrite	R,AP,CA
49119	678	Intraclast bearing micrite	R,AP,CA
49120	679	Fossiliferous micrite	R,AP,CA
49121	680	Dolostone	R,AP,CA
49122	681	Biomicrite	R,AP,CA
49123	682	Dolostone	R,AP,CA,D,P
49124	683	Fossiliferous micrite	R,AP,CA
49125	684	Biosparite	R,AP,CA
49126	685	"	R,AP,CA
49127	686	"	R,AP,CA
49128	687	Intraclast bearing fossiliferous micrite	R,AP,CA
49129	688	Biomicrite	R,AP,CA
49130	689	Biomicrite	R,AP
49131	690	Intraclast-bearing fossiliferous micrite	R,AP
49132	691	(micrite	R,AP
49133	692	Fossiliferous micrite	R,AP
49134	693	Biomicrite	R,AP
49135	694	Fossiliferous micrite	R,AP
49136	695	"	R,AP
49137	696	"	R,AP
49138	697	{Intraclast-bearing fossiliferous micrite	R,AP
49139	698	(micrite	R,AP
49140	300	Intraclast bearing fossiliferous micrite	R,AP,CA,D,P
49141	302	Biomicrite	R,AP
49142	303	Dismicrite	R,AP,CA
49143	304	Pelbiomicrite	R,AP,CA
49144	315	Intraclast bearing fossiliferous micrite	R,AP,CA
49145	306	"	R,AP,CA,D,P
49146	307	"	R,AP,CA,D,P

Catalogue Number	Field Number	Description	Sample Code
49147	308	Intraclast bearing fossiliferous micrite	R,AP,CA
49148	309	"	R,AP,CA
49149	310	Pelmicrite	R,AP,CA
49150	311	Fossiliferous micrite	R,AP,CA
49151	312	Biomicrite	R,AP,CA
49152	313	Fossiliferous micrite	R,AP
49153	314	"	R,AP,CA
49154	315	Intraclast bearing micrite	R,AP,CA
49155	316	Intraclast bearing fossiliferous micrite	R,AP,CA
49156	317	Biomicrite	R,AP,CA
49157	319	Fossiliferous micrite	R,AP,CA
49158	320	Biopelmicrite	R,AP,CA
49159	321	Biomicrite	R,AP,CA
49160	322	Pelbiomicrite	R,AP,CA
49161	323	Pelbiomicrite	R,AP
49162	324	"	R,AP
49163	326	Intraclast bearing fossiliferous micrite	R,AP
49164	336	"	R,AP,CA
49165	337	"	R,AP,CA
49166	338	"	R,AP,CA
49167	339	"	R,AP
49168	340	Biomicrite	R,AP,CA
49169	341	Intraclast bearing fossiliferous micrite	R,AP,CA
49170	342	Biomicrite	R,AP,CA
49171	344	Intraclast bearing fossiliferous micrite	R,AP,CA
49172	345	Fossiliferous micrite	R,AP
49173	346	Oolite, intraclast bearing fossiliferous micrite	R,AP,CA
49174	347	"	R,AP,CA
49175	348	Fossiliferous micrite	R,AP
49176	349	Intraclast bearing fossiliferous micrite	R,AP,CA
49177	350	Intramicroite	
49178	351	Intraclast bearing micrite	R,AP,CA
49179	352a	Intraclast bearing fossiliferous micrite	R,AP,CA
49180	352b	"	R,AP,CA
49181	353	Dolostone	R,AP,CA,D,P
49182	354	Dismicrite	R,AP
49183	355	"	R,AP,CA
49184	356	Intraclast bearing fossiliferous micrite	R,AP,CA
49185	357	Intraclast bearing micrite	R,AP,CA
49186	358	"	R,AP,CA
49187	359	"	R,AP,CA
49188	360	Biomicrite	R,AP,CA
49189	361	"	R,AP,CA
49190	362	"	R,AP,CA
49191	363	Intraclast bearing fossiliferous micrite	R,AP,CA

Catalogue Number	Field Number	Description	Sample Code
49192	364	Intraclast bearing fossiliferous micrite	R,AP,CA,D,P
49193	365	Biosparite	R,AP,CA
49194	366	"	R,AP,CA
49195	367	Biomicrite	R,AP
49196	368	"	R,AP,CA
49197	369	"	R,AP
49198	370	"	R,AP,CA
49199	371	Fossiliferous micrite	R,AP
49200	372	"	R,AP,CA
49201	373	Intraclast bearing fossiliferous micrite	R,AP,CA
49202	374		R,AP,CA
49203	375	Intrabiomicrite	R,AP
49204	376	Fossiliferous micrite	R,AP,CA
49205	377	Biomicrite	
49206	378	"	R,AP,CA
49207	379	"	R,AP,CA
49208	380	"	R,AP,CA
49209	381	Intraclast bearing fossiliferous micrite	
49210	382	"	R,AP
49211	383	"	R,AP,CA
49212	384	"	R,AP,CA,D,P
49213	385	Oolite, fossiliferous micrite	R,AP,CA
49204	386	Pclmicrite	R,AP,CA
49205	387	Intrabiopelmicrite	R,AP
49216	388	Fossiliferous micrite	R,AP
49217	389	Intrabiomicrite	R,AP,CA
49218	390		R,AP
49219	391	Intraclast bearing fossiliferous micrite	R,AP,CA
49220	392a	Intraoncosparudite	R,AP,CA
49221	392b	"	R,AP,CA
49222	393	Oncolite bearing intrabiomicrite	R,AP
49223	394	"	R,AP
49224	395	"	R,AP
49225	396	"	R,AP,CA
49226	397	Fossiliferous micrite	R,AP
49227	398	Intraclast bearing fossiliferous micrite	R,AP,CA
49228	399	"	R,AP,CA
49229	400	Pellet, intraclast bearing fossiliferous micrite	R,AP
49230	401	Pelmicrite	R,AP
49231	402	"	R,AP,CA
49232	403	Oncomicrite	R,AP,CA
49233	404	Fossiliferous micrite	R,AP
49234	405	"	R,AP,CA
49235	406	"	R,AP
49236	407	"	R,AP
49237	408	"	R,AP,CA
49238	409	Biomicrite	R,AP,CA
49239	410	"	R,AP,CA,D,P

Catalogue Number	Field Number	Description	Sample Code
49240	411	Dismicrite	R,AP,CA
49241	412	"	R,AP,CA
49242	413	Intraclast bearing fossiliferous micrite	R,AP,CA
49243	414	"	R,AP
49244	415	"	R,AP
49245	416	"	R,AP,CA
49246	417	Fossiliferous micrite	R,AP,CA
49247	418	"	R,AP
49248	419	Intraclast bearing fossiliferous micrite	R,AP
49249	420	"	R,AP
49250	421	"	R,AP,CA
49251	422	Biomcrite	R,AP,CA
49252	423	Fossiliferous micrite	R,AP,CA
49253	424	"	R,AP,CA
49254	425	"	R,AP,CA
49255	426	Intraclast bearing fossiliferous micrite	R,AP
49256	427	Fossiliferous micrite	R,AP
49257	428	"	R,AP,CA
49258	429	"	R,AP,CA
49259	430	Biomcrite	R,AP,CA
49260	431	Fossiliferous micrite	R,AP,CA
49261	432	Intraclast bearing fossiliferous micrite	R,AP,CA
49262	433	Biomcrite	R,AP,CA
49263	434	Fossiliferous micrite	R,AP
49264	435	"	R,AP,CA
49265	436	Intraclast bearing fossiliferous micrite	R,AP
49266	437	"	R,AP,CA
49267	438	Fossiliferous micrite	R,AP,CA
49268	439	"	R,AP,CA
49269	440	"	R,AP,CA
49270	441	"	R,AP,CA
49271	442	"	R,AP
49272	443	"	R,AP,CA
49273	444	"	R,AP,CA,D,P
49274	445	Pellet bearing fossiliferous micrite	R,AP,CA
49275	446	Fossiliferous micrite	R,AP,CA
49276	447	"	R,AP,CA
49277	448	"	R,AP
49278	449	Biomcrite	R,AP,CA
49279	450	"	R,AP,CA
49280	451	Fossiliferous micrite	R,AP,CA,D,P
49281	452	"	R,AP,CA
49282	453	"	R,AP
49283	454	Intraclast bearing fossiliferous micrite	R,AP,CA
49284	455	Fossiliferous micrite	R,AP
49285	456	"	R,AP
49286	457	Biomcrite	R,AP,CA
49287	458	"	R,AP,CA

Catalogue Number	Field Number	Description	Sample Code
49288	459	Intraclast bearing fossiliferous micrite	R,AP
49289	460	Biomicrite	R,AP,CA
49290	461	Fossiliferous micrite	R,AP,CA
49291	462	Intraclast bearing fossiliferous micrite	R,AP,CA
49292	463	Fossiliferous micrite	R,AP,CA
49293	464	"	R,AP,CA
49294	465	"	R,AP,CA
49295	467	"	R,AP,CA
49296	468	"	R,AP,CA
49297	469	Intramicroite	R,AP,CA
49298	470	Fossiliferous micrite	R,AP,CA
49299	471	Biomicroite	R,AP,CA
49300	472	"	R,AP,CA
49301	473	Fossiliferous micrite	R,AP,CA
49302	474	Oolite, fossiliferous micrite	R,AP,CA
49303	475	Oolite pellet " "	R,AP,CA
49304	476	Biomicroite	R,AP
49305	477	Fossiliferous micrite	R,AP
49306	478	"	R,AP,CA
49307	479	"	R,AP,CA
49308	480	Biomicroite	R,AP
49309	481	Fossiliferous micrite	R,AP,CA
49310	482	Intraclast bearing fossiliferous micrite	R,AP,CA
49311	483	Intrapelmicroite	R,AP
49312	484	Intraclast bearing fossiliferous micrite	R,AP,CA
49313	485	Fossiliferous micrite	R,AP,CA
49314	486	Pellet bearing fossiliferous micrite	R,AP
49315	487	Biomicroite	R,AP
49316	488	"	R,AP,CA
49317	489	Fossiliferous micrite	R,AP,CA
49318	490	"	R,AP,CA
49319	491	Biomicroite	R,AP
49320	492	Intraclast bearing fossiliferous micrite	R,AP,CA
49321	493	Oolite, intraclast bearing fossiliferous micrite	R,AP,CA
49322	494b	Biomicroite	R,AP,CA
49323	495	Intraclast bearing fossiliferous micrite	R,AP,CA
49324	496	"	R,AP
49325	497	"	R,AP,CA
49326	498	Fossiliferous micrite	R,AP,CA
49327	499	"	R,AP
49328	500	Biomicroite	R,AP,CA
49329	501	Biopelmicroite	R,AP,CA
49330	502	Biomicroite	R,AP,CA
49331	503	"	R,AP,CA
49332	504	"	R,AP
49333	505	"	R,AP,CA

Catalogue Number	Field Number	Description	Sample Code
49334	506	Intraclast bearing fossiliferous micrite	R,AP,CA
49335	507	"	R,AP,CA,D,P
49336	508	"	R,AP
49337	509	Biomicrite	R,AP
49338	510	Fossiliferous micrite	R,AP
49339	318	Biomicrite	R,AP,CA

APPENDIX B1Dissolution of Samples for Analyses

1. Dry powdered sample (ground into fine powder in gyratory swing mill using Colmonoy vessel for 15-20 seconds) in oven overnight.
2. Weigh about 10 g and dissolve in 500 ml of 1N HCl for one day with occasional stirring.
3. Filter through a weighed (dry) Whatman 542 filter paper, washing the residue with distilled water.
4. Dilute the filtrate to one litre. Fill plastic bottle containing 0.6 g of KCl (for 100x dilution) for trace element analysis.
5. Pipette 20 ml of the 100x dilution solution into a 100 ml flask.
6. Using distilled water, make up this solution to 100 ml. This is the 500x dilution standardised solution. Pour it into bottle containing 0.4 g of KCl for Ca and Mg analyses.

APPENDIX B2Preparation of Standard Solutions

2000 ppm potassium (as KCl) were added to all samples and standards to suppress ionisation. The standards were also matched with similar acid concentration as the samples.

Set 1 Ca and Mg

a) 800 ppm Ca, 100 ppm Mg, 2000 ppm K — 500 ml

1.0 g Merck CaCO_3

0.08289 g Merck MgO

1.91 g KCl (Analytical Reagent)

25 ml conc. HCl

b) 200 ppm Ca, 250 ppm Mg, 2000 ppm K — 500 ml

0.25 g Merck CaCO_3

0.2072 g Merck MgO

1.91 g A.R. KCl

25 ml conc. HCl

c) 500 ppm Ca, 50 ppm Mg, 2000 ppm K — 500 ml

0.625 g Merck CaCO_3

0.04144 g Merck MgO

1.91 g A.R. KCl

25 ml conc. HCl

Set 2 Na, Mn, Sr and Fe

a) 100 ppm Na, 100 ppm Mn, 100 ppm Sr, 200 ppm Fe — 1 litre

0.254 g NaCl

0.20927 g MnCO_3

0.16847 g SrCO_3

0.2859 g Fe_2O_3

3.82 g A.R. KCl

50 ml conc. HCl

Appendix B2 cont.

- b) 10 ppm Na, 10 ppm Mn, 10 ppm Sr, 20 ppm Fe, 2000 ppm K, Ca — 1 litre
100 ml of solution (a) from set 2

3.82 g A.R. KCl

5.0 g Merck CaCO_3

50 ml conc. HCl

- c) 5 ppm Na, 5 ppm Mn, 5 ppm Sr, 10 ppm Fe, 2000 ppm K, Ca — 1 litre
50 ml of solution (a) from set 2

3.82 g A.R. KCl

5.0 g Merck CaCO_3

50 ml conc. HCl

Set 3 Blank solutions (use same distilled water as for set 2)

- a) Blank with 2000 ppm K — 500 ml

1.91 g A.R. KCl

2.5 ml conc. HCl

- b) Blank with 2000 ppm Ca and K — 1 litre

5 g Merck CaCO_3

1.91 g A.R. KCl

50 ml conc. HCl

Appendix C.1

ATOMIC ABSORPTION SPECTROSCOPY

A Techtron AA-6 atomic absorption spectrophotometer was used to analyse the undermentioned elements using the following instrument settings.

Element	Wave Length nm	Lamp Current mA	Slit Width nm	Gas Mixture
calcium	239.9	5	0.2	air/acetylene
magnesium	202.5	5	1.0	air/acetylene
strontium	460.7	10	0.2	nitrous oxide/acetylene
sodium	589.0	10	0.2	air/acetylene
manganese	279.5	8	0.3	air/acetylene
iron	248.3	8	0.3	nitrous oxide/acetylene

Detection limits are Mn - 3ppm, Fe - 6 ppm, Sr - 4 ppm, and Na - 3 ppm.

APPENDIX C.2 CHEMICAL DATA - A.A.S.

Sample No.	I.R. %	Mg %	Ca %	Sr ppm	Mn ppm	Na ppm	Fe %	Mg/Ca	Sr $\times 10^3$ /Ca	Mn $\times 10^3$ /Ca	Na $\times 10^3$ /Ca	Fe $\times 10^2$ /Ca	Dolomite %	Dedolomite %
49041	6.89	0.75	38.25	496	93	131	0.110	0.0323	0.5931	0.1774	0.5969	0.2064	< 10	-
49042	9.25	2.36	35.65	335	104	64	0.159	0.1091	0.4298	0.2128	0.3129	0.3201	17	5
49043	12.19	2.42	33.75	372	117	0	0.175	0.1182	0.5042	0.2529	0.	0.3721	22	15
49044	11.88	1.53	35.65	479	113	114	0.180	0.0708	0.6146	0.2312	0.5574	0.3624	14	15
49045	5.94	0.74	38.35	502	92	84	0.098	0.0318	0.5987	0.1751	0.3817	0.1834		
49047	12.64	3.00	31.25	348	98	0	0.106	0.1583	0.5094	0.2289	0.	0.2434	31	20
49049	16.21	4.24	30.15	318	105	205	0.260	0.2318	0.4824	0.2541	1.1851	0.6169	40	14
49051	8.00	0.74	38.40	384	100	0	0.085	0.0318	0.4574	0.1900	0.4539	0.1589	< 10	-
49052	6.52	0.68	39.00	566	98	3	0.080	0.0287	0.6638	0.1833	0.0134	0.1472	< 10	-
49053	12.83	3.00	33.75	405	112	54	0.232	0.1465	0.5489	0.2421	0.2789	0.4934	42	45
49054	16.33	1.49	33.00	467	111	7	0.178	0.0744	0.6473	0.2454	0.0370	0.3871	< 10	-
49055	7.55	2.57	30.50	459	116	107	0.235	0.1389	0.6884	0.2775	0.6115	0.5530	37	40
49056	21.44	2.59	26.65	339	117	0	0.301	0.1602	0.5818	0.3203	0.	0.8106	46	46
49057	15.06	0.83	33.00	570	102	27	0.123	0.0415	0.7901	0.2255	0.1426	0.2675	-	-
49058	13.44	1.34	34.00	512	107	40	0.114	0.0650	0.6888	0.2296	0.2051	0.2406	12	10
49059	9.67	1.67	35.40	446	101	27	0.134	0.0778	0.5763	0.2081	0.1329	0.2717	15	15
49060	8.80	3.06	33.50	409	109	40	0.205	0.1506	0.5584	0.2374	0.2081	0.4392	30	21
49061	16.96	2.36	31.00	483	104	17	0.186	0.1255	0.7127	0.2447	0.0956	0.4306	31	35
49062	8.76	0.82	36.75	397	95	81	0.087	0.0368	0.4941	0.1886	0.3842	0.1699	< 10	-
49063	11.71	2.55	33.40	426	113	0	0.189	0.1259	0.5834	0.2468	0.	0.4061		
49064	13.83	2.13	32.00	401	87	104	0.175	0.1097	0.5732	0.1983	0.5665	0.3925	18	5
49065	8.18	0.90	38.00	517	84	101	0.065	0.0390	0.6223	0.1613	0.4633	0.1228	< 10	-
49066	10.43	1.73	35.65	471	94	64	0.098	0.0800	0.6043	0.1924	0.3129	0.1973	15	12
49067	9.39	1.33	35.75	459	94	0	0.092	0.0613	0.5873	0.1918	0.	0.1847	-	-
49069	13.41	1.49	34.00	413	93	0	0.099	0.0722	0.5556	0.1995	0.	0.2090		
49070	13.74	2.53	31.50	372	98	121	0.144	0.1324	0.5402	0.2270	0.6695	0.3281	28	22
49072	12.54	3.27	31.25	483	109	151	0.173	0.1725	0.7070	0.2545	0.8422	0.3972	44	39
49074	8.42	1.13	37.00	525	92	7	0.105	0.0503	0.6490	0.1814	0.0330	0.2037	< 10	-
49075	31.59	1.56	24.50	264	154	84	0.187	0.1013	0.4754	0.4423	0.5764	0.5284	< 10	-
49075	9.36	1.30	36.50	417	93	121	0.100	0.0587	0.5226	0.1859	0.5778	0.1966	< 10	-
49076	8.81	2.25	35.00	438	101	0	0.139	0.1060	0.5724	0.2105	0.0000	0.2850	22	21
49077	8.33	2.52	36.50	397	91	0	0.122	0.1138	0.4975	0.1819	0.0000	0.2399	18	5
49078	13.73	4.08	31.15	281	119	37	0.159	0.2159	0.4126	0.2787	0.2070	0.3663	58	44
49080	15.80	3.91	30.25	393	109	44	0.201	0.2131	0.5942	0.2629	0.2535	0.4769	38	19
49081	14.41	3.27	32.00	405	110	0	0.216	0.1685	0.5789	0.2508	0.0000	0.4844	36	27
49082	13.42	2.57	32.75	393	104	0	0.181	0.1294	0.5489	0.2317	0.0000	0.3967	23	10
49083	14.70	1.40	31.75	326	80	34	0.116	0.0727	0.4697	0.1838	0.1867	0.2622	14	13
49085	16.46	1.92	31.25	459	104	17	0.168	0.1013	0.6718	0.2428	0.0948	0.3858	21	14
49087	12.40	2.81	32.15	347	115	20	0.182	0.1441	0.4937	0.2609	0.1084	0.4063	27	15
49088	13.73	1.82	33.50	512	94	0	0.147	0.0896	0.6991	0.2047	0.0000	0.3149	16	8
49089	16.88	2.88	29.65	372	105	154	0.170	0.1601	0.5739	0.2583	0.9053	0.4115	29	13
49090	11.92	3.57	33.00	343	107	101	0.187	0.1783	0.4754	0.2365	0.5335	0.4067	37	25
49091	8.65	2.61	33.90	372	113	0	0.171	0.1269	0.5019	0.2431	0.0000	0.3620	28	27
49092	10.88	1.98	33.90	426	111	0	0.144	0.0963	0.5748	0.2389	0.0000	0.3049	19	16
49093	11.49	2.72	30.50	355	127	23	0.174	0.1470	0.5324	0.3038	0.1314	0.4094	48	51
49094	9.78	1.43	36.50	570	95	0	0.100	0.0646	0.7143	0.1899	0.0000	0.1966	10	5
49095	8.87	3.53	33.25	388	134	13	0.148	0.1750	0.5338	0.2940	0.0681	0.3195	43	36
49096	28.23	2.56	26.75	277	122	77	0.162	0.1578	0.4736	0.3327	0.5017	0.4346	48	48
49098	18.79	4.04	28.50	359	136	0	0.202	0.2337	0.5761	0.3481	0.0000	0.5087	59	41
49099	19.36	2.65	30.75	343	121	117	0.166	0.1421	0.5102	0.2871	0.6632	0.3874	39	42
49100	18.23	2.94	30.90	302	138	17	0.170	0.1569	0.4470	0.3258	0.0959	0.3949	62	60
49101	18.08	1.80	31.65	314	127	57	0.171	0.0938	0.4538	0.2927	0.3139	0.3878	35	55
49105	29.68	2.39	25.40	277	160	0	0.195	0.1551	0.4933	0.4595	0.	0.5510	78	69
49107	28.02	2.52	27.15	318	306	0	0.249	0.1530	0.5357	0.8222	0.	0.6582	72	67
49110	14.36	1.58	35.75	331	215	0	0.215	0.0729	0.4235	0.4387	0.	0.4316	26	52
49111	14.02	3.06	28.75	298	0	0	0.1850	0.4741	0.2523	0.	0.	0.2646	32	10
49112	12.72	0.74	36.65	331	95	0	0.106	0.033	0.4131	0.1891	0.	0.2076	< 10	-
49115	8.30	1.72	35.25	326	119	0	0.129	0.0804	0.4230	0.2463	0.	0.2626	20	31
49116	10.51	1.45	35.00	359	122	40	0.119	0.0683	0.4692	0.2543	0.1992	0.2440	16	28
49117	7.99	2.34	37.15	293	114	0	0.205	0.1038	0.3608	0.2239	0.	0.3960	18	7
49118	5.26	0.75	38.10	352	95	0	0.124	0.0325	0.4226	0.1820	0.	0.1225	-	-
49119	11.65	1.25	37.65	306	96	0	0.125	0.0547	0.3718	0.1898	0.	0.2383	10	10
49120	14.26	1.22	34.25	314	102	77	0.163	0.0587	0.4193	0.2173	0.3919	0.3416	-	-
49121	16.43	7.57	25.90	246	125	205	0.321	0.4818	0.4380	0.3521	1.3796	0.8895	86	28
49122	9.27	0.50	38.50	339	92	117	0.093	0.0214	0.4028	0.1743	0.5297	0.1734	< 10	-
49123	8.74	4.36	33.90	343	105	37	0.171	0.2120	0.4628	0.2260	0.1902	0.3620	54	40
49124	5.05	1.53	39.00	421	97	84	0.124	0.0647	0.4938	0.1814	0.3754	0.2282	< 10	-
49125	4.65	0.85	40.75	355	98	0	0.146	0.0344	0.3985	0.1754	0.	0.2571	< 10	-
49126	3.53	0.75	41.25	322	74	0	0.102	0.0300	0.0571	0.1309	0.	0.1775	< 10	-
49127	5.20	1.10	40.00	293	86	0	0.136	0.0453	0.3351	0.1568	0.	0.2440	< 10	-
49128	6.31	1.45	39.00	438	92	20	0.124	0.0613	0.5137	0.1721	0.0894	0.2282	< 10	-
49129	20.27	2.03	30.90	285	103	114	0.226	0.1083	0.4219	0.2432	0.6430	0.5249	26	32

APPENDIX C.2 cont.

Sample No.	I.R.%	Mg %	Ca %	Sr ppm	Mn ppm	Na ppm	Fe %	Mg/Ca	Sr $\times 10^3$ /Ca	Mn $\times 10^3$ /Ca	Na $\times 10^3$ /Ca	Fe $\times 10^2$ /Ca	Dolomite %	Dedolomite %
49140	11.13	0.41	34.35	636	82	47	0.118	0.0197	0.8469	0.1742	0.2385	0.2465	< 10	-
49142	8.82	1.75	32.18	767	163	60	0.140	0.0897	1.0902	0.3698	0.3250	0.3122	< 10	-
49143	5.73	0.76	37.39	963	81	161	0.101	0.0335	1.1781	0.1581	0.7505	0.1939	< 10	-
49144	6.63	2.17	34.36	748	87	164	0.234	0.1041	0.9957	0.1848	0.8319	0.4888	< 10	-
49145	8.66	2.90	31.62	589	75	47	0.179	0.1512	0.8520	0.1731	0.2591	0.4063	30	21
49146	6.20	3.80	31.62	565	83	56	0.252	0.1981	0.8173	0.1916	0.3087	0.5720	34	10
49147	6.40	2.40	31.73	488	89	117	0.212	0.1247	0.7035	0.2048	0.6427	0.4795	30	34
49148	10.93	1.77	33.99	657	85	97	0.171	0.0859	0.8841	0.1826	0.4974	0.3611	15	6
49149	7.57	1.90	33.40	636	80	103	0.141	0.0938	0.8710	0.1749	0.5375	0.3030	18	5
49150	9.05	1.04	35.49	694	74	30	0.119	0.0483	0.8944	0.1522	0.1473	0.2406	< 10	-
49151	4.70	1.08	35.81	660	53	43	0.070	0.0497	0.8430	0.1080	0.2093	0.1403	< 10	-
49153	7.04	1.11	36.71	682	75	27	0.122	0.0499	0.8498	0.1491	0.1282	0.2385	< 10	-
49154	7.99	1.03	37.62	688	83	43	0.087	0.0451	0.8365	0.1611	0.1992	0.1660	< 10	-
49155	5.53	1.05	37.17	727	68	23	0.121	0.0466	0.8946	0.1336	0.1079	0.2336	< 10	-
49156	11.19	1.46	33.22	640	81	161	0.174	0.0725	0.8812	0.1800	0.8447	0.3759	< 10	-
49339	7.20	2.12	33.68	545	78	40	0.184	0.1038	0.7402	0.1691	0.2070	0.3921	< 10	-
49157	7.75	0.80	33.09	625	77	117	0.113	0.0399	0.8639	0.1699	0.6163	0.2451	< 10	-
49158	6.99	2.15	33.18	510	75	13	0.166	0.1068	0.7031	0.1650	0.0683	0.3591	17	5
49159	6.81	0.81	36.49	760	71	57	0.085	0.0366	0.9527	0.1420	0.2723	0.1672	< 10	-
49160	9.64	1.90	30.37	531	87	110	0.219	0.1031	0.7997	0.2091	0.6313	0.5175	< 10	-
49164	6.42	2.40	33.86	569	89	158	0.201	0.1169	0.7686	0.1919	0.8133	0.4260	20	7
49165	12.04	2.55	29.46	452	97	115	0.232	0.1427	0.7018	0.2404	0.6804	0.5652	< 10	-
49166	15.12	1.60	29.69	446	102	102	0.199	0.0888	0.6871	0.2508	0.5988	0.4810	28	46
49168	10.44	1.80	35.67	561	90	90	0.155	0.0832	0.7194	0.1842	0.4398	0.3119	< 10	-
49169	10.22	1.90	32.50	554	95	17	0.167	0.0963	0.7797	0.2134	0.0911	0.3687	24	32
49170	6.90	1.80	35.04	570	90	10	0.210	0.0847	0.7441	0.1875	0.0497	0.4301	15	16
49171	7.16	2.00	33.31	525	79	138	0.199	0.0990	0.7209	0.1731	0.7221	0.4288	16	5
49173	6.93	0.45		492	80	70	0.148							
49174	6.48	1.97	34.67	533	81	138	0.202	0.0937	0.7032	0.1706	0.6938	0.4181	< 10	-
49176	4.92	0.80	34.10	542	77	109	0.126	0.0387	0.7270	0.1648	0.5572	0.2652	< 10	-
49178	7.44	3.24	33.68	500	85	10	0.222	0.1586	0.6790	0.1842	0.0518	0.4731	27	8
49179	7.25	4.06	32.32	492	95	156	0.300	0.2071	0.6963	0.2146	0.8413	0.6662	38	18
49180	7.29	2.45	34.81	508	79	13	0.235	0.1160	0.6675	0.1657	0.0651	0.4845	-	-
49181	15.64	3.95	29.46	529	104	107	0.292	0.2210	0.8213	0.2577	0.6331	0.7113	54	38
49183	11.52	2.70	34.00	561	95	13	0.188	0.1309	0.7547	0.2040	0.0666	0.3968	25	17
49184	10.57	1.01	35.58	599	87	40	0.124	0.0468	0.7701	0.1785	0.1960	0.2501	< 10	-
49185	11.12	2.10	31.62	577	95	77	0.137	0.1095	0.8347	0.2193	0.4245	0.3110	23	22
49186	9.70	2.25	33.06	609	83	30	0.160	0.1096	0.8227	0.1789	0.1544	0.3391	19	8
49187	9.80	2.25	34.45	566	95	148	0.197	0.1077	0.7515	0.2013	0.7488	0.4104	21	19
49188	9.13	1.20	32.86	636	100	26	0.127	0.0602	0.8853	0.2222	0.1379	0.2774	11	15
49189	10.90	2.00	31.82	593	105	94	0.207	0.1036	0.8524	0.2409	0.5149	0.4669	21	20
49190	11.03	2.02	34.67	587	102	34	0.220	0.0961	0.7744	0.2148	0.1709	0.4554	24	32
49191	16.50	1.23	30.37	609	120	51	0.228	0.0668	0.9172	0.2884	0.2927	0.5388	33	65
49192	23.63	2.20	26.74	478	128	9	0.278	0.1356	0.8176	0.3494	0.0587	0.7461	42	50
49193	7.43	0.85	33.86	731	110	158	0.134	0.0414	0.9875	0.2372	0.8113	0.2840	< 10	-
49194	8.73	0.80	35.81	698	114	107	0.131	0.0368	0.8916	0.2324	0.5208	0.2625	< 10	-
49196	12.86	0.60	32.86	759	133	81	0.176	0.0301	1.0565	0.2955	0.4297	0.3844	< 10	-
49198	18.31	0.77	32.41	587	121	154	0.215	0.0392	0.8284	0.2725	0.8282	0.4761	12	44
49200	11.02	0.40	32.18	678	112	146	0.166	0.0205	0.9637	0.2541	0.7908	0.3702	< 10	-
49201	8.37	0.64	37.17	901	94	81	0.131	0.0284	1.1087	0.1846	0.3798	0.2529	< 10	-
49202	6.90	0.65	37.76	814	96	37	0.106	0.0284	0.9860	0.1856	0.1708	0.2015	< 10	-
49204	7.03	0.53	36.49	917	65	34	0.106	0.0240	1.1495	0.1300	0.1624	0.2085	< 10	-
49206	9.73	0.60	35.58	773	100	20	0.149	0.0278	0.9937	0.2052	0.0980	0.3005	< 10	-
49207	6.55	0.70	37.39	949	90	68	0.129	0.0309	1.1609	0.1757	0.3170	0.2476	< 10	-
49208	5.94	0.71	36.49	880	72	156	0.088	0.0321	1.1031	0.1440	0.7452	0.1731	< 10	-
49211	8.85	1.84	34.36	756	97	156	0.176	0.0883	1.0064	0.2061	0.7914	0.3676	< 10	-
49212	8.54	2.47	33.54	690	95	10	0.197	0.1214	0.9410	0.2068	0.0520	0.4215	< 10	-
49213	5.91	2.08	35.49	678	82	54	0.171	0.0966	0.8738	0.1687	0.2652	0.3458	16	5
49214	8.97	3.45	30.59	534	175	47	0.271	0.1859	0.7985	0.4176	0.2678	0.6358	39	36
49217	9.61	2.71	33.54	661	95	40	0.222	0.1332	0.9014	0.2068	0.2079	0.4750	24	11
49219	5.55	0.63	36.40	674	87	10	0.100	0.0285	0.8469	0.1745	0.0479	0.1972	< 10	-
49220	5.68	1.19	36.94	620	64	34	0.085	0.0531	0.7677	0.1265	0.1604	0.1651	< 10	-
49221	7.06	2.45	32.50	490	79	90	0.216	0.1243	0.6896	0.1775	0.4827	0.4770	20	5
49225	7.03	0.54	37.17	674	72	60	0.093	0.0240	0.8294	0.1414	0.2814	0.1796	< 10	-
49227	8.71	1.35	33.09	447	85	47	0.155	0.0673	0.6179	0.1875	0.2476	0.3362	14	20
49228	3.95	0.85	38.66	554	74	37	0.103	0.0363	0.6555	0.1397	0.1668	0.1912	< 10	-
49231	5.40	0.62	38.53	723	72	117	0.093	0.0265	0.8583	0.1364	0.5293	0.1732	< 10	-
49232	8.42	0.60	36.85	674	77	64	0.109	0.0268	0.8366	0.1525	0.3027	0.2183	< 10	-
49234	8.69	0.73	32.18	545	87	187	0.126	0.0374	0.7747	0.1974	1.0129	0.2810	< 10	-
49237	15.52	1.85	31.73	550	88	27	0.234	0.0961	0.7929	0.2025	0.1483	0.5293	24	32
49238	9.62	1.90	33.09	589	163	81	0.186	0.0947	0.8142	0.3596	0.4267	0.4034	20	22
49239	14.20	2.00	32.50	510	100	34	0.186	0.1015	0.7178	0.2246	0.1823	0.4107		

APPENDIX C.2 cont.

Sample No.	I.R.%	Mg %	Ca %	Sr ppm	Mn ppm	Na ppm	Fe %	Mg/Ca	Sr 10 /Ca	Mn 10 /Ca	Na 10 /Ca	Fe 10 /Ca	Dolomite %	Dedolomite %
49240	10.78	0.95	33.18	589	95	21	0.114	0.0472	0.8120	0.2090	0.1103	0.2466	<10	-
49241	11.13	0.68	36.03	674	88	17	0.125	0.0311	0.8556	0.1783	0.0822	0.2490	<10	-
49242	9.26	0.83	36.40	620	86	34	0.112	0.0376	0.7791	0.1725	0.1628	0.2208	<10	-
49245	10.82	0.49	35.49	859	76	40	0.116	0.0228	1.1171	0.1553	0.1965	0.2346	<10	-
49246	8.67	0.45	36.71	822	63	34	0.072	0.0202	1.0342	0.1253	0.1614	0.1408	<10	-
49250	7.50	0.55	34.00	813	66	329	0.079	0.0267	1.0937	0.1417	1.6866	0.1668	<10	-
49251	3.98	0.50	32.86	828	56	123	0.086	0.0251	1.1525	0.1244	0.6524	0.1878	<10	-
49252	4.46	0.61	37.62	893	55	37	0.082	0.0267	1.0558	0.1067	0.1714	0.1564	<10	-
49253	3.37	0.65	37.84	896	51	129	0.073	0.0283	1.0331	0.0984	0.5942	0.1385	<10	-
49254	4.23	0.64	40.02	930	54	141	0.070	0.0264	1.0629	0.0985	0.6141	0.1255	<10	-
49257	7.74	1.64	29.57	523	71	145	0.152	0.0892	0.8590	0.1753	0.8547	0.3689	<10	-
49258	6.52	1.50	37.15	727	85	106	0.097	0.0666	0.8951	0.1670	0.4973	0.1874	11	5
49259	5.72	1.55	35.67	688	60	115	0.096	0.0716	0.8522	0.1228	0.5619	0.1932	12	5
49260	4.05	0.90	37.62	945	55	30	0.049	0.0394	1.1490	0.1067	0.1390	0.0935	<10	-
49261	5.03	0.67	37.39	1008	59	23	0.071	0.0295	1.2331	0.1152	0.1070	0.1363	<10	-
49262	3.86	0.93	38.98	719	73	115	0.053	0.0393	0.8437	0.1367	0.5142	0.0976	<10	-
49264	5.53	0.65	36.49	589	63	102	0.067	0.0294	0.7333	0.1260	0.4872	0.1318	<10	-
49266	6.27	2.10	34.22	711	73	209	0.118	0.1012	0.9504	0.1557	1.0645	0.2475	<10	-
49267	5.59	0.83	37.98	756	68	121	0.076	0.0360	0.9105	0.1307	0.5553	0.1436	<10	-
49268	5.98	0.95	36.12	715	63	124	0.078	0.0434	0.9554	0.1273	0.5984	0.1550	<10	-
49269	7.95	1.63	35.04	657	79	57	0.135	0.0767	0.8576	0.1646	0.2835	0.2765	<10	-
49270	8.82	1.01	36.26	694	78	67	0.107	0.0459	0.8754	0.1570	0.3221	0.2118	<10	-
49272	8.38	1.40	35.81	688	90	205	0.103	0.0645	0.8738	0.1835	0.9978	0.2064	<10	-
49273	9.06	0.93	31.05	644	75	107	0.109	0.0494	0.9487	0.1763	0.6006	0.2519	<10	-
49274	6.15	1.28	36.40	719	80	43	0.097	0.0580	0.9035	0.1604	0.2059	0.1913	<10	-
49275	8.08	1.35	33.54	621	83	43	0.114	0.0664	0.8469	0.1806	0.2235	0.2439	<10	-
49276	8.62	1.40	35.58	678	76	134	0.147	0.0649	0.8716	0.1559	0.6564	0.2965	<10	-
49278	9.18	1.17	36.85	517	81	17	0.133	0.0523	0.6417	0.1605	0.0804	0.2590	<10	-
49279	9.25	1.42	35.35	570	79	67	0.158	0.0662	0.7375	0.1631	0.3304	0.3208	<10	-
49280	6.13	0.69	38.07	735	70	188	0.076	0.0299	0.8631	0.1342	0.8607	0.1433	<10	-
49281	6.05	0.69	38.98	826	70	70	0.074	0.0292	0.9693	0.1311	0.3130	0.1362	<10	-
49283	6.91	0.75	36.40	569	100	30	0.065	0.0340	0.7150	0.2006	0.1437	0.1282	<10	-
49286	6.22	2.26	35.58	521	77	57	0.164	0.1047	0.6698	0.1580	0.2792	0.3308	12	5
49287	5.50	1.08	38.53	719	62	134	0.091	0.0462	0.8535	0.1175	0.6062	0.1695	<10	-
49289	5.52	0.78	35.67	569	95	102	0.069	0.0361	0.7296	0.1944	0.4984	0.1388	<10	-
49290	4.94	1.80	36.12	557	83	21	0.116	0.0822	0.7054	0.1678	0.1013	0.2305	13	5
49291	6.25	1.10	35.22	636	75	68	0.093	0.0515	0.8260	0.1555	0.3365	0.1895	<10	-
49292	7.10	0.75	36.12	834	73	111	0.068	0.0342	1.0561	0.1475	0.5356	0.1351	<10	-
49293	7.30	1.20	38.07	668	85	179	0.097	0.0520	0.8026	0.1630	0.8195	0.1829	<10	-
49294	6.71	0.86	36.94	649	67	117	0.101	0.0384	0.8036	0.1324	0.5521	0.1962	<10	-
49295	6.54	1.45	34.54	530	80	51	0.147	0.0692	0.7019	0.1691	0.2574	0.3054	<10	-
49296	5.96	1.10	35.81	644	90	47	0.074	0.0506	0.8226	0.1835	0.2288	0.1483	10	-
49297	14.90	0.65	36.71	802	70	34	0.070	0.0292	0.9993	0.1392	0.1614	0.1369	<10	-
49298	6.75	0.70	36.26	656	85	145	0.083	0.0318	0.8275	0.1711	0.6970	0.1643	<10	-
49299	7.15	0.70	35.35	640	75	244	0.098	0.0327	0.8281	0.1549	1.2031	0.1990	<10	-
49300	8.92	0.73	36.39	743	90	205	0.092	0.0331	0.9339	0.1805	0.9819	0.1814	<10	-
49301	10.29	0.70	33.40	775	90	30	0.093	0.0346	1.0613	0.1967	0.1566	0.1998	<10	-
49302	5.62	0.73	43.06	901	85	205	0.068	0.0279	0.9571	0.1441	0.8298	0.1133	<10	-
49303	5.87	0.73	36.71	806	80	77	0.081	0.0328	1.0042	0.1590	0.3656	0.1584	<10	-
49306	5.03	1.08	37.62	917	93	56	0.086	0.0473	1.1149	0.1805	0.2595	0.1641	<10	-
49307	5.23	0.81	36.26	1012	65	85	0.083	0.0368	1.2756	0.1309	0.4086	0.1643	<10	-
49309	4.97	1.03	37.17	925	75	90	0.082	0.0457	1.1323	0.1473	0.4220	0.1583	<10	-
49310	5.75	1.13	37.39	846	73	43	0.075	0.0498	1.0349	0.1425	0.2005	0.1440	<10	-
49312	3.56	0.85	35.67	909	70	107	0.079	0.0393	1.1656	0.1433	0.5229	0.1590	<10	-
49313	5.01	1.20	36.40	959	68	117	0.118	0.0544	1.2051	0.1364	0.5603	0.2327	<10	-
49316	11.35	1.33	33.54	585	95	103	0.141	0.0654	0.7978	0.2068	0.5353	0.3017	<10	-
49317	9.83	2.05	32.32	545	100	0	0.152	0.1046	0.7713	0.2259	0	0.3375	23	27
49318	7.33	1.50	37.62	684	93	167	0.117	0.0657	0.8316	0.1805	0.7737	0.2232	12	8
49320	5.53	2.35	34.54	632	93	81	0.197	0.1122	0.8369	0.1966	0.4088	0.4093	21	12
49321	5.05	1.20	36.26	814	80	43	0.065	0.0546	1.0268	0.1611	0.2067	0.1287	-	-
49322	5.30	1.18	30.59	455	93	0	0.134	0.0636	0.6603	0.2219	0	0.3144	14	24
49323	7.04	2.15	32.86	470	103	0	0.166	0.1079	0.6542	0.2288	0	0.3626	22	21
49325	10.38	2.70	31.27	565	100	17	0.218	0.1424	0.8255	0.2335	0.0948	0.5003	30	26
49326	7.53	1.18	35.67	553	85	397	0.114	0.0545	0.7031	0.1740	1.9399	0.2294	-	-
49328	4.12	0.98	36.71	616	67	0	0.099	0.0440	0.7675	0.1332	0	0.1935	-	-
49329	5.70	2.05	35.35	553	95	158	0.159	0.0956	0.7155	0.1962	0.7791	0.3228	17	8
49330	11.57	1.06	33.00	566	94	34	0.140	0.0530	0.7845	0.2079	0.1796	0.3045	<10	-
49331	9.13	1.10	33.54	545	80	81	0.103	0.0541	0.7432	0.1741	0.4209	0.2204	<10	-
49333	12.60	2.13	31.41	510	83	98	0.185	0.1118	0.7427	0.1929	0.5438	0.4227	-	-
49334	6.60	1.80	35.67	573	83	150	0.141	0.0832	0.7348	0.1699	0.7330	0.2837	-	-
49335	6.11	1.53	33.86	613	83	107	0.118	0.0745	0.8261	0.1789	0.5508	0.2501	-	-

Appendix D

X-RAY FLUORESCENCE ANALYSES (XRF)

XRF analyses were done under the guidance of Mr. P. Robinson on a Philips PW1410 X-ray spectrometer. Glass fusion discs used for the major element analyses were prepared from a mixture of lithium-lanthanum-borate flux and rock powder as described in Norrish and Chappell (1977). Trace elements were analysed in pressed pills prepared by backing finely powdered samples with boric acid.

Matrix correction coefficients for the major elements were taken from Norrish and Hutton (1969) and mass absorption coefficients for trace elements were calculated on the basis of the major element compositions following Norrish and Chappell (1977). Corrections were also made for the interfering elements.

Table D.1 gives instrument settings, precision, and detection limits used for the analyses.

Table D.1

INSTRUMENT SETTINGS FOR XRF ANALYSIS

Oxide/ Element	Tube	KV	mA	Crystal	Vaccum	Coll.	Counting time,sec.	Counting precision	Detection limit (3 standard deviations)
Fe ₂ O ₃	Cr	50	30	LiF ₂₀₀	yes	coarse	30	13.00±0.04%	0.01%
TiO ₂	Cr	50	30	LiF ₂₀₀	yes	fine	20	2.50±0.01%	0.002%
CaO	Cr	50	30	LiF ₂₀₀	yes	fine	20	6.50±0.02%	0.01%
K ₂ O	Cr	50	30	PE	yes	fine	20	1.8±0.01%	0.003%
SiO ₂	Cr	50	30	PE	yes	coarse	100	55.0±0.30%	0.02%
Al ₂ O ₃	Cr	50	30	PE	yes	coarse	100	13.30±0.05%	0.02%
P ₂ O ₅	Cr	50	50	GE	yes	coarse	50	1.04±0.01%	0.01%
MgO	Cr	50	50	TLAP	yes	coarse	100	10.00±0.07%	0.04%
Rb	Mo	50	30	LiF ₂₂₀	no	fine	20,20,20	200±2 ppm	2 ppm
Ba	Cr	50	50	LiF ₂₀₀	yes	fine	100,100,100	50±2 ppm	4 ppm
V	Cr	50	50	LiF ₂₀₀	yes	fine	100	30±3 ppm	4 ppm
Ga	Mo	50	40	LiF ₂₀₀	yes	fine	20	20±1 ppm	1 ppm
S	Cr	50	50	PE	yes	coarse	30	0.05±0.001	0.006%

APPENDIX E

A Phillips Diffraction unit, which generated Ni filtered Ai K_α radiation was used for X-ray diffraction (XRD) analysis. Powdered samples were smeared onto glass slides using non-diffracting grease.

The whole rock (powder) samples were analysed, by scanning at a rate of 1° , 2θ per minute over the range 25° to 34° , 2θ , within which the main calcite, dolomite and quartz peaks occur.

The insoluble residues were analysed at the same rate, but over the range 4° - 60° , 2θ to include any clay minerals.

XRD angles used for determination of the significant minerals are:

Mineral	dA°	$2\theta^\circ$
Calcite	3.04	29.36
Dolomite $\text{CaMg}(\text{CO}_3)_2$	2.89	30.92
Ferroan dolomite $\text{Ca}(\text{Mg}_{0.67}\text{Fe}_{0.33})(\text{CO}_3)_2$	2.90	30.8
Quartz	3.34	26.64
Illite	10	8.84
Muscovite	9.97	8.86
K-Feldspar	4.02	22.08
Plagioclase	4.03	22.04
Plagioclase	3.19	27.94

Diffraction patterns of several whole rock samples are shown below as Fig. E.1.

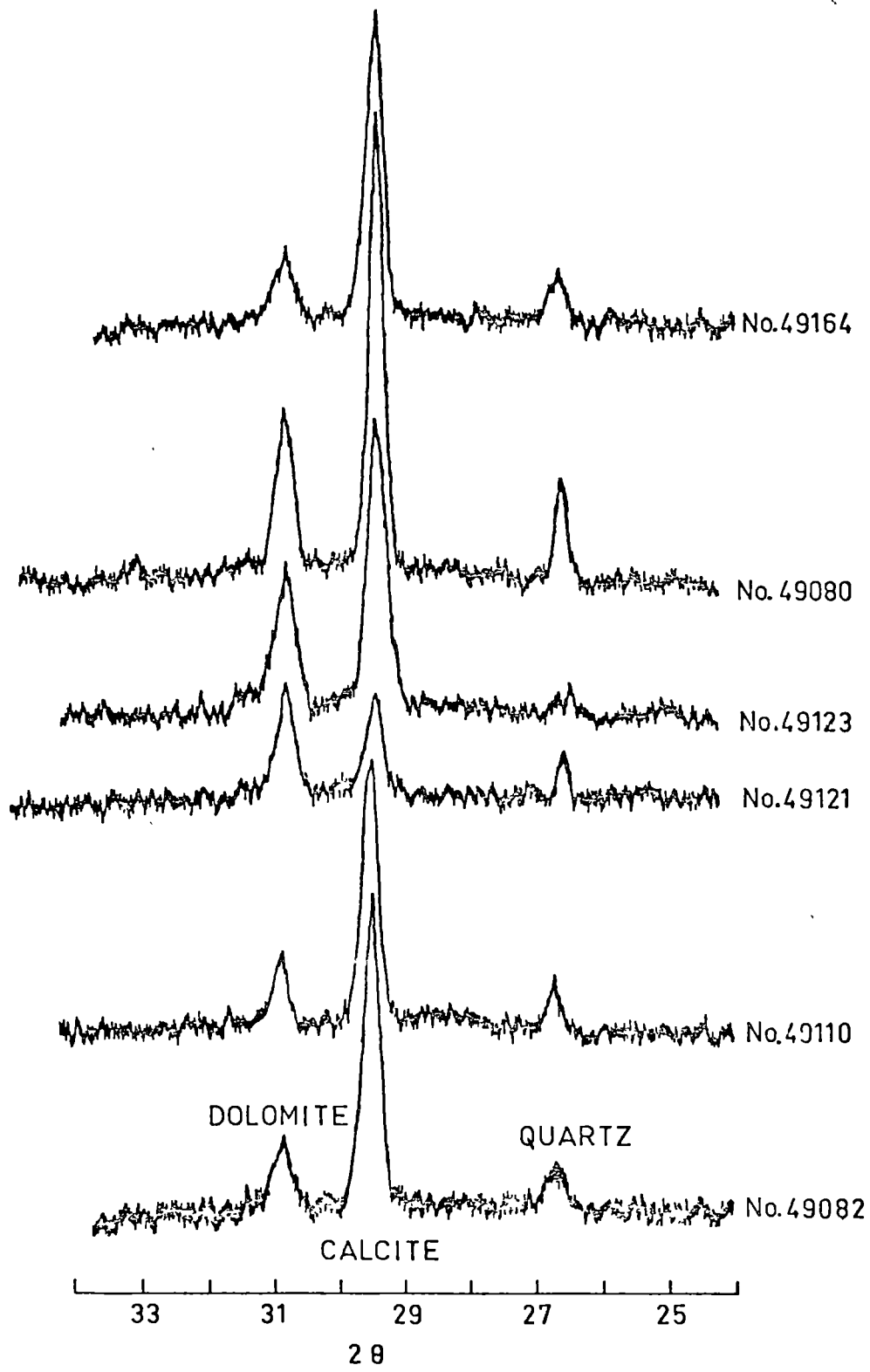


Table E.1 X-ray diffractograms showing the major peaks of dolomite, calcite and quartz.

APPENDIX F

Electron microprobe analyses.

The analyses were carried out on a JEOL JXA-50A scanning electron microprobe analyser under the guidance of Mr. W. Jablonski. EDAX spectra were used for analyses. Reductions of X-ray data incorporating corrections for absorption, fluorescence, ionization and backscattering were made with the aid of the incorporated computer programme TAS-SUEDS.

Back scattered electron images and X-ray distribution maps were obtained on a tilt of 20° with current 3×10^{-9} amps and accelerated voltage 15 kv.